LHC Phenomenology of the Three-Site Higgsless Model

Dissertation zur Erlangung des
naturwissenschaftlichen Doktorgrades
der Julius-Maximilians-Universität Würzburg

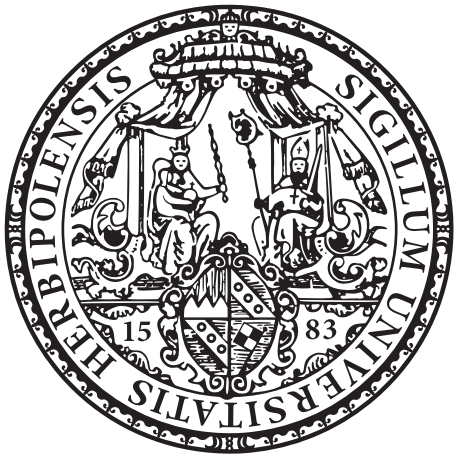

vorgelegt von

Christian Speckner

aus Würzburg

Würzburg, 2009

LHC Phenomenology of the Three-Site Higgsless Model

Dissertation zur Erlangung des
naturwissenschaftlichen Doktorgrades
der Julius-Maximilians-Universität Würzburg

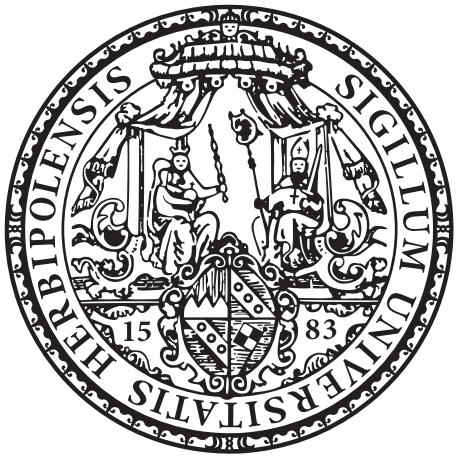

vorgelegt von

Christian Speckner

aus Würzburg

Würzburg, 2009

Einereicht am: _____

bei der Fakultät für Physik und Astronomie

1. Gutachter: _____

2. Gutachter: _____

3. Gutachter: _____

der Dissertation

1. Prüfer: _____

2. Prüfer: _____

3. Prüfer: _____

im Promotionskolloquium

Tag des Promotionskolloquiums: _____

Zusammenfassung

Das Standardmodell der Teilchenphysik, welches in den späten sechziger Jahren in seiner heutigen Form eingeführt wurde, hat sich über die letzten 40 Jahre hinweg in zahllosen Experimenten als eine außerordentlich genaue Beschreibung der Physik auf kleinsten Skalen erwiesen. Alle von dem Modell vorhergesagten Fermionen und Vektorbosonen wurden mittlerweile entdeckt, ihre Eigenschaften experimentell vermessen, und die Vorhersagen des Modells auf Basis dieser Daten haben sich auf Schleifen- und sogar Mehrschleifenniveau als gültig erwiesen.

Der letzte noch nicht entdeckte Baustein des Modells ist das Higgs-Boson. Da von den bisher durchgeführten Experimenten im wesentlichen der Skalenbereich unterhalb von $100\,\mathrm{GeV}$ abgedeckt wurde, ist dies jedoch noch kein Problem und immer noch mit der Theorie konsistent. Der LHC (der in der nahen Zukunft anlaufen sollte) wird den experimentell zugängliche Skalenbereich voraussichtlich um eine Größenordnung auf mehrere TeV erweitern. Sollte das Higgs auch bei diesen Energien nicht gefunden werden, so wäre das Standardmodell falsifiziert und aus den Grundlagen der Quantenmechanik würde folgen, daß entweder bei etwa $1\,\mathrm{TeV}$ die Störungstheorie zusammenbrechen oder neue Physik in Erscheinung treten müßte, welche die Perturbativität der Theorie gewährleistet — anderenfalls würde bei hohen Energien die Unitarität des Zeitentwicklungsoperators verlorengehen und die statistische Interpretation der Quantenmechanik zusammenbrechen.

Obwohl viele Modelle neuer Physik das Konzept der Symmetriebrechung durch fundamentale Skalarfelder vom Standardmodell übernehmen und lediglich die Details des entsprechenden Sektors modifizieren, gibt es auch eine große Gruppe von Szenarien, welche keine derartigen Felder enthalten. Unter diesen Higgslosen Modellen (und möglicherweise auch durch die berühmte AdS/CFT-Korrespondenz verknüpft) sind die wohl bekanntesten Beispiele Technicolor-Modelle sowie extradimensionale Higgslose Szenarien. Beiden Klassen von Modellen gemeinsam ist das Auftreten neuer Resonanzen im Spektrum oberhalb von etwa $100\,\mathrm{GeV}$, deren Austausch perturbative Unitarität bei hohen Skalen gewährleistet. Diese neuen Resonanzen stellen jedoch ebenfalls eine ernstzunehmende Gefahr für solche Szenarien dar, da ihr Austausch zusätzliche Beiträge zu den bei LEP / LEP-II sehr genau vermessenen Präzisionsobservablen liefert. Falls keine speziellen Vorkehrungen getroffen werden, haben diese Beiträge die Tendenz, derartige Modelle bereits auf der Basis existierender Daten auszuschließen.

In den letzten Jahren wurden extradimensionale Modelle vorgeschlagen, in wel-

chen die Fermionen des Standardmodells in der Extradimension delokalisiert sind, wodurch die Präzisionsobservablen durch Justage der Kopplungen an die neuen Resonanzen korrekt reproduziert werden können. Derartige Modelle sind ein gangbarer Weg, die elektroschwache Symmetrie zu brechen und die perturbative Unitarität an der TeV-Skala aufrecht zu erhalten, ohne ein fundamentales Higgs-Feld zu postulieren. Allerdings sind extradimensionale Modelle (von Trivialfällen abgesehen) nicht renormierbar und nur unterhalb einer Cutoff-Skala gültig, und die meisten neuen Resonanzen liegen oberhalb dieses Cutoffs. Eine „ehrliche" Erweiterung des Standardmodells sollte lediglich die Struktur unterhalb dieses Cutoffs enthalten und den extradimensionalen Mechanismus zur Symmetriebrechung und Verzögerung der Unitaritätsverletzung implementieren, ohne Annahmen über die Physik jenseits der Cutoff-Skala zu machen.

Das „Three-Site Higgsless Model" ist eine minimale Implementation dieser Idee. Obwohl dieses Modell durch extradimensionale Higgslose Modelle motiviert werden kann, enthält es lediglich eine Generation zusätzlicher Resonanzen, welche vollständig unterhalb des Cutoffs liegt und die Verletzung der Unitarität auf $2 - 3\,\mathrm{TeV}$ hinausschiebt. Der nicht mit dem Standardmodell übereinstimmende Teil des Spektrums besteht aus einem kompletten Satz von Partnern für alle Standardmodellteilchen mit Ausnahme des Gluons und des Photons. Eine Analyse der bestehenden experimentellen Einschränkungen zeigt, daß das Modell die Präzisionsobservablen korrekt reproduzieren kann, falls die Kopplungen zwischen den schweren Eichbosonpartnern und den Fermionen des Standardmodells sehr klein (etwa 1% des Isospinkopplung) und die Fermionpartner mit Massen $\geq 1.8\,\mathrm{TeV}$ verhältnismäßig schwer sind.

In dieser Doktorarbeit wurde die LHC-Phänomenologie dieses Szenarios untersucht. Zu diesem Zwecke wurden die Kopplungen und Breiten aller neuen Teilchen berechnet und das Modell in den Monte-Carlo-Generator WHIZARD / O'Mega implementiert. Diese Implementation wurde verwendet, um die Produktion der Fermion- und Eichbosonpartner auf Partonniveau in verschiedenen Kanälen zu simulieren, welche sich für die Entdeckung am LHC eignen könnten. In dieser Arbeit werden die Ergebnisse zusammen mit ein Einführung in das Modell sowie einer Diskussion der Modelleigenschaften präsentiert.

Obwohl ihre fermiophobe Natur die Entdeckung der schweren Eichbosonen an Teilchenbeschleunigern grundsätzlich erschwert, zeigt sich, daß der LHC die entsprechenden Resonanzen finden kann sowie sogar einige Rückschlüsse auf die Stärke der fermiophoben Kopplungen (was ein wesentlicher Test der Konsistenz eines solchen Szenarios wäre) zulassen sollte. Bei der Berechnung der Breite der schweren Fermionen stellt sich heraus, daß zu der großen Masse auch relative Breiten von 10% und mehr kommen, so daß diese Teilchen sich eher schlecht für eine direkte Entdeckung am LHC eignen. Trotzdem zeigen die Simulationen daß, hinreichend viel Zeit, Geduld sowie ein gutes Verständnis von Detektor und Hintergrund vorausgesetzt, eine direkte Entdeckung zumindest in einem Teil des Parameterraums möglich ist.

Abstract

The Standard Model of particle physics, conceived in the late 1960s, has been confirmed as an extremely accurate description of microscopic physics in a multitude of experiments conducted over the last 40 years. Over time, all fermions and vector bosons predicted by the model have been discovered, their properties have been measured, and the predictions of the model based upon these properties have shown to be accurate to the one loop and even multiloop level.

The last piece of the Standard Model which hasn't been discovered yet is the Higgs boson. As experiments have essentially only been probing scales below $100\,\mathrm{GeV}$, this is not necessarily a problem and still consistent with the theory. However, the LHC (which should be commencing operation anytime soon) will be hopefully extending the energy scale accessible to experiments by a an order of magnitude to several TeVs. If the Higgs is not discovered in this energy range, then the Standard Model would be falsified and the very fundamentals of quantum mechanics would tell us that either perturbation theory must break down at about $1\,\mathrm{TeV}$ or that new physics must enter the stage in order for the theory to remain perturbative — otherwise, unitarity would be lost at high energies and the probabilistic interpretation of quantum mechanics would break down.

While many models of new physics retain the concept of fundamental scalars in the spectrum being responsible for the symmetry breaking and just modify the details of the implementation, there is also a large group of scenarios which do not contain any such fields at all. Among these Higgsless models (and probably also connected by the celebrated AdS/CFT correspondence), the arguably most prominent examples are technicolor and extra dimensional Higgsless models. In both classes of models, new resonances appear in the spectrum above $100\,\mathrm{GeV}$, the exchange of which retains perturbative unitarity at high scales. However, at the same time, the presence of these new resonances also turns out to be a severe threat to such scenarios, their exchange leading to additional contributions to the precision observables measured in the LEP / LEP-II experiments to very high accuracy and tending to exclude such models if no special care is taken.

In the last years, extra dimensional models have been proposed which can evade these constraints by delocalizing the Standard Model fermions within the extra dimension, thus allowing to tune the couplings to the new resonances in order to avoid these constraints. This way, such models are a viable method of breaking the electroweak symmetry and retaining perturbative TeV scale unitar-

ity without introducing a fundamental Higgs field. However, extra dimensional models (excluding trivial cases) are intrinsically nonrenormalizable and valid only below a cutoff scale, with most of the new resonances lying in fact above the cutoff. Conceptionally, a honest extension of the Standard Model should only contain the structure below this cutoff, incorporating the extra dimensional mechanism of breaking the symmetry and delaying unitarity violation without making assumptions on the high energy physics above the cutoff scale.

The Three-Site Higgsless Model is a minimal implementation of this idea. While it can be motivated by extra dimensional Higgsless models of electroweak symmetry breaking, it in fact contains only one set of extra resonances which lies below the cutoff, delaying unitarity violation to $\approx 2 - 3\,\mathrm{TeV}$. The non-Standard Model part of the spectrum consists of a set of heavy partners for all Standard Model particles with the exception of photon and gluon. The analysis of the experimental constraints reveals that, while the model is consistent with the precision observables, the couplings between the new heavy gauge bosons and the Standard Model fermions have to be exceedingly small ($\approx 1\%$ of the isospin gauge coupling) while the new fermions are constrained to be rather heavy with masses above $1.8\,\mathrm{TeV}$.

In this thesis, we explored the LHC phenomenology of this scenario. To this end, we calculated the couplings and widths of all the new particles and implemented the model into the Monte-Carlo eventgenerator and WHIZARD / O'Mega. With this implementation, we simulated the parton-level production of the gauge boson and fermion partners in different channels possibly suitable for their discovery at the LHC. The results are presented in this work together with an introduction to the model and a discussion of the properties and couplings of the model.

We find that, while the fermiophobic nature of the new heavy gauge bosons does make them intrinsically difficult to observe at a collider, the LHC should be able to establish the existence of both resonances and even give some hints about the properties of their couplings which would be a vital test of the consistency of such a scenario. For the heavy fermions, we find that their large mass is accompanied by relative widths of more than 10%, making them ill-suited for a direct discovery at the LHC. Nevertheless, our simulations reveal that there is a part of parameter space where, given enough time, patience and a good understanding of detector and backgrounds, a direct discovery might be possible.

Contents

Chapter 1

Introduction

> *Of course our model has too many arbitrary features for these predictions to be taken very seriously...*
>
> (Steven Weinberg, "A theory of leptons")

This quote taken from [1] on what would later become the Standard Model of elementary particle physics may well be one of the most spectacular cases of false modesty in the history of science. Only six years after Steven Weinberg wrote these memorable lines on the then speculative unification of electromagnetic and charged current interactions in a spontaneously broken $\mathbf{SU}(2)_{\mathrm{L}} \times \mathbf{U}(1)_{\mathrm{Y}}$ gauge theory, the discovery of the neutral current interaction at the Gargamelle bubble chamber in 1973 at CERN suggested that there was more to this model than its authors originally had dared to hope.

Attempting to include the three known quarks into this model of weak interactions and explain the smallness of flavor violation, Glashow, Iliopoulos and Maiani postulated an additional quark (the charm) in 1970 [2], while in 1972 Kobayashi and Maskawa suggested another doublet of quarks (top and bottom) in order to explain the violation of CP symmetry observed in the hadron sector [3]. Again, nature chose to prove the theorists right, and in 1974, the charm quark was discovered in form of the J/Ψ charmonium state, while the Υ bottomonium state was discovered in 1977.

By the end of the 1970s, the Nobel prize committee in Stockholm deemed the evidence for the unified theory of electroweak interactions to be convincing enough to win Glashow, Salam and Weinberg the 1979 Nobel prize in physics, even before the postulated W and Z bosons were discovered as resonances at the UA1 and UA2 detectors in 1983, with the 1984 physics Nobel prize going to Rubbia and van der Meer for this discovery.

Up to this day, the success story of the Standard Model has continued with the impressive confirmation of the one loop structure of the model by the LEP / LEP-II experiments, the discovery of the top quark in 1995 at the Tevatron and the discovery of tau neutrino in 2000. Indeed, quite contrary to Weinbergs initial feelings,

every single prediction of the Standard Model has been confirmed in experiment, and all significant discoveries which are usually called "new physics" (e.g. neutrino oscillations) can be easily accommodated within the model.

The last remaining specimen from the Standard Model particle zoo is the Higgs boson. If it exists, then it must have managed to escape detection both at LEP / LEP-II and Tevatron, and together with indirect bounds on its mass coming from a global fit to the Standard Model, this implies that it most probably is lurking around $120\,\mathrm{GeV}$ and in any case must be lighter than several hundred GeV where the LHC together with the ATLAS and CMS experiments would surely find it. After all the past success of the model, it is arguably not the discovery but the absence of a Higgs resonance at the LHC which would be exciting news from the land of particle physics.

Still, there is much truth in Weinbergs statement (after all, it comes from a Nobel laureate), and the Standard Model does exhibit many features that deserve to be called arbitrary and seem to be unfitting for a deep model of nature, e.g. the large number of free parameters (especially the Yukawa sector), the seemingly magical cancellation of gauge anomalies which is essential for the celebrated renormalizability of the model or the three generations of fermions, each of which is an exact copy of the others, differing only in mass.

Also, at the very least, the Standard Model does not describe dark matter and is incompatible with general relativity, and this fact alone implies that it can be only an effective description of nature. If we accept this as fact and still want to keep the Standard Model as-is up to the Planck scale, then we must answer the question why nature would adjust the Higgs mass at the matching scale to ridiculous precision in order to achieve the moderate value we observe. This is the famous Hierarchy Problem which would leave an ugly aftertaste if the Higgs were the only "new" piece of nature waiting to be discovered at the LHC.

So, what happens if the LHC fails to discover the Higgs and puts an end to the success of the Standard Model? If there is no Higgs boson, then (unless our understanding of quantum field theory is fundamentally flawed) consistency conditions require that either new physics enters the game below $1\,\mathrm{TeV}$ or that the model becomes strongly interacting at this scale. In this sense, the LHC cannot fail in its mission: Higgs or not, something yet undiscovered most certainly has to lurk within its reach.

Over the last decades, particle physicists have invested a lot of time and thought into finding out what such a discovery might look like. The resulting models can be divided into two categories: renormalizable models which (even if they may not be candidates for a fundamental theory of nature due to their physics content) can be valid to arbitrarily high scales, and effective field theories which are only valid below a cut-off scale and which do not claim to cover physics at scales significantly higher than those probed by the LHC.

Models which fall into the first category are often motivated in a top-down fashion by theoretical concepts of how nature might organize itself at hight scales, for example supersymmetry or technicolor, while effective models are usually built

in a more pragmatic way as an extension of the low-energy Standard Model physics with little or no assumptions on the high energy structure of nature.

Either way, it turns out that building a model which is in agreement with all experimental constraints collected over the last decades is quite challenging. In particular, any model of electroweak symmetry breaking different from the usual Higgs mechanism tends to change the structure of the leptonic current-current interactions which have been very precisely mapped out in the LEP / LEP-II experiments. The major part of the resulting constraints can be summarized in only three numbers which, however, have a devastating effect on many models of electroweak symmetry breaking. In particular, technicolor models and models of Higgsless symmetry breaking from compact extra dimension tend to violate these precision constraints badly, and extra care has to be taken if models of this kind are to remain viable candidates for a description of nature[1].

In the specific case of compact extra dimensions, all particles usually come with a tower of partners of increasing mass which correspond to the higher excitations of the 5th momentum component (exceptions are particles which are explicitly localized on four-dimensional submanifolds by constuction), the so called Kaluza-Klein (KK) modes. Depending on the conditions enforced on the fields on the boundary of the extra dimensions, massless modes can be forbidden for the towers, thus facilitating the breaking of electroweak gauge symmetry without introducing a Higgs.

As stated above, if a model of new physics is to remain perturbative at the TeV scale, then it must contain some agent which retains perturbative unitarity at high scales, this part being played by the Higgs in the Standard Model. In Higgsless extra-dimensional models, this is achieved via the exchange of higher KK modes, which requires nonzero couplings between the Standard Model particles and their KK partners. However, these couplings also imply new contributions to the current-current interactions which lead to the aforementioned conflict with the LEP observables. Luckily, these constraints can be evaded by a moderate tuning of the wavefunctions of the Standard Model fermions, and this way, extra dimensions remain a potential candidate for the mechanism of electroweak symmetry breaking.

However, if we accept this fine-tuning of the parameters in order to comply with the precision observables, extra dimensional models contain another conceptional flaw. Although they are built in a top-down way with the high energy structure of spacetime in mind, the resulting models are in fact nonrenormalizable with a UV cutoff scale which is typically of the order of $5 - 10\,\mathrm{TeV}$. Therefore, most of the new physics in these models is meaningless as it lies above the cutoff, and an effective field theory which only describes the KK modes below the cutoff would be a more honest way to describe the remaining sector which is not dominated by other high energy physics.

The Three-Site Higgsless Model [4], the LHC phenomenology of which is the

[1] Of course, if the celebrated AdS/CFT correspondence is correct, then the difficulties technicolor and 5D theories are faced with are connected by this duality, and solutions in one formalism induce solutions in the other framework.

topic of this thesis, is an implementation of this idea. While it is clearly inspired by such Higgsless extra dimensional models of electroweak symmetry breaking, it only describes the Standard Model particles and the first generation of KK excitations, making no assumptions on the underlying high energy physics. The precision constraints severely restrict the couplings between the new heavy particles, and we will find that, albeit the structure of the model is simple compared to other, more ambitious extensions of the Standard Model, these restrictions lead to a quite interesting and rich LHC phenomenology.

In chapter 2, we motivate the model in a bottom-up approach, starting with the assumption of unitarity being maintained by W and Z partners in the absence of a Higgs boson and show that, while the model doesn't cure the arbitrariness in the Standard Model, most of the new structure is a straightforward consequence of this assumption. The explicit construction of the model using a more ideological top-down approach inspired by extra dimensions is shown in chapter 3, and in chapter 4 we will move on to discussing the bounds on the model, its parameter space, the couplings and the widths of the new particles. Chapter 5 elaborates on the tools we have been using for the phenomenology study, the results of which are presented in chapters 6 – 8.

Chapter 2

The Model — Bottom-up Approach

I have a cunning plan.

(Archetypical quote from Baldrick in "Blackadder")

The Three Site Model is only one example out of a multitude of models for physics beyond the Standard Model that have been proposed. Before examining the phenomenology of any such model in detail, we should have a clear notion why looking at this particular kind of new physics is worthwhile.

The purpose of this chapter is to give a bottom-up type motivation for the Three Site Model as a straightforward option for pushing the unitarity bounds of the Standard Model once the notion of a fundamental Higgs field that unitarizes scattering amplitudes is discarded.

Although this chapter contains some general remarks on quantum field theories, familiarity of the reader with the formalism and with the Standard Model ist assumed. These topics can be found covered in-depth in many textbooks, e.g. [5, 6, 7, 8].

2.1 Restrictions on Quantum Field Theories

Setting the stage

According to our current understanding of nature, the world at very small scales is properly described in the language of relativistic quantum field theories. To define such a theory, we need to specify the field content of the theory as well as the Lagrangian.

The field content tells us what different kinds of particles are described by the theory. The fields transform in different representations of the Poincaré group which are distinguished by spin and mass of the field.

The Lagrangian $\mathcal{L}$ of the theory is a Lorentz invariant local function of the fields and their derivatives and determines the time evolution of the states described by the theory. It is commonly assumed that $\mathcal{L}$ either is a polynomial of the fields and their derivatives or at least can be expanded in a series in a meaningful way.

The most useful known way to extract predictions out of this kind of description of nature is the use of perturbation theory to describe scattering experiments. Such experiments are modeled in an idealized way as a world that only consists of two particles with well-defined momenta in the asymptotic past, which then interact and scatter to finally evolve into a set of particles with well defined momenta in the distant future. This description relies on the hypothesis that there are such asymptotically free states and that all interactions between the particles are negligible at asymptotic times ("adiabatic switching"). The time evolution operator that mediates the transition from the free particle states in the asymptotic past ("in states") to those in the asymptotic future ("out states") is called the S matrix operator.

To describe the scattering process at finite times, the Lagrangian is split into a quadratic propagation part $\mathcal{L}_{\text{free}}$ and an interaction part $\mathcal{L}_{\text{int}}$ that consists of monomials of higher order in the fields[1] . It is then assumed that the interaction part is just a small perturbation on top of the free propagation, and time dependent perturbation theory is applied to calculate the transition amplitudes order for order as an expansion in the coupling constants appearing as prefactors at the monomials in $\mathcal{L}_{\text{int}}$. This formalism then leads to the well-known expansion of scattering amplitudes in terms of Feynman diagrams.

Although this setup suggests a lot of freedom in the construction of a quantum field theory, there are some properties any sensible theory has to fulfill. The severity of these constraints depends on whether we want our theory to be acceptable as a fundamental description of nature or whether we just want it to be an effective description of our world that breaks down at some energy scale.

Renormalization and renormalizability

Any physical model comes with a number of free parameters that have to be fixed before the theory can be used to quantitatively predict experimental results. One criterion for a sensible model is the existence of predictions that can be checked to potentially falsify the theory, and therefore, these free parameters must be such that they can be determined with a finite number of measurements.

When we set out to calculate higher orders in the perturbation expansion, we encounter loop diagrams that translate to unbounded integrals over four-momenta. Quite contrary to the assumption that higher order contributions are small compared to the leading order, the vast majority of these integrals is infinite. To study these infinities, it is useful to bound the integration domain and cut off the high energy contributions at some energy scale using a regularization scheme (e.g. a

[1] Because of the Lorentz invariance of the Lagrangian, linear terms in the fields are only allowed for scalars and generate a shift in the field vacuum expectation value in this case.

naïve cutoff, Pauli-Villars, dimensional regularization etc.). Calculations in the regularized theory then give finite predictions for observables which now carry an explicit dependence on the parameters and on the cutoff scale (in which they are divergent).

Interestingly, there is a class of theories in which the reexpression of the free parameters in terms of a finite set of measurable defining observables[2] leads to a cancellation of the divergences. In this case, the cutoff scale can be taken to infinity, leading to well-defined, finite observables that now only depend on a finite set of numbers that must be measured to completely fix the theory. This process is called renormalization, and theories which can be treated this way are called renormalizable.

Of course, there is a lot of freedom in the choice of defining observables. Different observables will lead to different convergence properties of the perturbation series. In particular, for a given observable, a clever choice of the scale μ at which the defining observables are measured can significantly reduce the contributions of higher orders; this corresponds to a resummation of the perturbation series.

In the limit of infinite cutoff scale, the parameters which are expressed through the defining observables are divergent. Therefore, the above renormalization trick can be equivalently achieved by splitting the parameters g into a finite part g_R and an infinite part δg which is called a counterterm. The finite part is fixed by measurement while the counterterm is chosen according to some prescription such that it cancels the infinities. If the splitting prescription depends on some renormalization scale μ like in $\overline{\text{MS}}$, then a change of this scale shifts contributions between g_R and δg, changing the value of g_R. This dependence of the g_R on μ is called the renormalization group flow of the parameters, and a suitable choice of μ again allows to resum the perturbation series and reduce the contributions from higher orders.

The whole process of renormalization can be interpreted as absorbing the effects of physics far above the renormalization scale into an (albeit infinite) redefinition of the couplings.

Effective field theories

Renormalizable field theories can be taken to be valid at arbitrarily high energies and therefore are candidates for a fundamental theory of nature. However, with any theory, the claim of it being fundamental is a very ambitious one and, furthermore, the renormalizability condition turns out to be very restrictive on the types of allowed Lagrangians.

However, if we drop the requirement of the theory being fundamental and instead think of it in terms of an effective field theory that is only valid below some scale Λ, then there is nothing bad in the idea of having a cutoff scale to make our integrals finite. Quite contrary, as the theory is only valid up to Λ, we should only include intermediate states below Λ anyway. Effects that come from high energy

[2] An introduction of a finite number of new free couplings that undergo the same treatment might also be necessary.

physics should be included as effective couplings in our low energy theory. The cutoff explicitly enters our calculations and again influences the convergence of the perturbation series.

If we change the cutoff scale Λ, we can calculate how we have to adjust the couplings in front of the operators to retain the predictions. This leads to a renormalization group flow of the couplings that can again be used to resum parts of the perturbation series and this way allow for a meaningful perturbative calculation of observables at different scales. The downside is that, as opposed to renormalizable theories, we must allow for infinitely many couplings as they will be introduced by the renormalization group flow anyway.

To keep our theory predictive, we must assume some kind of ordering scheme where the higher order operators are suppressed by some scale Λ_{NP} and therefore are negligible at low energies. If we construct an effective theory e.g. by integrating out heavy particles from a renormalizable theory, the new operators describing the effects of the degrees of freedom that have been removed obey exactly such an ordering scheme, so this is not an unnatural assumption. This way the theory can be predictive at low energies even though the Lagrangian describing it contains arbitrarily many operators.

If we want to calculate observables at some scale Λ, we must evolve the couplings to this scale in order to perform the perturbative calculation. The higher order interactions increase if we evolve to higher scales, and at some scale Λ_0, the ordering scheme will break down. At this scale the very latest, we have no control over the contributions from higher order operators anymore, and the effective theory is not predictive anymore. It then has to be replaced by another theory that might contain new degrees of freedom and which can either be a fundamental, renormalizable theory or again an effective theory.

This way, if we don't require our theory to be fundamental, renormalizability is not necessary for the theory to make sense. We only have to be aware that the energy range in which the theory is valid is limited and that we have to replace it by something else above Λ_0. Not insisting on renormalizability allows for a much larger class of theories which can be effective descriptions of nature even if quantum field theories should turn out not to be the suitable language for the "theory of everything". Even better, the scale Λ_0 as well as a self-consistent ordering scheme for the higher dimension operators can be estimated from the parameters of the theory by simple dimensional arguments without requiring any knowledge about the underlying high energy physics; this procedure is called NDA [9] ("naïve dimensional analysis").

The remainder of this chapter will be dealing with effective field theories, so renormalizability will not be an issue as long as we stay in the energy range where these theories are valid.

Unitarity — limits on the validity of the perturbation expansion

Unrelated to the issue of renormalizability, there is another criterion for the consistency of field theories. Because it is the limit of a time evolution operator, the axioms of quantum mechanics require the S matrix to be unitary. This is the prerequisite for the probabilistic interpretation of quantum mechanics.

The diagonal elements of the S matrix contain contributions from the case of direct propagation of the initial into the final state without any scattering. As we are usually not interested in these contributions, the cross section is conveniently defined as a flux normalization factor times the modulus of an T matrix element, T being defined as

$$S = iT + \mathbb{I} \tag{2.1}$$

The unitarity condition on S then implies a relation for T:

$$SS^\dagger = \mathbb{I} \quad \longrightarrow \quad i\left(T^\dagger - T\right) = TT^\dagger \tag{2.2}$$

Taking the matrix element between two states $|a\rangle$ and $|b\rangle$ and inserting a complete set of basis vectors, we obtain

$$i\left(\langle b|\, T\, |a\rangle^* - \langle a|\, T\, |b\rangle\right) = \sum_{|c\rangle} \langle a|\, T\, |c\rangle\, \langle b|\, T\, |c\rangle^* \tag{2.3}$$

From (2.3), important consequences for matrix elements can be derived. Restricting the equation to the forward scattering case $|a\rangle = |b\rangle$ yields

$$2\Im\, \langle a|\, T\, |a\rangle = \sum_{|c\rangle} |\langle a|\, T\, |c\rangle|^2 \tag{2.4}$$

This is the famous optical theorem which basically states that the imaginary part of the forward scattering amplitude of some state is equal to the probability for this state scattering into anything. If $|a\rangle$ is an eigenstate of T with eigenvalue $T\,|a\rangle = t\,|a\rangle$ and norm $\langle a \mid a\rangle = 1$, (2.4) further reduces to

$$2\Im t = |t|^2$$

which is solved by[3]

$$t = i + e^{i\delta} \tag{2.5}$$

(2.5) restricts the eigenvalue t to a "Argand circle" in the complex plane with center i and radius 1.

Due to rotational invariance, two particle angular momentum eigenstates below the inelastic threshold (the regime in which the total energy is not sufficient to create any new particles) are eigenstates of the T matrix. If we examine the cross

[3]The same result can also be directly obtained from the definition of T in terms of the unitary S matrix (2.1).

section between incident momentum eigenstates, then these states can be decomposed in a relativistic partial wave expansion [10], and (2.5) implies relations for the partial wave amplitudes. If we cross the inelastic threshold (2.5) changes into an inequality, and the amplitudes are constrained to lie within the Argand circle rather than on it. For a more complete discussion of unitarity and partial wave amplitudes see [10, 6]

If the Lagrangian is hermitian, then the S matrix will be unitary by definition[4]. However, as (2.2) – (2.5) are nonlinear in the T matrix elements, they don't hold order by order if the T matrix elements are expanded in a perturbation series[5]. Therefore, at a fixed order in perturbation theory, the partial wave amplitudes can violate the unitarity criteria. Worse, if an amplitude grows with energy in perturbation theory, then it will leave the Argand circle at some scale and higher orders must become increasingly large to compensate and restore consistency to the theory.

In particular, if the tree level amplitude for some scattering process grows with energy, then there will be a scale where the tree level scattering probability exceeds one and at which perturbation theory stops to be a trustworthy calculational instrument and breaks down. If we write down an effective field theory, this unitarity cutoff will limit the range of applicability of the theory independently from the NDA cutoff.

2.2 The Fermi Model

At "low" energies much smaller than the W mass, our world can be well described by the Fermi model. At this scale, the observable fundamental degrees of freedom are[6]:

- Three generations of leptons e^-, μ^-, τ^- which differ only by their mass and which are described by Dirac spinors L_j.
- The associated three generations of neutrinos ν_e, ν_μ, ν_τ which we will approximate to be massless and which are described by Dirac spinors N_j.
- The photon which mediates the electromagnetic interaction and which is described by the vector field A^μ.

The Fermi Lagrangian $\mathcal{L}_{\text{Fermi}}$ can be decomposed as

$$\mathcal{L}_{\text{Fermi}} = \mathcal{L}_{\text{QED}} + \mathcal{L}_4$$

[4]Exceptions can arise if the quantization is done incorrectly and states are inconsistently removed from the Hilbert space, e.g. due to improper quantization of gauge theories.

[5]Of course, the equations themselves can be expanded to hold order by order, but in this case, different orders in the expansion of the matrix elements will mix.

[6]As color and QCD are not related in any way to the line of reasoning aimed at in this chapter, all colored particles will be ignored for the remainder.

The first part is the usual QED Lagrangian $\mathcal{L}_{\text{QED}}$ given by

$$\mathcal{L}_{\text{QED}} = \sum_{j=1}^{3} \left(\overline{L}_j \left(i\partial\!\!\!/ + m_j \right) L_j + i\overline{N}_j \partial\!\!\!/ N_j \right) - eA_\mu J_Q^\mu - \frac{1}{4} F^{\mu\nu} F_{\mu\nu} \tag{2.6}$$

with the electromagnetic gauge coupling e, the electromagnetic current

$$J_Q^\mu = \sum_{j=1}^{3} \overline{L}_j \gamma^\mu L_j \tag{2.7}$$

and the electromagnetic field strength tensor

$$F^{\mu\nu} = \partial^\mu A^\nu - \partial^\nu A^\mu$$

Defining the left- and right-handed fermion fields Ψ_L and Ψ_R via (A.3), we can introduce the charged and neutral currents

$$\begin{aligned} J_\mu^+ &= \frac{1}{\sqrt{2}} \sum_{j=1}^{3} \overline{L}_{L,j} \gamma_\mu N_{L,j} \quad , \\ J_\mu^- &= J_\mu^{+\dagger} \\ J_\mu^0 &= \sum_{j=1}^{3} \left(\overline{L}_j \gamma_\mu \left(\sin^2 \theta_W - \frac{1}{2} \Pi_- \right) L_j + \frac{1}{2} \overline{N}_{L,j} \gamma_\mu N_{L,j} \right) \end{aligned} \tag{2.8}$$

(with the Weinberg angle θ_W) and write the second piece $\mathcal{L}_4$ as

$$\mathcal{L}_4 = -4\sqrt{2} G_F \left(J_\mu^+ J^{-\mu} + J_\mu^0 J^{0\mu} \right) \tag{2.9}$$

where the Fermi coupling G_F has mass dimension $[G_F] = -2$.

(2.6) contains the bilinear parts of the Lagrangian that generate the propagators as well as the three point gauge couplings of the photon to two leptons, while (2.9) encodes the charged and neutral current four point couplings among four fermions. Apart from the lepton masses, the only free parameters are the electromagnetic gauge coupling e, the Fermi coupling G_F and the Weinberg angle θ_W. Once these parameters are fixed, the Fermi model does a very good job at describing the low energy phenomenology of our world.

However, while pure QED is renormalizable, the four point interactions make the Fermi model a nonrenormalizable model that is only valid up to a UV cutoff scale Λ_{UV}. To estimate this scale, consider the one loop correction to the charged current four point interaction[7]:

[7] The t channel contribution can be avoided by considering the four point function for two different flavors (e.g. $e^- \bar{\nu}_e \to \mu^- \bar{\nu}_\mu$).

Naïve powercounting reveals a quadratic divergence in the one loop contribution, and we can estimate the leading contribution by

$$8{G_F}^2 N_f \int \frac{d^4p}{(2\pi)^4}\, \mathbf{Tr}\, \frac{\not{p}\not{p}}{p^4} = \frac{4}{\pi^2}{G_F}^2 N_f \int_0^{\Lambda_{\mathrm{UV}}} dp\; p = \frac{2}{\pi^2}{G_F}^2 \Lambda_{\mathrm{UV}}^2 N_f$$

where N_f is the number of flavors which can run in the loop. Considering only the leptons we have $N_f = 3$, and demanding that the one loop correction must not exceed the tree level contribution if perturbation theory is to make sense then leads to a estimate for the cutoff scale

$$\Lambda_{\mathrm{UV}} = \pi \sqrt{\frac{\sqrt{2}}{N_f G_F}} \approx 630\,\mathrm{GeV}$$

Of course, if we had also included the quarks into our version of Fermi theory, they would appear within the loop, and the cutoff would be lowered further to $\Lambda_{\mathrm{UV}} \approx 315\,\mathrm{GeV}$.

However, even when setting aside all issues related to renormalization, a straightforward calculation of the amplitude for $ff \longrightarrow ff$ type processes reveals terms induced by the four point couplings which grow quadratically with energy. Partial wave analysis yields a scale of $\approx 600\,\mathrm{GeV}$ [11, 12] at which the s wave amplitude exceeds the unitarity bound. At this scale the very latest, perturbation theory can't be trusted anymore. If our world is to be described by a perturbative quantum field theory, then new physics must come into play below this scale and unitarize the scattering amplitudes or at least delay the scale of unitarity violation.

2.3 The Standard Model

Indeed, experimentalists didn't have to go to scales of $600\,\mathrm{GeV}$ to discover new physics that supersedes the Fermi model: in the early eighties, the $W^\pm$ and Z bosons were discovered at the Super Proton Synchrotron SPS at CERN and at Fermilab with masses of $m_W \approx 80\,\mathrm{GeV}$ and $m_Z \approx 91\,\mathrm{GeV}$ [13].

Together with the photon, the $W^\pm$ and Z are understood as the gauge bosons of a $\mathbf{SU}(2)_L \times \mathbf{U}(1)_Y$ gauge group which unifies electromagnetism and weak interactions. In the following, we will denote the $\mathbf{SU}(2)_L$ gauge fields as $W^\mu = W_k^\mu \tau_k$ (with the $\mathbf{SU}(2)$ generators τ_k, see (A.2)) and the $\mathbf{U}(1)_Y$ gauge field as B^μ; the gauge couplings will be called g and g' respectively. Introducing the field strength tensors

$$F_W^{\mu\nu} = \partial^\mu W^\nu - \partial^\nu W^\mu - ig\,[W^\mu, W^\nu] \quad , \quad F_B^{\mu\nu} = \partial^\mu B^\nu - \partial^\nu B^\mu$$

the gauge kinetic Lagrangian can be written as

$$\mathcal{L}_{\mathrm{gauge}} = -\frac{1}{2}\mathbf{Tr}\, F_W^{\mu\nu} F_{W\,\mu\nu} - \frac{1}{4} F_B^{\mu\nu} F_{B\,\mu\nu}$$

As the W and Z are massive, the gauge symmetry must be broken, and the only known mechanism which achieves this while still allowing for a consistent quantization is spontaneous symmetry breaking. Without any assumptions on the underlying dynamics, the breaking can be parameterized by the introduction of a $\mathbf{SU}(2)$ valued field[8]

$$\Sigma = v e^{i\frac{\phi_k}{v}\tau_k}$$

where v is the vacuum expectation value[9] of Σ

$$\langle \Sigma \rangle = v\mathbb{I}$$

This field is assigned the transformation behavior

$$\Sigma \quad \xrightarrow{\mathbf{SU}(2)_L \times \mathbf{U}(1)_Y} \quad e^{i\lambda_{L,k}\tau_k} \Sigma e^{-i\lambda_Y \tau_3}$$

with the gauge transformation parameters $\lambda_{L,k}, \lambda_Y$. With this charge assignment, the covariant derivative of Σ reads (c.f. (A.1))

$$D^\mu \Sigma = \partial^\mu \Sigma - igW_k^\mu \tau_k \Sigma + ig' B^\mu \Sigma \tau_3$$

The minimal gauge invariant Lagrangian required to make Σ a dynamic field is

$$\mathcal{L}_\Sigma = \mathbf{Tr}\ \left(D^\mu \Sigma\right) \left(D_\mu \Sigma\right)^\dagger \tag{2.10}$$

Expanding (2.10) in the component fields ϕ_i, we find that the lowest order (aka the vacuum expectation value of Σ) leads to mass terms for the gauge bosons which can be written as

$$\frac{v^2}{2}\left(g^2 \sum_{k=1}^{2} W_k^\mu W_{k,\mu} + (W_{3,\mu}, B_\mu) \begin{pmatrix} g^2 & -gg' \\ -gg' & g'^2 \end{pmatrix} \begin{pmatrix} W_{3,\mu} \\ B_\mu \end{pmatrix}\right) \tag{2.11}$$

(2.11) is diagonalized by the mass eigenstates

$$W_\mu^\pm = \frac{W_{1,\mu} \pm iW_{2,\mu}}{\sqrt{2}} \quad , \quad Z_\mu = \frac{gW_{3,\mu} - g'B_\mu}{\sqrt{g^2 + g'^2}} \quad , \quad A_\mu = \frac{g'W_{3,\mu} + gB_\mu}{\sqrt{g^2 + g'^2}} \tag{2.12}$$

and yields the Z and W masses as eigenvalues

$$m_W = gv \quad , \quad m_Z = \sqrt{g^2 + g'^2}v \tag{2.13}$$

Classically, the Σ field can be put to $v\mathbb{I}$ at every point in spacetime by a gauge transformation, absorbing the three corresponding degrees of freedom into the gauge fields. This identifies the three ϕ_k fields as the Goldstone boson fields which are required by the Goldstone theorem [14] and which are "eaten" by the heavy

[8] More accurately, it is the rescaled field $\frac{1}{v}\Sigma$ which is valued in $\mathbf{SU}(2)$.

[9] Note that this definition of v differs by a factor of $\sqrt{2}$ from that usually used found textbooks.

gauge bosons to constitute the longitudinal degrees of freedom. As the ϕ_k transform in a nonlinear realization of the gauge group, Σ is called a nonlinear sigma field.

To reproduce the physics of the Fermi model, we have to specify the representation in which the leptons transform. The left-handed leptons of each generation are grouped in isospin doublets

$$\Psi_{L,j} = \begin{pmatrix} N_{L,j} \\ L_{L,j} \end{pmatrix}$$

that transform in the fundamental representation of the $\mathbf{SU}(2)_L$, the right-handed leptons are singlets under this group factor. The hypercharge transformation properties are derived from the electric charge of the fermions:

$$\Psi_L \xrightarrow{\mathbf{U}(1)_Y} e^{i\lambda_Y(Q-\tau_3)}\Psi_L \quad , \quad \Psi_R \xrightarrow{\mathbf{U}(1)_Y} e^{i\lambda_Y Q}\Psi_R$$

with the electric charge Q. These assignments completely fix the covariant derivative and the conserved currents which couple to the gauge bosons. Defining the electromagnetic gauge coupling e and the Weinberg angle θ_W as

$$e = \frac{gg'}{\sqrt{g^2+g'^2}} \quad , \quad \sin\theta_W = \frac{g'}{\sqrt{g^2+g'^2}} \tag{2.14}$$

the resulting fermionic Lagrangian including the kinetic terms can be written as

$$\mathcal{L}_{\text{fermion}} = i\sum_{j=1}^{3}\left(\overline{L}_k \not{\partial} L_k + \overline{N}_k \not{\partial} N_k\right) + \frac{e}{\sin\theta_W}\left(W^+_\mu J^{+\mu} + W^-_\mu J^{-\mu}\right) + \frac{2e}{\sin 2\theta_W} Z^\mu J_{0\mu} - eA^\mu J_{Q\mu} \tag{2.15}$$

The conserved currents appearing in (2.15) are the very same currents already defined in (2.7) and (2.8).

In the Fermi model, the fermion mass terms can be inserted into the Lagrangian directly. However, with the above $\mathbf{SU}(2)_L \times \mathbf{U}(1)_Y$ charge assignments, such terms would now violate gauge invariance. Fortunately, the nonlinear sigma field Σ allows to generate the necessary terms in a gauge invariant way from Yukawa couplings[10]:

$$\mathcal{L}_{\text{Yukawa}} = \sum_{j=1}^{3} \overline{\Psi}_{L,j} \Sigma \begin{pmatrix} 0 & 0 \\ 0 & \frac{m_j}{v} \end{pmatrix} \begin{pmatrix} N_{R,j} \\ L_{R,j} \end{pmatrix} \tag{2.16}$$

Putting together all pieces of the puzzle, the full Lagrangian of the theory reads

$$\mathcal{L} = \mathcal{L}_{\text{gauge}} + \mathcal{L}_{\text{fermion}} + \mathcal{L}_{\text{Yukawa}} + \mathcal{L}_\Sigma \tag{2.17}$$

[10]For the quark masses, the mass matrix in (2.16) is replaced by $\frac{1}{v}\mathbf{diag}\,(m_u, m_d)$.

The resulting model is the Standard Model, but without any assumptions on the dynamics of the electroweak symmetry breaking and therefore without the Higgs field.

The Standard Model without a Higgs is nonrenormalizable due to the dimension $6+$ operators appearing in the expansion of the Σ fields and therefore must be treated as an effective field theory. Even without knowing the physics responsible for the symmetry breaking, NDA[11] can be used to get an upper bound on the UV cutoff [9]:

$$\Lambda_{\text{NDA}} = 8\pi v = 8\pi \frac{m_W}{g} \approx 3.1\,\text{TeV} \tag{2.18}$$

How does the transition from the Fermi model to the Higgsless Standard Model affect tree level unitarity? In the Fermi model, the divergent parts violating unitarity in the $ff \longrightarrow ff$ amplitude stem from the four point fermion coupling. However, in the Higgsless Standard Model, these couplings are replaced by the exchange of the $W^{\pm}$ and Z bosons:

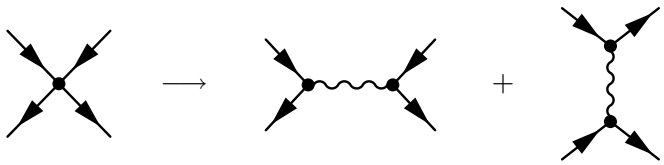

At low energies, the $W^{\pm}$ and Z can be integrated out by replacing the propagators by $-\frac{1}{m^2}$ to obtain the Fermi theory as an effective theory. However, above the W' mass scale, the propagators and the amplitude fall off as $\frac{1}{p^2}$. This damping removes the quadratic growth in energy from the partial wave amplitudes and eliminates the unitarity violating terms.

The entrance of the $W^{\pm}$ and Z bosons on the stage restores perturbative unitarity to the amplitudes for four fermion processes. However, the exorcism of unitarity violation is not complete — perturbative unitarity is still violated by amplitudes containing external heavy vectors. To understand this, recall the high energy limit of the longitudinal polarization vector

$$\epsilon_L^{\mu} \xrightarrow{E\to\infty} \frac{k^{\mu}}{m}$$

At high energies, ϵ_L behaves like the four-momentum and therefore, the amplitude for the scattering of longitudinal vector bosons

$\mathcal{M}_{V_LV_L\to V_LV_L} =$

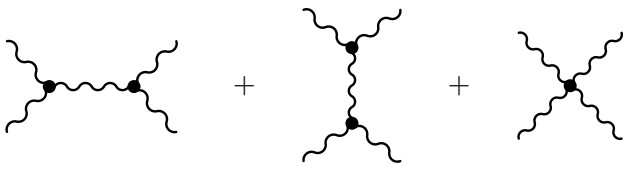

might develop a high energy behavior as bad as E^4. Explicit calculation [15] shows that, while the E^4 parts cancel, a quadratic divergence remains which leads to a

[11] (2.18) differs from [9] by a factor of 2 due to a difference in convention.

violation of tree level unitarity at approximately $1\,\mathrm{TeV}$, well below the NDA cut-off. Therefore, new physics that unitarizes the scattering amplitudes should be expected below $1\,\mathrm{TeV}$ if the theory is to remain perturbative.

2.4 The Higgs

The question of unitarity at the TeV scale is not the only terra incongnita not covered by the Higgsless version of the Standard Model. In particular, we didn't make any assumptions on the physics responsible for the dynamics of electroweak symmetry breaking. As simplicity always has been an effective guiding principle in physics, it is not unreasonable to assume that these questions have the same answer and that the physics responsible for breaking the electroweak symmetry also unitarizes the scattering amplitudes. This is exactly what happens in the Standard Model: a scalar Higgs field is introduced which dynamically develops the vacuum expectation value which breaks the electroweak symmetry and which at the same time unitarizes the scattering amplitudes.

The Higgs can be incorporated into the Higgsless Standard Model presented in the last section by replacing the vacuum expectation value of the Σ field with a dynamical field $H(x)$

$$\Sigma = v e^{\frac{i}{v}\phi_k(x)\tau_k} \quad \longrightarrow \quad \Sigma = H(x) e^{\frac{i}{v}\phi_k(x)\tau_k}$$

and adding the potential

$$\mathcal{L}_H = -V_H(x) = \frac{\mu^2}{2}\mathbf{Tr}\,\Sigma\Sigma^\dagger - \frac{\lambda}{4}\mathbf{Tr}\,\left(\Sigma\Sigma^\dagger\right)^2 = \mu^2 H^2 - \frac{\lambda}{2}H^4 \tag{2.19}$$

with the "mass" μ and the coupling constant λ to the Lagrangian. This potential is the famous Mexican Hat potential whose nontrivial minimum constitutes the tree level vacuum expectation of the Higgs

$$v = \langle H \rangle = \frac{\mu}{\sqrt{\lambda}}$$

Shifting $H(x)$ in order to perform the perturbation expansion around the ground state, we finally obtain $\mathcal{L}_H$ and Σ in terms of the physical Higgs field

$$\Sigma = (v + h(x))\, e^{i\frac{\phi(x)}{v}\phi_k(x)\tau_k}$$

$$\mathcal{L}_H = \frac{\mu^4}{2\lambda} - \mu^2 h^2 - 2\mu\sqrt{\lambda}h^3 - \frac{\lambda}{2}h^4 \tag{2.20}$$

Inserting the modified Σ into (2.17) and adding (2.20) finally leads to the usual Standard Model. The nonlinear representation of the Higgs and Goldstone fields may look unfamiliar compared to the linear doublet representation usually used in textbooks, but both formulations can be transformed into each other by means of a nonlinear field redefinition and therefore are equivalent [16].

What has changed with the introduction of the Higgs? In the Higgsless version of the Standard Model, the symmetry breaking was just parameterized by the introduction of the Goldstone bosons, but the physics responsible for the breaking was not included and the vacuum expectation value v was fixed by hand. In the version of the model including the Higgs, the vacuum expectation value arises dynamically from the Higgs potential, and the observable consequence is the appearance of a physical scalar in the particle spectrum.

The Higgs couples to every massive field and, in particular, new contributions to the scattering amplitude for longitudinal gauge bosons arise

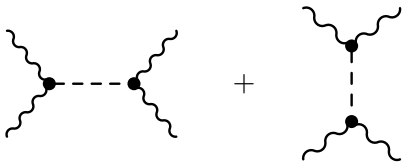

As already mentioned above, explicit calculation shows that these new diagrams completely cancel the divergent pieces and, if the Higgs is not too heavy, perturbative unitarity is restored at arbitrarily high scales [15].

In addition to resolving the unitarity problem, the inclusion of the Higgs makes the Standard Model a renormalizable theory [17], removing the remaining obstacle in interpreting it as a fundamental theory valid at arbitrarily high energies[12]. From this, one might draw the conclusion that the Higgs is the preferred candidate for the mechanism of electroweak symmetry breaking.

However, the Standard Model does not include gravity, and therefore, it cannot be a fundamental theory of nature but must be superseded by new physics at some (although possibly high) scale. Once we have accepted this fact, the Higgs looses much of its appeal through the so-called Hierarchy Problem. Consider the one loop corrections to the Higgs mass

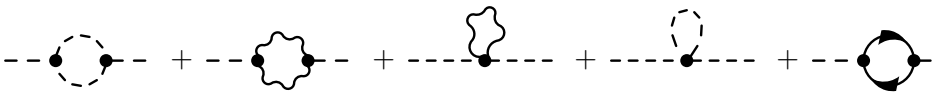

(2.21)

Apart from the first two diagrams, all pieces of (2.21) contain quadratic divergences inducing a quadratic running of the Higgs mass. Therefore, if the Higgs is to have a mass m_H at low scales, then the mass must be tuned with an accuracy of approximately $\frac{m_H}{\Lambda_{\mathrm{UV}}}$ at the scale Λ_{UV} where the Standard Model is matched to some more fundamental description of nature.

In order to preserve perturbative unitarity, the Higgs mass must be considerably smaller then $1\,\mathrm{TeV}$. If we insert the Planck scale as Λ_{UV}, this implies a fine tuning to a rather ridiculous precision of roughly $10^{-14}\%$! While this extreme sensitivity to the underlying high energy physics is not technically inconsistent, it arguably seems unfitting for a theory of nature which is deep enough to be valid over

[12] Even if the model is renormalizable and tree-level unitary at all energies, Landau poles in the renormalization group flow might limit the range of applicability of the model, so this statement is a bit oversimplified.

19 orders of magnitude. Apart from the Hierarchy Problem, there is also a more mundane issue concerning the Higgs boson: no trace of it has been yet discovered in collider experiments and, looking at current exclusion plots (see e.g. [18]) for the Higgs mass, the air is growing thin.

Considering the effective nature of the Standard Model in conjunction with the Hierarchy Problem and the reluctance of the Higgs to show up in experiments, the concept of a fundamental Higgs certainly drops in grace, and other mechanisms for electroweak symmetry breaking and/or maintaining perturbative unitarity become attractive.

2.5 An Alternative

If the amplitudes for the scattering of longitudinal gauge bosons are to fulfill the tree level unitarity requirement, then their high energy behavior must be modified. This can be achieved either through modifying the propagators of the particles or by introducing new particles into the model, the exchange of which cancels the dangerous growth with energy.

Of course, a scalar is not the only possible particle suitable for achieving this goal; an alternative ansatz would be the introduction of new vector bosons. These new vectors would have to be massive and rather heavy in order to have accomplished the escape from detection until now. However, the only known case of massive spin 1 particles that can be consistently quantized is that of gauge bosons of a spontaneously broken symmetry. So, let us introduce an additional $\mathbf{SU}(2)$ gauge group with new heavy gauge bosons which we will call W' and Z'. To parameterize the symmetry breaking, we will also need a new nonlinear sigma field Σ' which describes the three new Goldstone bosons that arise from the symmetry breaking.

If the new particles are to unitarize the scattering amplitudes, then they must couple to the $W^{\pm}$ and Z bosons. However, the couplings of gauge bosons are completely determined by gauge invariance, and if we have only kinetic and[13] mass terms, then we will only get couplings of the types

(assigning double lines to the new heavy particles), but no couplings that mix the Standard Model gauge bosons and the new heavy ones.

A way to lift this constraint is the introduction of terms into the mass matrix which mix the Standard Model gauge bosons and the new ones. As a results, the

[13] As this section focuses on the ideas behind the model, the discussion is qualitative and the details are postponed to the next chapter.

physical fields arise as mixtures of the old and the new fields

$$\begin{pmatrix} W_\mu^\pm \\ W_\mu^{\pm\prime} \end{pmatrix} = U \begin{pmatrix} \frac{W_{1\mu} \pm i W_{2\mu}}{\sqrt{2}} \\ \frac{W'_{1\mu} \pm i W'_{2\mu}}{\sqrt{2}} \end{pmatrix} \quad , \quad \begin{pmatrix} A_\mu \\ Z_\mu \\ Z'_\mu \end{pmatrix} = V \begin{pmatrix} B_\mu \\ W_{3\mu} \\ W'_{3\mu} \end{pmatrix}$$

with orthonormal mixing matrices U, V. This mixing induces the desired couplings, resulting in contributions to the longitudinal gauge boson scattering amplitude

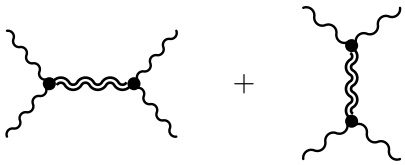

which can potentially restore perturbative unitarity.

The mixing between the gauge bosons also induces couplings of the W'/Z' to the standard model fermions, leading to contributions to the charged and neutral current four point function

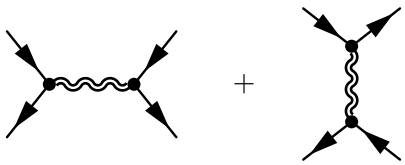

As new physics would also appear in loop contributions to the charged and neutral current correlators, this kind of processes was studied very precisely by the LEP-II experiments, resulting in an astonishing agreement with the one loop predictions of the Standard Model and leading to very stringent bounds on any kind of new physics which contributes to this kind of processes. The major part of this so-called electroweak precision data can be distilled into the famous αS, αT and αU parameters defined in [19, 20] or equivalently the three $\epsilon_{1/2/3}$ parameters defined in [21, 22].

If no special care is taken to avoid these constraints, most models of new physics that introduce copies of the W and Z which couple to Standard Model fermions are excluded. In our construction so far, these couplings are completely determined by the mixing matrices U and V, and as we have no further influence on the resulting couplings, we will almost certainly violate the electroweak precision bounds. Therefore, once we have introduced the W' and Z' this way, we have to think of a trick to gain control over the undesired couplings.

Of course, we could try to charge the Standard Model fermions under the new $\mathbf{SU}(2)$ gauge group, but the resulting couplings are completely fixed by gauge invariance, giving us no additional freedom that could be used to avoid the constraints. What could work, however, this the introduction of a partner fermion for each Standard Model fermion which is heavy, charged under the new $\mathbf{SU}(2)$ and mixes with its Standard Model partner. The price would be new set of new heavy

fermions f', but we could use the mixing parameters to control the unwanted fermion couplings and tune them away.

This way, we are rather naturally led to a model which contains a heavy copy of every Standard Model particle (with the exception of the gluon and the photon). There is no physical scalar in the spectrum and consequently there is no hierarchy problem. The task of unitarizing the scattering amplitudes is taken over by the new set of heavy vector bosons.

This structure of massive replica of the spectrum is a well-known feature of theories with one or more compact extra dimensions. In such theories, gauge symmetry can be broken without a Higgs by the introduction of suitable boundary conditions, and the massive gauge bosons that arise this way are known to delay the scale of unitarity violation [23]. Reducing the extra dimension to a finite point lattice, this can be exploited to build a model which has exactly the spectrum and features discussed above, the Three-Site Higgsless model [4]. The next chapter will be devoted to a detailed discussion of the construction and properties of this model.

Chapter 3

The Model — Top-down Approach

Percy: *Only this morning in the courtyard I saw a horse with two heads and two bodies.*
Blackadder: *Two horses standing next to each other?*

("Blackadder I — Witchsmeller Pursuviant")

In the last chapter the Three-Site Model was demonstrated to arise in a rather natural way when attempting to unitarize scattering amplitudes with heavy copies of the W and Z bosons instead of a Higgs. The actual construction was postponed and will now be carried out using a convenient framework.

The first two sections are devoted to introducing the concepts of extra dimensions and dimensional deconstruction, while the third then continues with the actual construction of the model.

3.1 Extra Dimensions

Manifolds and boundary conditions

The first ingredient to an extra dimensional field theory is, obviously, the spacetime manifold on which it is formulated. As the theory must match onto our known 4D physics at low energies, this manifold must contain the usual Minkowski spacetime (we are not going to consider general relativity), extended by one or more extra dimensions. For the same matching reason, these additional dimensions must decouple from the low energy phenomenology and are therefore usually chosen to be compact with some compactification scale R which suppresses the new physics arising from them.

In the following, we will specialize to a flat 5th dimension which (together with the case of "warped" extra dimensions with Randall-Sundrum metric [24]) is arguably the best-studied case in particle phenomenology. To complete the basic setup, we also need to specify the topology of the extra dimension. Common

choices are a circle with radius R or a compact interval $[0; 2R\pi]$. Out of these two examples, we now specialize to the latter. The boundaries of such an interval are also sometimes called "branes", while the open interval is called "bulk".

The second ingredient to the theory is the set of fields that propagate on the manifold. In analogy to the 4D case, these form representations of the 5D Poincaré group[1]. In 4D field theories, we require that the fields decay "fast enough" for asymptotic times and distances, and in a 5D theory, we need to specify boundary conditions on the boundaries of the compact extra dimension. On the interval, these are usually chosen either as Dirichlet or as Neumann boundary conditions[2]

$$\begin{aligned} &\text{Neumann:} && \partial_y \Phi(x,y)\big|_{y\in\{0,2R\pi\}} = 0 \\ &\text{Dirichlet:} && \Phi(x,y)\big|_{y\in\{0,2R\pi\}} = 0 \end{aligned} \tag{3.1}$$

It is also possible to mix these conditions and e.g. impose a Dirichlet boundary condition at one end of the interval and a Neumann one on the other one.

5D scalar field and Kaluza-Klein expansion

The simplest possible 5D theory is that of a real scalar field on an interval:

$$\Phi : (x,y) \in \mathbb{R}^4 \times [0; 2R\pi] \longrightarrow \Phi(x,y) \in \mathbb{R}$$

As an example for how to treat such theories, let us consider the Lagrangian for the flat 5D variant of Φ^4 theory (see appendix A for the conventions regarding Lorentz indices)

$$\mathcal{L}_{\Phi^4} = \frac{1}{2}(\partial_a\Phi)(\partial^a\Phi) - \frac{1}{2}M^2\Phi^2 - \frac{g}{4!}\Phi^4 \tag{3.2}$$

The action functional is then defined as the usual integral of the Lagrangian over spacetime, the y part of which is bounded

$$S[\Phi] = \int d^4x \int_0^{2R\pi} dy\, \mathcal{L}_{\Phi^4} = \int d^4x \int_0^{2R\pi} dy\, \left(\frac{1}{2}(\partial_a\Phi)(\partial^a\Phi) - \frac{1}{2}M^2\Phi^2 - \frac{g}{4!}\Phi^4\right) \tag{3.3}$$

It is noteworthy that, in order for the action (3.3) to be classically scale invariant, the mass dimensions of the scalar and of the coupling must be

$$[\Phi] = \frac{3}{2} \qquad , \qquad [g] = -1$$

Variation of the action to obtain the equations of motion proceeds as usual. However, the result

$$\delta S = \int d^4x \left(\partial_y \Phi \delta\Phi \Big|_{y=0}^{y=2R\pi} - \int_0^{2R\pi} dy\, \left(\partial_a\partial^a\Phi + M^2\Phi + \frac{g}{3!}\Phi^3\right)\delta\Phi \right)$$

[1] Usually, the compactification breaks the 5D Poincaré group down to the 4D one, resulting in a violation of 5D momentum conservation.

[2] Starting from a fifth dimension compactified on a circle, the case of compactification on an interval with Dirichlet or Neumann boundary conditions can also be obtained in a very elegant way by orbifolding [25].

contains a boundary term that results from partial integration. With the boundary conditions (3.1) or mixed ones, this term vanishes, and the resulting Euler-Lagrange equation is

$$\left(\partial_a \partial^a + M^2\right) \Phi = \left(\partial^2 - \partial_y^2 + M^2\right) \Phi = -\frac{g}{3!}\Phi^3 \tag{3.4}$$

It is convenient to partially decompose the solutions to (3.4) as a Fourier series with the basis functions $f_k(y)$ chosen such that they satisfy the boundary conditions and are eigenfunctions of ∂_y^2:

$$\begin{aligned} &\text{Neumann:} \quad \Phi(x,y) = \sum_{k=0}^{\infty} \phi_k(x) f_k(y) = \sum_{k=0}^{\infty} \phi_k(x) \frac{1}{\sqrt{R\pi(1+\delta_{k,0})}} \cos\left(\frac{k}{2R} y\right) \\ &\text{Dirichlet:} \quad \Phi(x,y) = \sum_{k=1}^{\infty} \phi_k(x) f_k(y) = \sum_{k=1}^{\infty} \phi_k(x) \frac{1}{\sqrt{R\pi}} \sin\left(\frac{k}{2R} y\right) \end{aligned} \tag{3.5}$$

Inserting the expansion into the Lagrangian (3.2) and defining the effective 4D action functional and Lagrangian as

$$\widetilde{S}[\phi] = \int d^4x \; \widetilde{\mathcal{L}}_{\Phi^4} \qquad , \qquad \widetilde{\mathcal{L}}_{\Phi^4} = \int_0^{2R\pi} dy \; \mathcal{L}_{\Phi^4}$$

we obtain

$$\widetilde{\mathcal{L}}_{\Phi^4} = \frac{1}{2} \sum_k \left(\left(\partial_\mu \phi_k\right)^2 - \left(M^2 + \frac{k^2}{4R^2} \right) \phi_k^2 \right) - \sum_{k_1,k_2,k_3,k_4} g_{k_1,k_2,k_3,k_4} \phi_{k_1} \phi_{k_2} \phi_{k_3} \phi_{k_4} \tag{3.6}$$

with the dimensionless coupling constants

$$g_{k_1,k_2,k_3,k_4} = \frac{g}{4!} \int_0^{2R\pi} dy \; f_{k_1}(y) f_{k_2}(y) f_{k_3}(y) f_{k_4}(y) \tag{3.7}$$

This expansion is the so-called Kaluza-Klein (KK) expansion of the theory.

What is the virtue of the KK expansion and of the effective Lagrangian (3.6)? While we started with a 5D theory of a single scalar field, we find that the physics can be equivalently described by an ordinary 4D field theory with an infinite number of 4D scalar fields ϕ_k. Each of these fields has an effective mass of

$$m_k^2 = \frac{k^2}{4R^2} + M^2$$

making them arbitrarily heavy for $k > 0$, the mass increasing with k. The 5D Lagrangian $\mathcal{L}_{\Phi^4}$ contains a single four point interaction of the Φ whereas the effective 4D version contains four point interactions involving all the different ϕ_k fields (although many of the coupling constants vanish).

The physics behind this is easy to understand: in the 5D version of the theory, the 5-momentum satisfies the mass shell condition

$$k_a k^a = k_\mu k^\mu - \left(k^5\right)^2 = M^2$$

with the fifth component of the momentum being discrete[3] rather than continuous

$$k_n^5 = \frac{n}{2R}$$

due to the compactification of the extra dimension. The straightforward interpretation is to think of Φ as a 5D field with a discrete fifth momentum component and mass M^2. However, it can be equivalently regarded as a tower of 4D fields with masses given by $M^2 + \left(k^5\right)^2$. In the same way we could think about a 4D particle as a continuum of 3D particles, but as the four-momentum is a continuous degree of freedom, this is not a very useful intuition.

At tree level, we have the liberty of setting the 5D mass M to zero. In the case of Neumann boundary conditions, there is a $k = 0$ mode in the tower of scalars which is massless. In the case of Dirichlet or mixed boundary conditions the flat wavefunction $f_0(k)$ is forbidden, and all the ϕ_k are massive, even if no tree level mass is put into the Lagrangian.

Applying naïve powercounting to the 5D version of the Lagrangian leads to the conclusion that it must describe a nonrenormalizable theory as can be easily understood by noting that the 5D coupling g has negative mass dimension. In the 4D theory, the coupling constants at the four point interactions are dimensionless and therefore, the theory might appear to be renormalizable at a casual glance. However, in higher order diagrams, all the infinitely many ϕ_k can run in the loops leading to a possibly divergent series over k. This enhances the divergences and recovers the nonrenormalizable character of the theory.

Although we have been examining just the simple case of a 5D Φ^4 theory, we have found a lot of interesting structure that generalizes to more complicated 5D theories. These theories can always be described by an effective 4D theory by virtue of the KK expansion. In this process, every 5D field gets replaced by a tower of 4D fields of increasing mass. Asymptotically, the masses of the modes in the tower are equidistantly spaced[4]. The presence of a zero mode which is massless in absence of an explicit mass term in the Lagrangian depends on the boundary conditions. Extra dimensional theories are usually[5] nonrenormalizable and valid only as effective field theories with an ultraviolet cutoff. Therefore, it is arguably inconsistent to include all modes in the KK towers in calculations. Instead, the towers should be cut off in some way at high scales, and if gauge fields are involved, extra care has to be taken to preserve gauge invariance in this step.

[3] To be a bit more precise, the f_k are not eigenfunctions of $i\partial_y$ but of ∂_y^2, so we should rather be talking about the square of the five momentum and not about the momentum itself.

[4] This changes if the metric of is chosen nontrivially, e.g. in Randall-Sundrum type models.

[5] Trivial counterexamples exist, e.g. ϕ^3 theory in 5 or 6 dimension (which, however, is a slightly pathological example as the potential is not bounded from below).

Gauge bosons

A 5D gauge field transforms in the vector representation of the five dimensional Poincaré group and hence has five components A^a. However, boundary conditions break this group down to its 4D subgroup, under which A^μ transforms as a vector and A^5 transforms as a scalar. Once we perform the KK expansion to get the 4D effective theory, the A^μ will give us a tower of 4D vector fields, while A^5 will become a tower of 4D scalars. In the following, we will restrict the discussion to the case of an abelian field for simplicity's sake.

Under a gauge transformation with parameter field λ, the fields A^μ and A^5 transform as

$$A^\mu(x,y) \longrightarrow A^\mu(x,y) + \frac{1}{g}\partial^\mu\lambda(x,y) \quad , \quad A^5(x,y) \longrightarrow A^5(x,y) - \frac{1}{g}\partial_y\lambda(x,y) \tag{3.8}$$

with the gauge coupling g. Similar to the scalar case, we have to choose boundary conditions for the fields. Let us choose Neumann boundary conditions for A^μ. We can then KK expand the 4D vector field as

$$A^\mu(x,y) = \sum_{k=0}^{\infty} A_k^\mu(x) \frac{1}{\sqrt{R\pi(1+\delta_{k,0})}} \cos\left(\frac{k}{2R}y\right)$$

Looking at (3.8), it is easy to see that the parameter field λ has to satisfy the same boundary conditions as A^μ and therefore can be KK expanded likewise

$$\lambda(x,y) = \sum_{k=0}^{\infty} \lambda_k(x) \frac{1}{\sqrt{R\pi(1+\delta_{k,0})}} \cos\left(\frac{k}{2R}y\right)$$

This implies that the shift in A^5 generated by such a gauge transformation is

$$A^5(x,y) \longrightarrow A^5(x,y) + \frac{1}{g}\sum_{k=1}^{\infty} \lambda_k \frac{k}{2R} \frac{1}{\sqrt{R\pi}} \sin\left(\frac{k}{2R}y\right)$$

which means that the field A^5 must obey Dirichlet boundary conditions and can be decomposed as

$$A^5(x,y) = \sum_{k=1}^{\infty} A_k^5(x) \frac{1}{\sqrt{R\pi}} \sin\left(\frac{k}{2R}y\right)$$

Therefore, after the KK decomposition, we obtain an infinite tower of 4D gauge transformations which leave the theory invariant, the 4D gauge bosons A^μ and the 4D scalars A^5 transforming as

$$\begin{aligned} A_k^\mu(x) &\longrightarrow A_k^\mu(x) + \frac{1}{g}\partial^\mu\lambda_k(x) && k \geq 0 \\ A_k^5(x) &\longrightarrow A_k^5(x) + \frac{1}{g}\frac{k}{2R}\lambda_k(x) && k \geq 1 \end{aligned} \tag{3.9}$$

A closer look at (3.9) reveals at least two things of special interest. First, there is a gauge transformation generated by λ_0 which only acts on A_0^μ and doesn't involve any of the 4D scalars A_k^5. Second, it is possible to perform gauge transformations which remove all of the A_k^5 and completely absorb them into the A_k^μ, fixing the gauge for all the 4D gauge fields with the exception of A_0^μ. This suggests an elegant interpretation.

As we chose Neumann boundary conditions for the A^μ, the fifth component of the 5-momentum k^5 vanishes for A_0^μ, leaving this mode as a massless gauge boson of an unbroken gauge symmetry generated by λ_0. All the other modes A_k^μ are massive and obtain their longitudinal modes from "eating" a A_k^5 field in a process very similar to the Goldstone mechanism in spontaneous symmetry breaking. Due to the mass terms, the gauge symmetry generated by the $\lambda_k,\ k \neq 0$ is hidden in a simultaneous transformation of the A_k^μ and the "Goldstone" fields A_k^5, which also is reminiscent of spontaneous symmetry breaking. Gauging away the A_k^5 corresponds to unitarity gauge in a spontaneously broken gauge theory.

Let's have a look at the Lagrangian to see whether this assertion is correct. The 5D gauge kinetic Lagrangian is given by

$$\mathcal{L}_{\text{gauge}} = -\frac{1}{4} F_{ab} F^{ab} \tag{3.10}$$

with the 5D field strength tensor

$$F^{ab} = \partial^a A^b - \partial^b A^a$$

The Lagrangian (3.10) can be split into 4D part $\mathcal{L}_{4D}$ and a 5D part $\mathcal{L}_{5D}$

$$\mathcal{L}_{\text{gauge}} = \underbrace{-\frac{1}{4} F^{\mu\nu} F_{\mu\nu}}_{\mathcal{L}_{4D}} + \underbrace{\frac{1}{2} \left(\partial_y A^\mu + \partial^\mu A^5\right)^2}_{\mathcal{L}_{5D}}$$

Performing the KK expansion and defining the KK masses m_k as

$$m_k = \frac{k}{2R}$$

we obtain the effective 4D Lagrangian

$$\widetilde{\mathcal{L}}_{\text{gauge}} = -\frac{1}{4} \sum_{k=0}^{\infty} \underbrace{F_k^{\mu\nu} F_{k,\mu\nu}}_{\widetilde{\mathcal{L}}_{k,4D}} + \sum_{k=1}^{\infty} \underbrace{\frac{1}{2} \left(-m_k A_k^\mu + \partial^\mu A_k^5\right)^2}_{\widetilde{\mathcal{L}}_{k,5D}} \tag{3.11}$$

The $\widetilde{\mathcal{L}}_{k,4D}$ are the kinetic Lagrangians for the 4D gauge fields, while the $\widetilde{\mathcal{L}}_{k,5D}$ are easily identified as gauge invariant Stueckelberg Lagrangians. The Stueckelberg action is a well-known trick for giving mass to $\mathbf{U}(1)$ gauge bosons by spontaneous symmetry breaking, introducing a scalar, massless Goldstone boson. Therefore, the above interpretation is quite correct; in the 4D effective theory, the masses of

the $A_k^\mu,\ k \geq 1$ fields arise from a mechanism equivalent to spontaneous symmetry breaking, yielding an infinite tower of massless Goldstone fields.

In addition to the mass terms for A_k^μ, $k \geq 1$ and the kinetic terms for A_k^5, the Lagrangian $\widetilde{\mathcal{L}}_{k,5D}$ also contains a bilinear term which mixes A_k^μ and $\partial^\mu A_k^5$. This can be removed by adding a suitable gauge fixing term to (3.10) similar to the R_ξ gauges in spontaneous broken gauge theories

$$\mathcal{L}_{GF} = \frac{1}{2\xi}\left(\partial_\mu A^\mu - \xi \partial_y A^5\right)^2$$

If we impose Dirichlet boundary conditions on A^μ, we find a result only slightly different. This boundary condition implies Neumann boundary conditions for the 4D scalar A^5. The massless A_0^μ vanishes from the spectrum, and at the same time, a physical scalar A_0^5 arises in which is not "eaten" by the gauge bosons. Imposing mixed boundary conditions would forbid the massless A_0^μ mode as well as the physical scalar A_0^5.

The analysis of nonabelian 5D gauge theories proceeds along the same lines as the abelian case but is more complicated due to the more complex group structure. This discussion can be found e.g. in [26] or [23]. The most exciting difference when compared to the abelian case is the possibility of assigning different boundary conditions to different component gauge fields. As an example, consider a 5D $\mathbf{SU}(2)$ gauge field $A^a = A_r^a \tau_r$. If we assign Dirichlet boundary conditions to the components belonging to the τ_1 and τ_2 generators and Neumann ones to the τ_3 component, then only the A_3^a tower will contain a massless mode mode in the KK decomposition. Thus, only the $\mathbf{U}(1)$ subgroup generated by τ_3 will make it into the 4D effective theory as an unbroken gauge symmetry; all other gauge symmetries of the KK fields get spontaneously broken.

Therefore, in a 5D version of the Standard Model, suitable boundary conditions could be used to break the $\mathbf{SU}(2)_L \times \mathbf{U}(1)_Y$ gauge symmetry down to the $\mathbf{U}(1)_{\mathrm{EM}}$ subgroup without introducing a Higgs field. The price to pay would be towers of massless KK partners for all Standard Model particles. However, such a scenario is excluded by electroweak precision observables. Still, if we could cut off the KK towers after the first mode, this theory could be a starting point for the model suggested in chapter 2.5.

Unfortunately, another feature of the nonabelian result is a more complicated transformation behavior of the KK modes under gauge transformation involving mixing between different modes [26]. In other words, we have to take all KK modes into account to retain gauge invariance. Simply cutting off the tower wouldn't do any good but instead destroy gauge invariance! However, there are loopholes: for example, dimensional deconstruction as discussed in section 3.2 provides a gauge invariant way of cutting off the KK towers.

Fermions

To describe 5D fermions, we have to find a five dimensional representation of the Clifford algebra, i.e. a set of five matrices γ^a obeying the anticommutation relations

$$\left\{\gamma^a, \gamma^b\right\} = 2g^{ab} \tag{3.12}$$

Fortunately, this search does not lead far from well-known territory: if we take the usual set of 4D gamma matrices γ^μ, then γ^5 has all the properties we need. Defining γ^4 as

$$\gamma^4 = i\gamma^5$$

we obtain a set of matrices that obey (3.12). As a result, 5D fermions can be described by 4 component complex spinors just as the 4D ones.

However, writing down the generators for 5D Lorentz transformations

$$\sigma^{ab} = \frac{i}{2}\left[\gamma^a, \gamma^b\right]$$

we note that the $\sigma^{5\mu}$ don't commute with the 4D chirality projectors $\Pi_\pm$ (c.f. (A.3)). This means that 5D Lorentz transformations mix left- and right-handed fields, defeating the notion of chirality: there is no such thing like a chiral fermion in five dimensions. Nevertheless, as 5D Lorentz invariance is broken down to the 4D subgroup anyway by the boundaries of the interval, it is possible to obtain a 4D effective theory that makes a distinction between the chiralities by choosing suitable chiral boundary conditions.

As an example consider a 5D fermion Ψ with left- and right-handed components $\Psi_{L/R} = \Pi_\pm \Psi$. The massless 5D kinetic Lagrangian reads

$$\begin{aligned}\mathcal{L}_\Psi = i\overline{\Psi}\gamma^a\partial_a\Psi = i\overline{\Psi}\not{\partial}\Psi - \overline{\Psi}\partial_y\gamma^5\Psi = \\ i\left(\overline{\Psi}_L\not{\partial}\Psi_L + \overline{\Psi}_R\not{\partial}\Psi_R\right) - \overline{\Psi}_L\partial_y\Psi_R + \overline{\Psi}_R\partial_y\Psi_L\end{aligned} \tag{3.13}$$

If we impose Neumann boundary conditions on the left-handed field Ψ_L and Dirichlet ones on the right-handed field Ψ_R and insert the corresponding KK expansions into (3.13), we obtain the effective 4D Lagrangian as

$$\widetilde{\mathcal{L}}_\Psi = \overline{\Psi}_{0,L}\not{\partial}\Psi_{0,L} + \sum_{k=1}^{\infty}\left(\overline{\Psi}_{k,L}\not{\partial}\Psi_{k,L} + \overline{\Psi}_{k,R}\not{\partial}\Psi_{k,R} - \frac{k}{2R}\left(\overline{\Psi}_{k,L}\Psi_{k,R} + \overline{\Psi}_{k,R}\Psi_{k,L}\right)\right) \tag{3.14}$$

From (3.14) it is then clear that the 4D effective theory contains a left-handed massless fermion $\Psi_{0,L}$ together with a tower of massive Dirac fermions.

Other types of boundary conditions as well as an explicit 5D mass term change this picture and may result in more complicated situations. In particular, a mixing between different KK modes is possible requiring further diagonalization to obtain the mass eigenstates. However, as this is of no importance for this work, we refrain from delving deeper into these issues and stop the discussion at this point. Some further remarks on fermions in compactified 5D theories can be found e.g. in [27].

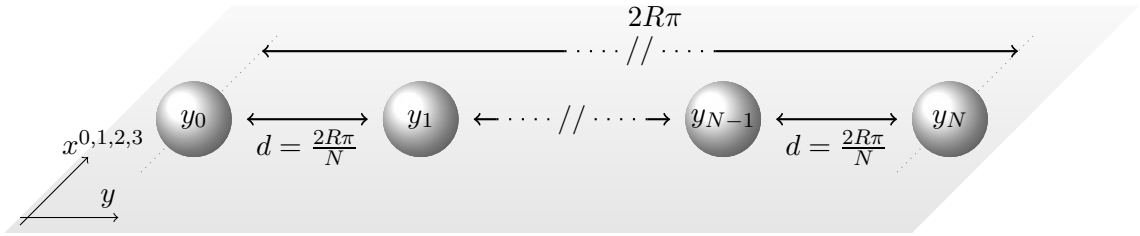

Figure 3.1: Sketch of the deconstruction of a fifth dimension compactified on an interval $[0; 2R\pi]$ to a lattice of $N + 1$ points.

3.2 Dimensional Deconstruction

Dimensional deconstruction is the reduction of one or more extra dimensions to a finite point lattice. This procedure is well-known from lattice gauge theory where Minkowski space is approximated by a four dimensional finite point lattice which allows for the numerical calculation of correlators by solving the path integral via Monte Carlo integration.

In the context of model building, the deconstruction of an extra dimension opens up a new class of models which are akin to extra dimensional models but differ in some important aspects. In particular, deconstruction allows to cut off the KK towers in a gauge invariant fashion and provides a class of possible UV completions.

Let us consider again the example of a 5D theory compactified on an interval which we discussed in the last section

$$(x, y) \in \mathbb{R}^4 \times [0; 2R\pi]$$

and replace the fifth dimension by a discrete lattice of $N + 1$ equidistantly spaced sites $y_0, \ldots, y_N$

$$y_n = nd \quad , \quad d = \frac{2R\pi}{N}$$

This setup is sketched in fig. 3.1.

Gauge theory revisited

In order to find out how a 5D gauge field A^a is properly represented in the deconstructed theory, let us briefly recall some basics about gauge theories. Such a theory is invariant under a group of spacetime dependent transformations[6]

$$\phi(x) \longrightarrow U(x)\phi(x)$$

[6]For the rest of this section, an unitary representation will be assumed together with the canonical trace normalization of the Lie algebra generators T_i

$$\mathbf{Tr}\, T_i T_j = \frac{1}{2}\delta_{ij}$$

of the fields ϕ.

This invariance gives rise to the necessity of some prescription for how to compare fields at different points in space time in a gauge invariant way. Even in a local field theory, this is necessary because the definition of the partial derivative

$$\partial^\mu \phi(x) = \lim_{\epsilon \to 0} \frac{\phi(x + \epsilon n^\mu) - \phi(x)}{\epsilon}$$

(with the unit vector n^μ pointing in direction μ) involves the field at two infinitesimally separated points and therefore is not gauge covariant

$$\partial^\mu \left(U(x)\phi(x) \right) \neq U(x)\partial^\mu \phi(x)$$

Such a prescription is given by Wilson lines $W(x_1, x_2)$, operators valued in the gauge group which transform as

$$W(x_1, x_2) \longrightarrow U(x_1) W(x_1, x_2) U(x_2)^\dagger \tag{3.15}$$

The gauge field A^μ is valued in the Lie algebra of the group and generates Wilson lines for infinitesimal displacements ϵ^μ

$$W(x, x + \epsilon) = \mathbb{I} - ig\epsilon_\mu A^\mu(x) + \mathcal{O}\left(\epsilon^2\right) \tag{3.16}$$

with an arbitrary nonzero number g which ends up as the gauge coupling in the covariant derivative. Different finite Wilson lines $W(x_1, x_2)$ can be generated by iterating (3.16) along paths connecting x_1 and x_2 (see e.g. [5] for details). (3.16) implies that the gauge field transforms as

$$A^\mu(x) \longrightarrow U(x) \left(A^\mu(x) + \frac{i}{g} \partial^\mu \right) U(x)^\dagger$$

Due to their transformation behavior, the Wilson lines can be used to connect different points on the manifold and define a covariant derivative:

$$D^\mu \phi(x) = \lim_{\epsilon \to 0} \frac{W(x, x + \epsilon n^\mu)\phi(x + \epsilon n^\mu) - \phi(x)}{\epsilon} \tag{3.17}$$

Inserting (3.16) into (3.17) we retrieve the well known expression for the covariant derivative

$$D^\mu \phi(x) = \partial^\mu \phi(x) - igA^\mu \phi(x)$$

which by construction is gauge covariant as desired.

The transformation law (3.15) also implies that Wilson lines can be plugged together to form new Wilson lines

$$W(x_1, x_2) W(x_2, x_3) = W(x_1, x_3)$$

In particular, it follows that the closed Wilson line defined as

$$K(x) = W(x, x + \epsilon) W(x + \epsilon, x + \epsilon + \eta) W(x + \epsilon + \eta, x + \eta) W(x + \eta, x) \tag{3.18}$$

with two small displacements ϵ^μ and η^μ transforms as

$$K(x) \longrightarrow U(x)K(x)U(x)^\dagger \tag{3.19}$$

Plugging (3.16) and the Taylor expansion of A^μ

$$A^\mu(x+\epsilon) = A^\mu(x) + \epsilon_\nu \partial^\nu A^\mu(x) + \mathcal{O}\left(\epsilon^2\right)$$

into the definition of $K(x)$ (3.18), we obtain

$$K(x) = \mathbb{I} - ig\epsilon_\mu\eta_\nu \underbrace{\left(\partial^\mu A^\nu(x) - \partial^\nu A^\mu(x) - ig\left[A^\mu(x), A^\nu(x)\right]\right)}_{F^{\mu\nu}} + \mathcal{O}\left(\eta^2, \mu^2\right)$$

recovering the well known expression for the field strength tensor $F^{\mu\nu}$. The transformation behavior (3.19) must hold in every order in ϵ^μ and η^μ, and it follows that

$$F^{\mu\nu}(x) \longrightarrow U(x)F^{\mu\nu}(x)U(x)^\dagger$$

Therefore, we can use $F^{\mu\nu}$ to write down a gauge invariant Lagrangian that involves bilinears in the derivatives of A^μ and which therefore is suitable to give dynamics to the gauge field

$$\mathcal{L}_{\text{gauge}} = -\frac{1}{2}\mathbf{Tr}\, F^{\mu\nu}F_{\mu\nu}$$

Summing up the discussion: the gauge field acts as connection that relates gauge transformations at adjacent points on the manifold to each other and therefore allows to compare the value of fields at different points in a gauge covariant way. This is strongly reminiscent of Riemannian geometry where the Christoffel symbols provide such a connection w.r.t. coordinate transformations. The connection can be integrated to provide a parallel transport along finite paths, much like the Wilson lines for gauge transformations. Indeed, there is a geometrical description of gauge theory in terms of fiber bundles [28]. The field strength tensor is built in a similar way as the curvature tensor by considering the transport along an infinitesimal parallelogram.

Deconstructing gauge theory

Let us now carry the above description of gauge invariance over to the deconstructed 5D theory. Going from the continuous coordinate y to discrete sites y_n, we've got a copy of the 4D gauge group $\mathcal{G}_n$ at every lattice site, and the theory is invariant under transformations of the fields

$$\phi(x, y_n) = \phi_n(x) \to U_n(x)\phi_n(x) \tag{3.20}$$

If we compare the values of one of the ϕ_n at two different 4D coordinates $\phi_n(x_1)$ and $\phi_n(x_2)$, then we can still use 4D gauge fields $A^\mu_n(x)$ localized at the lattice sites to generate Wilson lines $W_n(x_1, x_2)$ which compensate for the change in gauge.

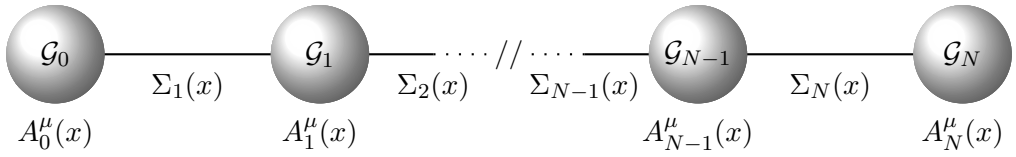

Figure 3.2: Deconstructing a gauge theory. At each lattice site, there is a 4D copy $\mathcal{G}_n$ of the gauge group $\mathcal{G}$ with the gauge field A_n^μ, the sites being linked with Wilson line fields Σ_n.

However, as far as the fifth coordinate is concerned, there is no such thing as an infinitesimal displacement in y anymore after deconstruction. Therefore, the notion of a field $A_n^5(x)$ which connects points infinitesimally separated in y doesn't make any sense at all. The smallest displacement in y we can manage in the deconstructed theory is a hop between adjacent lattice sites. Since this is a finite displacement, we need finite Wilson lines $\Sigma_n(x)$ which connect the sites and which transform as

$$\Sigma_n(x) \longrightarrow U_{n-1}(x)\Sigma_n(x)U_n(x)^\dagger \tag{3.21}$$

Therefore, in the deconstructed theory, we must replace the 5D gauge field $A^a(x,y)$ with $N+1$ 4D gauge fields $A_0^\mu(x),\ldots,A_N^\mu(x)$ and N Wilson line fields $\Sigma_1(x),\ldots,\Sigma_N$. This setup is shown in fig. 3.2. From these objects, we can build up Wilson lines that connect arbitrary points on the lattice (x_1,y_{n_1}) and (x_2,y_{n_2}). The Σ_n are valued in the gauge group and can be parameterized using the group generators T_k

$$\Sigma_n(x) = \exp\left(i\frac{\sigma_{nk}(x)}{v}T_k\right) \tag{3.22}$$

The scale v is introduced to make the component fields σ_{nk} dimensionful quantities and will later be fixed by matching the mass spectrum of the deconstructed theory to that of the continuous one. As the Σ_n are valued in the gauge group, they must have a nonvanishing vacuum expectation value. If the component fields σ_{nk} don't develop nontrivial vacuum expectation values, then (3.22) tells us

$$\langle\Sigma_n\rangle = \mathbb{I} \tag{3.23}$$

A kinetic term for the Σ_n can be obtained by finding the analog to $F^{\mu 5}(x,y)$ in the continuous case. According to our previous discussion, $F^{\mu 5}$ is obtained from the Wilson line along a parallelogram spanning an infinitesimal distance both in a 4D direction and in y. As we can only go finite distances d in the discrete theory, a deconstructed analog is the quantity

$$K_n(x) = \Sigma_n(x)W_n(x,x+\epsilon)\Sigma_n(x+\epsilon)^\dagger W_{n-1}(x+\epsilon,x) \tag{3.24}$$

which corresponds to an infinitesimal displacement ϵ^μ in 4D direction and a finite hop from y_{n-1} to y_n in the discrete extra dimension (c.f. fig. 3.3). Expanding (3.24)

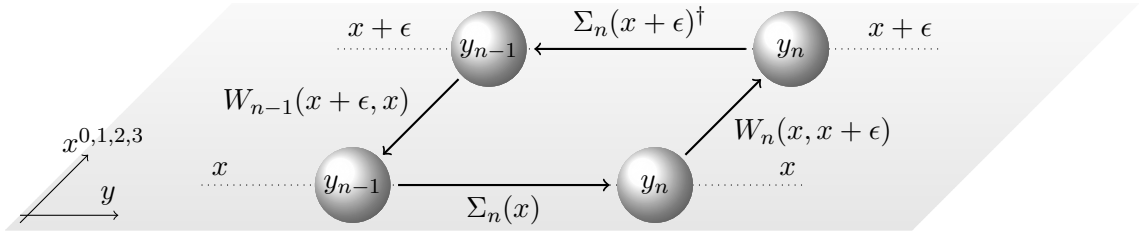

Figure 3.3: Definition of the quantity K_n as the Wilson line along a parallelogram spanning two adjacent lattice sites and an infinitesimal 4D distance.

in a similar fashion as (3.18), we obtain

$$K_n(x) = \mathbb{I} - \epsilon_\mu \underbrace{\left(\partial^\mu \Sigma_n(x) - ig\left(A^\mu_{n-1}(x)\Sigma_n(x) - \Sigma_n(x)A^\mu_n(x)\right)\right)\Sigma_n(x)^\dagger}_{F^\mu_n(x)} + \mathcal{O}\left(\epsilon^2\right)$$

By construction, F^μ_n must transform as

$$F^\mu_n(x) \to U_n(x) F^\mu_n(x) U_n(x)^\dagger$$

and therefore, we can write down a gauge invariant kinetic term for the Σ_n

$$\mathcal{L}_\Sigma = \sum_{n=1}^{N} v^2 \mathbf{Tr}\, F^\mu_n F^\dagger_{n\mu}$$

$\mathcal{L}_\Sigma$ is chosen such that the component fields σ_{nk} are canonically normalized.

As the covariant derivative of the Σ_n is fixed by their transformation behavior (3.21)

$$D^\mu \Sigma_n = \partial^\mu \Sigma_n - ig\left(A^\mu_{n-1}\Sigma_n - \Sigma_n A^\mu_n\right)$$

it follows that

$$F^\mu_n = \left(D^\mu \Sigma_n\right)\Sigma^\dagger_n$$

and finally, we can rewrite the complete Lagrangian for the deconstructed theory as

$$\mathcal{L}_{\text{dec}} = -\frac{1}{2}\sum_{n=0}^{N} \mathbf{Tr}\, F^{\mu\nu}_n F_{n\mu\nu} + v^2 \sum_{n=1}^{N} \mathbf{Tr}\, \left(D^\mu \Sigma_n\right)\left(D_\mu \Sigma_n\right)^\dagger \tag{3.25}$$

If we expand the Σ_n fields in their component fields σ_{nk} according to (3.22) we find that the lowest order (aka the vacuum expectation value of the Σ_n) generates mass terms for the component gauge fields $A^\mu_{n,k}$:

$$\mathcal{L}_{\text{mass}} = \frac{v^2 g^2}{2}\sum_{n=1}^{N}\left(A^2_{n-1,k} + A^2_{n,k} - 2A^\mu_{n-1,k}A_{n,k\mu}\right) = \frac{1}{2}M_{nm}A^\mu_{n,k}A_{m,k\mu}$$

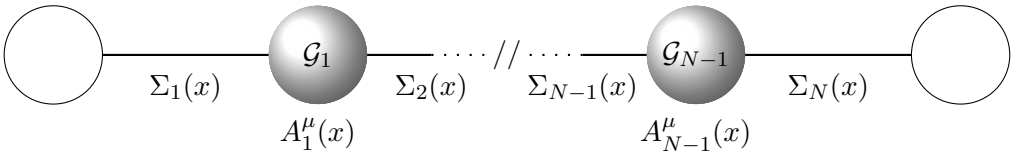

Figure 3.4: Deconstructing a gauge theory with Dirichlet boundary conditions. The condition $A^\mu(x,y)|_{y\in\{0,2R\pi\}} = 0$ removes the gauge groups and gauge fields at the y_0 and y_N sites of the lattice (c.f. fig. 3.2).

with the real, symmetric mass matrix

$$M = v^2 g^2 \begin{pmatrix} 1 & -1 & 0 & \cdots & 0 \\ -1 & 2 & -1 & \ddots & \vdots \\ 0 & -1 & \ddots & \ddots & 0 \\ \vdots & \ddots & \ddots & 2 & -1 \\ 0 & \cdots & 0 & -1 & 1 \end{pmatrix}$$

The eigenvalues of this matrix (see e.g. [29] for the eigenvectors) give the gauge boson masses

$$m_n^2 = 4v^2 g^2 \sin^2 \frac{n\pi}{2\,(N+1)} \quad , \quad n = 0, \ldots, N \tag{3.26}$$

For every component gauge field, the spectrum contains a massless mode together with N massive ones. As we have N sigma fields, we additionally get N scalar fields for every group generator which is just the amount of Goldstone bosons that are required to constitute longitudinal modes for the massive vector bosons.

In the limit of large N we can approximate (3.26) by

$$m_n^2 \approx \left(vg \frac{n\pi}{N+1} \right)^2$$

Therefore, if we fix the scale v as

$$v = \frac{N+1}{2gR\pi} \approx \frac{1}{gd}$$

we recover the mass spectrum of the continuous case with Neumann boundary conditions from the deconstructed theory in the large N limit. It seems that our way of deconstructing the theory has been the correct prescription for a 5D gauge field compactified with Neumann boundary conditions.

What about Dirichlet or mixed boundary conditions on $A^\mu(x,y)$? Setting one or all components to zero at both ends of the interval corresponds to setting the gauge fields at y_0 and / or y_N to zero and basically kills gauge invariance at these sites (c.f. fig. 3.4). However, we have no way of transferring the appropriate boundary

conditions on $A^5(x, y)$ to the deconstructed version of the theory and can only hope that the theory takes care of this itself.

This is indeed the case as can been seen by counting the scalar and vector fields involved: if we remove the A_0^μ and A_N^μ fields, we obtain $N-1$ massive gauge fields for every generator, while the number of scalars remains N. After all the Goldstone bosons have been eaten, a physical scalar remains for every generator, which we have argued in the last section also happens in the continuous case with Dirichlet boundary conditions. In the mixed case, we have N massive vectors and N scalars which all get eaten for every generator, also matching the continuous case nicely.

Although deconstruction as presented here does a rather nice job at approximating 5D gauge theories, the formalism had first been proposed in [30] as a tool for constructing renormalizable UV completions to 5D theories. At low scales, the deconstructed theory virtually cannot be distinguished from a true 5D theory. However, while such a theory is inherently nonrenormalizable and must break down at some cutoff scale, the deconstructed version can be made renormalizable rather easily.

For example, note that the Σ_n are similar to the Σ field introduced in chapter 2.3 to describe the spontaneous breaking of electroweak gauge symmetry. Therefore, the deconstructed theory can be UV completed just like the Standard Model by introducing Higgs fields H_n for each of the Σ_n fields.

A different, technicolor-like approach to an UV completion is to describe the Σ_n fields similar to the Pions in QCD as the excitation of a condensate of strongly interacting fermions. At energies above the confinement scale of this new strong interaction, the Σ_n fields would be replaced by the "quarks" and "gluons" of the new strongly interacting sector, a theory which is known to be renormalizable.

For our purposes, it is important to note that deconstructing the theory retains gauge invariance. Therefore, deconstruction presents a consistent gauge invariant way for cutting off the infinite KK towers that arise in the continuous case.

Matter fields

The correct prescription for the discretization of matter fields has already been given in (3.20): the field $\phi(x, y)$ is replaced by a set of $N+1$ fields $\phi_n(x)$. The Wilson line fields Σ_n then allow for a straightforward discretization of the covariant derivative[7] D^5

$$\partial_y \phi(x, y_n) \longrightarrow D_n = \frac{\Sigma_n(x)\phi_n(x) - \phi_{n-1}(x)}{d}$$

The discretized covariant derivative can be used to build a discretized version of the Lagrangian for the matter fields, e.g. for a real scalar

$$\mathcal{L}_\phi = \frac{1}{2}\sum_{n=0}^{N} \left(D^\mu \phi_n D_\mu \phi_n - m^2 \phi_n^2\right) - \frac{1}{2}\sum_{n=1}^{N} D_n^\dagger D_n \tag{3.27}$$

[7] In fact, different possible discretization prescriptions can be devised, each leading to a slightly different mass spectrum, but all having the same high energy limit.

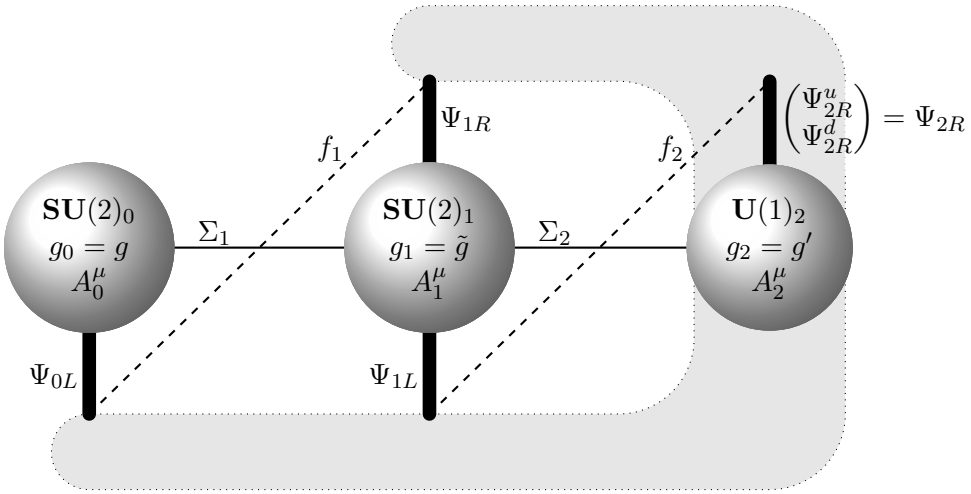

Figure 3.5: The structure of the Three-Site Higgsless Model in moose notation. See the text for explanation.

Expanding the second term in (3.27) we obtain

$$D_n^\dagger D_n = \frac{1}{d^2}\left(\phi_n^T\phi_n + \phi_{n-1}^T\phi_{n-1} - \phi_n^T\Sigma_n^\dagger\phi_{n-1} - \phi_{n-1}^T\Sigma_n\phi_n\right)$$

We find that the discretized covariant derivative terms yield contributions to the diagonal mass terms of the ϕ_n as well as Yukawa-type "hopping" terms that couple fields at adjacent lattice sites and contribute off-diagonal elements to the mass matrix. Diagonalization of the mass matrix then leads to a finite tower of massive modes which matches the infinite KK tower in the $N \to \infty$ limit.

If the discretization procedure is applied to fermions, a new issue arises. Plugging in the discretized derivative and calculating the mass spectrum, an unphysical doubling of modes is observed: for every mode in the continuous theory, two modes arise in the lattice approximation, one of which is unphysical. This problem of fermion doubling as well as the solution by adding a so-called Wilson term to the Lagrangian is well known from lattice gauge theory. A detailed discussion of the issue in the context of deconstructed QED can be found in [31]. In the Three-Site Model, however, this problem does not arise due to the extremely small size of the lattice, so we won't elaborate on this point. Instead, the interested reader is referred to above reference.

3.3 Constructing the Lagrangian

With the introduction of 5D gauge theories and dimensional deconstruction in the last two sections, we now have the tools at hand for the actual construction of a Lagrangian implementing the Three-Site Higgsless Model [4] sketched in chapter 2.5.

In [23] it is shown that in 5D gauge theories the unitarity cutoff is pushed to the NDA cutoff scale by the exchange of KK gauge bosons. Therefore, a 5D gauge theory is a good starting point for a theory in which unitarity violation is delayed by heavy W' and Z' partners. Dimensional deconstruction can then be used to cut off the higher KK modes in gauge invariant way, retaining only the Standard Model particles and one generation of KK partners.

Fig. 3.5 shows the structure of the Three Site Model in moose notation [32]. The gauge group consists of two $\mathbf{SU}(2)$ factors and one $\mathbf{U}(1)$ factor which can be understood as a 5D $\mathbf{SU}(2)$ gauge theory broken by boundary conditions to $\mathbf{U}(1)$ on the right brane and deconstructed to three lattice sites. All three group factors are given their own gauge couplings g, $\tilde{g}$ and g' which is required in order to allow the model to be consistent with experimental data and which corresponds to a y dependent gauge coupling $g(y)$ in the continuous version of the theory. QCD is left unchanged in the Three-Site Model with only one set of gluon fields G^μ in the spectrum. The gauge kinetic Lagrangian is

$$\mathcal{L}_{\text{gauge}} = -\frac{1}{2}\sum_{n=0}^{1} \mathbf{Tr}\, F_n^{\mu\nu} F_{n\mu\nu} - \frac{1}{4} F_2^{\mu\nu} F_{2\mu\nu} - \frac{1}{2}\mathbf{Tr}\, G^{\mu\nu} G_{\mu\nu} \tag{3.28}$$

It should be noted that this setup is identical to the BESS model [33].

Deconstructing the gauge group gives us two nonlinear sigma type Wilson line fields Σ_1 and Σ_2 which connect adjacent lattice sites. Under gauge transformations generated by parameter fields $\lambda_0 = \lambda_{0k}\tau_k$, $\lambda_1 = \lambda_{1k}\tau_k$ and λ_2, the Wilson lines transform as

$$\Sigma_1 \longrightarrow e^{i\lambda_0}\Sigma_1 e^{-i\lambda_1} \qquad , \qquad \Sigma_2 \longrightarrow e^{i\lambda_1}\Sigma_2 e^{-i\lambda_2\tau_3} \tag{3.29}$$

The transformation behavior (3.29) fixes the covariant derivative of the Σ fields

$$\begin{aligned} D^\mu\Sigma_1 &= \partial^\mu\Sigma_1 - igA_0^\mu\Sigma_1 + i\tilde{g}\Sigma_1 A_1^\mu \\ D^\mu\Sigma_2 &= \partial^\mu\Sigma_2 - i\tilde{g}A_1^\mu\Sigma_2 + ig' A_2^\mu\Sigma_2\tau_3 \end{aligned} \tag{3.30}$$

With the covariant derivatives fixed, we can write down the kinetic term for the $\Sigma_{1/2}$ fields

$$\mathcal{L}_\Sigma = v^2 \sum_{n=1}^{2} \mathbf{Tr}\, \left(D^\mu\Sigma_n\right)^\dagger \left(D_\mu\Sigma_n\right) \tag{3.31}$$

Expanding (3.31) in terms of the component fields of $\Sigma_{1/2}$ gives mass terms for the gauge bosons. The mass scale is set by v and fixed by the W and Z masses.

The fermion sector is inspired by deconstructing 5D fermions with chiral boundary conditions. The Three-Site Model comes with two copies of each Standard Model fermion, the chiral components of which are distributed according to fig. 3.5. Each Standard Model isospin doublet gives rise to left-handed doublets under the respective $\mathbf{SU}(2)$ at sites 0 and 1, a right-handed $\mathbf{SU}(2)_1$ doublet at site 1 and two right-handed fermions at site 2. As shown in tab. 3.1, the fermions at site 2 inherit

	Ψ_{0L} / Ψ_{1L} / Ψ_{1R}	Ψ_{2R}
Neutrinos	$-\frac{1}{2}$	0
Leptons	$-\frac{1}{2}$	-1
Up type Quarks	$\frac{1}{6}$	$\frac{2}{3}$
Down type Quarks	$\frac{1}{6}$	$-\frac{1}{3}$

Table 3.1: $\mathbf{U}(1)_2$ charge assignments for the fermions on the three site moose.

their $\mathbf{U}(1)_2$ charge from the electromagnetic charge of the corresponding Standard Model fields, while those at the other two sites inherit the hypercharge[8].

According to the above charge assignments, the covariant derivatives of the fermions (omitting the gluon contribution in the case of quarks) read

$$D^\mu \Psi_{0L} = \left(\partial^\mu - igA_0^\mu - ig' A_2^\mu Y\right) \Psi_{0L} \quad , \quad D^\mu \Psi_{1L} = \left(\partial^\mu - i\tilde{g} A_1^\mu - ig' A_2^\mu Y\right) \Psi_{1L}$$
$$D^\mu \Psi_{1R} = \left(\partial^\mu - i\tilde{g} A_1^\mu - ig' A_2^\mu Y\right) \Psi_{1R} \quad , \quad D^\mu \Psi_{2R}^{u/d} = \left(\partial^\mu - ig' A_2^\mu Q\right) \Psi_{2R}^{u/d}$$

with the charge operator Q and the hypercharge operator Y. The fermion Lagrangian then reads[9]

$$\mathcal{L}_f = \sum_{n=0}^{1} \overline{\Psi}_{nL} \not{D} \Psi_{nL} + \sum_{n=1}^{2} \overline{\Psi}_{nR} \not{D} \Psi_{nR}$$
$$+ v \left(\lambda \overline{\Psi}_{0L} \Sigma_1 \Psi_{1R} + \tilde{\lambda} \overline{\Psi}_{1L} \Psi_{1R} + \overline{\Psi}_{1L} \Sigma_2 \begin{pmatrix} \lambda'_u & 0 \\ 0 & \lambda'_d \end{pmatrix} \Psi_{2R} + \text{h.c.} \right) \quad (3.32)$$

In (3.32), the Yukawa couplings between fermions at adjacent lattice sites are left as free parameters, an effect which can be achieved in the continuous theory by the introduction of brane kinetic terms. In particular, the Yukawa couplings $\lambda'_{u/d}$ between Ψ_{L1} and the $\Psi_{R2}^{u/d}$ allow to accommodate the different masses of up- and down-type fermions observed in nature. The $\lambda'_{u/d}$ are the only Yukawa couplings that have a nontrivial flavor structure, all other couplings are taken as flavor universal[10].

With the definitions (3.28), (3.31) and (3.32), the complete Three-Site Lagrangian reads

$$\mathcal{L}_{\text{3-site}} = \mathcal{L}_{\text{gauge}} + \mathcal{L}_\Sigma + \mathcal{L}_f \quad (3.33)$$

[8] While being a slight deviation from straightforward deconstruction as it corresponds to a nonlocal coupling of the fermion fields to the gauge field on the right brane in the continuous theory, this setup is necessary in order to reproduce the correct hypercharges of the Standard Model fermions without introducing additional neutral vectors.

[9] In all expressions containing fermions, an implicit sum over all fermion flavors present in the Standard Model is assumed.

[10] Flavor mixing is not included in the original model, but CKM-type mixing can be easily achieved through the $\lambda'_{u/d}$, retaining the flavor-universal nature of the other couplings [4].

How does this model relate to that sketched in chapter 2.5? In the limit of large $\tilde{g}$ and large $\tilde{\lambda}$ we can integrate out the fields at the bulk site in order to obtain a "two site model" with one linear sigma field

$$\Sigma = \Sigma_1 \Sigma_2$$

Comparison to chapter 2.3 identifies this two site model as the ordinary Standard Model with $\mathbf{SU}(2)_0$ playing the role of $\mathbf{SU}(2)_L$ and $\mathbf{U}(1)_2$ that of $\mathbf{U}(1)_Y$! The bulk lattice site adds the additional $\mathbf{SU}(2)$ group factor and the set of fermion partners suggested in chapter 2.5, and the desired mixings arise from the terms that connect the lattice sites via the $\Sigma_{1/2}$ fields, corresponding to the 5D kinetic terms in the deconstructed setting.

In accordance with [4], we introduce the following definitions for later convenience

$$\begin{aligned} x &= \frac{g}{\tilde{g}} & y &= \frac{g'}{\tilde{g}} & t &= \tan\theta = \frac{g'}{g} = \frac{\sin\theta}{\cos\theta} \\ \epsilon_L &= \frac{\lambda}{\tilde{\lambda}} & \epsilon'_f &= \frac{\lambda'_f}{\tilde{\lambda}} \end{aligned} \tag{3.34}$$

As argued above (and discussed in more detail in the next chapter), the Standard Model is recovered in the limit of large $\tilde{g}$ and $\tilde{\lambda}$, and therefore, we should expect that x, y, ϵ_L and ϵ'_f are small quantities if the new structure is indeed a small perturbation on top of the Standard Model.

Chapter 4

Model Properties

Who ordered that?

(I. I. Rabi on the discovery of the muon on 1936)

At the end of the last chapter, the Lagrangian of the Three-Site Model as presented in [4] was assembled. The present chapter is devoted to a detailed discussion of the model. In the first section, the mass spectrum is calculated. In the second section, the free parameters present in the model in addition to the Standard Model parameters are identified. A number of experimental constraints together with the resulting parameter space is discussed. With the third section follows a brief discussion of the couplings between the Standard Model particles and their new heavy partners, and the last section is devoted to the widths of the new heavy particles. An autogenerated sample spectrum is printed in appendix B.

4.1 Masses

The first step in studying the phenomenology of the Three-Site Model is the calculation of the mass spectrum. The mass terms for the gauge bosons can be readily extracted from (3.31)

$$\mathcal{L}_{\text{mass,gauge}} = M_{ij}^{CC} W_i^{+\mu} W_{j\mu}^{-} + \frac{1}{2} M_{ij}^{NC} B_i^{\mu} B_{j\mu} \tag{4.1}$$

with the charged gauge bosons

$$W_n^{\pm\mu} = \frac{A_{n1}^{\mu} \pm i A_{n2}^{\mu}}{\sqrt{2}} \quad (n = 0, 1)$$

the neutral gauge bosons

$$B_n^{\mu} = A_{n3}^{\mu} \quad (n = 0, 1) \quad , \quad B_2^{\mu} = A_2^{\mu}$$

and the mass matrices

$$M^{CC} = v^2\tilde{g}^2 \begin{pmatrix} x^2 & -x \\ -x & 2 \end{pmatrix} \quad , \quad M^{NC} = v^2\tilde{g}^2 \begin{pmatrix} x^2 & -x & 0 \\ -x & 2 & -tx \\ 0 & -tx & t^2x^2 \end{pmatrix} \tag{4.2}$$

where we have used the definitions (3.34).

The fermion mass terms follow from the Yukawa couplings in (3.32)

$$\mathcal{L}_{\text{mass,fermions}} = \left(\overline{\Psi}^f_{0L}, \overline{\Psi}^f_{1L}\right) M_f \begin{pmatrix} \Psi^f_{1R} \\ \Psi^f_{2R} \end{pmatrix} \tag{4.3}$$

(an implicit sum over all fermions present in the Standard Model is assumed) with the fermion mass matrices

$$M_f = v\tilde{\lambda} \begin{pmatrix} \epsilon_L & 0 \\ 1 & \epsilon'_f \end{pmatrix} \tag{4.4}$$

Integrating out the bulk: the two-side model

To get some intuition about the connection between the Standard Model and the Three-Site Model, let's pick up again the argument presented at the end of chapter 3.3 and integrate out the bulk lattice site in the limit

$$\tilde{g} \to \infty \qquad , \qquad \tilde{\lambda} \to \infty \tag{4.5}$$

where we keep the other parameters (in particular λ and λ') finite in the limiting process such that the limit implies

$$x = \frac{g}{\tilde{g}} \to 0 \quad , \quad y = \frac{g'}{\tilde{g}} \to 0 \quad , \quad \epsilon_L = \frac{\lambda}{\tilde{\lambda}} \to 0 \quad , \quad \epsilon'_f = \frac{\lambda'_f}{\tilde{\lambda}} \to 0$$

for the quantities defined in (3.34).

The masses of the bulk gauge bosons and of the bulk fermions that are to be integrated out can be read off from (4.1) and (4.3)

$$M_{A_1} = \sqrt{2}\tilde{g}v \qquad , \qquad M_{\text{bulk}} = v\tilde{\lambda} \tag{4.6}$$

The resulting model lives on only two lattice sites, connected by one nonlinear sigma field

$$\Sigma = \Sigma_1\Sigma_2$$

To stress the connection to the Standard Model, we will use the same identifiers as in chapter 2.3 for the two-side model fields

$$W^\mu = A^\mu_0 \quad , \quad B^\mu = A^\mu_2 \quad , \quad \Psi_L = \Psi_{0L} \quad , \quad \Psi_R = \Psi_{2R}$$

The covariant derivative of Σ is then

$$D^\mu\Sigma = \partial^\mu\Sigma - igW^\mu\Sigma + ig'B^\mu\Sigma\tau_3 \tag{4.7}$$

and the kinetic Lagrangian for Σ is

$$\mathcal{L}_{\Sigma,2S} = \tilde{v}^2 \mathbf{Tr}\ (D_\mu \Sigma)^\dagger (D^\mu \Sigma) \tag{4.8}$$

As we want to reproduce the Standard Model in the limit (4.15), we can express $\tilde{v}$ through m_W and g by virtue of (2.13)

$$\tilde{v} = \frac{m_W}{g}$$

To find out how $\tilde{v}$ relates to v, let's perform the matching to the Three-Site Model and integrate out the bulk gauge field from the diagram

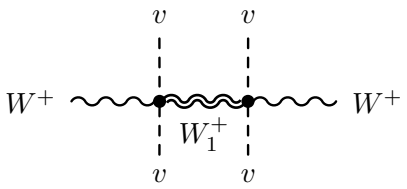

(4.9)

The vertices can be read off (4.1), and the resulting change in the Lagrangian is

$$\Delta\mathcal{L}_{m,W} = (-i)\left(-iv^2 g\tilde{g}\right)\frac{i}{2v^2\tilde{g}^2}\left(-iv^2 g\tilde{g}\right) W^{+\mu}W^-_\mu = -\frac{1}{2}v^2 g^2 W^{+\mu}W^-_\mu$$

modifying the mass term for $W^\pm_\mu$

$$\mathcal{L}_{m,W} = v^2 g^2 W^{+\mu}W^-_\mu + \Delta\mathcal{L}_{m,W} = \frac{1}{2}v^2 g^2 W^{+\mu}W^-_\mu$$

Comparing this to (4.7) and (4.8) identifies $\tilde{v}$ as

$$\tilde{v} = \frac{v}{\sqrt{2}} \tag{4.10}$$

The factor $\sqrt{2}$ has an interesting effect: plugging v into the formula for the NDA cutoff (2.18) in order to estimate the UV cutoff of the Three-Site Model, we obtain

$$\Lambda_{\text{NDA}} = 8\pi v = 8\sqrt{2}\pi\tilde{v} = 8\sqrt{2}\pi\frac{m_W}{g} \approx 4.4\,\text{TeV}$$

Comparison to (2.18) shows that the NDA cutoff scale is elevated by a factor $\sqrt{2}$ in the Three-Site Model above that of the Standard Model.

In fermion sector, Yukawa couplings between the left-handed fermions sitting at site 0 and the right-handed ones at site 1 (formerly site 2) are obtained by integrating out the bulk fermions from diagrams of the type

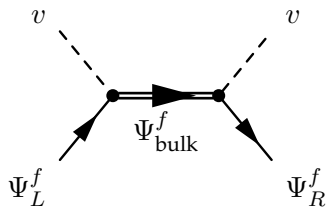

(4.11)

The vertex factors can be read off from (4.4) and inserted to obtain the effective Yukawa couplings

$$\mathcal{L}_{\text{Yukawa,2S}} = v\left(\overline{\Psi}^f_L \epsilon_L \lambda' \Psi^f_R + \text{h.c.}\right) = M_{\text{bulk}}\left(\overline{\Psi}^f_L \epsilon_L \epsilon'_f \Psi^f_R + \text{h.c.}\right) \tag{4.12}$$

with an implicit sum over all Standard Model fermions. We can read off the fermion masses from (4.12)

$$m_f = M_{\text{bulk}} \epsilon_L \epsilon'_f$$

After choosing the flavor-universal ϵ_L, the ϵ'_f are to be chosen for each Standard Model fermion separately to yield the correct Yukawa couplings and masses.

If we would drop the assumption of taking the limit $\tilde{\lambda} \to \infty$ such that $\epsilon'_f \to 0$ and instead keep the ϵ'_f finite (which is perfectly possible by letting ϵ_L go to zero fast enough), diagrams like

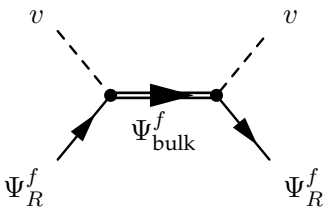

(4.13)

would induce finite wave function renormalizations[1]

$$\Psi^f_R \longrightarrow \sqrt{1+{\epsilon'_f}^2}\,\Psi^f_R$$

In addition, diagrams of the type

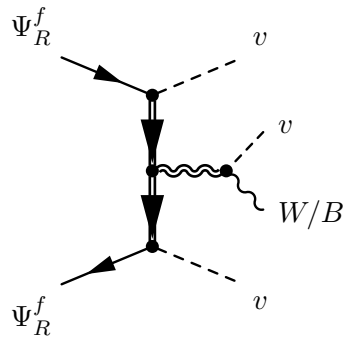

(4.14)

would induce finite couplings e.g. of two Ψ^f_R to a $W^\pm$, leading to deviations from the Standard Model even in the limit $\tilde{g} \to \infty$, $\tilde{\lambda} \to \infty$! Similar arguments apply if

[1]Due to the chirality of Ψ^f_R, the momentum expansion of the diagram (4.13) starts at the order $\not{p}$, leading to the change in the Lagrangian

$$\Delta\mathcal{L} = i{\epsilon'_f}^2 \overline{\Psi}^f_R \not{\partial} \Psi^f_R$$

ϵ_L is kept finite, and therefore, the correct limit for recovering the Standard Model is in fact

$$x \to 0 \quad , \quad M_{\text{bulk}} \to \infty \quad , \quad \epsilon_L \to 0 \quad , \quad \epsilon'_f \to 0 \tag{4.15}$$

while keeping g, g' and v finite[2].

In the limit (4.15), we fully recover the Standard Model and obtain the matching conditions (4.10) and (4.12). By comparison to chapter 2.3 we can immediately write down the spectrum to lowest order in an expansion in x, ϵ_L and ϵ'_f:

- The massless photon and gluons.
- The Standard Model $W^{\pm}$ and Z bosons with masses

$$m_W = \frac{vg}{\sqrt{2}} \quad , \quad m_Z = v\sqrt{\frac{g^2 + g'^2}{2}}$$

- The Standard Model fermions with masses given by

$$m_f = M_{\text{bulk}} \epsilon_L \epsilon'_f$$

- Two $W^{\pm\prime}$ and one Z' which are degenerate with mass

$$m_{W'} = m_{Z'} = \sqrt{2}\tilde{g}v$$

- One partner fermion for each Standard Model fermion with mass

$$M_{\text{bulk}} = \tilde{\lambda} v \tag{4.16}$$

Exact spectrum

To get the corrections for finite x, ϵ_L and ϵ'_f to the above picture, we must explicitly diagonalize the mass matrices (4.2) and (4.4). This was done analytically with the results then being expanded as a series in x resp. ϵ_L in order to obtain the expressions for masses and wavefunctions presented in this section.

As the gauge sector of the Three-Site Model corresponds to a deconstructed 5D $\mathbf{SU}(2)$ gauge group with Neumann boundary conditions for the τ_3 component field and mixed ones for the other two, an unbroken $\mathbf{U}(1)$ gauge symmetry together with a massless gauge boson is to be expected. Indeed, setting

$$\lambda_0 = \lambda_1 = \lambda_2 \tau_3$$

in (3.29), we find that the vacuum expectation value of the $\Sigma_{1/2}$ is not changed under the transformation and, therefore, this combination generates an unbroken

[2]Indeed, while being more intuitive considering the parameterization of the model we will be developing in the remainder of this chapter, (4.15) together with the requirement of keeping g, g' and v finite is just a rephrasing of the limiting conditions stated already at the beginning of this section.

$m_W^2 = \frac{g^2v^2}{2}\left(1 - \frac{x^2}{4} + \mathcal{O}\left(x^6\right)\right)$	$f_0^W = 1 - \frac{x^2}{8} - \mathcal{O}\left(x^4\right)$
	$f_1^W = \frac{x}{2} + \frac{x^3}{16} - \mathcal{O}\left(x^5\right)$
$m_{W'}^2 = 2\tilde{g}^2v^2\left(1 + \frac{x^2}{4} + \mathcal{O}\left(x^4\right)\right)$	$f_0^{W'} = -\frac{x}{2} - \frac{x^3}{16} + \mathcal{O}\left(x^5\right)$
	$f_1^{W'} = 1 - \frac{x^2}{8} - \mathcal{O}\left(x^4\right)$
$m_Z^2 = \frac{g^2v^2}{2c^2}\left(1 - \frac{x^2\left(c^2-s^2\right)^2}{4c^2} + \mathcal{O}\left(x^6\right)\right)$	$f_0^Z = c - \frac{x^2c^3\left(1+2t^2-3t^4\right)}{8} + \mathcal{O}\left(x^4\right)$
	$f_1^Z = \frac{xc\left(1-t^2\right)}{2} + \frac{x^3c^3\left(1-t^2\right)^3}{16} + \mathcal{O}\left(x^5\right)$
	$f_2^Z = -s - \frac{x^2sc^2\left(3-2t^2-t^4\right)}{8} + \mathcal{O}\left(x^4\right)$
$m_{Z'}^2 = 2\tilde{g}^2v^2\left(1 + \frac{x^2}{4c^2} + \mathcal{O}\left(x^4\right)\right)$	$f_0^{Z'} = -\frac{x}{2} - \frac{x^3\left(1-3t^2\right)}{16} + \mathcal{O}\left(x^5\right)$
	$f_1^{Z'} = 1 - \frac{x^2\left(1+t^2\right)}{8} + \mathcal{O}\left(x^4\right)$
	$f_2^{Z'} = -\frac{xt}{2} + \frac{x^3t\left(3-t^2\right)}{16} + \mathcal{O}\left(x^5\right)$

Table 4.1: Masses and wavefunctions of the gauge bosons as obtained from diagonalizing the mass matrices M^{CC} and M^{NC} (c.f. (3.34) for the abbreviations).

$\mathbf{U}(1)$ gauge symmetry. Looking at the fermion charges tab. 3.1 this is readily identified as the electromagnetic $\mathbf{U}(1)_{\text{em}}$, and defining the electromagnetic gauge coupling e

$$\frac{1}{e^2} = \frac{1}{g^2} + \frac{1}{\tilde{g}^2} + \frac{1}{g'^2} \tag{4.17}$$

the corresponding photon field A^μ is

$$A^\mu = \frac{e}{g}B_0^\mu + \frac{e}{\tilde{g}}B_1^\mu + \frac{e}{g'}B_2^\mu \tag{4.18}$$

The masses and wavefunctions[3] of the massive gauge bosons are given in tab. 4.1 as an expansion in x. As expected, the masses coincide at lowest order with the above result obtained by integrating out the bulk site. The most noticeable effect of the corrections is to lift the degeneracy between the W' and the Z'. Turning our attention to the wavefunctions, we find that the Standard Model $W^\pm$ and Z bosons are localized at the brane lattice sites with f_1 vanishing in the limit $x \to 0$, while the $W^{\pm\prime}$ and Z' are localized at the bulk site with f_0 and f_2 being of order $\mathcal{O}\left(x\right)$.

[3]The wavefunctions are to be read as e.g.

$$Z'^\mu = \sum_{n=0}^{2} f_n B_n^\mu$$

$m_f = \frac{M_{\text{bulk}}\epsilon_L\epsilon'_f}{\sqrt{1+{\epsilon'_f}^2}} \times \left(1 - \frac{\epsilon_L^2}{2\left({\epsilon'_f}^2+1\right)^2} + \mathcal{O}\left(\epsilon_L^4\right)\right)$	$f^f_{0L} = -1 + \frac{\epsilon_L^2}{2\left(1+{\epsilon'_f}^2\right)^2} + \mathcal{O}\left(\epsilon_L^4\right)$
	$f^f_{1L} = \frac{\epsilon_L}{1+{\epsilon'_f}^2} + \frac{\left(2{\epsilon'_f}^2-1\right)\epsilon_L^3}{2\left({\epsilon'_f}^2+1\right)^3} + \mathcal{O}\left(\epsilon_L^5\right)$
	$f^f_{1R} = -\frac{\epsilon'_f}{\sqrt{1+{\epsilon'_f}^2}} + \frac{\epsilon_L^2\epsilon'_f}{\left(1+{\epsilon'_f}^2\right)^{\frac{5}{2}}} + \mathcal{O}\left(\epsilon_L^4\right)$
	$f^f_{2R} = \frac{1}{\sqrt{1+{\epsilon'_f}^2}} + \frac{\epsilon_L^2{\epsilon'_f}^2}{\left(1+{\epsilon'_f}^2\right)^{\frac{5}{2}}} + \mathcal{O}\left(\epsilon_L^4\right)$
$m_{f'} = M_{\text{bulk}}\sqrt{1+{\epsilon'_f}^2} \times \left(1 + \frac{\epsilon_L^2}{2\left({\epsilon'_f}^2+1\right)^2} + \mathcal{O}\left(\epsilon_L^4\right)\right)$	$f^{f'}_{0L} = -\frac{\epsilon_L}{1+{\epsilon'_f}^2} - \frac{\left(2{\epsilon'_f}^2-1\right)\epsilon_L^3}{2\left({\epsilon'_f}^2+1\right)^3} + \mathcal{O}\left(\epsilon_L^5\right)$
	$f^{f'}_{1L} = -1 + \frac{\epsilon_L^2}{2\left(1+{\epsilon'_f}^2\right)^2} + \mathcal{O}\left(\epsilon_L^4\right)$
	$f^{f'}_{1R} = -\frac{1}{\sqrt{1+{\epsilon'_f}^2}} - \frac{{\epsilon'_f}^2\epsilon_L^2}{\left(1+{\epsilon'_f}^2\right)^{\frac{5}{2}}} + \mathcal{O}\left(\epsilon_L^4\right)$
	$f^{f'}_{2R} = -\frac{\epsilon'_f}{\sqrt{1+{\epsilon'_f}^2}} + \frac{\epsilon'_f\epsilon_L^2}{\left(1+{\epsilon'_f}^2\right)^{\frac{5}{2}}} + \mathcal{O}\left(\epsilon_L^4\right)$

Table 4.2: Fermion masses and wavefunctions expanded in ϵ_L as obtained from diagonalizing the fermion mass matrix (c.f. (3.34) for the abbreviations).

The masses and wavefunctions resulting from diagonalizing the fermion mass matrix (4.4) are given in tab. 4.2 as an expansion in ϵ_L. Again, in the limit (4.15) the result from integrating out the bulk site is recovered, with the corrections lifting the degeneracy between the heavy partner fermions. As in the case of the gauge bosons, the Standard Model fermions are predominantly localized at the brane sites, while their heavy partners reside mainly in the bulk with the modes becoming fully localized in the limit (4.15).

In order to illustrate the formulae in tab. 4.1 and tab. 4.2, fig. 4.1 shows the wavefunctions of W, Z and massless left- and right-handed fermions as well as those of their heavy KK partners, the values being taken from app. B. These profiles are representative for the whole allowed region of parameters space and clearly exhibit the (de)localization properties of the different modes as discussed above. The wavefunctions of t/t' and b/b' differ slightly from those shown in fig. 4.1 due the comparatively large mass of the respective KK light modes, the most notable difference being a slight delocalization of the right-handed components which are

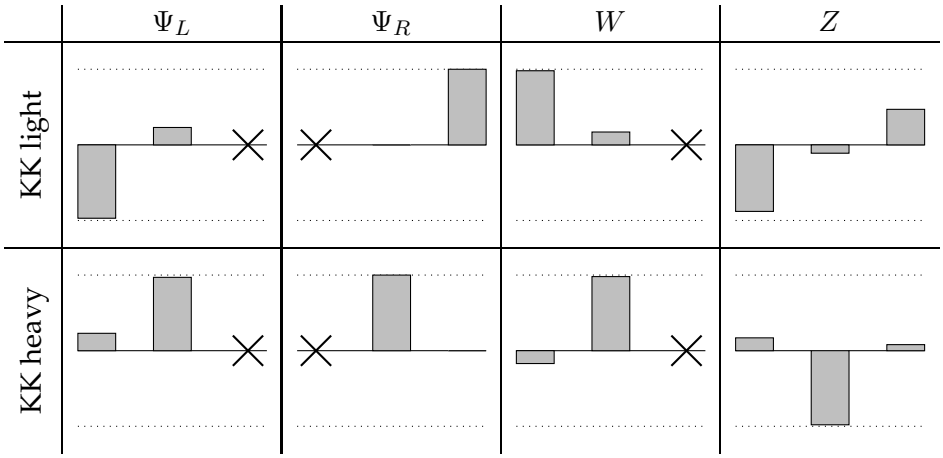

Figure 4.1: The wavefunctions f_n of W, Z and massless left- and right-handed fermions as well as those of their heavy KK partners for $m_{W'} = 500\,\mathrm{GeV}$, $M_{\text{bulk}} = 3.5\,\mathrm{TeV}$ and $\epsilon_L = 0.237$ (ideal delocalization, see section 4.2 below), the values are taken from app. B. The scale is linear, and the dotted lines correspond to $f_n = \pm 1$.

(nearly) completely localized for the (almost) massless fermions and their KK partners.

4.2 Parameter space and constraints

While it indeed manages to delay the unitarity cutoff without invoking any scalar fields, the Three-Site Higgsless Model is not an improvement over the Standard Model as far as the number of free parameters is concerned. To fix the model and make predictions, all parameters present in the Standard Model (except for the Higgs mass, obviously) must be specified in addition to a couple of additional ones.

In the gauge sector we've got four free parameters: the three gauge couplings g, g' and $\tilde{g}$ as well as the scale[4] v. After fixing the W and Z masses as well as the electric charge, only one degree of freedom remains in this sector, which can be chosen as x. From the expansions in tab. 4.1 it follows that to leading order in x

$$\frac{m_W^2}{m_{W'}^2} = \frac{x^2}{4} \tag{4.19}$$

Therefore, we can fix x from the mass ratio of W and W', and the limit $x \to 0$ for recovering the Standard Model is equivalent to $m_{W'} \to \infty$.

Going over to the fermion sector we have two flavor-universal parameters ϵ_L and $\tilde{\lambda}$ and one set of parameters ϵ'_f that are to be chosen separately for each fermion

[4]It is possible to choose two different scales v_1 and v_2 for the link fields $\Sigma_{1/2}$. The choice $v_1 = v_2 = v$ maximizes the delay of unitarity violation [34], however, this relation is not honored by loop corrections [35].

flavor. The ϵ'_f are fixed by the masses of the Standard Model fermions, while $\tilde{\lambda}$ and ϵ_L remain as free parameters. We choose to replace $\tilde{\lambda}$ by the heavy fermion mass scale M_{bulk} (4.16) which has a more intuitive physical meaning.

Electroweak precision observables at tree level: ideal delocalization

In chapter 2.5, the introduction of heavy fermions was suggested as a loophole for evading the bounds coming from precision measurements at LEP and LEP-II. In these experiments, the neutral- and charged current correlators were measured very precisely, revealing an astonishing degree of agreement with the higher order predictions of the Standard Model and putting tight bounds on any contributions from new physics.

Under the assumption that all contributions of new physics manifest themselves as modification to the gauge boson self energies, the resulting constraints can be summarized as bounds on a small number of parameters. The LEP bounds are commonly parameterized by the αS, αT and αU parameters [19] or equivalently by the three $\epsilon_{1/2/3}$ parameters [21] which correspond to bounds on the coefficients in an expansion of the self-energies to order p^2.

The data obtained at LEP-II allows for additional constraints on new physics contributions to the self-energies, corresponding to an expansion to order p^4. Together with the LEP-I constraints, these bounds can be expressed by a set of 7 parameters introduced in [36] which also cover the bounds expressed by αS, αT and αU.

While these parameters were designed to parameterize deviations from the Standard Model that appear only as "oblique corrections" in the gauge boson self-energies, the authors of [37] show that non-oblique corrections appearing in Higgsless models can also be absorbed into the extended set of parameters defined in [36].

An generic analysis of the precision observables in a large class of deconstructed Higgsless models which also contains the Three-Site Model was published in [38]. There, the general form of the charged and neutral current scattering amplitudes in the vicinity of the Z and W poles was derived and it was shown that a suitable tuning of the fermion wavefunctions dubbed "ideal delocalization" can minimize the tree level corrections to the precision observables. In particular, the $\Delta\rho$ parameter which measures the low energy difference between the charged and neutral current coupling strengths vanishes, and the tree level contributions to αS and αT reduce to

$$\alpha S = 4 s_W^2 c_W^2 m_Z^2 \sum_n \left(\frac{1}{m_{Z_n}^2} - \frac{1}{m_{W_n}^2} \right) \quad , \quad \alpha T = s_W^2 m_Z^2 \sum_n \left(\frac{1}{m_{Z_n}^2} - \frac{1}{m_{W_n}^2} \right) \tag{4.20}$$

where the sums run over all KK gauge bosons and c_W and s_W are sine and cosine of the Weinberg angle

$$c_W = \cos\theta_W = \frac{m_W}{m_Z}$$

For the case of the Three-Site Model, plugging the expansions of the masses tab. 4.1 into (4.20) and using (4.19) as well as

$$c = \frac{m_W}{m_Z} + \mathcal{O}\left(x\right) \tag{4.21}$$

gives the naturally small results

$$\alpha S = -4\frac{m_W^2}{m_Z^2}\frac{\left(m_Z^2 - m_W^2\right)^2}{m_{W'}^4} + \mathcal{O}\left(x^6\right) \quad , \quad \alpha T = -\frac{\left(m_Z^2 - m_W^2\right)^2}{m_{W'}^4} + \mathcal{O}\left(x^6\right)$$

The condition for ideal delocalization is the vanishing of the couplings of the light Standard Model fermions to the heavy W partners. In the Three-Site Model there is only one W', and the corresponding coupling is given by the overlap of the wavefunctions

$$g_{W'ff} = \frac{1}{\sqrt{2}}\left(g f_0^{W'} f_{0L}^{f_1} f_{0L}^{f_2} + \tilde{g} f_1^{W'} f_{1L}^{f_1} f_{1L}^{f_2}\right)$$

As ϵ_f' vanishes for massless fermions and the other two parameters of the fermion sector M_{bulk} and ϵ_L are flavor-universal, all massless fermions have the same wavefunctions f^f. Due the mass matrix being symmetric, the wavefunctions f^W and $f^{W'}$ are orthogonal and, therefore, choosing

$$\begin{pmatrix} \left(f_{0L}^f\right)^2 \\ \left(f_{1L}^f\right)^2 \end{pmatrix} \propto \begin{pmatrix} \frac{1}{g} f_0^W \\ \frac{1}{\tilde{g}} f_1^W \end{pmatrix}$$

or equivalently

$$\left(\frac{f_{1L}^f}{f_{0L}^f}\right)^2 = x\frac{f_1^W}{f_0^W} \tag{4.22}$$

is sufficient to implement ideal delocalization. Examining the wavefunctions given in tab. 4.1 and tab. 4.2 reveals that (4.22) encodes a relationship between ϵ_L and x

$$\epsilon_L^2 = \frac{x^2}{2} + \mathcal{O}\left(x^2\right) \tag{4.23}$$

which reduces the number of free parameters by one, allowing us to fix the Three-Site Model by specifying just $m_{W'}$ and M_{bulk} in addition to the Standard Model parameters, (in the case of ideal delocalization). Also, (4.23) automatically implies $\epsilon_L \to 0$ in the limit $x \to 0$ as required by (4.15) in order to recover the Standard Model.

Electroweak precision observables at one loop

Due to the extremely efficient suppression of the tree level contributions to the precision observables in the case of ideal delocalization, the loop contributions can

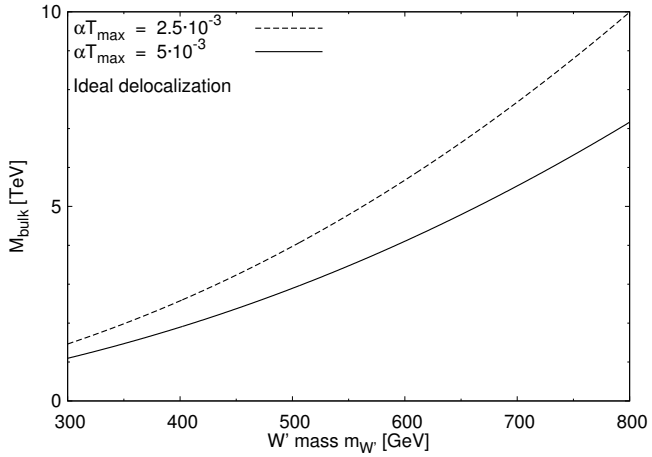

Figure 4.2: Lower bound on M_{bulk} from estimating the t' / b' one loop contribution to αT in the ideally delocalized scenario.

be expected to be dominant. Because the model contains heavy copies of the top and the bottom quarks, new contributions to αT can arise from diagrams of the type

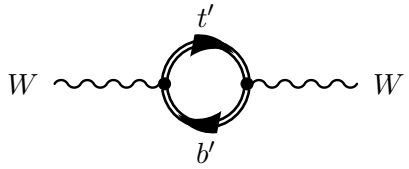

As ϵ_L honors isospin, the isospin violating effect of this diagram persists in the limit $\epsilon_L \to 0$. The leading contribution to αT in this limit is estimated in [4] as

$$\alpha T = \frac{1}{32\pi^2} \frac{M_{\text{bulk}}^2}{v^2} \epsilon_t'^4 \tag{4.24}$$

From tab. 4.2 we can approximate ϵ_t' as

$$\epsilon_t' \approx \frac{m_t}{M_{\text{bulk}} \epsilon_L} \tag{4.25}$$

Plugging this into (4.24) with an upper bound αT_{max} on αT and using the condition for ideal delocalization (4.23), we obtain a lower bound on M_{bulk}

$$M_{\text{bulk}} \geq \frac{1}{4\pi\sqrt{2\alpha T_{\text{max}}}} \frac{m_t^2}{v\epsilon_L^2} = \frac{1}{8\pi\sqrt{2\alpha T_{\text{max}}}} \frac{m_t^2 m_{W'}^2}{v m_W^2} \tag{4.26}$$

This constraint is shown in fig. 4.2 for two different values of αT_{max} (the exact value depends on the "reference Higgs boson mass" chosen for the determination of αT, see [19]).

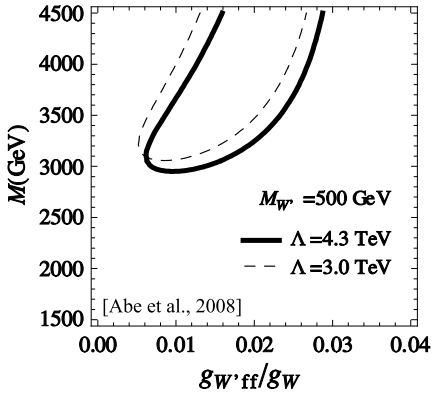

Figure 4.3: Region in the $M_{\text{bulk}} - g_{W'ff}$ plane consistent with αS and αT at one loop for $m_{W'} = 500\,\text{GeV}$ and different values of the UV cutoff Λ; g_W is the isospin gauge coupling. Plot taken from [35].

A nice consequence of (4.26) is the fact that it also induces an upper bound on the ϵ'_f

$$\epsilon'_f \leq 4\pi\sqrt{2\alpha T_{\text{max}}}\frac{m_f v \epsilon_L}{m_t^2}$$

Together with (4.23) and (4.19), this implies that any limit $m_{W'} \to \infty, M_{\text{bulk}} \to \infty$ which respects the precision constraints leads to $\epsilon'_f \to 0$ and therefore recovers the Standard Model according to (4.15)[5].

A complete one loop calculation of αS and αT was started in [39, 40] and completed in [35]. The result is quite interesting as, although a sizable piece of parameter space remains, the case of ideal delocalization is excluded. As an example, fig. 4.3 shows the region in the $M_{\text{bulk}} - g_{W'ff}$ plane which is consistent with αS and αT at 95% confidence level for $m_{W'} = 500\,\text{GeV}$. The resulting $g_{W'ff}$ coupling is constrained to be smaller than some $2-3\%$ of the isospin gauge coupling, but still finite.

As the Three-Site Model must be treated as an effective field theory, a logarithmic dependence on the UV cutoff scale Λ remains in the result which fig. 4.3 demonstrates to be very moderate. Increasing the W' mass moves the allowed area to higher values of M_{bulk} in agreement with the bound (4.26) obtained from αT for ideal delocalization. At some value of the W' mass, the bound on M_{bulk} crosses the UV cutoff, indicating the breakdown of the theory that contains the bulk fermions

[5]Two comments are in order. First, if M_{bulk} exceeds the UV cutoff, then the above estimate of αT from loops with dynamical KK fermions is inconsistent. Instead, an analysis in the effective theory obtained by integrating out the heavy fermions from an UV-completed version of the model should be performed. This is carried out in [4] with a toy completion and the result is shown to be unchanged.

Second, the case of ideal delocalization is excluded by the one-loop result for αS (see below). However, $g_{W'ff}$ has still to be very close to zero, so the above constraints on M_{bulk} and the ϵ'_f are still realistic.

as physical degrees of freedom. While this is of little consequence to tree level calculations, the effective field theory analysis performed in [35] breaks down at this point.

Triple gauge boson couplings

After the discovery of the W and Z, LEP-II was the first experiment capable of measuring the triple gauge boson couplings predicted by nonabelian gauge theory. The results put bounds on these couplings which differ between the Three-Site Model and the Standard Model.

In the absence of CP-violation, all[6] possible dimension 4 operators that generate couplings between two charged and one neutral gauge bosons can be parameterized in Hagiwara-Zeppenfeld notation [41]

$$\begin{aligned}\mathcal{L}_{3g} = &-ie\left(1+\Delta\kappa_A\right)W^+_\mu W^-_\nu A^{\mu\nu} - ie\left(1+\Delta g_1^A\right)\left(W^{+\mu\nu}W^-_\mu - W^{-\mu\nu}W^+_\mu\right)A_\nu - \\ &ie\frac{c_W}{s_W}\left(1+\Delta\kappa_Z\right)W^+_\mu W^-_\nu Z^{\mu\nu} - ie\frac{c_W}{s_W}\left(1+\Delta g_1^Z\right)\left(W^{+\mu\nu}W^-_\mu - W^{-\mu\nu}W^+_\mu\right)Z_\nu\end{aligned} \tag{4.27}$$

In order to obtain the values of the couplings and the parameters $\Delta\kappa_{A/Z}$ and $\Delta g_1^{Z/A}$, the mass eigenstates W, Z and A must be expressed through the gauge eigenstates situated at the lattice sites. The normalization of the wavefunctions together with the photon wavefunction (4.18) implies $\Delta\kappa_A = \Delta g_1^A = 0$ by electromagnetic gauge invariance. The remaining two parameters must be equal and evaluate to

$$e\frac{c_W}{s_W}\left(1+\Delta\kappa_Z\right) = e\frac{c_W}{s_W}\left(1+\Delta g_1^Z\right) = gf_0^Z\left(f_0^W\right)^2 + \tilde{g}f_1^Z\left(f_1^W\right)^2$$

Plugging in the wavefunctions and masses tab. 4.1, we obtain

$$\Delta g_1^Z = \Delta\kappa_Z = \frac{x^2}{8c^2} + \mathcal{O}\left(x^3\right)$$

Using (4.19) and (4.21) results in a lower bound on the W' mass

$$m_{W'} = \frac{1}{2}\frac{m_Z^2}{\Delta g_1^Z}$$

From [42], the upper bound on Δg_1^Z is 0.028, and we obtain

$$m_{W'} \geq 380\,\mathrm{GeV} \tag{4.28}$$

[6]The Hagiwara-Zeppenfeld parameterization excludes operators containing pieces like $\partial_\mu Z^\mu$ whose contributions are suppressed with the electron mass at LEP and which are therefore not observable in the LEP / LEP-II data.

Note that, together with the above bounds on M_{bulk}, this implies a lower bound on M_{bulk}[7] which we can read off from fig. 4.2 as

$$M_{\text{bulk}} \geq 1.8\,\text{TeV} - 2\,\text{TeV} \tag{4.29}$$

(depending on the exact bound on αT assumed, see above).

4.3 Couplings

The calculation of couplings in the Three-Site Model follows the pattern already shown for $g_{W'ff}$ and g_{WWZ} in the last section: the couplings are obtained from reexpressing the mass eigenstates (which are delocalized over the whole lattice) in terms of the gauge eigenstates localized at each lattice site, e.g. for couplings of arity three

$$g_{XYZ} = \sum_n g_n f_n^X f_n^Y f_n^Z$$

In the language of deconstruction, these sums are the deconstructed version of the overlap integrals which give the couplings in the continuous case (c.f. (3.7))

$$g_{XYZ} = \int dy\; g(y) f_X(y) f_Y(y) f_Z(y)$$

(allowing for a possible dependence of the 5D couplings on y).

Gauge sector

The only free parameter in the gauge sector of the Three-Site Model not present in the Standard Model is x and, therefore, all gauge sector couplings must be independent of M_{bulk} (and ϵ_L in the the case of nonideal delocalization).

As shown at the beginning of the previous section, the Three-Site Model is identical to the Standard Model without a Higgs in the limit (4.15). This implies that couplings between the Standard Model gauge bosons match those in the Standard Model up to corrections of order $\mathcal{O}\left(x^2\right)$ or higher[8], where x is constrained to be smaller than ≈ 0.42 by (4.28) and (4.19).

By the same reasoning, the couplings g and g' at the lattice sites 0 and 2 are equal to the isospin and hypercharge gauge couplings up to corrections of order $\mathcal{O}\left(x^2\right)$. The coupling $\tilde{g}$ at the bulk site can be written as

$$\tilde{g} = \frac{g}{x} \approx \frac{g}{2}\frac{m_{W'}}{m_W}$$

[7] An additional bound on M_{bulk} arises from potential dangerous contributions to $b \to s\gamma$ originating from the small but finite right-handed Wtb coupling present in the model. However, this constraint is weaker than (4.29), see [4] for details.

[8] As the sign of the gauge couplings is purely conventional and can be changed by redefining the gauge field, all couplings have to be either even or odd in x which is the reason why the corrections to couplings between Standard Model particles start at $\mathcal{O}\left(x^2\right)$.

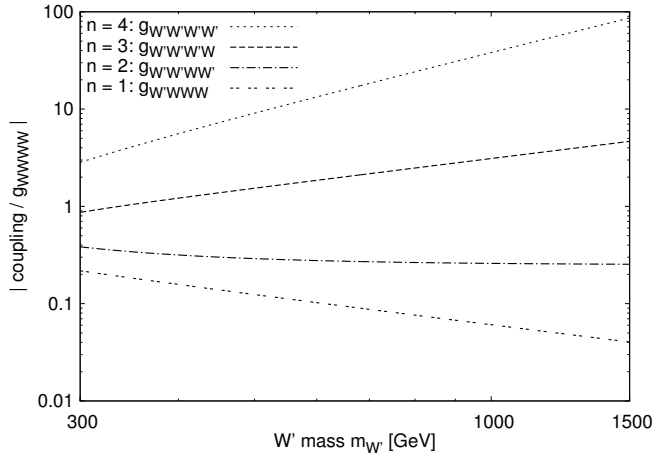

Figure 4.4: The four-point coupling between different combinations of W and W', double logarithmic plot to emphasize the leading order dependence on x.

and exhibits a linear growth with m_W. We can't reasonably expect the delay of unitarity to work out of the W' is heavier than $\mathcal{O}(1\,\mathrm{TeV})$ and, therefore

$$\tilde{g} \leq \tilde{g}|_{m_{W'}=1.5\,\mathrm{TeV}} \approx 6.2 < 4\pi$$

This means that the gauge coupling of the $\mathbf{SU}(2)$ at site 1 is moderately strong with radiative corrections being roughly of order $\frac{\tilde{g}^2}{16\pi^2} \approx 25\%$ in the worst case.

In the limit $x \to 0$, the Standard Model gauge bosons are localized on the branes with the f_1 being of order x, while the W' and Z' are localized in the bulk with $f_{0/2}$ of $\mathcal{O}(x)$ (c.f. tab. 4.1). Naively, one would therefore expect that all couplings involving different KK modes are suppressed by powers of x. However, this is not true because the coupling at the bulk lattice site is proportional to x^{-1}. Taking this into account and recalling the definition of x (3.34), it is not difficult to see that a coupling between gauge bosons involving n W' or Z' (for $n > 0$) must be of order $\mathcal{O}\left(x^{2-n}\right)$ relative to the corresponding Standard Model coupling. This behavior is demonstrated in fig. 4.4.

The only exception from this rule are couplings involving only W, W' and photons. In this case, orthonormality of f^W and $f^{W'}$ together with the photon wavefunction (4.18) implies that all couplings apart from

$$g_{WW\gamma} = g_{W'W'\gamma} = e \quad , \quad g_{WW\gamma\gamma} = g_{W'W'\gamma\gamma} = e^2$$

vanish.

As QCD is not touched by the additional structure in the Three-Site Model, the couplings between the gluons are unchanged with respect to the Standard Model.

Fermion sector: ideal delocalization

The fermion sector is more complicated as it depends on x as well as on M_{bulk}. However, the Standard Model must be recovered in the limit (4.15), so all couplings

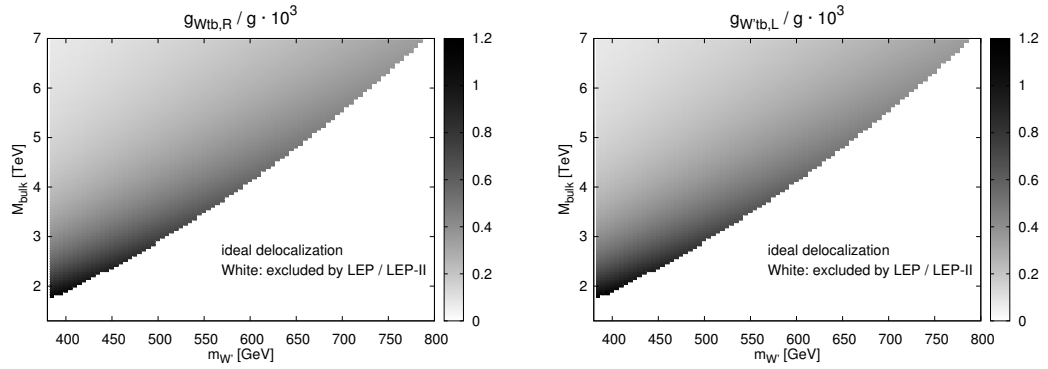

Figure 4.5: *Left:* Right-handed Wtb coupling relative to the isospin gauge coupling g (forbidden in the Standard Model) in the Three-Site Model in as a function of the $m_{W'}$ and M_{bulk}.
Right: Similar plot of the left-handed $W'tb$ coupling which vanishes for massless fermions due to ideal delocalization.

involving only KK light particles must equal the respective Standard Model values up to corrections of order $\mathcal{O}\left(x^2\right)$ and $\mathcal{O}\left({\epsilon'_f}^2\right)$ (this also covers the dependence on ϵ_L as it is proportional to x by ideal delocalization).

In the ideally delocalized scenario, x enters the wavefunctions of the fermions through their dependence on ϵ_L, while M_{bulk} enters through ϵ'_f. For a massless fermion we have $\epsilon'_f = 0$ and therefore, the wavefunctions and couplings of massless fermions only depend on x. In addition, the right-handed zero modes of the massless fermions have to completely decouple from their left-handed counterparts and therefore are completely localized at site 2, while the KK-heavy modes are completely localized in the bulk in this case.

Consulting tab. 4.2 shows that the massless KK-light fermions are localized at the branes with f_1^f suppressed like $\mathcal{O}\left(\epsilon_L\right)$ while their KK-heavy partners are localized in the bulk with $f_{0/2}^f$ similarly suppressed. This implies that the counting rule derived for the gauge sector also holds for W coupling to massless fermions or their KK-partners. In the case of massive fermions, ϵ'_f goes to zero as M_{bulk} goes to infinity, recovering the same pattern in this limit and yielding corrections of order ϵ'_f for finite M_{bulk}.

The left-handed couplings between a W' and two massless fermions are not only suppressed by $\mathcal{O}\left(x^2\right)$ but fully vanish as required by ideal delocalization due to a cancellation between the contributions from different lattice sites. In the case of massive Standard Model fermions, the cancellation is not complete, but the resulting coupling is still very small as demonstrated in fig. 4.5 right by the example of $W'tb$.

As the right-handed KK-light modes of the massive fermions and the W have a nonvanishing overlap in the bulk, a small right-handed coupling between the W

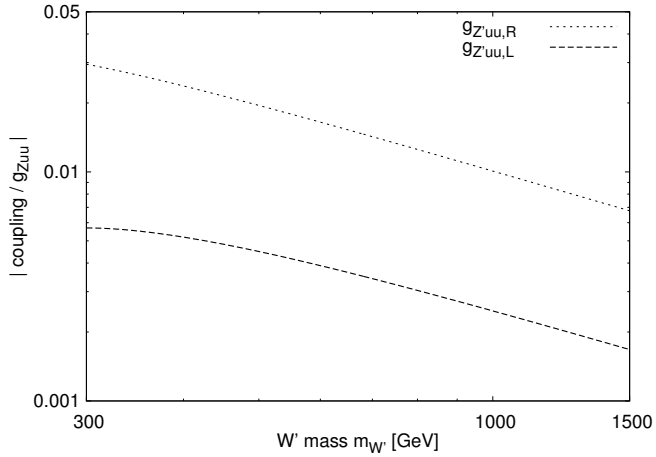

Figure 4.6: The left- and right-handed $Z'uu$ couplings relative to their Zuu counterpart as a function of the W' mass $m_{W'}$. Double logarithmic plot.

and the massive Standard Model fermions suppressed like $\mathcal{O}\left(\epsilon_f'^{\,2}\right)$ is present in the Three-Site Model. This coupling is showcased in fig. 4.5 left for Wtb.

The couplings to the Z are more complicated due to the nontrivial charge of the fermions at site 0 and 1 under the $\mathbf{U}(1)$ at site 2. Taking this into account, the left- and right-handed couplings read

$$\begin{aligned} g_{Zf_1f_2,L} =& T_3 \left(g\, f_{0L}^{f_1}\, f_{0L}^{f_2}\, f_0^Z + \tilde{g}\, f_{1L}^{f_1}\, f_{1L}^{f_2}\, f_1^Z \right) - Y g'\, f_2^Z \left(\sum_{n=0}^{1} f_{nL}^{f_1}\, f_{nL}^{f_2} \right) \\ g_{Zf_2f_2,R} =& T_3 \tilde{g}\, f_{1R}^{f_1}\, f_{1R}^{f_2}\, f_1^Z + Q g'\, f_{2R}^{f_1}\, f_{2R}^{f_2}\, f_2^Z + Y g'\, f_2^Z\, f_{1R}^{f_1}\, f_{1R}^{f_2} \end{aligned} \tag{4.30}$$

The first two terms of both couplings come from the wave function overlap and directly fall under the same counting rule as above in the $\epsilon_f' = 0$ case. The third term comes from the part of the coupling to B_2^μ which is nonlocal on the lattice and could potentially violate our counting rule. To see that this is not the case, note that the contributions of these terms are either of order $\mathcal{O}(x)$ or $\mathcal{O}(1)$, and the latter only if the Standard Model Z is involved. However, in both cases, the only combination of KK modes that could give a $\mathcal{O}(1)$ contribution is $Zf'f'$ for which the counting rule also gives $\mathcal{O}(1)$ and therefore, the leading order in x as given by the rule is unchanged for all possible combinations of modes at the vertex.

The submatrix of the neutral gauge boson mass matrix M^{NC} (c.f. (4.2)) which links the gauge fields at sites 0 and 1 is identical to the charged gauge boson mass matrix M^{CC}. Therefore, we can expect the wave function of the Z' at these lattice sites to be approximately proportional to that of the W' (a conjecture which can be confirmed by a look at the actual wave functions in tab. 4.1). Thus, the cancellation leading to ideal delocalization also suppresses the left-handed couplings between the Z' and the Standard Model fermions. This is confirmed by fig. 4.6 which shows the right- and left-handed couplings of $Z'uu$ relative to their Zuu counterparts.

While the right-handed coupling is of order x as expected if there is no special relation between the wave functions at different lattice sites, the left-handed coupling is suppressed by roughly another order of magnitude by the incomplete cancellation.

Putting the pieces together, in the limit $\epsilon'_f \to 0$ (either by vanishing Standard Model mass or large M_{bulk}), the couplings of the KK-light fermions to W and Z are equal to their Standard Model model values up to corrections of $\mathcal{O}\left(x^2\right)$, while couplings involving n ($n \geq 1$) KK-heavy particles go like $\mathcal{O}\left(x^{2-n}\right)$[9]. As far as the left-handed couplings to the Standard Fermions are concerned, the W' is completely fermiophobic and the Z' at least close to it.

Due to electromagnetic gauge invariance, the photon doesn't couple to fermions of different mass. The couplings of a photon to two Standard Model fermions (or both the KK partners) are equal to the Standard Model couplings. Similarly, the gluons either couple to two KK-light or two KK-heavy quarks with the couplings borrowed from the Standard Model.

Nonideal delocalization

In [35] it is shown that, in contrast to the ideally delocalized scenario, a nonvanishing coupling between the W' and the light fermions is necessary for compatibility with the precision observables at the one loop level. This coupling $g_{W'ff}$ for which the bounds are derived is defined in the low-energy effective theory obtained by integrating out the heavy fermions and renormalized at the W' mass scale.

There are two operators contributing to $g_{W'ff}$ in the one loop analysis. The first one

$$O_1 = \overline{\Psi}_{0L} \Sigma_1 \not{A}_1 \Sigma_1^\dagger \Psi_{0L}$$

arises from integrating out the bulk fermions from diagrams of the type

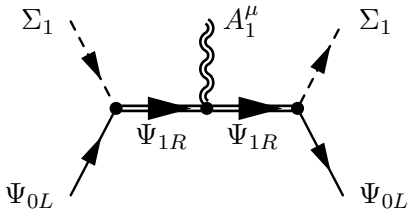

and corresponds to the Yukawa coupling ϵ_L in the full model which includes the heavy fermions. The second operator arises from loop corrections

$$O_2 = \overline{\Psi}_{0L} \left(D_\nu \left(\Sigma_1 F_1^{\mu\nu} \Sigma_1^\dagger \right) \right) \gamma_\mu \Psi_{0L}$$

Although this operator also encodes a coupling between the left-handed Standard Model fermions and the W', it has a nontrivial momentum structure. However, a

[9] As a slight exception to this rule, several couplings to right-handed fermions vanish completely due to the exact localization of the right-handed components of the massless fermions and their KK partners.

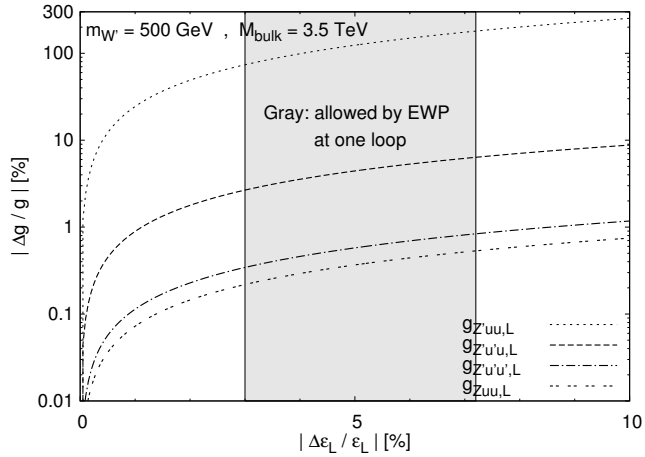

Figure 4.7: Examples of the change induced in the left-handed Zuu type couplings by tuning ϵ_L always from ideal delocalization.

nonlinear field redefinition in the spirit of on-shell effective field theory [43] can be used to apply the equation of motion to A_1 and convert O_2 to the same form as O_1 at the price of introducing additional higher dimension operators which are suppressed by a power of the gauge couplings and two powers of v. After the redefinition, O_2 also gives a contribution to $g_{W'ff}$ which is accounted for by ϵ_L in the full theory. Therefore, at tree level, the finite $g_{W'ff}$ can be accommodated in the full theory by tuning ϵ_L away from the value required by ideal delocalization.

From the fermion and gauge boson wavefunctions tab. 4.2 and tab. 4.1 we can estimate the value of ϵ_L required to generate a given $g_{W'ff}$

$$\epsilon_L \approx \frac{g_{W'ff}}{\tilde{g}} + \frac{x^2}{2}$$

Using the condition for ideal delocalization (4.23), we can solve for the relative change in ϵ_L

$$\epsilon_L \approx \epsilon_{L,0}\left(1 + x\frac{g_{W'ff}}{g}\right)$$

with $\epsilon_{L,0}$ being the value required for ideal delocalization. According to [35], $g_{W'ff}$ is constrained to be smaller than some $2-3\%$ of g, and we find that the required change to ϵ_L is of the same order.

At leading order, the wavefunctions of the right-handed fermions are independent of ϵ_L (c.f. tab. 4.2), and therefore, only the left-handed couplings are sensitive to the departure from ideal delocalization. Naively, we would expect the resulting relative change in the left-handed couplings to be of the same order of magnitude as the relative change in ϵ_L. However, this is not true for the couplings of the Standard Model fermions to the W' and the Z'.

For these couplings, the change of ϵ_L disrupts the cancellation among the contributions from different lattice sites, leading to a potentially much bigger change.

This is demonstrated in fig. 4.7 which shows the change induced in several of the left-handed Zuu type couplings. All couplings change within a few percent or even significantly less, with the exception of the $Z'uu$ coupling which changes by nearly 300% when ϵ_L is changed by 10%! However, although the relative change is sizable, the coupling still remains nearly two orders of magnitude smaller than the isospin gauge coupling and therefore close to fermiophobic. As the corresponding right-handed couplings to the Z' are considerably larger and not affected by nonideal delocalization, we shouldn't expect a big change in most physical observables.

For the W' couplings to Standard Model fermions, the situation is different: although the coupling is still virtually fermiophobic, the change induced by nonideal delocalization opens up the possibility of producing this resonance from fermions which is impossible in the case of the ideally delocalized scenario (c.f. chapter 8).

The gauge sector as well as the couplings to photons and gluons are not affected by nonideal delocalization.

Goldstone bosons

From expanding the Wilson lines $\Sigma_{1/2}$ in terms of the component fields and inserting the expansion into the Three-Site Lagrangian, we would obtain infinitely many couplings involving arbitrarily many Goldstone bosons. However, choosing unitarity gauge completely removes the Goldstone bosons from the spectrum, which is what we will be doing for the remainder of this work.

4.4 Widths and decay channels

In order to regularize the mass poles appearing in transition amplitudes, we have to calculate the widths of the new heavy resonances. In addition, some knowledge on the decay channels and branching ratios is required in order to identify suitable final states for the discovery of these particles. In this section we will only state the results of the calculation, the details of which can be found in appendix C.

Heavy gauge bosons

At leading order, the W' and Z' can either decay into two Standard Model gauge bosons or two Standard Model fermions fermions

All other potential $1 \to 2$ decay channels are forbidden due to the near-degeneracy of W' and Z'

$$\frac{m_{W'}}{m_{Z'}} = 1 + \mathcal{O}\left(x^2\right)$$

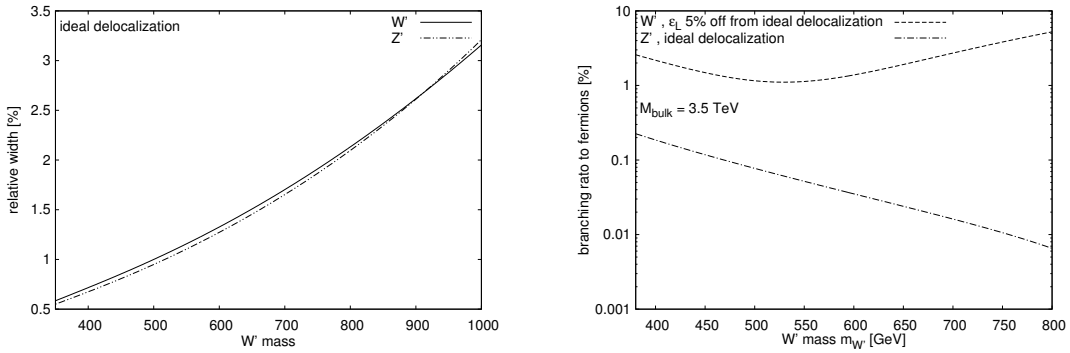

Figure 4.8: *Left:* Relative widths of W' and Z' as a function of $m_{W'}$.
Right: Branching ratio of the heavy gauge bosons going to fermions as a function of $m_{W'}$.

and the bound on the heavy fermion mass scale (4.26). The resulting relative widths are shown in fig. 4.8 left to be very similar for W' and Z' and of the order of $1-3\%$.

Compared to the fermionic decay channel, the bosonic decay channel receives an enhancement factor

$$\frac{m_{Z'}^4}{16 m_W^2 m_Z^2}$$

which is of order 100 and which comes from the decay into longitudinal modes. Therefore, although there are more final states and phasespace available for the fermionic channel, the bosonic final state is highly favored. This is demonstrated in fig. 4.8 right which shows the fermionic branching ratio of Z' and W' as a function of $m_{W'}$ (in the case of the latter, ϵ_L is tuned away from ideal delocalization by 5%). Evidently, the W' decays to more than 95% into gauge bosons, while the fermionic branching ratio of Z' is even lower than 1%.

Heavy fermions

For the heavy fermions there are two two possible decay channels at leading order:

The decay into the heavy isospin partners is forbidden due to the near-degeneracy of the heavy fermions. The $\mathcal{O}(\alpha_s)$ QCD contributions to the decays of the heavy quarks can be expected to be of order of several percent and may therefore be

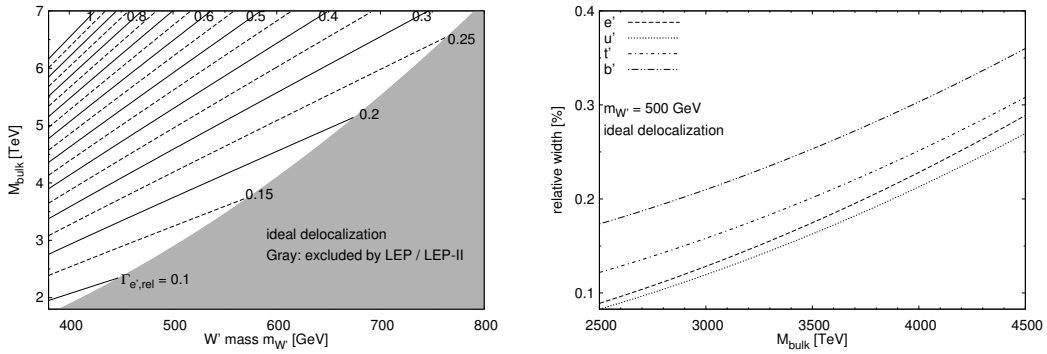

Figure 4.9: *Right:* Contour lines of constant relative e' width $\Gamma_{e',\text{rel}} = \frac{\Gamma_{e'}}{m_{e'}}$ in the $m_{W'}$ – M_{bulk} plane.
Left: Relative widths of e', u', t' and b' (including one loop QCD corrections) as a function of M_{bulk}.

worthwhile to include. These corrections can be written diagrammatically as

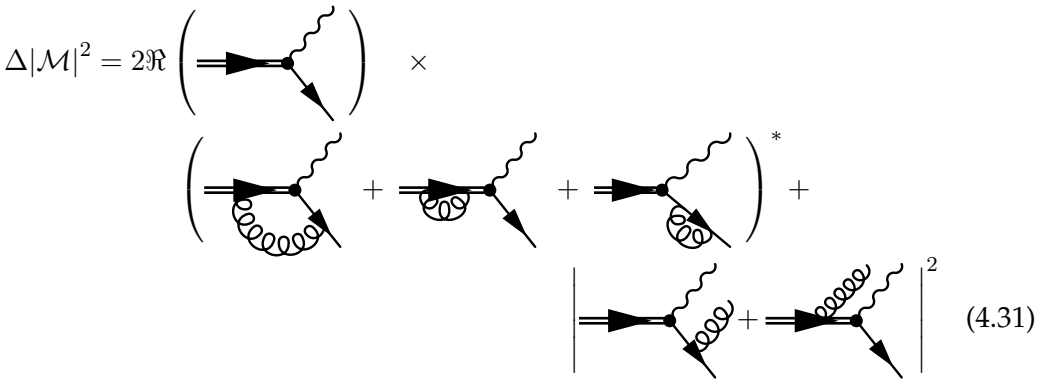

(4.31)

and are included in the calculation of the heavy fermions widths presented here; the analytical result can be found in appendix C.

Fig. 4.9 left shows contour lines of constant relative width $\Gamma_{e',\text{rel}}$ for the e' in the $m_{W'} - M_{\text{bulk}}$ plane. Evidently, there is a huge range of possible values from about 10% to more than 100%. However, direct detection as resonances at the LHC will only be possible for moderate values of M_{bulk}, say $\leq 4\,\text{TeV}$ anyway, and in this part of parameter space, the relative width does not exceed $30 - 40\%$.

The right-hand plot of fig. 4.9 shows the relative width of e', u', b' and t' as a function of M_{bulk} for $m_{W'} = 500\,\text{GeV}$. As the tree-level widths of the heavy fermions (with exception of the t' and b') turn out to be virtually identical, the difference between the e' and the u' width is solely due to the QCD loop corrections which are around 7.5% and show only very little variation over the parameter space. The t' is considerably broader than the partners of the light quarks, which is due to the wavefunctions of the t being fairly nonlocal to accommodate the high top mass, enhancing the couplings between t' and t.

The big surprise, however, is the b' which turns out to be nearly two times as broad as the partners of the light quarks. The reason for this unexpected effect is the right-handed $W^{(\prime)}b't$ coupling which is considerably enhanced by the nonlocal wavefunction of the right-handed top quark. This can be confirmed by looking at the sample spectrum in appendix B.

Concerning the branching ratios, fig. 4.10 left shows the fraction of d' decaying to heavy gauge bosons as a function of $m_{W'}$ for different values of M_{bulk}. While this varies a bit over parameter space, it's always around 50%. For d' which decay versus the light resp. heavy decay channels, fig. 4.10 right shows the fractions which goes into a W resp. W', demonstrating these channels to be preferred with branching ratios of around 65% over the Z / Z' channels. Both results are representative for the other heavy fermions with little variation over different values of M_{bulk}, again excluding the t' and b' due to the high top mass.

For these two, the respective results are shown in fig. 4.11 and fig. 4.12. Although the functional dependence on $m_{W'}$ and M_{bulk} is different, the branching ratio of both t' and b' into heavy gauge bosons is around 50% similarly to the partners of the light fermions. However, the branching ratios into $W^{(\prime)}$ and W are very different and exhibit a strong dependence on $m_{W'}$. Further investigation shows that, while still not drastic, the dependence on M_{bulk} is much more pronounced as for the other KK fermions.

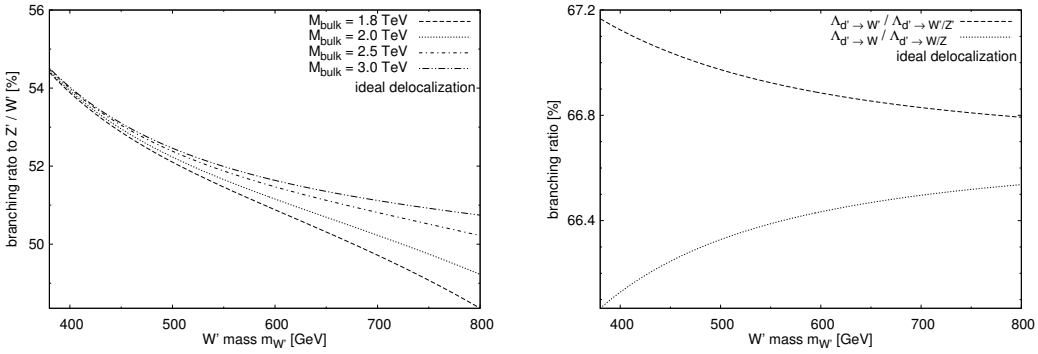

Figure 4.10: *Left:* The branching ratio of the d' into heavy gauge bosons as a function of $m_{W'}$ for different values of M_{bulk}.
Right: The fraction of the d' taking the light / heavy decay channels going to W / W'.

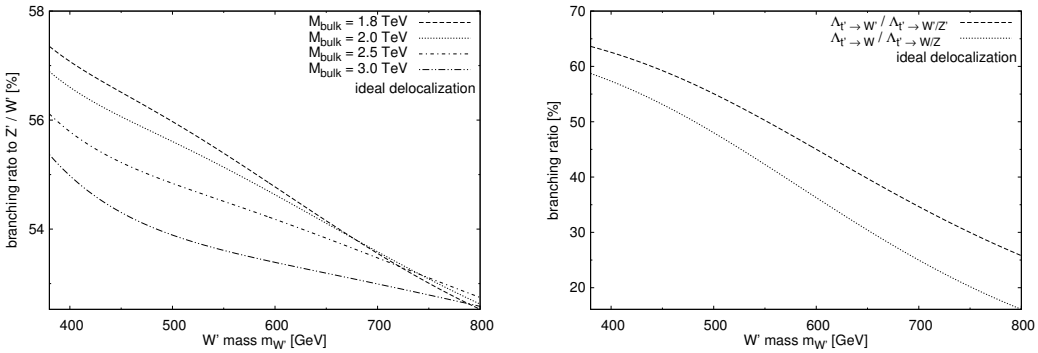

Figure 4.11: The same type of plots as fig. 4.10 for the t'.

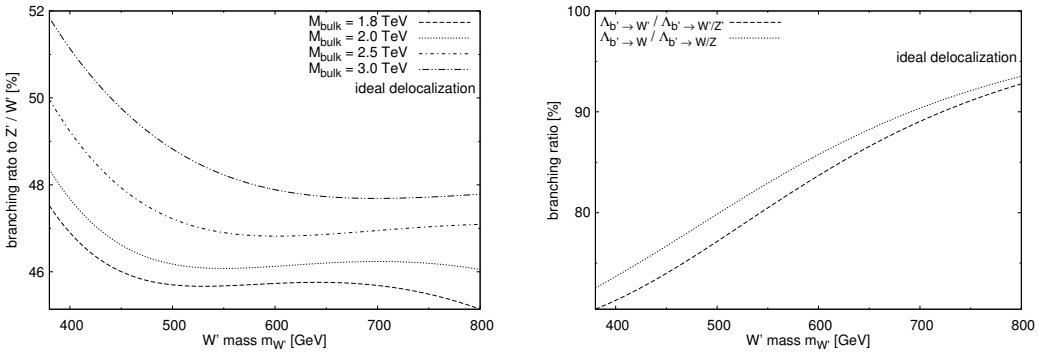

Figure 4.12: The same type of plots as fig. 4.10 for the b'.

Chapter 5

Tools for Phenomenology

> *This admitted, we may propose to execute, by means of machinery, the mechanical branch of these labours, reserving for pure intellect that which depends on the reasoning faculties.*
>
> (L. Menabrea, "Sketch of The Analytical Engine, invented by Charles Babbage", translated by Lady A. Lovelace)

So far, we have dealt with the formal structure of a quantum field theory (the Three-Site Model in our case) which defines the theory and allows to calculate observables such as scattering probabilities. To test the theory, we must connect these observables to the quantities that are measured in collider experiments or, more specific to this work, at the LHC. This is usually done with the help of computers via Monte Carlo eventgenerators.

In this chapter, we first briefly review the general structure of an event simulation. After that, the WHIZARD / O'Mega package which has been used for the numerical simulations presented in this thesis is introduced together with a small review of the challenges which have to be tackled by Monte-Carlo eventgenerators. In the third section, the implementation of the Three-Site Model into WHIZARD / O'Mega done as part of this thesis is discussed. Finally, in the last section, a brief overview over an interface between FeynRules [44] and WHIZARD / O'Mega is given.

5.1 The structure of an event simulation

The simulation of collision events at particle colliders can be roughly split into three building blocks. The first is the calculation and integration of the differential cross section which consists of evaluating the squared matrix elements and performing the phase space integration. The second block is the actual generation of an ensemble of events that is distributed according to the differential cross section. The third block consists of simulating the characteristics of the detector used for the actual observation of the particles produced in the events.

Obviously, the calculation and integration of the differential cross section is the necessary prerequisite for the generation of events. However, the detector simulation part completely factorizes from the other two steps. As it also is time consuming and requires an intricate knowledge of the inner workings of the actual machinery employed in the experiment, it is usually a good idea to perform studies on the feasibility of detecting new physics without a detailed detector simulation first. The result then is a machine-independent assessment of the chances for detection which, if it is positive, can be further improved by adding a detector simulation.

The calculation of the cross section also is an intricate process. The complications start with the initial state which, at a hadron collider like the LHC, consists of complicated bound states of quarks and gluons which we cannot describe from first principles. The final state usually consist of leptons, photons and mesons, and the latter again are bound states of QCD whose formation cannot be described with perturbation theory. Luckily, nature has arranged for asymptotic freedom and the factorization theorems of QCD [45] which allow us to split this complicated process of hadrons $\longrightarrow$ mesons $+ X$ into different regimes which decouple in good approximation.

More specifically, we may describe the initial hadrons at high energies as ensembles of non-interacting partons with the probability of finding a given parton carrying a given momentum fraction being described by parton distribution functions (PDFs) which are universal and independent of the process under consideration. In addition, the QCD interactions that lead to the fragmentation of the hard partons and the final hadronization to the observable bound states can also be approximately factorized.

In the end, as a good approximation, we can reduce the complicated scattering process to a "hard" core process consisting of two ingoing partons scattering into a handful of hard outgoing partons, photons and leptons. This then is convoluted with the PDFs to accommodate the hadronic initial state, and parton showers are added to describe the evolution of the small number of hard partons to a large number of soft ones. In a final step, empirical models can be applied to describe the formation of bound states from these soft partons in a process called "hadronization".

The only piece of this decomposition which we can calculate in perturbation theory is the hard matrix element describing the partonic core process (which fortunately usually also is the only part sensitive to new physics). Algorithms for performing the parton shower can also be obtained from first principles. However, there is to this day no way of calculating the PDFs from first principles, and only empirical models exist for the hadronization process.

In this work, we concentrate on the hard process and don't include parton showers, hadronization or a detector simulation. This is called a "parton-level" simulation which essentially relies upon the assumption that every parton produced in the hard scattering event is distinctly observable as a jet in experiment. While this is certainly not correct, it is a good assumptions for embarking on a study of the phenomenology of the Three-Site Model: it is only in the case of signif-

icant deviations from the Standard Model at this level that we can hope to observe something at the LHC.

5.2 WHIZARD / O'Mega

In this thesis, the software package WHIZARD / O'Mega [46] is used for the simulation of parton level events. This package actually consists of at least two separate programs, the optimizing matrix element compiler O'Mega and the core Monte Carlo and infrastructure code of WHIZARD.

O'Mega: fast generation of tree level matrix elements

Easy as it may seem from calculating the matrix elements for $2 \to 2$ by straightforward application of the Feynman rules, the evaluation of tree level matrix elements actually is very demanding on computer hardware and requires clever algorithms if it is to run in finite time.

The reason for this is the enormous growth of the number of Feynman diagrams if we increase the number of external lines. Consider, for example, ϕ^3 theory[1]. If we know all the tree level diagrams contributing to the n-point correlator of n particles with momenta $p_1, \ldots, p_n$, we can easily obtain those for the $n+1$-point function as all possible ways of attaching the p_{n+1} leg to one of the lines in the n-point diagrams, e.g.

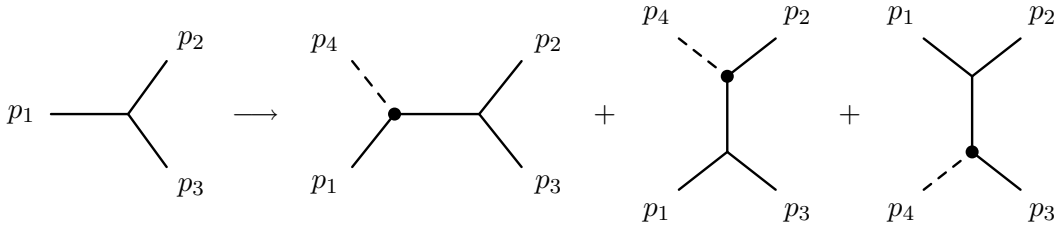

Therefore, we can calculate the number N_{n+1} of diagrams contributing to the $n+1$-point function from the number N_n of n-point diagrams as

$$N_{n+1} = L_n \cdot N_n$$

with the number of lines in any n-point diagram L_n. As attaching a leg increases L_n by 2, we deduce

$$L_n = 2n - 3$$

and therefore find

$$N_n = (2n-5)N_{n-1} = (2n-5)(2n-7) \cdot \ldots \cdot 1 = \prod_{k=2}^{n-1}(2k-3)$$

[1] While this is a pathological example of a field theory due to the indefinite potential, it actually is the easiest example when it comes to the combinatorics of Feynman diagrams. The only difference to other, physical models with arity three couplings (like QED) is the "dressing" of the ϕ^3-topologies with particle flavors which doesn't affect the asymptotic combinatorics.

By induction we have

$$N_n = (2n-5)!! = \frac{(2n-4)!}{2^{n-2}(n-2)!} \geq 2^{n-3}(n-3)!$$

Thus, the number of diagrams grows like factorial , and while we only have three diagrams for $n = 4$, we already have 105 diagrams for $n = 6$ and 10395 diagrams for $n = 8$.

Keeping in mind that the matrix element has to be evaluated at every phase space point under consideration it is obvious that this factorial growth of the number of Feynman diagrams kills off any attempt to perform a brute-force, diagram-by-diagram calculation. Things get even worse if a straightforward analytic calculation is attempted and therefore, traditional tools like CalcHEP [47] which perform very well for $2 \to 2$ processes have severe problems handling more than four particles in the final state.

Luckily, this is not the end of the story. If we consider again the addition of an additional leg to a diagram, we note that recalculating the whole diagram is a waste of resources. Reconsider the insertion of a line

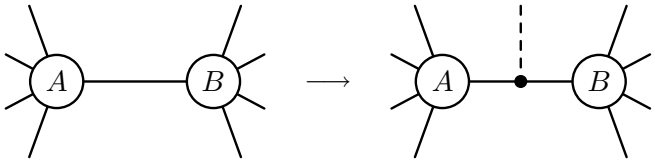

Evidently, we don't have to recalculate the blobs A and B, but just have to cut the line connecting the blobs and reattach them to a vertex together with the new leg. Also, if A and B are not only pieces of Feynman diagrams but instead complete correlation functions with all legs amputated except the leg extending to the middle vertex in the above diagrams (so-called "one particle off-shell wavefunctions" 1POWs), we can calculate a whole class of diagrams in this way. This observation suggests an iterative approach to the calculation of Feynman amplitudes which is potentially much more efficient than a straightforward calculation of all Feynman diagrams.

The potential savings in choosing a clever algorithm can be acknowledged by counting the number of possible 1POWs. In our example of ϕ^3 theory, these are uniquely enumerated by the distinct nonzero combinations of momenta which can be formed from external lines, the number of which

$$P_n = \binom{n}{1} + \binom{n}{2} + \ldots + \binom{n}{n-1} = (1+1)^n - 2 = 2^n - 2$$

only grows exponentially. Algorithms like the one used in the optimizing matrix element generator O'Mega exploit this redundancy to reduce the factorial growth in complexity of the calculation to an exponential one [48].

O'Mega represents the amplitude as a directed acyclical graph (DAG) of 1POWs from which it weeds out all redundancies that would arise from the recalculation

of 1POWs. Finally, this DAG is transferred to a backend which translates it into a representation suitable for performing numerical calculations. The only complete backend included in the O'Mega distribution is a FORTRAN 95 backend which emits a process library coded in FORTRAN 95 that can be called to evaluate the amplitude. The resulting code is clean, human readable, fast and can be automatically instrumented for numerical checks of gauge invariance. The matrix element is calculated in a completely numerical way by numerically multiplying spinors, four-vectors, Lorentz tensors etc.

WHIZARD: phase space, Monte Carlo integration and more

Once we have a way of calculating the matrix elements, we can go over to integrating them over phasespace, a step which turns out to be challenging for a number of reasons.

First, the dimensionality is high — subtracting four degrees of freedom due to momentum conservation and one due to rotational invariance around the beam axis, we have $3n - 5$ phasespace dimensions for n final state particles plus two additional dimensions for the parton distributions. Therefore, in a $2 \to 4$ process, we already have a 9-dimensional integral to evaluate. The complexity of deterministic numerical methods (e.g. Gauss-Kronrod) grows exponentially with the number of dimensions and therefore, such algorithms are not suitable for this type of integral.

This problem can be overcome by Monte Carlo methods. A simple method for Monte Carlo integration is drawing N random points $\mathfrak{p}_k$ in the integration domain Ω and then approximating the integral of f by

$$\int_\Omega dx\ f(x) \approx V \langle f \rangle = \frac{V}{N} \sum_{k=1}^{N} f(\mathfrak{p})_k$$

with the volume V of Ω.

If f is a probability density bounded from above by a number F_0, then we can use the set of pairs

$$\mathcal{W} = \{(\mathfrak{p}_1, f(\mathfrak{p}_1)), \ldots, (\mathfrak{p}_N, f(\mathfrak{p}_N))\}$$

to obtain an ensemble of points distributed according to f by drawing N numbers z_k between 0 and F_0 and then discarding all points $\mathfrak{p}_k$ for which $f(\mathfrak{p}_k)$ exceeds z_k. The resulting set of n surviving points

$$\mathcal{U} = \{\mathfrak{p}_{k_1}, \ldots, \mathfrak{p}_{k_n}\} = \left\{ \mathfrak{p}_k \;\middle|\; f(\mathfrak{p}_k) \leq z_k \right\}$$

can be significantly smaller than $\mathcal{W}$ but will obey the desired distribution. The set $\mathcal{W}$ is usually called a set of "weighted events" with statistical weights given by the $f(\mathfrak{p}_k)$, while $\mathcal{U}$ is called a set of "unweighted events" with the processes leading from $\mathcal{W}$ to $\mathcal{U}$ termed as "unweighting". If we want to simulate events at a particle collider, then it is the unweighted events we are interested in as they give a realistic estimate of the fluctuations induced by the statistics.

It can be shown that this Monte Carlo integration comes with an error that scales with $\frac{\alpha}{\sqrt{N}}$ for large N independently of the number of dimensions of the integral. The coefficient α is determined from the variance functional Δ

$$\Delta[f] = \int_\Omega dx\ f(x)^2 - \left(\int_\Omega dx\ f(x)\right)^2$$

Evidently, this is a small number only if the function f is well-behaved over Ω (aka doesn't fluctuate much).

However, the differential cross section we want to integrate is far from well-behaved: by the virtue of the propagators which have mass singularities, it fluctuates wildly, being close to zero in large regions of phasespace and nearly singular in others. The obvious problems arising from this large variation can be alleviated by choosing the ensemble of points $\mathfrak{p}_n$ not uniformly distributed in Ω but instead with respect to a nontrivial probability density $g(x)$. Provided we perform the replacement

$$f(x) \longrightarrow \frac{f(x)}{g(x)}$$

the Monte-Carlo method presented remains correct, but with the error coefficient α now determined by $\Delta\left[\frac{f}{g}\right]$.

Choosing a suitable g allows to reduce the Monte Carlo error drastically at the expense of more calculational time spent on the generation of the $\mathfrak{p}_i$. Therefore, g should be chosen such that the generation of the points is cheap enough to retain the speed gained by reducing Δ. As manual tuning of g usually is too cumbersome, a suitable density is usually determined in an adaptive process designed to minimize Δ over a restricted function space[2].

Monte-Carlo eventgenerators like WHIZARD usually start with an adaption phase during which g is optimized, then proceed with an integration phase where the integral is obtained and finally an event generation phase where (unweighted) events are generated. Ideally, new points are generated in all three phases to avoid pollution of the error estimates by statistical correlations.

In order to choose a suitable class of functions over which the density g is optimized, WHIZARD has some limited knowledge of diagrammatics and needs information on the vertices of the model. Prior to the start of the adaption phase WHIZARD then classifies all singular regions in phasespace that might contribute to the integral ("integration channels"). This information is passed to the Monte-Carlo core VAMP [49] (a multichannel modification of the VEGAS algorithm [50]) which chooses a suitable phasespace map ϕ_k for each channel. In these coordinates,

[2] It is an interesting fact that, for a restricted function space, the g_Δ which minimizes the variance functional Δ usually does not maximize the acceptance in the unweighting step (the percentage of points in $\mathcal{W}$ that is kept). It is also possible to optimize the acceptance instead of the variation in the adaption phase, increasing the performance of the unweighting step at the price of reducing the accuracy of the estimate for the integral.

a multidimensional grid function g_k together with a weight α_n is assigned to each channel, and the full parameterization of g reads

$$g(x) = \sum_{k=1}^{N} \alpha_k \left(g_k \circ \phi_k\right)(x)$$

with the sum running over all channels.

In the adaption process, g is optimized by adjusting the grids g_n as well as the weights α_n. After the adaption, the best g obtained in the adaption phase is used to calculate the Monte Carlo integral of the cross section. Finally, WHIZARD can use the grid and the integral to generate an ensemble of unweighted events which correspond to a given integrated luminosity.

The emphasis of the WHIZARD package lies on the fast generation of parton level events for BSM physics. Although its primary source of matrix elements is O'Mega, it can also interface other matrix element codes[3] like MadGraph [51] or CalcHep. It is capable of convoluting the partonic cross section with PDFs (via PDFLIB [52] or LHAPDF [53]) and can interface PYTHIA [54] for parton showering. The high numerical speed achieved by the combination WHIZARD / O'Mega allows for the simulation of processes with $6 - 8$ final state particles which is very hard to achieve with other tools. Other features include an integrated facility for event analysis which allows to create histograms on-the-fly from the generated event data.

The package is written in FORTRAN 95 with some perl glue being used to assemble the source and the matrix element code prior to compilation and evaluation[4]. For the exact treatment of color, the color flow decomposition [55] of Feynman amplitudes is used.

5.3 Implementation

In order to study the phenomenology of the Three-Site model with WHIZARD / O'Mega we have implemented the model into this package. In its current state, the code implements the Three-Site Model in unitarity gauge without flavor mixing and supports both ideal and non-ideal delocalization. It has been validated by numerical checks of the Ward identities in the limit $v \to 0$ as well as by direct comparison to the CalcHEP implementation used by [34] and (lately) to the FeynRules version done by N. Christensen et al. (see chapter 5.4).

The model implementation will be part of a future version of WHIZARD. In the meantime, the coupling library as well as modified versions of the O'Mega and WHIZARD packages which include the model can be downloaded from

`http://theorie.physik.uni-wuerzburg.de/~cnspeckn/`

[3] This functionality is present in the 1.9x branch of WHIZARD but will be dropped from version 2.0 onwards.

[4] This is only true for the 1.9x branch. WHIZARD 2.0 and higher compile the matrix elements at run time and link them dynamically without relying the perl component which is dropped.

O'Mega

In order to perform its duties as a matrix element generator, O'Mega needs some information about the model under consideration. This comes under the guise of a O'Caml module which contains the necessary definitions and functions needed by O'Mega to operate. We have written such a module implementing the Three-Site Model.

The implementation offers several options that can be (de)activated at the users leisure to change the set of particles vertices included. More specifically, it is possible to allow for flavor off-diagonal couplings (although these are set to zero at the moment, so this would currently just be a waste of resources), to leave out the heavy fermions and to discard the couplings of the W' to the leptons and to the first two quark generations. In addition, it is possible to replace the unitarity gauge propagators with Feynman gauge ones (this is necessary for using the massless limit).

Upon compilation of O'Mega, binaries are generated from the model modules which can then be called to generate code for the desired matrix elements. For the Three-Site Model, different binaries are generated for the different vertex sets described above both in colored and colorless versions (the colorless ones completely exclude QCD). A command line switch can be used to replace the unitarity gauge propagators.

More details on the implementation together with some snippets of the actual code can be found in app. D.2.

WHIZARD

In addition to the model implementation in O'Mega, WHIZARD requires a model file which defines the particles and vertices present in the model together with all parameters that can be changed at run time (and optionally also a list of secondary parameters calculated from these).

Writing the model file is a straightforward task. The only part which requires some trickery is the vertex list which WHIZARD requires to be loosely sorted with respect to the mass of the particles meeting at the vertex. Even if flavor violating couplings are excluded, the Three-Site Model contains 220 electroweak three-point couplings. To avoid the cumbersome and error-prone task of collecting and sorting all these couplings per hand, the list in the model file is generated directly from the O'Mega module by an O'Caml script.

The resulting vertex list may be too long for processes with 6+ particle final states, causing the phasespace mapping step to take forever or fail altogether. In this case, removing all vertices containing KK fermions provides a workaround without affecting the quality of the result overmuch.

The parameters[5] defined in the model file allow to set all Standard Model masses, the t, W and Z widths, the electromagnetic and strong coupling constants, the W'

[5]The actual names of the parameters are documented in the model file.

mass and M_{bulk}. This is enough to fix the model in the case of ideal delocalization (c.f. chapter 4.2). Nonideal delocalization can be activated by toggling a flag[6], making it necessary to supply a value ϵ_L to complete the set of model parameters in this case. The widths of the KK partners and the couplings are automatically calculated from the input parameters (see below). The inclusion of the QCD corrections into the heavy quark widths can be toggled by a flag, and another flag can be used to dump the spectrum and couplings (similar appendix B) to a file.

Unfortunately, the architecture of WHIZARD in its current form (version 1.9x) requires some patches to WHIZARD itself to make the model work. However, in a future version of WHIZARD, it will be possible to use the model without any changes to the actual WHIZARD code, allowing for the integration of the Three-Site Model into the package. More details on the required changes can be found in app. D.3.

Coupling library

To make the implementation work, a helper is required which calculates all masses, couplings and widths from the input parameters (c.f. chapter 4). This task is handled by a dedicated FORTRAN 90 library.

This library takes the input parameters and uses them to first calculate the masses and wavefunctions of the particles. The calculation is performed using exact analytic formulae in contrast to the expansions in x and ϵ_L given in chapter 4.2. The wavefunctions are then used to calculate the couplings as shown in chapter 4.3 (with the exception of the couplings to the photon which are determined by electromagnetic gauge invariance). After the couplings are calculated, the library then calculates the widths of the KK particles by looping over all possible two particle final states, using the analytical formulae given in app. C.1.

If activated, the $\mathcal{O}(\alpha_s)$ corrections to the heavy are also included using the analytic expressions of app. C.2. In this case, the LoopTools library [56] is utilized for the numerical evaluation of the one loop integrals appearing in the virtual corrections and for the dilogarithm appearing in the three-particle phase space integrals.

In order to validate the O'Mega implementation of the model by numerical checks of the Ward identities, the library supports a setup in which the full $\mathbf{SU}(2)_0 \times \mathbf{SU}(2)_1 \times \mathbf{U}(1)_2$ gauge symmetry is left unbroken. In this mode, the model is initialized from x, e, t and an arbitrary angle ϕ. The scale v and the Yukawa couplings $\lambda, \tilde{\lambda}, \lambda'$ are set to zero, resulting in vanishing mass matrices. The gauge couplings are initialized as

$$g = e\sqrt{1 + x^2 + t^{-2}} \quad , \quad \tilde{g} = \frac{g}{x} \quad , \quad g' = gt$$

As the mass matrices vanish, we can choose the wavefunctions freely (provided the wavefunction for KK partners are orthonormal). The W / W' and the fermion

[6] As WHIZARD only supports real numbers as parameters, a negative number is read as "false" and a positive number as "true".

wavefunctions are parameterized by the angle ϕ

$$f^W = f^{f_L} = \begin{pmatrix} \cos\phi \\ \sin\phi \end{pmatrix} \qquad f^{W'} = f^{f'_L} = \begin{pmatrix} -\sin\phi \\ \cos\phi \end{pmatrix}$$
$$f^{f_R} = \begin{pmatrix} \sin\phi \\ \cos\phi \end{pmatrix} \qquad f^{f'_R} = \begin{pmatrix} -\cos\phi \\ \sin\phi \end{pmatrix}$$

The wavefunction of the photon is left unchanged to avoid a change in the couplings to the photon (which are hardcoded), and the Z and Z' wavefunctions are chosen to form an orthonormal system together with f^γ

$$f^\gamma = e \begin{pmatrix} \frac{1}{g} \\ \frac{1}{\tilde{g}} \\ \frac{1}{g'} \end{pmatrix} \qquad f^{Z'} \propto \begin{pmatrix} -\frac{g}{2} \\ \tilde{g} \\ -\frac{g'}{2} \end{pmatrix} \qquad f^{Z} \propto \begin{pmatrix} -\frac{g'}{2\tilde{g}} - \frac{\tilde{g}}{g'} \\ \frac{g'}{2g} - \frac{g}{2g'} \\ \frac{\tilde{g}}{g} + \frac{g}{2\tilde{g}} \end{pmatrix}$$

with the normalization factors being suppressed for the sake of readability. This setup tries to avoid accidental cancellations in the couplings which would impair the effectiveness of the desired consistency check.

The library is not tied to WHIZARD but can also be used in a standalone fashion. Several tools are included which generate spectra (like e.g. app. B), density plots (e.g. fig. 4.5) etc. together with a wrapper that allows to access the masses, widths and couplings from Mathematica (in fact, many of the plots shown in chapter 4 were generated from Mathematica this way).

More information about implementation and usage of the library can be found in app. D.1 together with some snippets of code; more documentation can be found in the README file and in the woven source contained in the distribution which can be downloaded from the URL quoted at the beginning of this chapter.

5.4 FeynRules → WHIZARD interface driver

The implementation of a new model into an eventgenerator usually is a time-consuming and error-prone process, and careful testing is necessary to ensure that everything works as expected. The situation isn't improved by the fact that every eventgenerator has its very own format for specifying new models, follows its own conventions and has its own deficiencies and weak points which need to be worked around. Therefore, a generic format for specifying new models models which is as close as possible to the formal representation by a set of fields and a Lagrangian would be desirable.

The FeynRules package [44] is a step in this direction. FeynRules is a Mathematica package which can be used for the automatic generation of model files for different Monte Carlo eventgenerators. To this end, the particles in the model are specified in a format which is derived from FeynArts [57]. FeynRules then takes the Lagrangian (which can be entered in a way which is very close to the usual formal

notation) and calculates the Feynman rules from it. The generated rules can then be passed to an interface driver which generates a model file suitable for use with the event generator of choice.

This way, the cumbersome task of implementing the model has to be done just once and can be performed at a fairly abstract level with all the particularities of the different generators being take care of by the interface drivers. Having the model available in different eventgenerators is a very important step as all of them have their own strengths and weaknesses and cross-checking a result over different generators greatly improves the reliability of a prediction.

So far, the list of eventgenerators officially supported by FeynRules consists of CompHEP / CalcHEP, Sherpa [58] and MadGraph. During the preparation of this thesis, a new interface driver has been developed in corporation with N. Christensen which generates output for WHIZARD / O'Mega which will be included in a future distribution of FeynRules.

The driver is capable of producing the model module for O'Mega together with the model file and FORTRAN glue required by WHIZARD. It supports nearly all the features offered by FeynRules, including the free choice of any R_ξ gauge. The generated code has been successfully validated for the Standard Model and for the Three-Site Model, validation for the MSSM is in progress.

Chapter 6

W' Strahlung

After giving an overview over the model and the tools used for studying it in the last chapters, we now move on to presenting the results of the actual Monte Carlo simulations performed in this thesis. In this chapter, we start off with a discussion of the production of W' which are radiated from a light gauge boson in a process similar to Higgsstrahlung [59]. The process is presented in the first section, the details of the simulation are discussed in the second section and the result of the simulation is presented in the last part.

6.1 The Process

As the Three-Site Model is designed to mimic the Standard Model up to small corrections as far as the Standard Model particles are concerned, the most prominent signatures of the model at the LHC should be the resonances of the new heavy particles. While the LHC runs at an energy of $14\,\mathrm{TeV}$ in the proton center-of-mass system, the energy typically available for the partonic hard process is much smaller due to the parton distributions and only in the range of several TeV. Therefore, the heavy fermions will be hard to detect as resonances due their large mass $\geq 1.8\,\mathrm{TeV}$ (c.f. chapter 8), and the W'/Z' are thus the preferred candidates for direct detection.

The couplings between the heavy gauge bosons and the Standard Model fermions are suppressed due to their fermiophobic nature, and diagrams containing KK fermions are suppressed with the bulk mass M_{bulk} at the W'/Z' mass scale. Therefore, the processes that first spring into mind as promising candidates for producing the heavy gauge bosons on-shell involve the coupling of the KK particle to a W or Z line. Of this type there are basically two kinds of processes which are shown in fig. 6.1, namely the radiation from SM gauge bosons or the fusion of two SM gauge bosons.

As shown in chapter 4.4, the heavy gauge bosons decay to nearly 100% into Standard Model gauge bosons which then subsequently decay into fermions. Excluding all final states with more than two jets due to the large QCD backgrounds and all final states with more than one neutrino due to the missing momentum in-

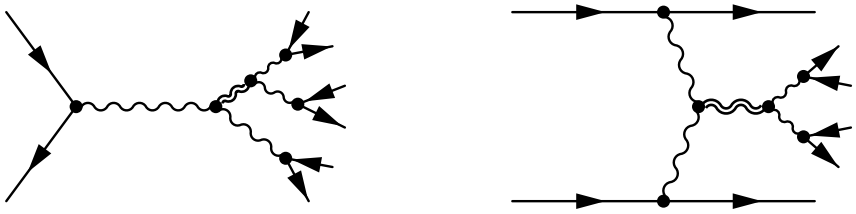

Figure 6.1: Diagrams contribution to the signal for the production of KK gauge bosons in strahlung type (*left*) and fusion type (*right*) processes.

formation, the following final states suitable for W'/Z' production remain:

strahlung		fusion	
W'	Z'	W'	Z'
$jj + 4l$ $jj + 3l + \nu$ $5l + \nu$	—	$jj + 3l + \nu$	—

Thus, W' strahlung seems to be the most promising candidate as it can be studied without involving any neutrinos, the missing momentum information of which would have to be made up for with tricks like using the transverse mass [60] instead of the invariant one or reconstructing the neutrino momentum from kinematic relations (see chapter 7).

The only source of notable contributions from the additional structure in the Three-Site Model to this process is the gauge sector, and therefore, the W' mass $m_{W'}$ is the only free parameter which has an influence on the result of the simulation. In particular, we are free to perform the simulations in the ideally delocalized scenario and can infer the dependence of the result on parameter space solely from varying $m_{W'}$[1].

In the context of this thesis, a simulation of the W' strahlung process via the $jj + 4l$ final state was performed using WHIZARD / O'Mega and the implementation of the Three-Site Model presented in chapter 5. Unfortunately, after the simulation was started, an already finished study of W' production via strahlung and fusion was published in [34]. However, the simulation performed in the context of this thesis still is of some value as it simulates the full six particle partonic final state using unweighted events, while the simulation performed in above reference uses CalcHEP and only simulates the four particle intermediate state $jjZZ$ using weighted events.

[1] Tuning ϵ_L away from ideal delocalization in principle allows for an additional contribution from a W' in the s channel, the coupling of which to the radiated W' is larger than that of the W. However, the coupling of the W' to the Standard Model fermions is still so small in this that the resulting change to the cross section in the peak region is only about 20% at best.

6.2 Simulation Details

In order to study the visibility of the W' resonance at the LHC, we have performed a full parton level simulation of the process $pp \longrightarrow jj + 4l$ with

$$p \in \{g, u, d\} \quad , \quad j \in \{g, u, d, c, s, b\} \quad , \quad l \in \left\{e^-, \mu^-\right\} \tag{6.1}$$

(and any of the respective antiparticles) for a total energy of $14\,\mathrm{TeV}$ in the proton CMS. Unweighted events have been generated for an integrated luminosity of $\int\mathcal{L} = 100\,\mathrm{fb}^{-1}$. The parton distributions were taken from the CTEQ6M series [61] and evaluated at the parton CMS energy in a running scale scheme.

All diagrams contributing to the signal are of the form

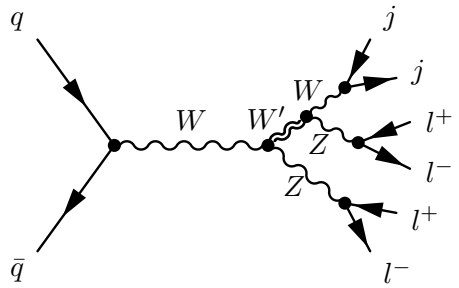

(the three-point couplings of the photon don't mix KK modes) and therefore, invariant mass cuts can be used to reduce the non-resonant contributions to the background. In particular, we have applied a cut

$$60\,\mathrm{GeV} \leq m_{jj} \leq 100\,\mathrm{GeV}$$

on the invariant mass of the jet pair and a cut

$$71\,\mathrm{GeV} \leq m_{ll} \leq 111\,\mathrm{GeV}$$

on the invariant mass of the lepton pairs, trying both possible combinations in the case of four leptons of the same generation and discarding events where no unique identification of the Z bosons could be achieved this way.

To further suppress the background, a p_T cut of

$$p_T \geq 20\,\mathrm{GeV}$$

was imposed on the final state particles. Another cut

$$-0.99 \leq \cos\theta \leq 0.99$$

was applied to the polar and intermediate angles of all final state particles, and in order to avoid infrared singularities, we imposed the condition

$$E \geq 10\,\mathrm{GeV}$$

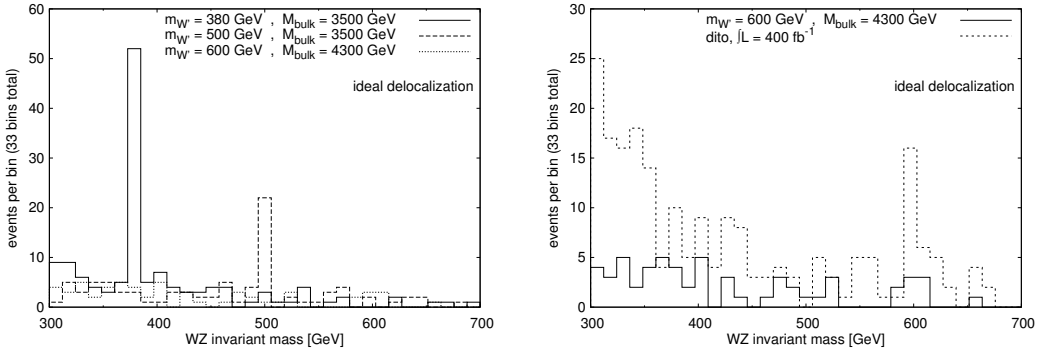

Figure 6.2: *Left*: W' resonance in the invariant mass of the Z/W pair for the W' strahlung process; different values of $m_{W'}$ and $\int\mathcal{L} = 100\,\mathrm{fb}^{-1}$.
Right: The W' resonance for $m_{W'} = 600\,\mathrm{GeV}$ and $\int\mathcal{L} = 100\,\mathrm{fb}^{-1}$, $400\,\mathrm{fb}^{-1}$.

on the energy of the incoming partons which corresponds to a small x cut

$$x \geq 1.4 \cdot 10^{-3}$$

(x being the fraction of the proton momentum which is carried by the parton).

As there is no way of determining which Z originated from the W', we have counted both possible combinations into the histograms similar to the analysis in [34]. Simulations have been performed in the ideally delocalized scenario at three points in parameter space

$$(m_{W'}, M_{\text{bulk}}) \in \{(380\,\mathrm{GeV}, 3.5\,\mathrm{TeV}), (500\,\mathrm{GeV}, 3.5\,\mathrm{TeV}), (600\,\mathrm{GeV}, 4.3\,\mathrm{TeV})\} \tag{6.2}$$

where M_{bulk} has been varied only for consistency in order to satisfy the precision constraints as discussed in chapter 4.2.

6.3 Results and Conclusions

Fig. 6.2 left shows the W' resonance peaks in the invariant mass distribution of the W/Z pair obtained from the simulation as described above. For $m_{W'} = 380\,\mathrm{GeV}$ and $m_{W'} = 500\,\mathrm{GeV}$, the peaks are clearly visible above the background, while only a very small bump is present in the data for $m_{W'} = 600\,\mathrm{GeV}$. This bump is reproduced in fig. 6.2 right together with the corresponding distribution for a higher integrated luminosity of $400\,\mathrm{fb}^{-1}$. With this increased luminosity, the $m_{W'} = 600\,\mathrm{GeV}$ resonance can also be clearly discerned.

In order to get a quantitative estimate of the significance of the resonances, let's define the signal N_s as the number N of events in the $\pm 20\,\mathrm{GeV}$ region around the peak in the Three-Site Model minus the the same quantity N_b in the Standard Model.

$$N_s = N - N_b$$

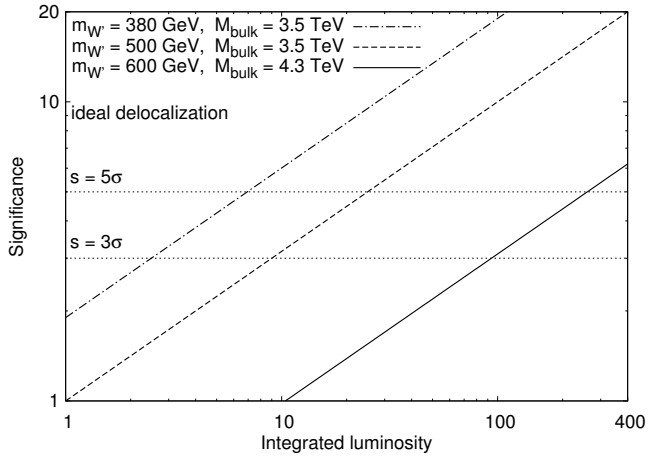

Figure 6.3: The statistical significance of the W' resonance peaks in W' strahlung as a function of the integrated luminosity together with 3σ and 5σ discovery thresholds.

We can then define the statistical significance of the signal as the deviation from the Standard Model relative to the standard deviation

$$s = \frac{N_s}{\sigma_{N_b}} = \frac{N - N_b}{\sqrt{N_b}}$$

which scales like $\sqrt{\int \mathcal{L}}$.

For the determination of the background N_b, we have performed a Standard Model simulation of the process for an integrated luminosity of $\int \mathcal{L} = 4000\,\mathrm{fb}^{-1}$ and downscaled the result by a factor of 40 in order to reduce the error on the significance induced by uncertainties in the background estimate. Fig. 6.3 shows the resulting significance as a function of the integrated luminosity together with the 3σ and 5σ discovery thresholds. The result for $m_{W'} = 380\,\mathrm{GeV}, 500\,\mathrm{GeV}$ looks encouraging with a 5σ discovery being possible within the first $7\,\mathrm{fb}^{-1}$ resp. $25\,\mathrm{fb}^{-1}$. For $m_{W'} = 600\,\mathrm{GeV}$ however, things are different, and nearly $300\,\mathrm{fb}^{-1}$ would be required for a 5σ discovery in this channel, which is (hopefully) at least still within LHC running time.

These results should be compared to the results obtained from simulating the $ZZjj$ intermediate state in [34]. To this end, the W' resonance for $m_{W'} = 500\,\mathrm{GeV}$ published by these authors is reprinted in fig. 6.4 left. The number of events contained in the peak is about 30 which is slightly smaller than the same number in our simulation (50 events, c.f. fig. 6.2 left). However, as the CalcHEP implementation of the model used in [34] and our WHIZARD / O'Mega implementation completely agree on the $2 \to 2$ process $pp \to W'Z$ and have also been validated against each other in numerous other processes, this discrepance is not overly disturbing and can be attributed to differences in the cuts, parameters and to the simulation of an intermediate state in [34].

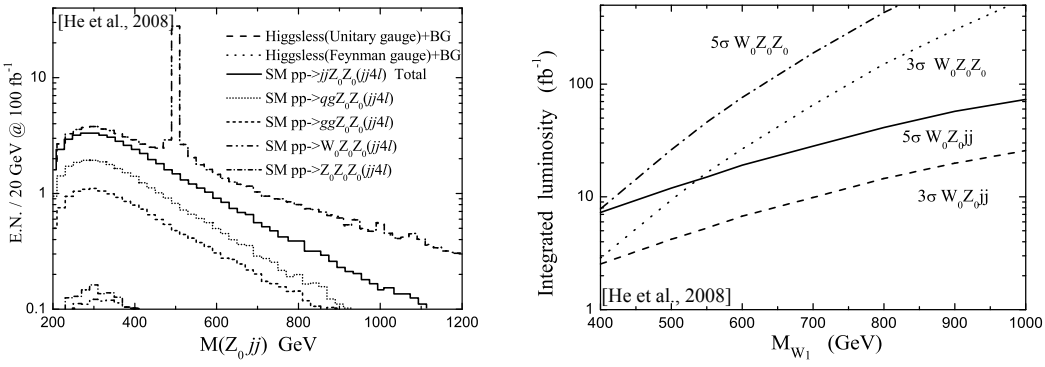

Figure 6.4: *Left*: The W' resonance peak in the W' strahlung process for $m_{W'} = 500\,\mathrm{GeV}$ as simulated in [34], plot taken from the same reference.
Right: The integrated luminosity required for a 3σ resp 5σ discovery as a function of the W' mass as obtained in [34], plot taken from the same reference. $W_0Z_0Z_0$ refers to the W' strahlung process, while W_0Z_0jj refers to the fusion process (see chapter 6.1).

Reprinted in fig. 6.4 right is the integrated luminosity required for a 3σ or 5σ discovery as a function of the W' mass as estimated in [34], the $W_0Z_0Z_0$ line referring to the W' strahlung process under consideration. The 5σ results are $10\,\mathrm{fb}^{-1}$, $20\,\mathrm{fb}^{-1}$ for $m_{W'} = 380\,\mathrm{fb}^{-1}$, $500\,\mathrm{fb}^{-1}$ and roughly consistent with our results quoted above. However, according to the authors of [34], a 5σ discovery for $m_{W'} = 600\,\mathrm{GeV}$ should be possible within $100\,\mathrm{fb}^{-1}$ which is much more optimistic than our estimate of $300\,\mathrm{fb}^{-1}$.

Unfortunately, [34] gives no details about how fig. 6.4 right was obtained and whether the higher mass region of the curve reflects the results of actual simulations or is an extrapolation. However, the strong decay of the signal observed in our simulations when going from $m_{W'} = 380\,\mathrm{GeV}$ to $m_{W'} = 600\,\mathrm{GeV}$ which leads to the high luminosity required for discovery is completely consistent with the result from performing a simulation of $pp \to W'Z$.

Concluding the discussion of our W' strahlung simulation, the discovery of the W' in this process at the LHC would be possible for the whole segment of parameter space shown to be compatible with the electroweak precision observables in [35]. However, depending on the W' mass, a huge amount of data taking might be necessary before any conclusive result is within reach. Another disadvantage of this process is that it only probes the electroweak structure of the Three-Site Model which coincides with other models, e.g. BESS [33]. In order to probe the fermion sector of the Three-Site Model which distinguishes it from other scenarios, other processes like the s channel production discussed in the next chapter must be explored.

Chapter 7

KK Gauge Bosons in the s Channel

In the previous chapter, a study of W' strahlung was presented. The major drawback of this process is that it only probes the gauge sector and doesn't reveal any information about the fermion sector. In sharp contrast, the production of the W' and Z' in the s channel is highly sensitive to the structure of the fermion sector due to the fermiophobic nature of the couplings between the KK gauge bosons and the light fermions. In this chapter, we discuss the prospects of exploiting this kind of process at the LHC.

After presenting an overview over the different channels of this type that might be accessible at the LHC in 7.1, we move on to the details of our simulations in 7.2. In 7.3 and 7.4 respectively, the results for Z' and W' production are discussed. It turns out that there are contributions from both W' and Z' to $jjl\nu$ type final states, and a possible strategy do disentangle these is presented in 7.5. The chapter is concluded in 7.6, and 7.7 contains a small collection of additional plots which have been omitted from the other sections for the sake of clarity.

Most of the work presented in this chapter is also covered in [62]. The results presented here at the parton level were supplemented by a detector simulation in the master's thesis of F. Bach [63].

7.1 The Processes

The main motivation behind the Three-Site Model is the delay of unitarity violation without introducing a Higgs while still satisfying the precision constraints imposed by the LEP / LEP-II data. As discussed in chapters 2 and 3, this implies strong constraints on the couplings between the KK gauge bosons (which are responsible for delaying unitarity violation) and the Standard Model fermions in this scenario. Therefore, if the LHC were to discover new resonances compatible with a W' and a Z', further tests of the fermion sector would be necessary in order to probe for such a type of new physics.

While sufficient for the bare discovery of the W' resonance, the W' strahlung process discussed in chapter 6 does not probe the structure of the fermion sector

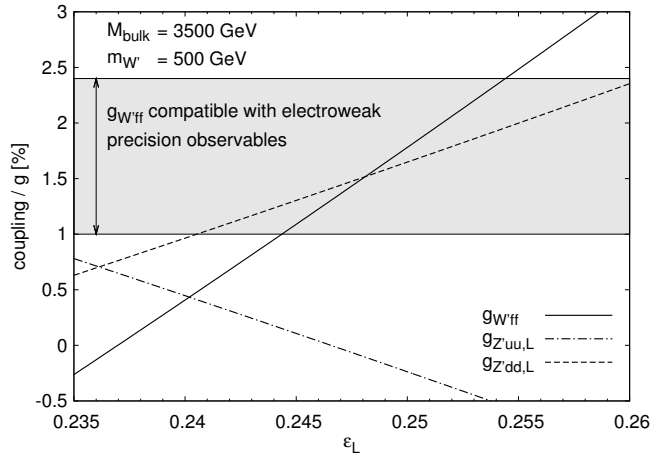

Figure 7.1: $g_{W'ff}$, $g_{Z'uu,L}$ and $g_{Z'dd,L}$ normalized to the site 0 gauge coupling g as a function of the delocalization parameter ϵ_L. The gray rectangle marks the range for $g_{W'ff}$ allowed by the precision observables as derived by the authors of [35].

and needs to be supplemented by other channels more sensitive to this part of the Three-Site Model. At a hadron collider, the simplest process involving the coupling of the W'/Z' to the light fermions is the production of these particles in the s channel. As the KK gauge bosons decay to nearly 100 percent into light gauge bosons (c.f. chapter 4.4), the signal in this kind of process is provided by diagrams of the type

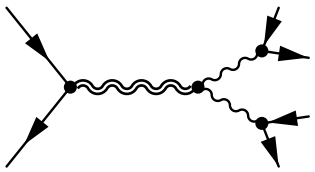

which involve one order of the heavily constrained couplings between light fermions and KK gauge bosons. Depending on the magnitude of those couplings, the total invariant mass of such final states should exhibit a W'/Z' resonance, the magnitude of which depends on the fermion (de)localization.

As discussed in chapter 4.3, the relevant couplings are restricted to be non-vanishing at the order of several percent of the isospin gauge coupling. Fig. 7.1 shows the coupling of the left-handed[1] light quarks to the W' and to the Z' for $m_{W'} = 500\,\mathrm{GeV}$ as a function of the fermion delocalization parameter ϵ_L (c.f. chapter 4.2), the corresponding plots for $m_{W'} = 380\,\mathrm{GeV}$, $600\,\mathrm{GeV}$ can be found in fig. 7.11. Remarkably, the left-handed coupling of the Z' to the up quark $g_{Z'uu,L}$ and that to the down quark $g_{Z'dd,L}$ change in exactly opposite ways under a variation of

[1]Recall that in the case of (approximately) massless fermions, the right-handed couplings to the W' vanish and those to the Z' are independent of ϵ_L (c.f. chapter 4.3).

the delocalization parameter. This is no accident and can be understood by using the normalization of the fermion wavefunction to recast the expression for the $Z'ff$ type couplings (4.30) as

$$g_{Z'ff,L} = \pm\frac{1}{2}\left(gf_0^{Z'}\left(f_{0,L}^f\right)^2 + \tilde{g}f_1^{Z'}\left(f_{1,L}^f\right)^2\right) + Yg'f_2^{Z'} \tag{7.1}$$

where Y is the hypercharge and the sign depends on the isospin of the fermion (recall that the only source of a dependence of (7.1) on ϵ_L is the wavefunction of the left-handed fermion f_L^f).

As the proton contains both up- and down quarks (albeit in the ratio $2:3$) and $g_{Z'uu,L}$ and $g_{Z'dd,L}$ both start with a positive value at the point of ideal delocalization, the effect of tuning ϵ_L away from nonideal delocalization partially cancels out from the Z' production cross section. In addition, there are also right-handed couplings of the same order of magnitude which don't depend on ϵ_L at all and therefore, we shouldn't expect Z' production in the s channel to be very sensitive to ϵ_L. W' production, however, is completely forbidden in the case of ideal delocalization and therefore highly sensitive to the value of ϵ_L.

The partonic final state of the processes is reached through a cascade of the KK gauge boson going into two Standard Model bosons which then in turn decay into two fermion pairs. Excluding final states with four jets due to the QCD background and final states with more than one neutrino due to the missing momentum information, the following final states remain:

W'	Z'
$jjl\nu$	$jjl\nu$
$jjll$	
$lll\nu$	

Evidently, the only such state suitable for the detection of the Z' resonance consists of two jets, a lepton and a neutrino, while we can choose from three different final states in the case of the W', $jjl\nu$ featuring the biggest branching ratio and $lll\nu$ the smallest one.

7.2 Simulation Details

If we want to have any chance of observing the Z' in the s channel or to take advantage of all three final states suitable for the observation of the W', we have to cope with final states containing one neutrino. Because the neutrino escapes the detector without leaving any traces, we have no direct information on its momentum which we require in order to measure the total invariant mass of the final state. Therefore, some trickery is necessary either to reconstruct the missing information or to live without it.

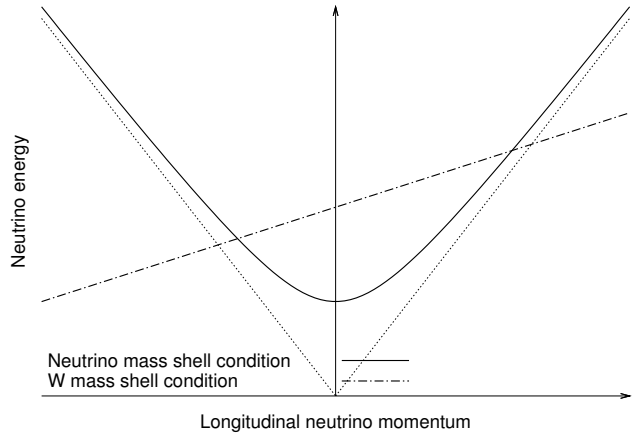

Figure 7.2: The two curves generated by the mass shell conditions for W and neutrino in the case of a W decaying to $l\nu$. The two points of intersection give the two possible solutions for the neutrino momentum.

The problem of missing momentum information is well known e.g. from SUSY decay chains where the transverse mass [60] is usually used instead of the invariant one in order to observe a resonance without requiring the full momentum information. However, our attempt to apply the transverse mass to the Z'/W' production processes under consideration was rather fruitless, the resonance in this observable being almost completely washed out.

Luckily, this is not the only trick available for dealing with the missing neutrino momentum. Even though we cannot observe the particle itself, we still can infer the projection $\vec{p}_\perp$ of its momentum on the transverse plane from transverse momentum conservation (assuming that the whole missing transverse momentum $p_{T,\text{miss}}$ originates from the neutrino). The mass shell conditions of neutrino and W boson (assuming that the neutrino originates from a W approximately on-shell) then give two additional conditions for the energy p_0 and the longitudinal momentum component p_L

$$p_0^2 - p_L^2 - |\vec{p}_\perp|^2 = 0 \tag{7.2a}$$

$$p_0 q_0 - p_L q_L - \vec{p}_\perp \vec{q}_\perp = \frac{m_W^2}{2} \tag{7.2b}$$

(with the momentum q of the corresponding lepton and the W mass m_W).

(7.2a) describes a hyperbola in the p_L - p_0 plane, while (7.2b) describes a straight line as depicted in fig. 7.2. These curves can have up to two points of intersection, one of which corresponds to the correct momentum of the neutrino. The two solutions can be obtained analytically as

$$p_0 = \frac{q_0^2\left(m_W^2 + 2\vec{p}_\perp\vec{q}_\perp\right) \pm q_L A}{2q_0\left(q_0^2 - q_L^2\right)} \quad , \quad p_L = \frac{q_L\left(m_W^2 + 2\vec{p}_\perp\vec{q}_\perp\right) \pm A}{2\left(q_0^2 - q_L^2\right)} \,,$$

with the abbreviation

$$A = q_0 \sqrt{\left(m_W^2 + 2\vec{p}_\perp \vec{q}_\perp\right)^2 + 4\vec{p}_\perp^{\,2}\left(q_L^2 - q_0^2\right)}\,.$$

It is easy to see from (7.2b) that the modulus of the slope of the straight line is always smaller than 1

$$\left|\frac{q_L}{q_0}\right| = \frac{|q_L|}{\sqrt{q_L^2 + |\vec{q}_\perp|^2}} < 1$$

while the asymptotes of the hyperbola (7.2a) have the slopes ± 1

$$p_0 = \sqrt{p_L^2 + |\vec{p}_\perp|^2} \to |p_L|$$

Therefore, there will be always (excluding the rare case of straight line being a tangent of the hyperbola) either two points of intersection or none at all, and this method of reconstructing the neutrino momentum will always yield two solutions, only one of which will usually be close to the correct value.

To cope with this, one can either try to find a kinematical criterion for discriminating between the two solutions (at the price of losing part of the signal) or count them both into the histograms. Of these two approaches, we have chosen the latter as it does not waste any precious signal events. The price to pay, however, is a doubling of the background.

Performing the actual simulation reveals that for roughly 10% (a number quite sensitive to the W' mass used in the reconstruction) of the events, the straight line doesn't intersect the hyperbola at all but instead lies slightly below the minimum, missing it by a small margin. Although we have chosen to simply remove these events from the histograms, more elaborate ways could be devised to deal with this, for example choosing the point on the hyperbola closest to the straight line or keeping m_W as a free parameter which is determined for each event such that (7.2a) – (7.2b) have one degenerate solution and using it as a cut variable. A more in-depth discussion of this issue can be found in [63].

In order to determine the discovery potential of the LHC in these processes at parton level, we have performed a Monte-Carlo simulation similar to that presented in the last chapter using our implementation of the model in WHIZARD / O'Mega with $\sqrt{s} = 14\,\mathrm{TeV}$ and an integrated luminosity of $\int\mathcal{L} = 100\,\mathrm{fb}^{-1}$. We have performed a complete simulation of the partonic processes $pp \to X$ with X being one of $jjl\nu$, $jjll$ and $lll\nu$ (using the assignments (6.1) and the same parton distributions as in chapter 6).

Fig. 7.3 shows the general structure of the diagrams contribution to the resonance signal. As the final state fermions are decay products of Standard Model gauge bosons, we can leverage cuts on the invariant mass m_{ff} of the visible final state fermion pairs in order to reduce the background[2]. More specifically, we

[2]Note that after the momentum reconstruction, the invariant mass $m_{l\nu}$ of the lepton-neutrino pairs is equal to m_W per definition, rendering an invariant mass cut on $m_{l\nu}$ pointless.

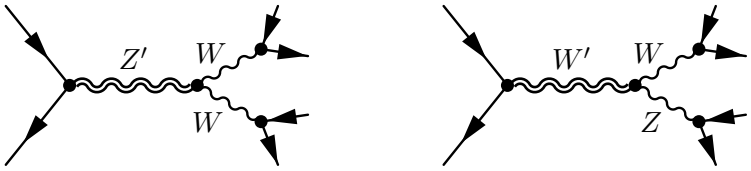

Figure 7.3: *Left*: General structure of the signal diagrams for Z' production in the s channel. *Right*: Dito, but W' production.

demanded m_{ff} to lie within the $\pm 5\,\mathrm{GeV}$ region around the invariant mass of the gauge boson which the fermions are to reconstruct:

$pp \to Z' \to jjl\nu$	$75\,\mathrm{GeV} \leq m_{jj} \leq 85\,\mathrm{GeV}$
$pp \to W' \to jjl\nu$	$86\,\mathrm{GeV} \leq m_{jj} \leq 96\,\mathrm{GeV}$
$pp \to W' \to jjll$	$75\,\mathrm{GeV} \leq m_{jj} \leq 85\,\mathrm{GeV}$ $86\,\mathrm{GeV} \leq m_{ll} \leq 96\,\mathrm{GeV}$
$pp \to W' \to lll\nu$	$86\,\mathrm{GeV} \leq m_{ll} \leq 96\,\mathrm{GeV}$

Note that the narrow cut window of $\pm 5\,\mathrm{GeV}$ is necessary in order to discriminate between the W' and Z' contributions to $jjl\nu$ (as the masses of Z' and W' are quasidegenerate, the resonance peaks fall together). However, it is quite unclear if ATLAS or CMS will be able to achieve enough precision in the measurement of the jet momenta for the separation to work out this way. This issue is discussed at length in section 7.5.

In the case of three leptons of the same generation in the final state, it is unknown which of the leptons originates from a decaying W. Therefore, we tried both possible combinations in this case and discarded the event if no unique identification of Z and W could be achieved this way.

In addition to the invariant mass cuts, we also applied p_T cuts of

$$p_T \geq 50\,\mathrm{GeV}$$

on the momenta of all visible particles and also on $p_{T,\mathrm{miss}}$ in order to suppress the background even more. Another cut of

$$-0.95 \leq \cos\theta \leq 0.95$$

was applied to the polar and intermediate angles of all visible particles, and as in the last chapter, we demanded

$$E \geq 10\,\mathrm{GeV}$$

for the incoming partons in order to avoid infrared divergences.

For each final state, we performed simulations for the three parameter space points (6.2), choosing three different values for ϵ_L from the interval allowed by [35]

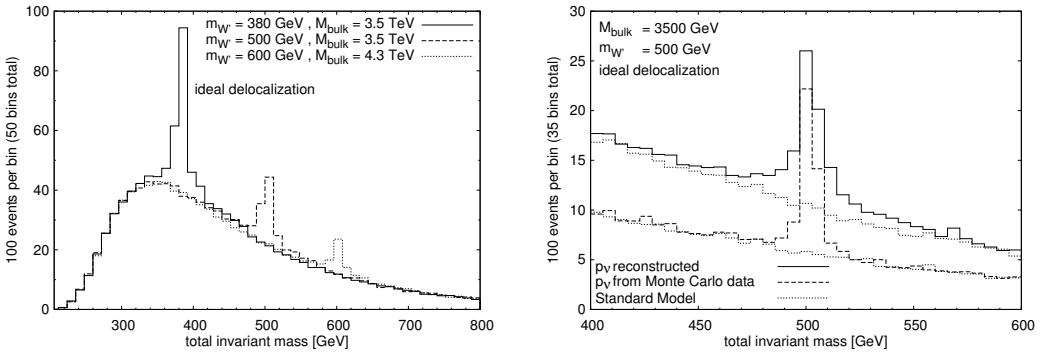

Figure 7.4: *Left*: Invariant mass distribution in $pp \to jjl\nu$ for different values of $m_{W'}$ and M_{bulk} (Z' production).
Right: The $m_{W'} = 500\,\text{GeV}$ peak obtained from the reconstructed neutrino momenta vs. the corresponding distribution obtained directly from Monte Carlo data.

in addition to the point of ideal delocalization (c.f. fig. 7.1 and 7.11) for each value of $m_{W'}$. As in the case of W' strahlung, the influence of M_{bulk} (which was varied only for consistency) on the processes is much too small to be resolved, with the results depending virtually only on $m_{W'}$ and the fermion delocalization ϵ_L.

7.3 Z' Production

Fig. 7.4 left shows the invariant mass distributions for $pp \to Z' \to jjl\nu$ for $m_{W'} = 380\,\text{GeV}$, $500\,\text{GeV}$ and $600\,\text{GeV}$ (again, recall that $m_{W'} \approx m_{Z'}$) in the case of ideal delocalization. For all three values of the mass, the resonance peaks are clearly visible, their overall size declining with growing W' mass as expected from the behavior of the parton distribution of the antiquark.

In order to check the reliability of the neutrino momentum reconstruction, fig. 7.4 right compares the $m_{W'} = 500\,\text{GeV}$ resonance peak obtained by reconstructing the neutrino momenta to the distributions created from the exact momenta taken directly from the eventgenerator. As expected, the reconstruction roughly doubles the number of background events, while the size of the peak remains more or less the same. However, the peak in the reconstructed data exhibits broad "sidebands" which closer investigation reveals to originate from the second solutions to the neutrino momentum in events within the peak.

The histograms in fig. 7.4 have been generated for the case of ideal delocalization in spite of the claim made in [35] (and discussed in chapter 4.2) that this case is in fact excluded by electroweak precision data. Instead, ϵ_L must be tuned away from ideal delocalization in order to allow for a small but nonvanishing $W'ff$ coupling. The resulting variation of the $m_{W'} = 500\,\text{GeV}$ resonance is shown in fig. 7.5 left for three different ϵ_L chosen from the allowed interval (c.f. fig. 7.1).

As argued in 7.1, this is rather small and causes a small increase of the event

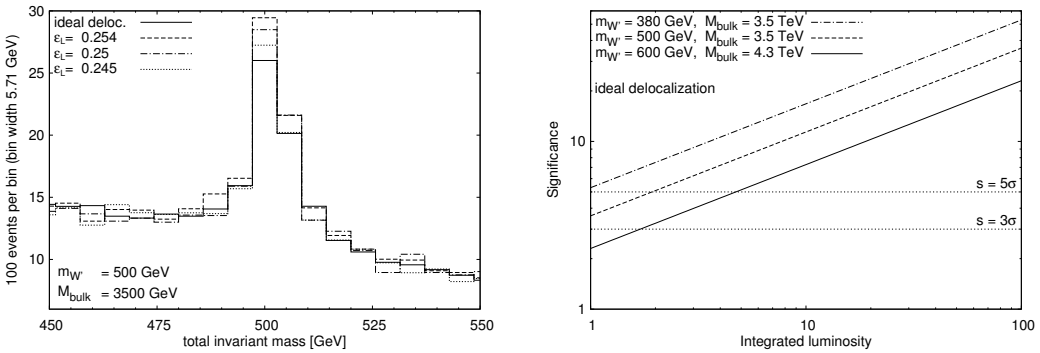

Figure 7.5: *Left*: The effect of tuning ϵ_L away from ideal delocalization (cf. fig. 7.1, 7.11) on the Z' peak.
Right: The significance as defined in the text as a function of the integrated luminosity. The dotted lines mark the 3σ resp. 5σ discovery thresholds.

count in the peak as compared to the case of ideal delocalization. Therefore, we will confine ourselves to presenting the results for this scenario, with the effect caused by varying ϵ_L being small and pushing in the direction of slightly larger significance.

To get a quantitative handle on the significance of the signal and to estimate the minimal luminosity necessary for discovering the Z', let's proceed similarly to the analysis in chapter 7.3 and define the raw signal N to be the number of events in the $\pm 20\,\mathrm{GeV}$ region around the peak. In order to estimate the background, we have generated SM events for an integrated luminosity of $\int\mathcal{L} = 400\,\mathrm{fb}^{-1}$, analyzed this data the in the same way as the Monte-Carlo data for the Three-Site Model and then downscaled the resulting distributions by a factor of 4 to reduce the error coming from fluctuations in the background. We denote the number of background events in the $\pm 20\,\mathrm{GeV}$ region around the peak obtained this way by N_b.

We then again define the signal N_s as

$$N_s = N - N_b$$

The determination of the standard deviation of the background is complicated by the fact that the pairs of entries in the histograms for the different solutions to the neutrino momentum lead to a nontrivial statistical correlation in the histograms. For simplicity, let's assume that the background is simply doubled by the momentum reconstruction

$$N_b = 2N_b'$$

The standard deviation of σ_{N_b} of N_b must scale accordingly

$$\sigma_{N_b} = 2\sigma_{N_b'} = 2\sqrt{N_b'} = \sqrt{2N_b}$$

resulting in the statistical significance defined as in chapter 6.3 being reduced by a

factor of $\sqrt{2}$

$$s = \frac{N_s}{\sigma_{N_b}} = \frac{N - N_b}{\sqrt{2N_b}}$$

which nevertheless scales like $\sqrt{\int \mathcal{L}}$.

The significance of the signal in the ideally delocalized scenario thus calculated is shown in figure 7.5 right as a function of the integrated luminosity together with the 5σ and 3σ discovery thresholds. The 5σ thresholds are approximately $1\,\mathrm{fb}^{-1}$, $2\,\mathrm{fb}^{-1}$, $5\,\mathrm{fb}^{-1}$ for $m_{W'} = 380\,\mathrm{GeV}$, $500\,\mathrm{GeV}$, $600\,\mathrm{GeV}$, respectively. Considering the fact that tuning ϵ_L into the region allowed by the precision observables does not significantly change the signal, the Three-Site Z' may be discovered in this process as early as in the first $1 - 2\,\mathrm{fb}^{-1}$ and even in the worst case can be expected to manifest itself in the first $10 - 20\,\mathrm{fb}^{-1}$ of data.

7.4 W' Production

In the case of W' production we have the three different final states $jjl\nu$, $jjll$ and $lll\nu$ which we can use to look for the resonance peak. The left column of fig. 7.6 shows the resulting invariant mass distributions for these final states, again for all three $m_{W'}$ values (6.2) under consideration with ϵ_L chosen to yield roughly the maximum allowed value of $g_{W'ff}$ (c.f. fig. 7.1 and fig. 7.11). The peaks are clearly visible in all three final states, with the total number of events contained in them dropping in the order (biggest to smallest)

$$jjl\nu \quad \longrightarrow \quad jjll \quad \longrightarrow \quad lll\nu$$

due to the declining branching ratio (as can be easily seen by simply counting the number of final states).

However, going from $jjl\nu$ to $jjll$, the need for the reconstruction of the neutrino momentum with the associated doubling of the background events also goes away, and the possibility of cutting on the invariant mass of the W enhances the ratio of signal to background. Furthermore, the hadronic background is completely removed when going to the fully leptonic final state $lll\nu$, leading to the much cleaner signal visible in fig. 7.6 in spite of the even smaller branching ratio.

Contrary to the Z' case, the signal in the W' production process must be proportional to the square of the $g_{W'ff}$ coupling and is therefore highly sensitive to the fermion delocalization parameter ϵ_L. The corresponding dramatic change in the $m_{W'} = 500\,\mathrm{GeV}$ resonance induced by changing ϵ_L within the allowed part of parameter space is shown in the right column of fig. 7.6, the change in the peaks for the other W' masses in fig. 7.10. From these distributions, it is evident that the peak can be nearly completely removed within the allowed region of parameter space by choosing a suitable value for ϵ_L.

As would be expected, the resonance completely vanishes in the (albeit forbidden) case of ideal delocalization. The histograms show that this is also true for the

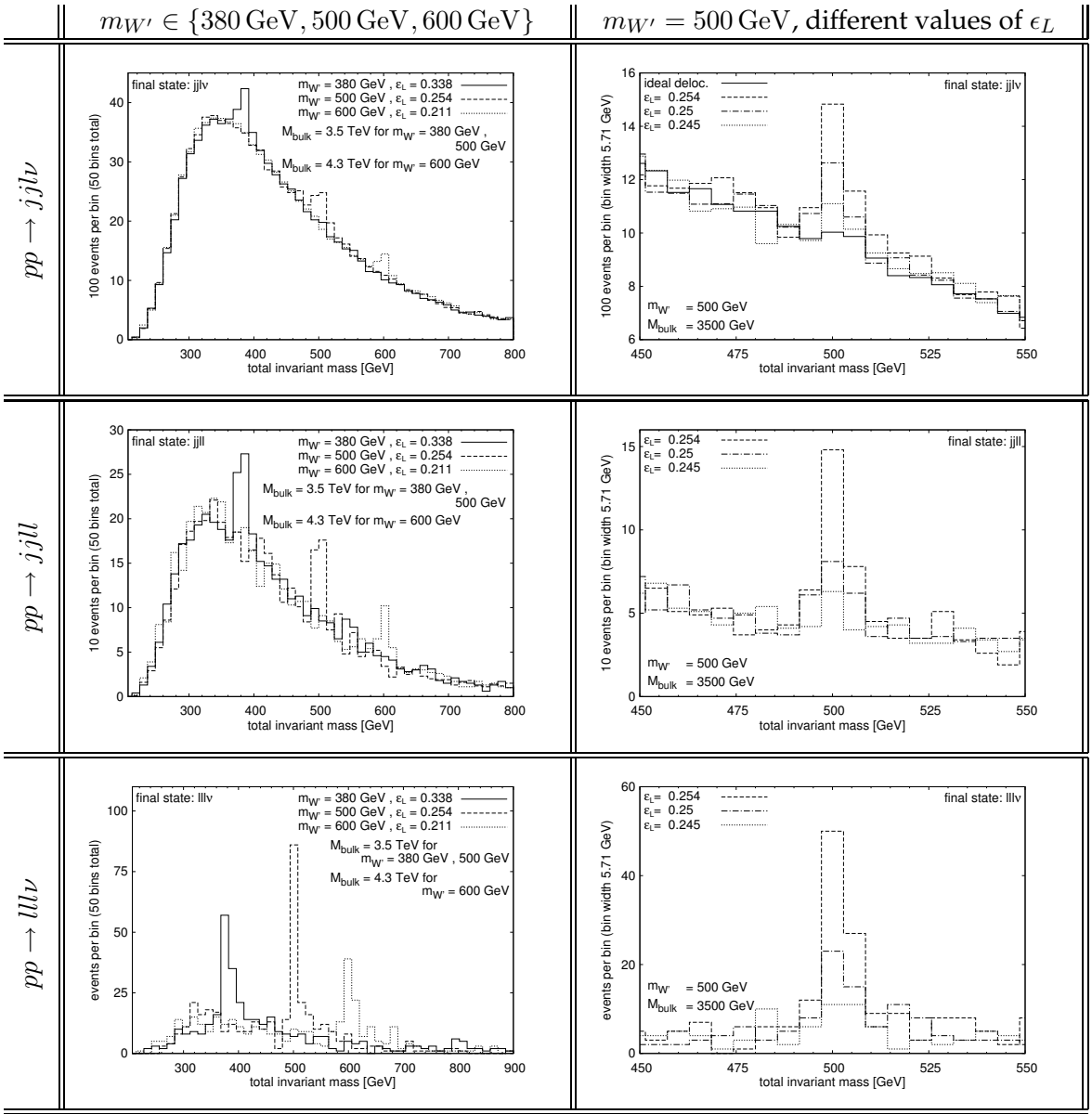

Figure 7.6: *Left column:* The W' resonance peaks for the three different final states under consideration. Different values of $m_{W'}$, near-maximal $g_{W'ff}$.
Right column: Close-up of the $m_{W'} = 500\,\mathrm{GeV}$ resonance peak for different values of ϵ_L from the interval allowed by the precision observables.

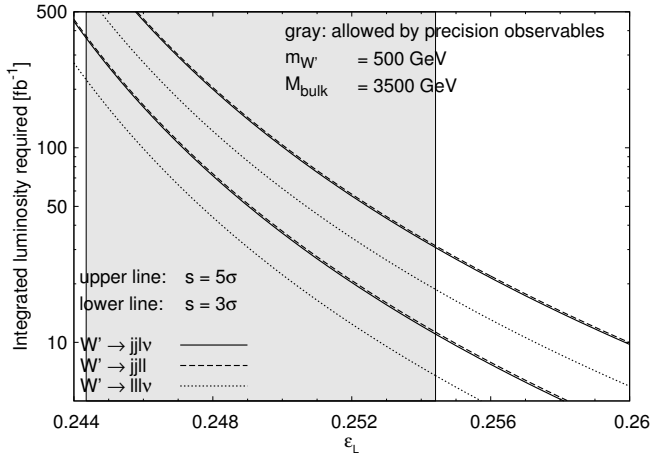

Figure 7.7: The integrated luminosities required for a 3σ resp. 5σ discovery of the W' in the s channel as a function of ϵ_L. Different final states, $m_{W'} = 500\,\mathrm{GeV}$.

$jjl\nu$ final state(with the exception of $m_{W'} = 380\,\mathrm{GeV}$ in which case a small peak from misidentified Z' events remains), demonstrating that the $\pm 5\,\mathrm{GeV}$ cut around the W mass is sufficient to separate W' and Z' contributions to this final state at least at parton level if the smearing cause by measurement errors is not take into account.

Defining the significance of the signal in exactly the same way[3] as in 7.3 for Z' production (without the additional factor $\sqrt{2}$ for $jjll$), we can exploit the quadratic dependence of the signal on $g_{W'ff}$ in order to obtain an estimate of the integrated luminosity required to yield a signal with a given significance. The 5σ resp. 3σ result is shown in fig. 7.7 as a function of ϵ_L for $m_{W'} = 500\,\mathrm{GeV}$; the corresponding plots for the other two masses are shown in fig. 7.12.

From these curves it is clear that, while the actual result varies a bit over parameter space, the performance of the different final states is fairly comparable at the parton level. However, once detector effects are included, it is likely that the fully leptonic final state is preferred due to the more precise measurement of the lepton momentum and the absence of complicated QCD backgrounds — an assertion which is confirmed by the detector simulation performed in [63].

As far as the prospects of discovering the W' in this process are concerned, fig. 7.7 and 7.12 clearly demonstrate that there are regions in parameter space easily accessible in the first $10 - 20\,\mathrm{fb}^{-1}$, while it would take more than $500\,\mathrm{fb}^{-1}$ for a 5σ discovery in other regions which is most likely out of question at the LHC.

[3] As the total number of events is much lower in the $jjll$ resp. $llll\nu$ final states when compared to $jjl\nu$, we generated the Standard Model backround for these by downscaling simulations for $\int\mathcal{L} = 1000\,\mathrm{fb}^{-1}$ resp. $\int\mathcal{L} = 5000\,\mathrm{fb}^{-1}$.

7.5 Disentangling the $jjl\nu$ final states

Since flavor tagging is impossible for light quark flavors, we have to rely on invariant mass cuts on the jet pairs in order to be able to separate the case of the two jets in $jjl\nu$ coming from the decay of a W in Z' production from that of the jets being produced by a decaying Z in W' production. However, it may very well be impossible to obtain a resolution of order $\pm 5\,\mathrm{GeV}$ in the jet invariant mass from experimental data. In the following, we model the effect of the measurement error on the W'/Z' separation with a gaussian smearing of the invariant mass of the jets.

In the ideal case of exact m_{jj} measurement, events coming from the decay of a intermediary $W\,/\,Z$ are distributed according to a Breit-Wigner distribution

$$p_b(x, m, \Gamma)\, dx = \frac{n_b(m,\Gamma)^{-1}}{\left(x^2 - m^2\right)^2 + \Gamma^2 m^2}\, dx$$

with the normalization factor

$$n_b(m,\Gamma) = \frac{\pi}{4m^3}\left(1 + \frac{\Gamma^2}{m^2}\right)^{-\frac{3}{4}} \sin^{-1}\left(\frac{1}{2}\operatorname{atan}\frac{\Gamma}{m}\right)$$

Emulating the measurement error in the jet mass by convoluting p_{bw} with a gaussian of standard deviation σ

$$p_{\mathrm{g}}(x, \sigma)\, dx = \frac{1}{\sqrt{2\pi}\sigma} e^{-\frac{x^2}{2\sigma^2}}\, dx$$

we obtain the smeared distribution

$$p_{\mathrm{sm}}(x, m, \Gamma, \sigma)\, dx = \int_0^\infty dy\, p_b(y, m, \Gamma) p_{\mathrm{g}}(x - y, \sigma)$$

Figure 7.8 shows the effect of this smearing on the Breit-Wigner peaks of the Z and the W. Turning on the smearing and increasing σ causes the sharp Breit-Wigner peaks to decay rapidly, and for $\sigma = 10\,\mathrm{GeV}$, only two very broad bumps are left. The consequence is that, if a cross section has one contribution which stems from the decays of a virtual Z and one coming from a virtual W, any attempt to isolate the Z contribution by cutting on the resonance will inevitably also select events coming from the W decay contaminating the sample (and vice versa). Therefore, our analysis of the $jjl\nu$ final state will show a W' peak even in the case of ideal delocalization which is caused by jet pairs from a decaying W misidentified as a Z.

If we try to isolate the W peak with a cut on the invariant mass m_{jj}

$$L_W \leq m_{jj} \leq U_W$$

and the Z peak with a cut

$$L_Z \leq m_{jj} \leq U_Z$$

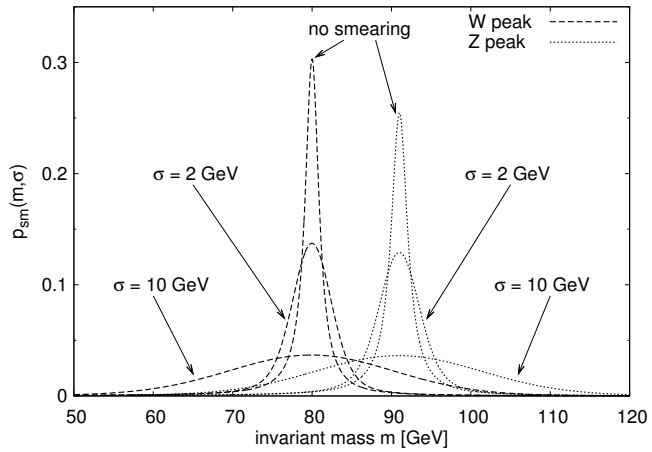

Figure 7.8: The effect of a gaussian smearing on the Breit-Wigner shape of the W and Z resonances for various widths σ of the gaussian.

then the resulting event counts $\widetilde{N}_W, \widetilde{N}_Z$ can be calculated from the true event counts N_W, N_Z coming from a decaying W or Z via a matrix T as

$$\begin{pmatrix} \widetilde{N}_W \\ \widetilde{N}_Z \end{pmatrix} = \begin{pmatrix} T_{WW} & T_{WZ} \\ T_{ZW} & T_{ZZ} \end{pmatrix} \begin{pmatrix} N_W \\ N_Z \end{pmatrix}$$

with entries

$$T_{ij} = \int_{L_i}^{U_i} dm\, p_{\text{sm}}(m, m_j, \Gamma_j, \sigma)$$

Inverting T we can calculate the event counts N_W and N_Z

$$\begin{pmatrix} N_W \\ N_Z \end{pmatrix} = T^{-1} \begin{pmatrix} \widetilde{N}_W \\ \widetilde{N}_Z \end{pmatrix} \tag{7.3}$$

The entries of T give the probability of (mis)identifying an event and can be readily calculated numerically; for example, choosing cuts

$$L_W = 60\,\text{GeV} \quad , \quad U_W = 85\,\text{GeV} \quad , \quad L_Z = 86\,\text{GeV} \quad , \quad U_Z = 111\,\text{GeV}$$

yields

$$T \approx \begin{pmatrix} 0.64 & 0.27 \\ 0.29 & 0.62 \end{pmatrix} \quad , \quad T^{-1} \approx \begin{pmatrix} 1.9 & -0.85 \\ -0.89 & 2.0 \end{pmatrix}$$

This way, we can in principle use T to disentangle the contributions from the W and Z resonances to the signal in the presence of a measurement error which causes the Breit-Wigner peaks to lose their shape. However, in order to apply this to actual data, it is vital to separate the signal from both the reducible and the irreducible backgrounds as these don't obey a Breit-Wigner distribution.

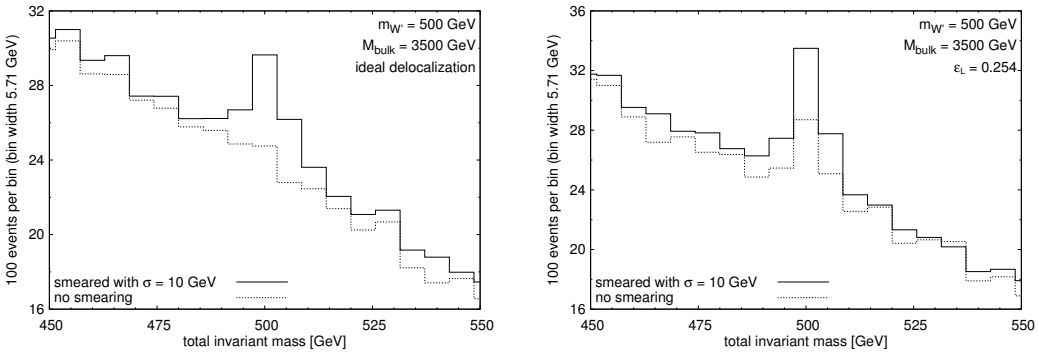

Figure 7.9: *Left*: Signal in the W' detection channel for the case of ideal delocalization smeared with a gaussian error.
Right: The same for the case of nonzero $g_{W'ff}$

In order to estimate the significance of a signal obtained this way, we calculate the standard deviation σ_{N_i} of N_i according to

$$\sigma_{N_i} = \sqrt{\sum_{j \in W,Z} \left(T_{ij}^{-1}\right)^2 \sigma_{\widetilde{N}_j}^2} \tag{7.4}$$

Calculating the fluctuations of $\widetilde{N}_j$ is a bit tricky as the neutrino momentum reconstruction adds statistically correlated pairs of events to the sample. According to the analysis performed in the last two sections 7.3 and 7.4, we obtain the number of events $\widetilde{N}$ in the peak by subtracting the background (aka Standard Model expectation) N_b from the total number of events N_{tot}

$$\widetilde{N} = N_{\text{tot}} - N_b$$

The Standard Model value N_b comes from a theoretical calculation and is by definition free of statistical fluctuations[4]. The total number of events N_{tot} contains $\widetilde{N}$ events originating from the resonance which we idealize to be free of double-counting and N_b background events which contain the correlated double counts. Putting the pieces together, we have

$$\sigma_{\widetilde{N}} = \sigma_{N_{\text{tot}}} = \sqrt{\widetilde{N} + 2N_b} = \sqrt{N_{\text{tot}} + N_b}$$

which we can now plug into (7.4) in order to calculate the statistical fluctuation we have to expect for the reconstructed event counts and finally arrive at

$$\sigma_{N_i} = \sqrt{\sum_{j \in W,Z} \left(T_{ij}^{-1}\right)^2 (N_{t,j} + N_{b,j})} \tag{7.5}$$

[4]Of course, this is a simplification which is not quite true in our analysis where we obtain N_b from a Monte-Carlo simulation. However, due to our generating and downscaling a surplus of events, the error on N_b is smaller than that on N_{tot}, and in a more serious analysis of experimental data, σ_{N_b} could be made arbitrarily small by investing enough time into its determination.

ideal delocalization				
	$\widetilde{N}_i$	s_i	N_i	$\frac{N_i}{\sigma_{N_i}}$
$i = W$	3193	17	5126	13
$i = Z$	1371	7.5	-96.10	0.24

$\epsilon_L = 0.254$				
	$\widetilde{N}_i$	s_i	N_i	$\frac{N_i}{\sigma_{N_i}}$
$i = W$	3767	21	5628	14
$i = Z$	2083	11	811.6	2.0

Table 7.1: Comparison of the signals $\widetilde{N}_{W/Z}$ obtained with an gaussian smearing of the invariant mass of the jets with $\sigma = 10\,\mathrm{GeV}$ to the "true" signals $N_{W/Z}$ calculated from the measured ones via the transfer matrix T^{-1}.

For a simulation of the effect of the measurement error our analysis we have randomly distributed the invariant mass of the jet pairs within a gaussian with width $\sigma = 10\,\mathrm{GeV}$ centered around the correct value calculated from Monte Carlo data. We then performed the same analysis as in the last two sections 7.3 and 7.4 with $m_{W'} = 500\,\mathrm{GeV}$ and $m_{\text{bulk}} = 3.5\,\mathrm{TeV}$ both for $\epsilon_L = 0.254$ and for the ideally delocalized scenario. The only difference to the previous analysis are the cuts on m_{jj} which we enlarged to

$$60\,\mathrm{GeV} \leq m_{jj} \leq 85\,\mathrm{GeV} \quad \text{resp.} \quad 86\,\mathrm{GeV} \leq m_{jj} \leq 111\,\mathrm{GeV}$$

Fig. 7.8 shows the resulting effect on the W' peak for the cases of ideal delocalization (left) and for $\epsilon_L = 0.254$ (right). In both cases a peak is clearly visible, which in the ideally delocalized scenario is only composed of events with jets coming from a decaying W misidentified as a Z.

The number of signal events $\widetilde{N}_{W/Z}$ after smearing, the significance $s_{W/Z}$ of these calculated similarly to the last sections, $N_{W/Z}$ obtained from applying the transfer matrix T^{-1} (7.3) and the resulting significance N_i/σ_{N_i} obtained from (7.5) are shown in table 7.1. All peaks are significant with $s > 5\sigma$; however, after applying the transfer matrix, the W' peak vanishes within one standard deviation for ideal delocalization[5], while in the case of $\epsilon_L = 0.254$ a residue as big as 2σ remains. The Z' peak remains significant after applying the transfer matrix although, however, the significance is reduced because the transfer matrix enlarges the error.

7.6 Conclusions

What is the message to be taken from the simulations presented in this chapter? At the beginning, we have argued that W'/Z' production in the s channel is a very sensitive probe of the fermion sector in the Three-Site Model and in particular of the delicate interplay of fermion and KK gauge boson wavefunction which allows the model to evade the precision constraints.

In the simulations presented here we have shown that the heavy gauge bosons, albeit fermiophobic, can indeed lead to observable resonances in the s channel

[5]The negative event count in the W' peak is an artifact of the multiplication with T^{-1}.

at the LHC. In the case of the Z', we have found that the corresponding resonance shows only little dependence on the fermion delocalization parameter ϵ_L and should be expected to be visible within the first $10 - 20\,\mathrm{fb}^{-1}$ in the $jjl\nu$ channel for any point in parameter space. At the LHC, such a signal together with the absence (or near-absence) of a corresponding signal in the dilepton and Drell-Yan channels would be a strong sign for a fermiophobic, heavy neutral vector resonance like the Three-Site Z'.

As far as the W' is concerned, the simulations have also shown that the resonance might be accessible at the LHC. However, the magnitude of the signal is highly dependent on ϵ_L, and there are regions in parameter space in which no signal would be observed at the LHC. Even in this case though, the existence of the W' could be established via the strahlung process presented in the last chapter (which is essentially independent of ϵ_L), and the absence of a corresponding peak in the s channel processes would be a clear sign of its fermiophobic nature.

We have found three different possible discovery channels for the W', all of which show a comparable discovery potential at the parton level. However, the $jjl\nu$ type final states contain contributions from both W' and Z', and if ATLAS and CMS turn out to be unable to resolve the jet momenta with the accuracy required for separating the resonances via cuts on the invariant jet mass, some trick like the one presented in 7.5 needs to be applied if this final state is to be exploited for W' production. Otherwise, only the combined resonance of Z' and W' can be observed in this channel which, luckily, at least wouldn't hurt the Z' detection much as the signal is stronger than the W' one anyways, and the amount of W' events contained in the peak could be inferred from the other two W' final states available.

All simulations presented in this thesis have been performed at the parton level only with no detector effects taken into account. In the case of those presented in this chapter, an ATLAS detector simulation was added in the master's thesis of F. Bach [63]. This also includes additional backgrounds which were purposefully not taken into account in the parton level simulations as they depend on details of the detector and of the jet identification algorithm, e.g. the background coming from $t\bar{t}$ production with two jets escaping down beam pipe.

The result shows that the Z' signature is rather robust and persists with a 5σ effect still being visible in the first $5 - 30\,\mathrm{fb}^{-1}$ even if detector effects are taken into account. The W' resonance turns out to be more fragile, with the separation trick for $jjl\nu$ not working well after the detector simulation and the signal in $jjll$ being diminished by the measurement error on the jet momenta and additional backgrounds. In light of this result, $lll\nu$ becomes the preferred final state for this process at the LHC, and the detector simulation suggests that the parton level results carry over to the actual experiment in this case. For more details on these issues see [63].

7.7 Additional plots

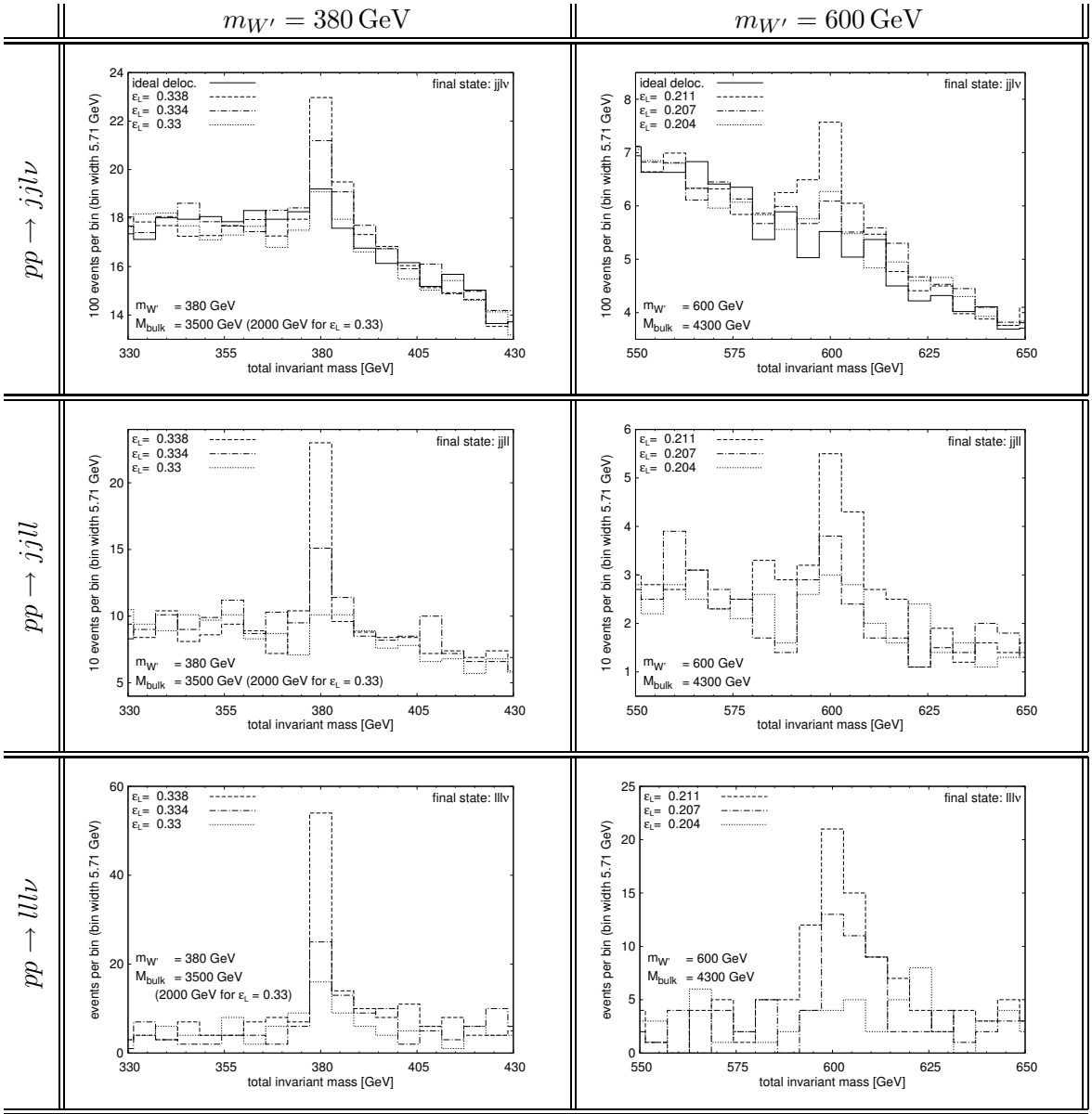

Figure 7.10: The W' resonance peaks not covered by fig. 7.6 for the different final states under consideration. Different values of $m_{W'}$ and ϵ_L.

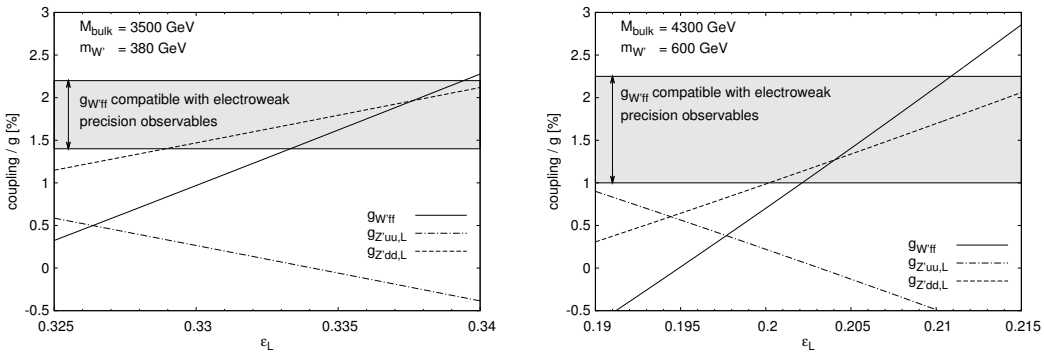

Figure 7.11: The same plots as fig. 7.1 for $m_{W'} = 380\,\mathrm{GeV}, 600\,\mathrm{GeV}$.

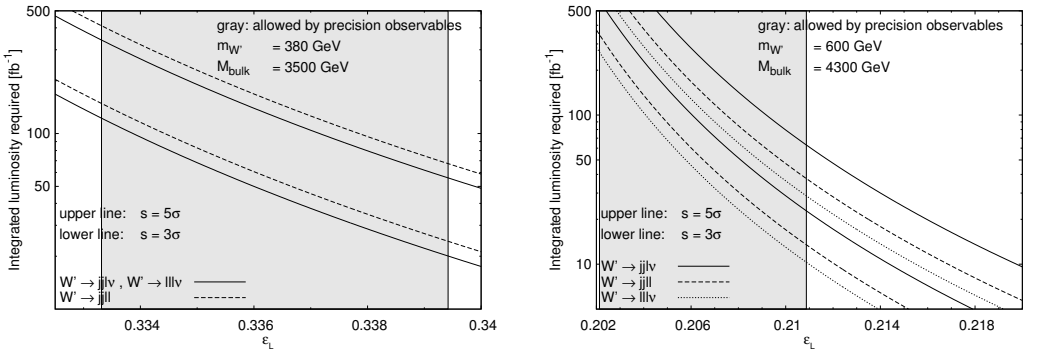

Figure 7.12: The same as fig. 7.7 for $m_{W'} = 380\,\mathrm{GeV}, 600\,\mathrm{GeV}$.

Chapter 8

Heavy Fermion Production

Oliphaunt am I,
Biggest of all.

(Excerpt from the "Oliphaunt song" in J.R.R. Tolkien's "Lord of the Rings")

After discussing at length the prospects of discovering the KK partners of the Z and W as well as the possibility of getting a handle on their fermiophobic nature, the only aspect of the model which we have not addressed in our simulations so far are the heavy fermion partners. With masses above $1.8\,\mathrm{TeV}$ and widths of several $100\,\mathrm{GeV}$ (c.f. chapter 4), these particles certainly are near the limit of what may be accessible as a resonance at the LHC. Nevertheless, we will see in this chapter that this may be feasible at least in some portions of parameter space.

As in chapters 6 and 7, we will first discuss the different processes that could be exploited for probing for this kind of new physics in 8.1. Subsequently, the details of the simulations we performed will be discussed in 8.2, while the results are presented and discussed in 8.3.

8.1 Processes

Besides the fermiophobic W' and Z', the main feature of the Three-Site Model are the new heavy fermion resonances. As we have seen in chapter 2, their introduction was required in the Three-Site setup in order to allow for the tuning of the couplings between the Standard Model fermions and the KK gauge bosons which in turn is necessary for evading the electroweak precision constraints. Therefore, regardless of their large mass scale $M_{\text{bulk}} > 1.8\,\mathrm{TeV}$, these particles are an integral part of the phenomenology of the Three-Site Model, and if other experimental results would hint at such a kind of new physics, a way to access these particles would be desirable.

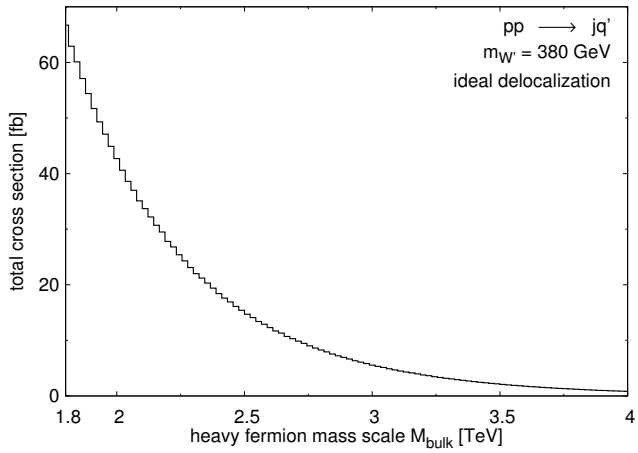

Figure 8.1: Total cross section for $pp \to jq'$ as a function of M_{bulk}.

The production mechanism which might first come to mind are simple Drell-Yan like processes of the type

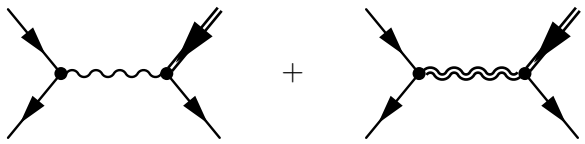

However, such processes always involve a quark-antiquark pair in the initial state which is very unlikely to deliver the large amount of energy necessary for the creation of a heavy fermion at a pp collider like LHC, and simulating $pp \to e^+e^{-\prime}$ with WHIZARD / O'Mega indeed reveals a cross section of the order of $0.5\,\text{ab}$ at the LHC. Clearly, even if we multiply this with with an optimistic factor of 42 in order to take all Standard Model fermions visible to the detector into account[1], the resulting cross section is still pathetic, and detecting the heavy fermions this way is out of question.

However, there is another kind of potential production processes which are mediated by t channel interactions

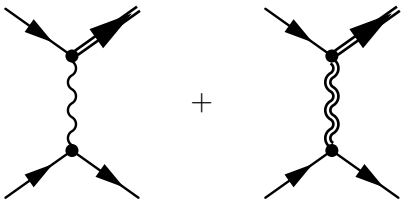

This kind of process can contain two valence quarks in the initial state with much more energy being typically available in the partonic CMS than in the above case of a valence and a sea quark. The resulting cross section for $pp \to jq'$ (q' being any

[1] (6 quarks $\times$ 3 colors $+$ 3 leptons) $\times$ 2 (fermions + antifermions) $=$ 42

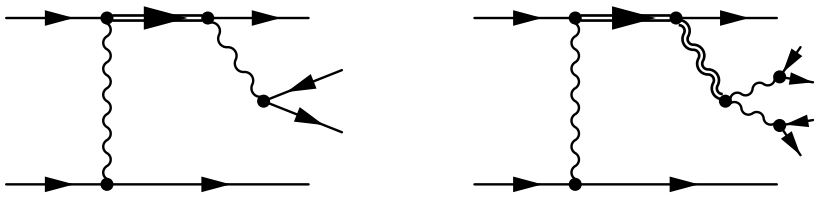

Figure 8.2: Signal diagrams for t channel induced production of heavy fermions with the two final states as obtained from the different decay channels of the heavy fermions.

of $u', \bar{u}', d', \bar{d}'$) is shown in fig. 8.1 as a function of M_{bulk}, exploiting the fact that the heavy partners of the light Standard Model fermions are degenerate (c.f. chapter 4.1) by summing over fermion flavors in order to enhance the signal. Evidently, the available energy is much higher, and the resulting cross section can be as big as $\approx 66\,\text{fb}$ for the smallest $M_{\text{bulk}} = 1.8\,\text{TeV}$, dropping only moderately with nearly $10\,\text{fb}$ being still available for $M_{\text{bulk}} = 3\,\text{TeV}$. These numbers are much more encouraging than those in the Drell-Yan like case, and we can indeed hope that it might be possible to dig out a heavy quark resonance this way if M_{bulk} is not too high.

As discussed in chapter 4.4, the heavy fermions decay into a Standard Model fermion and a gauge boson, the ratio between decays into light and heavy gauge bosons being roughly 1:1. The Standard Model W and Z then decay into two fermions, leading to four particle final states like fig. 8.1 left, while the W' and Z' cascade into four fermions by means of two intermediary gauge bosons, resulting in a six particle final state similar to fig. 8.1 right.

The six particle final states come with the advantage that a cut on the invariant mass of the heavy gauge boson can be leveraged in order to reduce the number of background events (given that the W'/Z' mass has been previously determined). However, a preliminary study of the six particle final state containing four jets turned out to be quite involved due to the large number of background processes already present at the parton level, and the resulting event count in the signal channels was not big enough to leave much hope for a significant discovery potential in this process. The investigation of six particle final states of the form $jjlll\nu$ is still an ongoing project, but as processes leading to this final state are suppressed relative to those with four particles in the final state by another gauge boson branching factor, it is unlikely that they will offer any advantage over these.

Therefore, we only present results for the four fermion processes in this work. Excluding the case of four jets due to the large QCD backgrounds, we remain with $jjl\nu$ and $jjll$ as potential final states. However, as the branching ratio into $Z \to ll$ is significantly smaller than that of $W \to l\nu$, we should expect the $jjl\nu$ final state to perform much better than $jjll$, provided that we can cope with the missing neutrino momentum.

Apart from the mass and couplings of the heavy fermions, the prospects for discovering these particles as a resonance also depend on their total width. As the

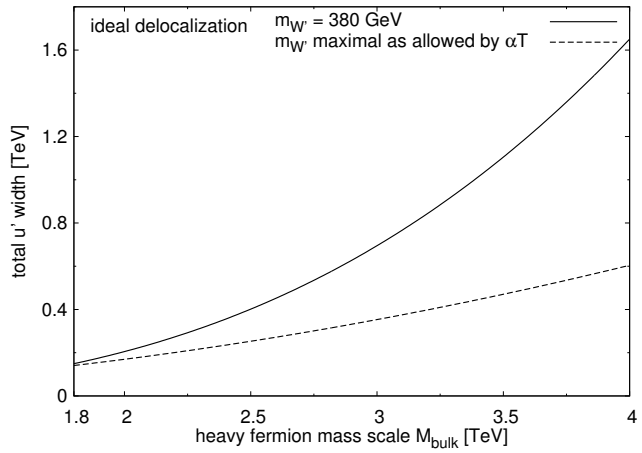

Figure 8.3: The total u' width as a function of M_{bulk} for the minimal value of the W' mass $m_{W'} = 380\,\text{GeV}$ and for the highest $m_{W'}$ allowed by the constraint $\alpha T \leq 0.005$.

amount of phasespace available for the decay of a particle depends on the mass of the decay products, we should expect that the total width exhibits a strong dependence on $m_{W'}$. Fig. 8.3 shows the total u' width as a function of M_{bulk} both for $m_{W'} = 380\,\text{GeV}$ (which is the smallest value allowed by the LEP constraint on the triple gauge boson couplings) and for the highest W' mass which is still in accordance with the condition $\alpha T \leq 0.005$ (c.f. chapter 4.2). This plot demonstrates that the range of potential values for the width grows significantly with increasing M_{bulk}, and for $M_{\text{bulk}} = 3\,\text{TeV}$, the difference is more than $200\,\text{GeV}$. Clearly, this variation of the width with $m_{W'}$ is big enough to have an influence on the significance of the resonance.

An additional dependence on $m_{W'}$ comes from the $Wf'f$ / $Zf'f$ couplings which scale with x (c.f. chapter 4.3). Looking at (4.19), it is obvious that, while the resonance becomes more narrow and easier to detect with growing W' mass, the couplings responsible for the production of the heavy quark in fact go down, and it is not clear a priori which effect dominates the significance of the signal in the end.

In contrast to the s channel production of heavy gauge bosons discussed in the last chapter, we have no reason to expect a large influence of the delocalization parameter ϵ_L on this process. The only possible source of such a dependence ore processes involving a W' in the t channel, the relative contribution to the amplitude of which would be

$$\frac{g_{W'qq',L}\; g_{W'qq,L}}{g_{Wqq',L}\; g_{Wqq,L}}$$

(the right-handed components of massless fermions sit completely at the right brane with their partners residing in the bulk and therefore, the right-handed couplings $g_{W'q'q,R}$ vanish). This turns out to be less than 10% over the whole parameter space

and therefore, we are free to perform the simulation in the ideally delocalized scenario with the effect of nonideal delocalization on the result being small and negligible when compared to other uncertainties.

8.2 Simulation Details

In order to examine whether it might indeed be possible to discover the heavy fermions at the LHC, we have performed full parton level simulations of the processes $pp \to jjll$ and $pp \to jjl\nu$ for an integrated luminosity of $\int\mathcal{L} = 400\,\mathrm{fb}^{-1}$ and a total energy of $14\,\mathrm{TeV}$, again with the definitions (6.1) and the same parton distributions as in chapters 6 and 7. In the case of the final state containing a neutrino, we have applied the reconstruction method already used in chapter 7 and presented in 7.2, again double counting the event if both solutions pass the cuts. To get a sufficiently smooth estimate of the background, additional simulations in the Standard Model were performed for an integrated luminosity of $\int\mathcal{L} = 1600\,\mathrm{fb}^{-1}$ and the result then downscaled by a factor of 4.

In order to suppress the backgrounds and identify the jet which originates from the heavy fermion, we concentrate on events in which the total energy available in the parton CMS is just barely enough to create the KK particle which is therefore only weakly boosted in this frame. In the CMS, this implies that the jet coming from the decaying heavy quark is emitted isotropically in all directions and is approximately back-to-back to the W/Z coming from the decay, while the jet originating from the proton will be aligned with the beam axis. Note that these kinematics are very different from those exhibited by gauge boson fusion processes like

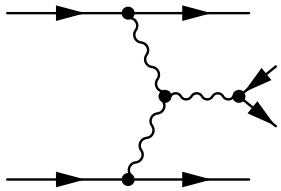

which feature two high rapidity jets aligned with the beam axis and which can be expected to constitute the largest part of the irreducible background.

To facilitate the selection of events whose kinematics match these criteria we applied the following cuts in the parton CMS

polar angle of jet j' originating from heavy quark	$0 \leq \left\lvert\cos\theta_{j'}\right\rvert \leq 0.7$
polar angle of jet j originating from proton	$0.95 \leq \lvert\cos\theta_j\rvert \leq 1$
angle between j' and W/Z	$-1 \leq \cos\theta_{jW} \leq -0.8$
p_T of heavy quark	$0 \leq \quad p_{T,q'} \quad \leq 200\,\mathrm{GeV}$
p_T of j' and W	$500\,\mathrm{GeV} \leq \quad p_{T,j'}\,, p_{T,W}$

We also applied a p_T cut on all observable momenta (and also on $p_{T,\mathrm{miss}}$ in the case of $pp \to jjl\nu$)

$$p_T \geq 50\,\mathrm{GeV}$$

as well as a cut on the total invariant mass

$$m_{\mathrm{tot}} \geq 1\,\mathrm{TeV}$$

for additional background suppression. In order to avoid infrared divergences and for simulating the acceptance region of the detector, we demanded

$$-0.99 \leq \cos\theta \leq 0.99$$

for the polar and intermediate angles of all observable particles in the hadron CMS, and the same small x cut already used in the last two chapters 7 – 8

$$x \geq 1.4 \cdot 10^{-4}$$

was applied on the incoming partons (also in the hadron CMS). In the case of the $jjll$ final state, we also applied an identification cut on the invariant mass of the dilepton system

$$81\,\mathrm{GeV} \leq m_{ll} \leq 101\,\mathrm{GeV}$$

In order to identify the part of parameter space in which the heavy quarks might be visible at the LHC, we have conducted simulations of the $jjl\nu$ final state at ten different points in parameter space as shown in tab. 8.1. For each value of M_{bulk}, a simulation at $m_{W'} = 380\,\mathrm{GeV}$ (which is the lower limit given by the LEP / LEP-II constraint on the triple gauge boson couplings, c.f. chapter 4.2) was performed. In addition, for $M_{\mathrm{bulk}} > 2\,\mathrm{TeV}$, another simulation near the upper limit on $m_{W'}$ (see fig. 8.3) was conducted in order to probe the dependence of the result on the W' mass. As the simulations of $pp \to jjll$ at the points I and II already show that $jjl\nu$ yields a much better signal, no simulations of $jjll$ were performed at IIIa/b – VIa/b.

parameters		heavy quark properties		point label
M_{bulk} [TeV]	$m_{W'}$ [GeV]	m [TeV]	Γ [GeV]	
1.8	380	1.90	150	I
2.0	380	2.10	205	II
2.2	380	2.31	273	IIIa
	430	2.29	204	IIIb
2.5	380	2.63	401	IVa
	460	2.58	257	IVb
2.7	380	2.84	506	Va
	480	2.78	294	Vb
2.9	380	3.05	628	VIa
	500	2.98	333	VIb

Table 8.1: The parameter space points at which the simulations of heavy quark production were performed. The first two columns define the parameter space point (we always assume ideal delocalization, c.f. section 8.1), the second two give mass and width of the KK partners to the light Standard Model quarks, and the labels used to identify the points in the analysis are given in the last column.

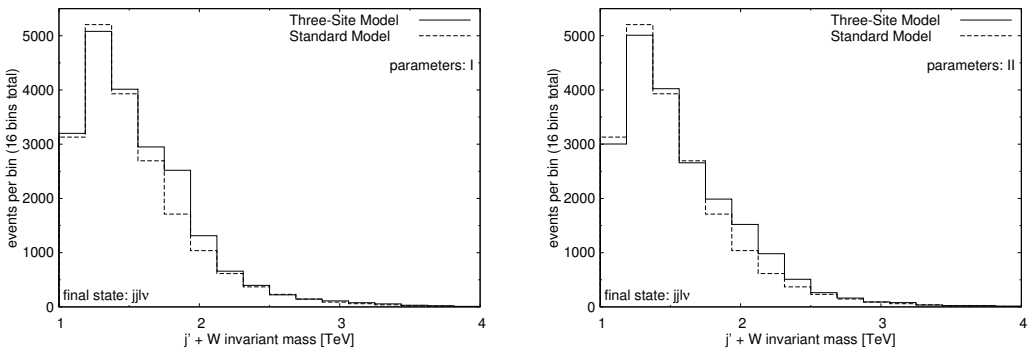

Figure 8.4: The heavy quark resonance in the $jjl\nu$ final state for the parameter space points I (*left*) and II (*right*), visible as an excess over the Standard Model background.

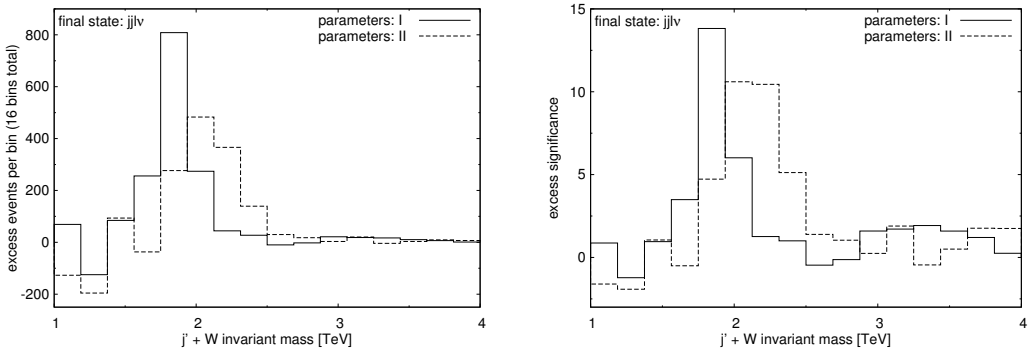

Figure 8.5: *Left*: The excess in the $j' + W$ invariant mass with the heavy quark resonance. *Right*: The per-bin significance of the excess calculated as described in the text.

8.3 Simulation Results

Let's start our discussion of the simulation results with the $jjl\nu$ final state. Fig. 8.4 shows the invariant mass of the combination of the jet j' potentially originating from a heavy quark (as identified by our cuts, see the preceding section) and the W for the parameter space points I and II (see tab. 8.1). While the background is considerable, an excess in the histogram at the invariant mass of the heavy quark over the Standard Model background is clearly visible (the peak in the distribution around $1.2\,\mathrm{TeV}$ is not related to the new physics, but a kinematical artifact induced by the cuts).

Calculating the difference between the event counts in the Three-Site Model and those in the Standard Model as shown in fig. 8.5 left for points I and II, we find that the excess is quite big, containing about 1000 events, and indeed has the shape of a broad resonance peak. In order to calculate its significance, we follow the same reasoning as in chapter 7.3 and assume that the double counting performed in the neutrino momentum reconstruction step simply doubles the event count and define the significance of the excess by

$$s_i = \frac{N_{s,i} - N_{b,i}}{\sqrt{2N_{b,i}}} \tag{8.1}$$

where the $N_{s,i}$ are the event counts in the Three-Site Model and the $N_{b,i}$ are the counts in the Standard Model. The resulting significance is shown on a per-bin basis in fig. 8.5 right, demonstrating the excess in the bins lying within the peak to be significant with $s > 10$. In addition, while the "naked" difference shown in fig. 8.5 left also exhibits a noticeable difference in the leftmost bins around $1\,\mathrm{TeV}$, fig. 8.5 right reveals this to be not significant and in fact just a statistical fluctuation, the conspicuous magnitude of which is solely due to the number of background events in this energy range.

In order to get a quantitative estimate of the significance of the whole resonance, we define the signal N_s to be the number of events within the $\pm\Gamma$ range around

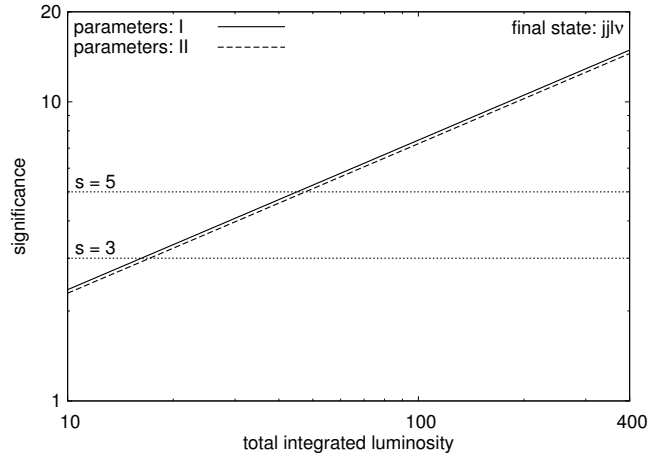

Figure 8.6: The significance of the heavy quark resonance as defined in the text at the points I and II as a function of the integrated luminosity together with the 3σ and 5σ discovery thresholds.

the invariant mass[2] of the heavy quarks. From this, we calculate the significance according to (8.1) just as we did for the individual bins. The result for the points I and II is shown in fig. 8.6 as a function of the integrated luminosity together with the 3σ and 5σ discovery thresholds. At both points, the signal exhibits nearly the same significance of $\approx 15\sigma$ for $\int\mathcal{L} = 400\,\mathrm{fb}^{-1}$ and intersects the 5σ threshold already around $45\,\mathrm{fb}^{-1}$.

The upper two rows of fig. 8.7 show the difference in the $j' + W$ invariant mass between the Three-Site Model and the Standard Model for the parameter space points III/IV/VIa and III/IV/VIb (Va/b has been excluded in order to make the figures more legible) with the left column giving the raw event count (similar to fig. 8.5 left) and the right column again the significance of the excess (like fig. 8.5). For both the points with minimal and maximal $m_{W'}$, the resonance remains visible while broadening as it moves to higher invariant mass values.

Similar to fig. 8.6, the bottom row of fig. 8.7 shows the significance of the resonance peaks as a function of $\int\mathcal{L}$ for the points IIIa/b – VIa/b. While the significance crosses the 5σ threshold below $400\,\mathrm{fb}^{-1}$ for IIIa/b – Va/b, the significance is just barely 5σ for VIa and even below that for VIb at $400\,\mathrm{fb}^{-1}$. For nearly all values of M_{bulk}, the significance is worse for the maximum value of $m_{W'}$ even though the resonances are considerably broader for $m_{W'} = 380\,\mathrm{GeV}$ (c.f. tab. 8.1). The only exceptions are Va/b ($M_{\text{bulk}} = 2700$) for which Vb gives a slightly better result than Va. However, as the determination of the significance comes with an uncertainty of about 1σ at $\int\mathcal{L} = 400\,\mathrm{fb}^{-1}$, this may well be a statistical fluctuation.

Let us now move on to the $jjll$ final state. For this process, fig. 8.4 shows the

[2]Choosing a wider interval gives a slightly higher significance of the signal at parameter space points with low Γ, but actually turns out degrade the signal at points with high width like Va and VIa.

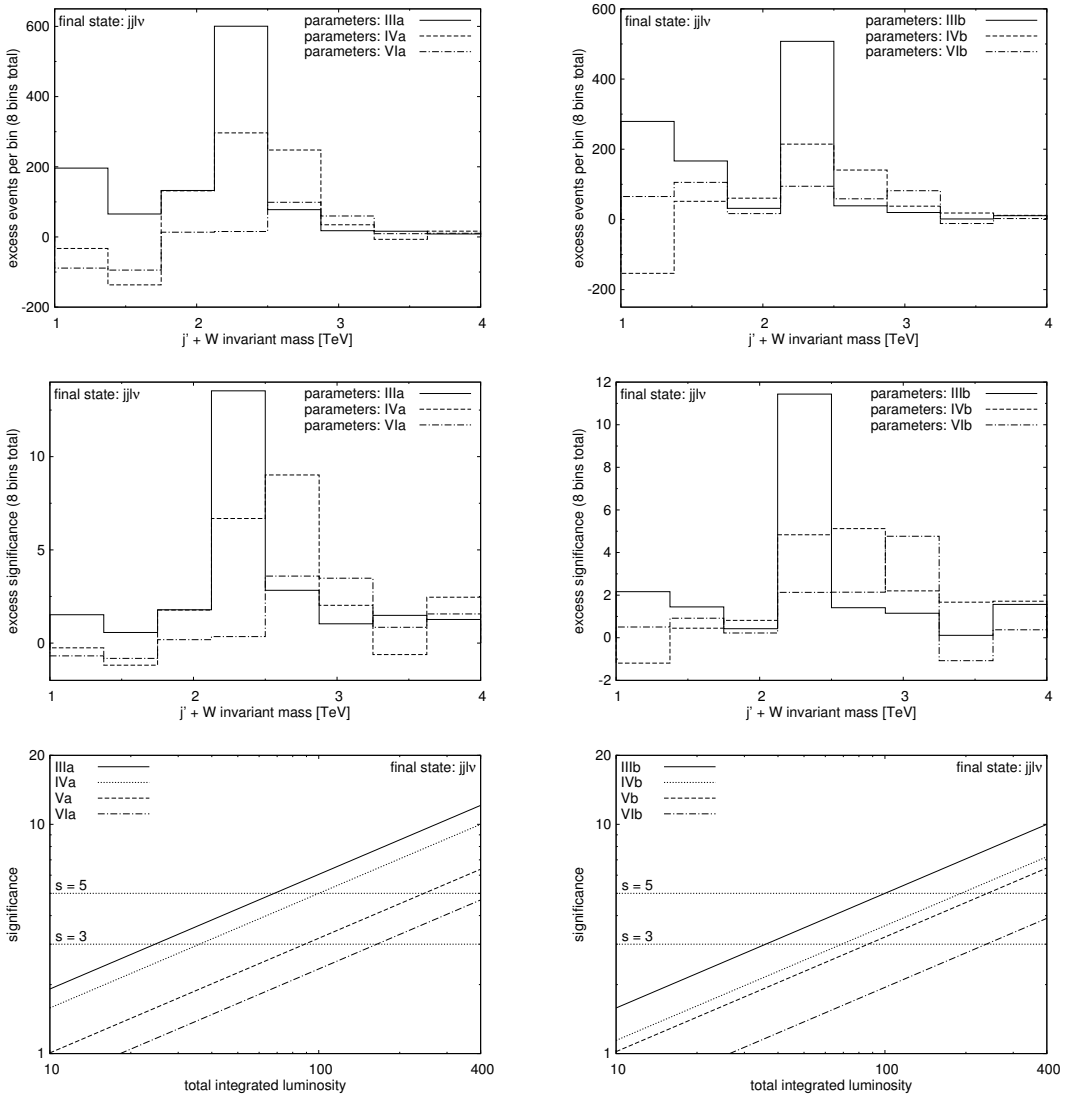

Figure 8.7: *Top row*: Similar to fig. 8.5 left, but for the points III/IV/VIa and III/IV/VIb. *Middle row*: Similar to fig. 8.5 right, but for III/IV/VIa/b. *Bottom row*: Like fig. 8.6, but for IIIa/b – VIa/b.

$j' + W$ invariant mass in the Three-Site Model versus the Standard Model expectation in a fashion similar to fig. 8.8 for the parameter space points I and II. Again, the resonance is clearly visible as an excess over the Standard Model background, but the total event count is much (more than an order of magnitude) lower than in the $jjl\nu$ case. The corresponding difference of the Three-Site Model and the Standard Model is shown in fig. 8.9 left, making the resonance peak manifest, but the fluctuations are much higher than in the $jjl\nu$ case due to the lower total event count.

This is emphasized by the significance of the excess showcased in fig. 8.9 right (with the significance again being calculated via (8.1), but now without the factor $\sqrt{2}$ in the denominator due to the absence of double counting). Already in this histogram, the significance of the signal turns out to be much lower than that observed in fig. 8.5 right for the $jjl\nu$ case. The total significance of the signal is shown in fig. 8.10 as a function of $\int\mathcal{L}$. For $400\,\mathrm{fb}^{-1}$, it is only about $\approx 6.5\sigma$ at point I and even below 5σ for II, which is clearly much worse than what we observed for $jjl\nu$ in fig. 8.6. As evidently $jjl\nu$ is much better suited for the detection of the heavy quarks in this process, with a 5σ discovery already being difficult for $M_{\text{bulk}} = 2\,\mathrm{TeV}$ in the $jjll$ final state, we didn't perform any more simulations for $pp \to jjll$.

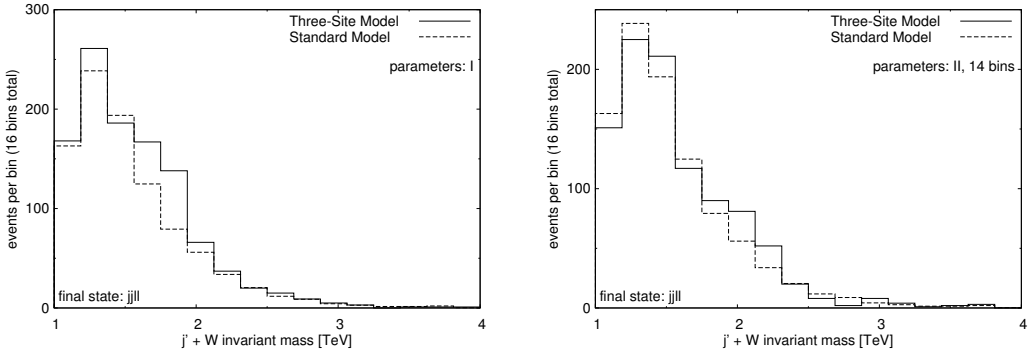

Figure 8.8: Like fig. 8.4, but for the $jjll$ final state.

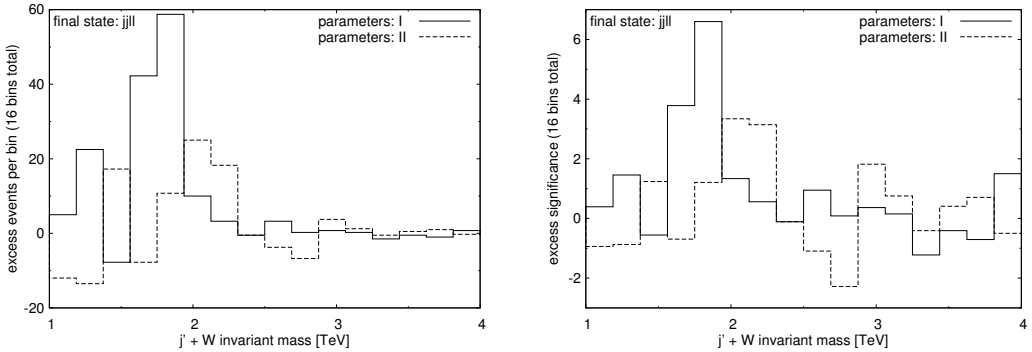

Figure 8.9: Like fig. 8.5, but for the $jjll$ final state.

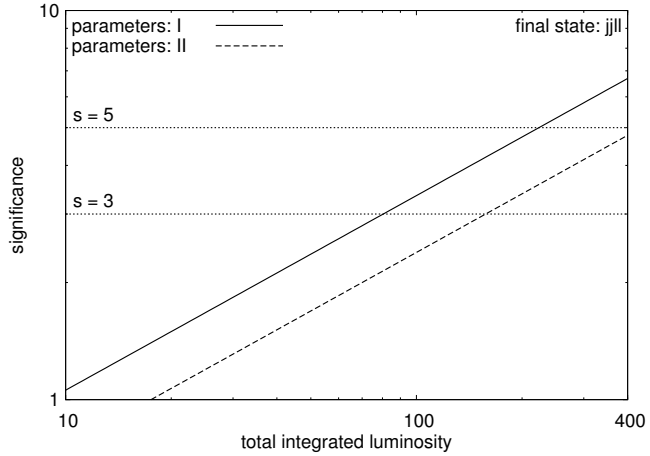

Figure 8.10: Like fig. 8.6, but for the $jjll$ final state.

8.4 Conclusions

While the detection of the heavy fermions at the LHC is challenging due to their large mass and considerable width, our parton level results show that this should indeed be possible in the $jjl\nu$ (and to a lesser extend in $jjll$) final states at least in the domain of the parameter space with M_{bulk} smaller than $2.9\,\text{TeV}$. While the signal significance depends heavily on M_{bulk}, the dependence on $m_{W'}$ turns out to be less than might be expected form the associated change in the width of the resonance which indeed turns out to be (over)compensated by the decrease of the relevant couplings. In addition, as argued in the beginning of this chapter, the effect of changing the delocalization parameter ϵ_L should be small and not more than 20% in the worst case.

However, even in the accessible part of parameter space, several caveats remain. First, this kind of processes is restricted to the heavy quarks, and no information on the heavy leptons or neutrinos can be obtained this way. Second, due to the near-degeneracy of the heavy fermions masses, only the heavy quarks as a whole (and, if small contributions from flavor mixing are ignored, of these only the u' and d') are accessible. For a resolution of individual flavors, tagging would be required which is impossible for the light flavors. Third, the background is rather large, reducing the broad resonances to an excess in the histograms, from which the Standard Model background must be subtracted in order to be able to resolve the resonance, and it is not clear a priori whether a sufficiently good background estimate will be available.

On the pro side, we can expect that the inclusion of hadronization and detector effects into our parton-level results would not harm the outcome overmuch. The main effect of these effects would supposedly be a smearing of the invariant mass distribution due to the finite jet resolution, but as the resonances are very broad anyway, no big harm should come from that. More dangerous is the potential increase in the reducible background coming from other final states which we did not take into account in our parton level analysis; this should be studied carefully if such an analysis of the experimental date should ever be performed.

So, can the heavy fermions be seen at the LHC? In the light of the results of our simulations, the answer to this question is a definitive “maybe”, with the final verdict depending on the actual value of M_{bulk}, the accuracy of our understanding of the Standard Model background, the amount of data the LHC will be able to collect and, also important, the actual energy the collider will reach — our simulations were performed for $14\,\text{TeV}$, and less energy would diminish the result considerably.

Chapter 9

Conclusions

The physics is theoretical, but the fun is real.

(Tagline of Sheldon's "Research Lab" game from "The Big Bang Theory — The Guitarist Amplification")

While it certainly does not solve most of the issues the Standard Model is usually criticized for (apart from the hierarchy problem which obviously is void in Higgsless model), we have argued in chapter 2 that a scenario like the Three-Site Model does arise in a rather natural fashion once we try to replace the Higgs with a set of $\mathbf{SU}(2)$ vector bosons as agents for the preservation of perturbative unitarity at the TeV scale. Discussing the properties of the new structure in the model and the consequences of the experimental constraints in chapter 4, we have found that these constraints imply that the new physics is well hidden from discovery by forcing the W'/Z' to be essentially fermiophobic and the KK partners of the fermions to be very heavy.

The goal of this thesis was the implementation of the model into the WHIZARD / O'Mega framework and the application of this implementation to studying the phenomenology exhibited by the model at the LHC. The implementation as presented in chapter 5 is complete and has been cross-checked against two independent implementations in CalcHep and FeynRules. In addition, the FeynRules → WHIZARD driver also developed in the context of this thesis and presented in chapter 5.4 will greatly simplify the future implementation of other models of new physics into WHIZARD / O'Mega.

Due to the constraints on the masses and couplings of the new particles, the LHC phenomenology of the Three-Site Model turns out to be quite interesting even though the new structure cannot compete with other extension of the Standard Model (e.g. SUSY) in terms of complexity. Using our WHIZARD / O'Mega implementation, we have performed a study of the discovery prospects of the new heavy particles in three different types of processes, the results of which we presented in chapters 6 – 8.

For the heavy gauge bosons, essentially two classes of production mechanisms

exist with the W'/Z' coupling either to a Standard Model gauge boson or to a Standard Model fermion. As a representative of the first class, we have showcased a simulation of the W' strahlung process in chapter 6. We find that this process indeed has the potential of uncovering the W' at the LHC. However, while a 5σ discovery of the W' should be possible in this process with considerably less than $100\,\mathrm{fb}^{-1}$ for W' masses of between $380\,\mathrm{GeV}$ and $500\,\mathrm{GeV}$ (the first value being the lower bound on $m_{W'}$ from existing experimental data), the integrated luminosity necessary for a 5σ discovery rises to $400\,\mathrm{fb}^{-1}$ for $m_{W'} = 600\,\mathrm{GeV}$ (which is the W' mass where the heavy fermions move above the UV cutoff). Considering that no detector effects are taken into account in these numbers, $m_{W'} = 600\,\mathrm{GeV}$ should present the upper limit on the reach of the LHC in this process.

As the W' strahlung process is essentially mediated by the gauge sector and does not contain any information on the fermiophobic couplings of the heavy gauge bosons to the Standard Model fermions, we have performed another set of simulations presented in chapter 7 where we studied the production of the W'/Z' in the s channel. For the Z', the only viable discovery channel leads to the final state $jjl\nu$ which our simulations show to be suitable for the discovery of the Z' with the first $10 - 20\,\mathrm{fb}^{-1}$ over the whole parameter space. For the W', three potential discovery channels exists with the final state $jjl\nu$, $jjll$ and $lll\nu$. However, the separation of the W' resonance from the Z' peak in $jjl\nu$ turns out to be difficult due to the finite experimental resolution of the jet momenta, leaving $jjll$ and $lll\nu$ as the most promising channels. We find that the discovery potential of these ranges from "possible within the first $100\,\mathrm{fb}^{-1}$" to "utterly impossible" for all W' masses depending on the exact value of the delocalization parameter ϵ_L. As the previously discussed W' strahlung process allows for a discovery of the W' independent of the delocalization parameter, the combination of these two processes might not only facilitate the discovery of the W' but even give some hints about its fermiophobic nature.

Apart from the heavy gauge bosons, the second major component of the new structure in the Three-Site Model are the heavy partners to the Standard Model fermions. In chapter 8, a simulation of the t channel induced production of heavy quarks leading to either a $jjll$ oder a $jjl\nu$ final state was discussed. The result suggests that, while the mass and width of the heavy fermions makes them hard to be detected as a resonance, such a measurement might indeed be possible at least for values of M_{bulk} below $2.9\,\mathrm{TeV}$. However, the success of this in the "real world" would be highly dependent on the exact value of M_{bulk} and the accuracy of our understanding of the expected Standard Model background which must be subtracted in order to establish the resonance. Still, the situation is not hopeless, and if physics reminiscent of the Three-Site Model W'/Z' were to be found at the LHC, the heavy fermions could in principle be probed for.

Combining the results of all our simulations, it is safe to say that the LHC would be capable of probing for all major components of the new physics in the Three-Site Model. However, there are areas in parameter space which would remain partially dark at the LHC, and while the W' and Z' should eventually turn up, the heavy fermions might remain completely invisible.

Of course, the Three-Site Model is just one example of Higgsless new physics, and there is no reason why nature should choose this particular scenario (or why nature should be Higgsless anyway). Still, even in the likely case of it not being a valid description of nature, the the Three-Site Model remains an interesting example of a model of new physics which is quite successful at (partially) hiding its new structure from quick discovery. In fact, as all Higgsless models in which heavy vectors are responsible for the delay of unitarity violation must manage to pass the precision constraints, phenomena like the fermiophobic couplings of the heavy gauge bosons or additional heavy fermions occur in other such models as well, with similar difficulties concerning the detection at the LHC.

Appendix A

Notation and Conventions

All covariant derivatives appearing in this work are defined with a minus sign

$$D^\mu = \partial^\mu - igA^\mu \tag{A.1}$$

In several places, the generators of the fundamental representation of $\mathbf{SU}(2)$ are referred to which are defined as

$$\tau_i = \frac{\sigma_i}{2} \tag{A.2}$$

with the Pauli matrices σ_i. Left- and right-handed fermions are defined via the chirality projectors $\Pi_\pm$ as

$$\Psi_{L/R} = \Pi_\pm \Psi = \frac{1 \pm \gamma^5}{2} \Psi \tag{A.3}$$

In the introduction to 5D gauge theories given in chapter 3, a convention is used of Greek Lorentz indices going from 0 to 3 (thus labeling the 4D part of 5D vectors), while Roman Lorenz indices go from 0 to 4. The 5th coordinate is labeled either as x^5, y or (implicately in sums) x^4. For the metric, the mostly minus convention is used

$$g^{\mu\nu} = \mathbf{diag}\,(1,-1,-1,-1)^{\mu\nu} \quad , \quad g^{ab} = \mathbf{diag}\,(1,-1,-1,-1,-1)^{ab} \tag{A.4}$$

It is also necessary to establish a convention on the nomenclature regarding the Standard Model particles and their heavy partners. If not explicitly stated differently in the text, we refer to the Standard Model particles as "light" or "KK light" and to their partners as "heavy", "KK heavy" or "KK particles".

Appendix B

A sample spectrum

The following is a sample spectrum generated by running the `spektrum` program described in appendix D.1. It is calculated for ideal delocalization $m_W = 500\,\mathrm{GeV}$ and $M_{\text{bulk}} = 3.5\,\mathrm{TeV}$ and gives all masses, wavefunctions, widths and couplings (excluding QED and QCD). The heavy quark widths include the one loop QCD correction (c.f. chapter 4.4 and appendix C.

Note that the scale `v` given in the first few lines must be divided by $\sqrt{2}$ to obtain the symmetry breaking scale v defined in chapter 3.3 due to a difference in convention. For similar reasons, the parameter `lambda` must be multiplied by 2 to get the bulk Yukawa coupling $\tilde{\lambda}$.

```
g0 =  0.6915048     g1 =  2.0914001     g2 =  0.3565523
     -> x =  0.3306421     t =  0.5156179     e =  0.3133290
     -> eps_L =  0.2369703
v =     235.7870519     lambda =     10.4962241


electron neutrino : light lepton with isospin +1/2 belonging to generation 0
 eps_r:       0.0000000
 wavefunction L :     -0.9730523           0.2305845
 wavefunction R :      0.0000000           1.0000000
 mass:       0.0000000
 width:      0.0000000

heavy electron neutrino : heavy lepton with isospin +1/2 belonging to generation 0
 eps_r:       0.0000000
 wavefunction L :      0.2305845           0.9730523
 wavefunction R :      1.0000000           0.0000000
 mass:    3596.9289707
 width:    628.3857980

up quark : light quark with isospin +1/2 belonging to generation 0
 eps_r:       0.0000000
 wavefunction L :     -0.9730523           0.2305845
 wavefunction R :      0.0000000           1.0000000
 mass:       0.0000000
 width:      0.0000000

heavy up quark : heavy quark with isospin +1/2 belonging to generation 0
 eps_r:       0.0000000
 wavefunction L :      0.2305845           0.9730523
 wavefunction R :      1.0000000           0.0000000
 mass:    3596.9289707
 width:    585.6279797

electron : light lepton with isospin -1/2 belonging to generation 0
 eps_r:       0.0000000
 wavefunction L :     -0.9730523           0.2305845
 wavefunction R :      0.0000000           1.0000000
 mass:       0.0000000
 width:      0.0000000
```

```
heavy electron : heavy lepton with isospin -1/2 belonging to generation 0
 eps_r:       0.0000000
 wavefunction L :      0.2305845           0.9730523
 wavefunction R :      1.0000000           0.0000000
 mass:    3596.9289707
 width:    628.3857980

down quark : light quark with isospin -1/2 belonging to generation 0
 eps_r:       0.0000000
 wavefunction L :     -0.9730523           0.2305845
 wavefunction R :      0.0000000           1.0000000
 mass:       0.0000000
 width:      0.0000000

heavy down quark : heavy quark with isospin -1/2 belonging to generation 0
 eps_r:       0.0000000
 wavefunction L :      0.2305845           0.9730523
 wavefunction R :      1.0000000           0.0000000
 mass:    3596.9289707
 width:    585.6279797

muon neutrino : light lepton with isospin +1/2 belonging to generation 1
 eps_r:       0.0000000
 wavefunction L :     -0.9730523           0.2305845
 wavefunction R :      0.0000000           1.0000000
 mass:       0.0000000
 width:      0.0000000

heavy muon neutrino : heavy lepton with isospin +1/2 belonging to generation 1
 eps_r:       0.0000000
 wavefunction L :      0.2305845           0.9730523
 wavefunction R :      1.0000000           0.0000000
 mass:    3596.9289707
 width:    628.3859271

charm quark : light quark with isospin +1/2 belonging to generation 1
 eps_r:       0.0015489
 wavefunction L :     -0.9730524           0.2305840
 wavefunction R :     -0.0014665           0.9999989
 mass:       1.2500000
 width:      0.0000000

heavy charm quark : heavy quark with isospin +1/2 belonging to generation 1
 eps_r:       0.0015489
 wavefunction L :      0.2305840           0.9730524
 wavefunction R :      0.9999989           0.0014665
 mass:    3596.9328385
 width:    585.6454626

muon : light lepton with isospin -1/2 belonging to generation 1
 eps_r:       0.0001313
 wavefunction L :     -0.9730523           0.2305845
 wavefunction R :     -0.0001244           1.0000000
 mass:       0.1060000
 width:      0.0000000

heavy muon : heavy lepton with isospin -1/2 belonging to generation 1
 eps_r:       0.0001313
 wavefunction L :      0.2305845           0.9730523
 wavefunction R :      1.0000000           0.0001244
 mass:    3596.9289985
 width:    628.3858577

strange quark : light quark with isospin -1/2 belonging to generation 1
 eps_r:       0.0011771
 wavefunction L :     -0.9730524           0.2305842
 wavefunction R :     -0.0011145           0.9999994
 mass:       0.9500000
 width:      0.0000000

heavy strange quark : heavy quark with isospin -1/2 belonging to generation 1
 eps_r:       0.0011771
 wavefunction L :      0.2305842           0.9730524
 wavefunction R :      0.9999994           0.0011145
 mass:    3596.9312047
 width:    585.6492771

tauon neutrino : light lepton with isospin +1/2 belonging to generation 2
 eps_r:       0.0000000
 wavefunction L :     -0.9730523           0.2305845
 wavefunction R :      0.0000000           1.0000000
 mass:       0.0000000
 width:      0.0000000
```

```
heavy tauon neutrino : heavy lepton with isospin +1/2 belonging to generation 2
 eps_r:       0.0000000
 wavefunction L :      0.2305845           0.9730523
 wavefunction R :      1.0000000           0.0000000
 mass:    3596.9289707
 width:    628.4222032

top quark : light quark with isospin +1/2 belonging to generation 2
 eps_r:       0.2202501
 wavefunction L :     -0.9752869           0.2209422
 wavefunction R :     -0.2046066           0.9788443
 mass:     174.0000000
 width:      1.5230000

heavy top quark : heavy quark with isospin +1/2 belonging to generation 2
 eps_r:       0.2202501
 wavefunction L :      0.2209422           0.9752869
 wavefunction R :      0.9788443           0.2046066
 mass:    3674.4892058
 width:    739.9590965

tauon : light lepton with isospin -1/2 belonging to generation 2
 eps_r:       0.0022056
 wavefunction L :     -0.9730525           0.2305835
 wavefunction R :     -0.0020883           0.9999978
 mass:       1.7800000
 width:      0.0000000

heavy tauon : heavy lepton with isospin -1/2 belonging to generation 2
 eps_r:       0.0022056
 wavefunction L :      0.2305835           0.9730525
 wavefunction R :      0.9999978           0.0020883
 mass:    3596.9368138
 width:    628.4026301

bottom quark : light quark with isospin -1/2 belonging to generation 2
 eps_r:       0.0052042
 wavefunction L :     -0.9730536           0.2305789
 wavefunction R :     -0.0049275           0.9999879
 mass:       4.2000000
 width:      0.0000000

heavy bottom quark : heavy quark with isospin -1/2 belonging to generation 2
 eps_r:       0.0052042
 wavefunction L :      0.2305789           0.9730536
 wavefunction R :      0.9999879           0.0049275
 mass:    3596.9726381
 width:    910.9435197

W boson : light W boson
 wavefuntion:       0.9858825           0.1674384
 mass:      80.4030000
 width:      2.0480000

heavy W boson : heavy W boson
 wavefuntion:      -0.1674384           0.9858825
 mass:     500.0000000
 width:      5.0007454

Z boson : light Z boson
 wavefuntion:      -0.8759133          -0.1084404           0.4701241
 mass:      91.1880000
 width:      2.4430000

heavy Z boson : heavy Z boson
 wavefuntion:       0.1657276          -0.9827488           0.0820918
 mass:     501.6804843
 width:      4.7681804

-----------------------------------------
W boson:                light
isospin +1/2 lepton:    light
isospin -1/2 lepton:    light

left-handed coupling matrix (rows <-> iso-up,  columns <-> iso-down):

           0.6641137           0.0000000           0.0000000
           0.0000000           0.6641137           0.0000000
           0.0000000           0.0000000           0.6641137

right-handed coupling matrix (rows <-> iso-up,  columns <-> iso-down):

           0.0000000           0.0000000           0.0000000
           0.0000000           0.0000000           0.0000000
```

```
           0.0000000           0.0000000           0.0000000

-------------------------------------------


-------------------------------------------
W boson:                light
isospin +1/2 quark:     light
isospin -1/2 quark:     light

left-handed coupling matrix (rows <-> iso-up,  columns <-> iso-down):

           0.6641137           0.0000000           0.0000000
           0.0000000           0.6641137           0.0000000
           0.0000000           0.0000000           0.6648179

right-handed coupling matrix (rows <-> iso-up,  columns <-> iso-down):

           0.0000000           0.0000000           0.0000000
           0.0000000           0.0000006           0.0000000
           0.0000000           0.0000000           0.0003530

-------------------------------------------


-------------------------------------------
W boson:                light
isospin +1/2 lepton:    light
isospin -1/2 lepton:    heavy

left-handed coupling matrix (rows <-> iso-up,  columns <-> iso-down):

          -0.0743928           0.0000000           0.0000000
           0.0000000          -0.0743928           0.0000000
           0.0000000           0.0000000          -0.0743921

right-handed coupling matrix (rows <-> iso-up,  columns <-> iso-down):

           0.0000000           0.0000000           0.0000000
           0.0000000           0.0000000           0.0000000
           0.0000000           0.0000000           0.0000000

-------------------------------------------


-------------------------------------------
W boson:                light
isospin +1/2 quark:     light
isospin -1/2 quark:     heavy

left-handed coupling matrix (rows <-> iso-up,  columns <-> iso-down):

          -0.0743928           0.0000000           0.0000000
           0.0000000          -0.0743928           0.0000000
           0.0000000           0.0000000          -0.0780258

right-handed coupling matrix (rows <-> iso-up,  columns <-> iso-down):

           0.0000000           0.0000000           0.0000000
           0.0000000          -0.0005135           0.0000000
           0.0000000           0.0000000          -0.0716484

-------------------------------------------


-------------------------------------------
W boson:                light
isospin +1/2 lepton:    heavy
isospin -1/2 lepton:    light

left-handed coupling matrix (rows <-> iso-up,  columns <-> iso-down):

          -0.0743928           0.0000000           0.0000000
           0.0000000          -0.0743928           0.0000000
           0.0000000           0.0000000          -0.0743932

right-handed coupling matrix (rows <-> iso-up,  columns <-> iso-down):

           0.0000000           0.0000000           0.0000000
           0.0000000          -0.0000435           0.0000000
           0.0000000           0.0000000          -0.0007313

-------------------------------------------
```

```
-----------------------------------------
W boson:                light
isospin +1/2 quark:     heavy
isospin -1/2 quark:     light

left-handed coupling matrix (rows <-> iso-up,  columns <-> iso-down):

          -0.0743928           0.0000000           0.0000000
           0.0000000          -0.0743926           0.0000000
           0.0000000           0.0000000          -0.0678180

right-handed coupling matrix (rows <-> iso-up,  columns <-> iso-down):

           0.0000000           0.0000000           0.0000000
           0.0000000          -0.0003903           0.0000000
           0.0000000           0.0000000          -0.0016890

-----------------------------------------


-----------------------------------------
W boson:                light
isospin +1/2 lepton:    heavy
isospin -1/2 lepton:    heavy

left-handed coupling matrix (rows <-> iso-up,  columns <-> iso-down):

           0.3678096           0.0000000           0.0000000
           0.0000000           0.3678096           0.0000000
           0.0000000           0.0000000           0.3678095

right-handed coupling matrix (rows <-> iso-up,  columns <-> iso-down):

           0.3501807           0.0000000           0.0000000
           0.0000000           0.3501807           0.0000000
           0.0000000           0.0000000           0.3501799

-----------------------------------------


-----------------------------------------
W boson:                light
isospin +1/2 quark:     heavy
isospin -1/2 quark:     heavy

left-handed coupling matrix (rows <-> iso-up,  columns <-> iso-down):

           0.3678096           0.0000000           0.0000000
           0.0000000           0.3678095           0.0000000
           0.0000000           0.0000000           0.3670548

right-handed coupling matrix (rows <-> iso-up,  columns <-> iso-down):

           0.3501807           0.0000000           0.0000000
           0.0000000           0.3501801           0.0000000
           0.0000000           0.0000000           0.3427682

-----------------------------------------


-----------------------------------------
W boson:                heavy
isospin +1/2 lepton:    light
isospin -1/2 lepton:    light

left-handed coupling matrix (rows <-> iso-up,  columns <-> iso-down):

           0.0000000           0.0000000           0.0000000
           0.0000000           0.0000000           0.0000000
           0.0000000           0.0000000          -0.0000005

right-handed coupling matrix (rows <-> iso-up,  columns <-> iso-down):

           0.0000000           0.0000000           0.0000000
           0.0000000           0.0000000           0.0000000
           0.0000000           0.0000000           0.0000000

-----------------------------------------


-----------------------------------------
W boson:                heavy
isospin +1/2 quark:     light
```

```
isospin -1/2 quark:     light

left-handed coupling matrix (rows <-> iso-up,  columns <-> iso-down):

           0.0000000           0.0000000           0.0000000
           0.0000000          -0.0000004           0.0000000
           0.0000000           0.0000000          -0.0048388

right-handed coupling matrix (rows <-> iso-up,  columns <-> iso-down):

           0.0000000           0.0000000           0.0000000
           0.0000000           0.0000034           0.0000000
           0.0000000           0.0000000           0.0020788

-----------------------------------------


-----------------------------------------
W boson:                heavy
isospin +1/2 lepton:    light
isospin -1/2 lepton:    heavy

left-handed coupling matrix (rows <-> iso-up,  columns <-> iso-down):

           0.4886032           0.0000000           0.0000000
           0.0000000           0.4886032           0.0000000
           0.0000000           0.0000000           0.4886032

right-handed coupling matrix (rows <-> iso-up,  columns <-> iso-down):

           0.0000000           0.0000000           0.0000000
           0.0000000           0.0000000           0.0000000
           0.0000000           0.0000000           0.0000000

-----------------------------------------


-----------------------------------------
W boson:                heavy
isospin +1/2 quark:     light
isospin -1/2 quark:     heavy

left-handed coupling matrix (rows <-> iso-up,  columns <-> iso-down):

           0.4886032           0.0000000           0.0000000
           0.0000000           0.4886022           0.0000000
           0.0000000           0.0000000           0.4693173

right-handed coupling matrix (rows <-> iso-up,  columns <-> iso-down):

           0.0000000           0.0000000           0.0000000
           0.0000000          -0.0030238           0.0000000
           0.0000000           0.0000000          -0.4218681

-----------------------------------------


-----------------------------------------
W boson:                heavy
isospin +1/2 lepton:    heavy
isospin -1/2 lepton:    light

left-handed coupling matrix (rows <-> iso-up,  columns <-> iso-down):

           0.4886032           0.0000000           0.0000000
           0.0000000           0.4886032           0.0000000
           0.0000000           0.0000000           0.4886012

right-handed coupling matrix (rows <-> iso-up,  columns <-> iso-down):

           0.0000000           0.0000000           0.0000000
           0.0000000          -0.0002564           0.0000000
           0.0000000           0.0000000          -0.0043058

-----------------------------------------


-----------------------------------------
W boson:                heavy
isospin +1/2 quark:     heavy
isospin -1/2 quark:     light

left-handed coupling matrix (rows <-> iso-up,  columns <-> iso-down):
```

```
           0.4886032           0.0000000           0.0000000
           0.0000000           0.4886026           0.0000000
           0.0000000           0.0000000           0.4885680

right-handed coupling matrix (rows <-> iso-up,  columns <-> iso-down):

           0.0000000           0.0000000           0.0000000
           0.0000000          -0.0022981           0.0000000
           0.0000000           0.0000000          -0.0099449

-------------------------------------------


-------------------------------------------
W boson:                heavy
isospin +1/2 lepton:    heavy
isospin -1/2 lepton:    heavy

left-handed coupling matrix (rows <-> iso-up,  columns <-> iso-down):

           1.9460904           0.0000000           0.0000000
           0.0000000           1.9460904           0.0000000
           0.0000000           0.0000000           1.9460909

right-handed coupling matrix (rows <-> iso-up,  columns <-> iso-down):

           2.0618749           0.0000000           0.0000000
           0.0000000           2.0618749           0.0000000
           0.0000000           0.0000000           2.0618704

-------------------------------------------


-------------------------------------------
W boson:                heavy
isospin +1/2 quark:     heavy
isospin -1/2 quark:     heavy

left-handed coupling matrix (rows <-> iso-up,  columns <-> iso-down):

           1.9460904           0.0000000           0.0000000
           0.0000000           1.9460908           0.0000000
           0.0000000           0.0000000           1.9508340

right-handed coupling matrix (rows <-> iso-up,  columns <-> iso-down):

           2.0618749           0.0000000           0.0000000
           0.0000000           2.0618714           0.0000000
           0.0000000           0.0000000           2.0182299

-------------------------------------------


couplings to the light Z
------------------------
2x electron neutrino:
 L:      -0.3765880     R:       0.0000000

2x up quark:
 L:      -0.2648388     R:       0.1117492

2x heavy electron neutrino:
 L:      -0.2072812     R:      -0.1972081

2x heavy up quark:
 L:      -0.0955319     R:      -0.0854589

electron neutrino , heavy electron neutrino:
 L:       0.0425077     R:       0.0000000

up quark , heavy up quark:
 L:       0.0425077     R:       0.0000000

2x electron:
 L:       0.2089642     R:      -0.1676238

2x down quark:
 L:       0.3207134     R:      -0.0558746

2x heavy electron:
 L:       0.0396573     R:       0.0295843

2x heavy down quark:
 L:       0.1514065     R:       0.1413335
```

```
electron , heavy electron:
 L:      -0.0425077     R:       0.0000000

down quark , heavy down quark:
 L:      -0.0425077     R:       0.0000000

2x muon neutrino:
 L:      -0.3765880     R:       0.0000000

2x charm quark:
 L:      -0.2648388     R:       0.1117488

2x heavy muon neutrino:
 L:      -0.2072812     R:      -0.1972081

2x heavy charm quark:
 L:      -0.0955319     R:      -0.0854585

muon neutrino , heavy muon neutrino:
 L:       0.0425077     R:       0.0000000

charm quark , heavy charm quark:
 L:       0.0425076     R:       0.0002892

2x muon:
 L:       0.2089642     R:      -0.1676238

2x strange quark:
 L:       0.3207134     R:      -0.0558744

2x heavy muon:
 L:       0.0396573     R:       0.0295843

2x heavy strange quark:
 L:       0.1514065     R:       0.1413332

muon , heavy muon:
 L:      -0.0425077     R:      -0.0000245

strange quark , heavy strange quark:
 L:      -0.0425077     R:      -0.0002198

2x tauon neutrino:
 L:      -0.3765880     R:       0.0000000

2x top quark:
 L:      -0.2656636     R:       0.1034933

2x heavy tauon neutrino:
 L:      -0.2072812     R:      -0.1972081

2x heavy top quark:
 L:      -0.0947071     R:      -0.0772030

tauon neutrino , heavy tauon neutrino:
 L:       0.0425077     R:       0.0000000

top quark , heavy top quark:
 L:       0.0408237     R:       0.0394964

2x tauon:
 L:       0.2089642     R:      -0.1676229

2x bottom quark:
 L:       0.3207138     R:      -0.0558698

2x heavy tauon:
 L:       0.0396573     R:       0.0295834

2x heavy bottom quark:
 L:       0.1514061     R:       0.1413287

tauon , heavy tauon:
 L:      -0.0425075     R:      -0.0004118

bottom quark , heavy bottom quark:
 L:      -0.0425067     R:      -0.0009717

couplings to the heavy Z
------------------------
2x electron neutrino:
 L:      -0.0150208     R:       0.0000000
```

```
2x up quark:
 L:       0.0044925     R:       0.0195133

2x heavy electron neutrino:
 L:      -0.9846090     R:      -1.0422955

2x heavy up quark:
 L:      -0.9650956     R:      -1.0227822

electron neutrino , heavy electron neutrino:
 L:      -0.2434336     R:       0.0000000

up quark , heavy up quark:
 L:      -0.2434336     R:       0.0000000

2x electron:
 L:      -0.0142492     R:      -0.0292700

2x down quark:
 L:       0.0052642     R:      -0.0097567

2x heavy electron:
 L:       0.9553390     R:       1.0130255

2x heavy down quark:
 L:       0.9748523     R:       1.0325389

electron , heavy electron:
 L:       0.2434336     R:       0.0000000

down quark , heavy down quark:
 L:       0.2434336     R:       0.0000000

2x muon neutrino:
 L:      -0.0150208     R:       0.0000000

2x charm quark:
 L:       0.0044928     R:       0.0195111

2x heavy muon neutrino:
 L:      -0.9846090     R:      -1.0422955

2x heavy charm quark:
 L:      -0.9650959     R:      -1.0227800

muon neutrino , heavy muon neutrino:
 L:      -0.2434336     R:       0.0000000

charm quark , heavy charm quark:
 L:      -0.2434331     R:       0.0015285

2x muon:
 L:      -0.0142492     R:      -0.0292700

2x strange quark:
 L:       0.0052640     R:      -0.0097554

2x heavy muon:
 L:       0.9553390     R:       1.0130255

2x heavy strange quark:
 L:       0.9748525     R:       1.0325376

muon , heavy muon:
 L:       0.2434336     R:      -0.0001296

strange quark , heavy strange quark:
 L:       0.2434333     R:      -0.0011617

2x tauon neutrino:
 L:      -0.0150208     R:       0.0000000

2x top quark:
 L:       0.0092162     R:      -0.0241212

2x heavy tauon neutrino:
 L:      -0.9846090     R:      -1.0422955

2x heavy top quark:
 L:      -0.9698193     R:      -0.9791477

tauon neutrino , heavy tauon neutrino:
 L:      -0.2434336     R:       0.0000000
```

```
top quark , heavy top quark:
 L:       -0.2337897     R:        0.2087489

2x tauon:
 L:       -0.0142497     R:       -0.0292655

2x bottom quark:
 L:        0.0052614     R:       -0.0097314

2x heavy tauon:
 L:        0.9553395     R:        1.0130210

2x heavy bottom quark:
 L:        0.9748551     R:        1.0325136

tauon , heavy tauon:
 L:        0.2434326     R:       -0.0021766

bottom quark , heavy bottom quark:
 L:        0.2434281     R:       -0.0051358


couplings between gauge bosons
------------------------------

2xW boson , Z boson :       -0.5950754

2xW boson , heavy Z boson :        0.0537663

2xheavy W boson , Z boson :       -0.2374152

2xheavy W boson , heavy Z boson :       -1.9944859

W boson , heavy W boson , Z boson :        0.0625477

W boson , heavy W boson , heavy Z boson :       -0.3581991

4x W boson , 0x heavy W boson :        0.4551806

3x W boson , 1x heavy W boson :       -0.0564797

2x W boson , 2x heavy W boson :        0.1322188

1x W boson , 3x heavy W boson :        0.6995732

0x W boson , 4x heavy W boson :        4.1325152

2x W boson , Z boson , photon :       -0.1864544

2x W boson , heavy Z boson , photon :        0.0168466

2x heavy W boson , Z boson , photon :       -0.0743891

2x heavy W boson , heavy Z boson , photon :       -0.6249303

W boson , heavy W boson , Z boson , photon :        0.0195980

W boson , heavy W boson , heavy Z boson , photon :       -0.1122342

2x W boson , 2x Z boson :        0.3580269

2x W boson , 2x heavy Z boson :        0.1311974

2x W boson , Z boson , heavy Z boson :       -0.0543996

2x heavy W boson , 2x Z boson :        0.0602782

2x heavy W boson , 2x heavy Z boson :        4.1062808

2x heavy W boson , Z boson , heavy Z boson :        0.4511168

W boson , heavy W boson , 2x Z boson :       -0.0520704

W boson , heavy W boson , 2x heavy Z boson :        0.6951640

W boson , heavy W boson , Z boson , heavy Z boson :        0.0884049
```

Appendix C

Two-body decays — Analytical Results

In this chapter the analytical results for the decay widths presented in chapter 4.4 are given.

C.1 Tree level

Consider a heavy particle with momentum p_1 and mass m_1 decaying into two particles with momenta p_2 / p_3 and masses m_2 / m_3.

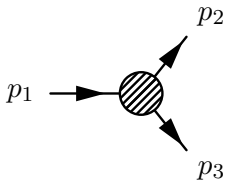

In the center-of-mass system, we can parameterize the momenta as

$$p_1^\mu = (m_1, 0, 0, 0)^\mu \quad , \quad p_2^\mu = (E_2, \vec{p})^\mu \quad , \quad p_3^\mu = (E_3, -\vec{p})$$

Furthermore, momentum conservation and the mass shell conditions can be leveraged to express the energies and the modulus of the three-momentum as

$$E_2 = \frac{m_1^2 + m_2^2 - m_3^2}{2m_1} \quad , \quad E_3 = \frac{m_1^2 + m_3^2 - m_2^2}{2m_1}$$
$$|\vec{p}|^2 = \frac{1}{4m_1^2}\left(m_1^2 - (m_2 + m_3)^2\right)\left(m_1^2 - (m_2 - m_3)^2\right) \quad \text{(C.1)}$$

The total width of the decaying particle can be expressed as the product of a phasespace factor and the square of the transition matrix element $|\mathcal{M}|^2$ (see e.g. [64])

$$\Gamma = \frac{1}{16\pi}\frac{|\vec{p}|}{m_1^2}\left(\prod_f 2m_f\right)\int_{-1}^{1} d\cos\theta\, |\mathcal{M}|^2$$

with the product $\prod_f 2m_f$ running over all external fermions. After performing the spin sum (including an averaging factor $\frac{1}{N}$ in front of Γ), Lorentz invariance requires $|\mathcal{M}|^2$ to be independent of θ. Inserting (C.1) and adopting the convention of absorbing the fermion factor into the squared matrix element, we arrive at the result

$$\Gamma = \frac{1}{N}\frac{1}{16\pi}\frac{1}{m_1^3}\sqrt{\left(m_1^2-(m_2+m_3)^2\right)\left(m_1^2-(m_2-m_3)^2\right)}|\mathcal{M}|^2$$

which is completely expressed in terms of the particle masses, the squared matrix element $|\mathcal{M}|^2$ and the averaging factor $\frac{1}{N}$ which is determined from the spin of the initial state particle[1].

The remaining quantity that has to be determined is the squared matrix element $|\mathcal{M}|^2$ which is given in the following for the different spin combinations that are relevant for calculating the widths of the KK particles in the Three-Site Model.

Spin $1 \longrightarrow$ **Spin** 1 **+ Spin** 1

- Coupling: standard triple gauge boson coupling
- Mass assignment:

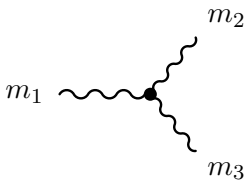

- Amplitude:

$$\sum_{\text{spin}}|\mathcal{M}|^2 = g^2\left(-8\left(m_1^2+m_2^2+m_3^2\right)+2\left(\frac{m_2^4+m_3^4}{m_1^2}+\frac{m_1^4+m_3^4}{m_2^2}+\frac{m_1^4+m_2^4}{m_3^2}\right)\right.$$
$$\left.-\frac{9}{2}\left(\frac{m_2^2m_3^2}{m_1^2}+\frac{m_1^2m_3^2}{m_2^2}+\frac{m_1^2m_2^2}{m_3^2}\right)+\frac{1}{4}\left(\frac{m_1^6}{m_2^2m_3^2}+\frac{m_2^6}{m_1^2m_3^2}+\frac{m_3^6}{m_1^2m_2^2}\right)\right)$$

Spin $1 \longrightarrow$ **Spin** $\frac{1}{2}$ **+ Spin** $\frac{1}{2}$

- Coupling: $g_V - g_A\gamma_5$
- Mass assignment:

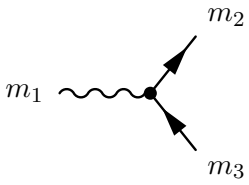

[1] An additional symmetry factor of $\frac{1}{2}$ could arise if there were identical particles in the final state. However, this does not occur for the decays relevant to the calculation presented here.

- Amplitude:

$$\sum_{\text{spins}} |\mathcal{M}|^2 = \left(g_V^2 + g_A^2\right)\left(2\left(2m_1^2 - m_2^2 - m_3^2\right) - 2\frac{m_2^4 + m_3^4}{m_1^2} + 4\frac{m_2^2 m_3^2}{m_1^2}\right) + 12\left(g_V^2 - g_A^2\right) m_1 m_3$$

Spin $\frac{1}{2}$ $\longrightarrow$ Spin $\frac{1}{2}$ + Spin 1

- Coupling: $g_V - g_A\gamma_5$
- Mass assignment:

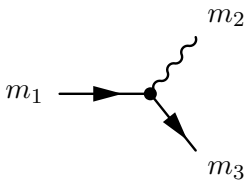

- Amplitude:

$$\sum_{\text{spins}} |\mathcal{M}|^2 = \left(g_V^2 + g_A^2\right)\left(2\left(m_1^2 + m_3^2 - 2m_2^2\right) + 2\frac{m_1^4 + m_3^4}{m_2^2} - 4\frac{m_1^2 m_3^2}{m_2^2}\right) - 12\left(g_V^2 - g_A^2\right) m_1 m_3 \quad \text{(C.2)}$$

C.2 $\mathcal{O}(\alpha_s)$ corrections to the heavy quark widths

According to (4.31), the calculation of the $\mathcal{O}(\alpha_s)$ QCD corrections to the heavy quark widths can be split into the calculation of the virtual correction and that of the real ones. In order to subtract the divergences arising in the loop integrals, we have to specify a renormalization scheme. For this calculation, we use a modified $\overline{\text{MS}}$ scheme where the heavy particle masses are renormalized on-shell such that the masses obtained by diagonalizing the Lagrangian are treated as pole masses.

The consistency of the result has been checked by confirming infrared finiteness. In addition, it has been cross-checked against the calculation of the $\mathcal{O}(\alpha_s)$ correction to the top decay in [65].

Virtual corrections

For computing the corrections which arise from the exchange of virtual gluons, we decompose the squared and spin summed two body decay matrix element as

$$\sum_{\text{spin}} |\mathcal{M}|^2 = M_0 + \alpha_s\left(M_{1,\text{1PI}} + M_{1,\delta Z}\right) + \mathcal{O}\left(\alpha_s^2\right) \quad \text{(C.3)}$$

The first term in the decomposition is just the tree level matrix element

$M_0 =$ 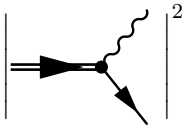

given by (C.2). The second term is the interference between the tree level matrix element and the QCD vertex correction

$M_{1,\mathrm{1PI}} = 2\Re$ 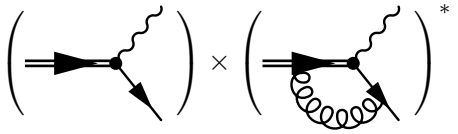

The third term $M_{1,\delta Z}$ arises from the wave function renormalization

$M_{1,\delta Z} = 2\Re$ 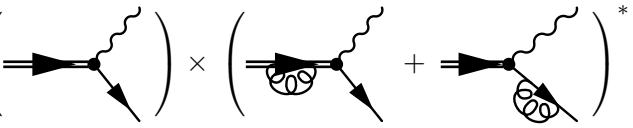

In order to better understand the origin of this term and how to calculate it, consider the full two point function $\hat{\Sigma}(p^2)$ of a scalar[2]

$\hat{\Sigma}(p^2) \quad =$ 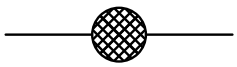

In the vicinity of the mass pole, $\hat{\Sigma}$ has a Laurent expansion

$$\hat{\Sigma}(p^2) = \frac{Zi}{p^2 - m^2} + \mathcal{O}(1)$$

with the pole mass m and residual Z. At tree level, the residual is $Z = 1$. However, loop corrections give rise to a nontrivial value of Z which depends on the renormalization scheme chosen. If we apply LSZ reduction (see e.g. [6]) and amputate legs from a Green's function to obtain a transition matrix element, we have to keep track of the potentially nontrivial residual

$\mathcal{M} = \frac{-i}{\sqrt{Z}} \lim_{p^2 \to m^2} (p^2 - m^2)$ 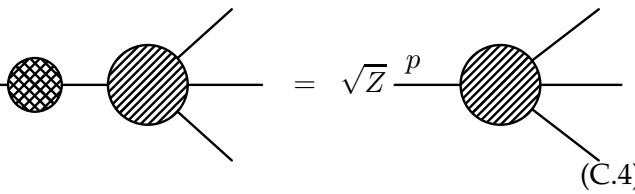 (C.4)

(C.4) shows that we have to multiply the amputated Greens function with the proper residual $\sqrt{Z}$ for each external leg in order to correctly obtain the transition

[2]Choosing a scalar is convenient to make the argument more transparent. Of course, the same reasoning applies to fields of arbitrary spin.

matrix element. This is precisely the origin of $M_{1,\delta Z}$. If we work in perturbation theory, then the residual can be expanded as

$$Z = 1 + \alpha_s \Delta Z_1 + \mathcal{O}\left(\alpha_s^2\right) \tag{C.5}$$

and $M_{1,\delta Z}$ is correctly calculated as

$$M_{1,\delta Z} = M_0 \left(\Delta Z_{1,f'} + \Delta Z_{1,f}\right)$$

with the residuals of the two fermions f and f'.

For the actual calculation of the residual, decompose the one particle irreducible (1PI) two point function as

$i\Pi(p^2)$ = 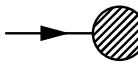 = $i\left(\not{p}\Delta(p^2) + m\Sigma(p^2)\right)$ (C.6)

with scalar functions Δ and Σ. The full two point function is then obtained by Dyson resummation of the 1PI function

$$\hat{\Sigma} = \frac{i}{\not{p} - m} + \frac{i}{\not{p} - m}\left(i\Pi\right)\frac{i}{\not{p} - m} + \ldots = \frac{i}{\not{p} - m}\frac{1}{1 + \frac{\Pi}{\not{p} - m}} = \frac{i}{\not{p} - m + \Pi}$$

Using the decomposition (C.6), this can be more properly written as

$$\hat{\Sigma} = \frac{i}{1 + \Delta} \cdot \frac{\not{p} + m\frac{1-\Sigma}{1+\Delta}}{p^2 - m^2\left(\frac{1-\Sigma}{1+\Delta}\right)^2}$$

As we have chosen to renormalize the mass on-shell[3], the self energy $\hat{\Sigma}$ must have a pole at $p^2 = m^2$, and we can perform Laurent expansions around m

$$\frac{1 - \Sigma(p^2)}{1 + \Delta(p^2)} = 1 + \mathcal{O}\left(p^2 - m^2\right)$$

$$\frac{i}{B(p^2)} = \frac{1}{1 + \Delta} \cdot \frac{i}{p^2 - m^2\left(\frac{1-\Sigma}{1+\Delta}\right)^2} = \frac{iZ}{p^2 - m^2} + \mathcal{O}\left(1\right) \tag{C.7}$$

(C.7) implies that the self energy can be expanded around the pole as

$$\hat{\Sigma} = \frac{iZ}{\not{p} - m} + \mathcal{O}\left(1\right)$$

[3] If the calculation is performed in a different renormalization scheme, then we can always perform a finite renormalization of the mass

$$m \to m - m\delta m \quad , \quad \Sigma \to \Sigma + \delta m + \mathcal{O}\left(\alpha_s^2\right)$$

such that the on-shell condition is fulfilled. As the final $\mathcal{O}\left(\alpha_s\right)$ result (C.8) only depends on the derivative Σ' which is independent on the finite renormalization δm to order $\mathcal{O}\left(\alpha_s\right)$, it is in fact valid for any renormalization scheme (provided that we set m to the pole mass in (C.8)).

with Z being the residual we are looking for and which therefore can be calculated as

$$\frac{1}{Z} = \frac{d}{dp^2} B(p^2) \Big|_{p^2=m^2}$$

Plugging in (C.7) and expanding in α_s, we finally obtain

$$\Delta Z = -\Delta(m^2) - 2m^2 \left(\Delta'(m^2) + \Sigma'(m^2)\right) \tag{C.8}$$

The actual calculation of $M_{1,\mathrm{1PI}}$ and ΔZ was carried out using FeynArts [57] and FormCalc [66]. The result for $M_{1,\mathrm{1PI}}$ is

$$\begin{aligned}
M_{1,\mathrm{1PI}} = \\
&-\frac{2}{3\pi} M_0 \\
&+\frac{4g_V}{3\pi m_2^2}\left((m_1-m_3)^2 - m_2^2\right)\Big(\\
&\quad + B_0\left({m_1}^2 + 2m_3m_1 + 2{m_2}^2 + {m_3}^2\right) \\
&\quad + C_0\left({m_1}^4 + 2m_3{m_1}^3 + \left({m_2}^2 + 2{m_3}^2\right){m_1}^2 + \left(2{m_3}^3 - 2{m_2}^2m_3\right)m_1\right. \\
&\qquad \left. - 2{m_2}^4 + {m_3}^4 + {m_2}^2{m_3}^2\right) \\
&\quad + C_1\left({m_1}^4 + 2m_3{m_1}^3 + \left({m_2}^2 + 2{m_3}^2\right){m_1}^2 + m_3\left({m_2}^2 + 2{m_3}^2\right)m_1\right. \\
&\qquad \left. -2{m_2}^4 + {m_3}^4 + 4{m_2}^2{m_3}^2\right) \\
&\quad + C_2\left({m_1}^4 + 2m_3{m_1}^3 + 2\left(2{m_2}^2 + {m_3}^2\right){m_1}^2 + m_3\left({m_2}^2 + 2{m_3}^2\right)m_1\right. \\
&\qquad \left. -2{m_2}^4 + {m_3}^4 + {m_2}^2{m_3}^2\right) \\
&\quad - C_{00}\left(2\left({m_1}^2 + 2m_3m_1 + 2{m_2}^2 + {m_3}^2\right)\right) \\
&\quad - C_{11}\left(m_3(m_1+m_3)\left({m_1}^2 + 2m_3m_1 - {m_2}^2 + {m_3}^2\right)\right) \\
&\quad - C_{12}\left((m_1+m_3)^2\left({m_1}^2 + 2m_3m_1 - {m_2}^2 + {m_3}^2\right)\right) \\
&\quad - C_{22}\left(m_1(m_1+m_3)\left({m_1}^2 + 2m_3m_1 - {m_2}^2 + {m_3}^2\right)\right)\Big) \\
&+\frac{4g_A}{3\pi m_2^2}\left((m_1+m_3)^2 - m_2^2\right)\Big(\\
&\quad + B_0\left({m_1}^2 - 2m_3m_1 + 2{m_2}^2 + {m_3}^2\right) \\
&\quad + C_0\left({m_1}^4 - 2m_3{m_1}^3 + \left({m_2}^2 + 2{m_3}^2\right){m_1}^2 + 2m_3\left({m_2}^2 - {m_3}^2\right)m_1\right. \\
&\qquad \left. -2{m_2}^4 + {m_3}^4 + {m_2}^2{m_3}^2\right) \\
&\quad + C_1\left({m_1}^4 - 2m_3{m_1}^3 + \left({m_2}^2 + 2{m_3}^2\right){m_1}^2 - m_3\left({m_2}^2 + 2{m_3}^2\right)m_1\right. \\
&\qquad \left. -2{m_2}^4 + {m_3}^4 + 4{m_2}^2{m_3}^2\right) \\
&\quad + C_2\left({m_1}^4 - 2m_3{m_1}^3 + 2\left(2{m_2}^2 + {m_3}^2\right){m_1}^2 - m_3\left({m_2}^2 + 2{m_3}^2\right)m_1\right. \\
&\qquad \left. -2{m_2}^4 + {m_3}^4 + {m_2}^2{m_3}^2\right)
\end{aligned}$$

$$
\begin{aligned}
&- C_{00}\left(2\left({m_1}^2 - 2m_3m_1 + 2{m_2}^2 + {m_3}^2\right)\right) \\
&- C_{11}\left((m_3 - m_1)m_3\left({m_1}^2 - 2m_3m_1 - {m_2}^2 + {m_3}^2\right)\right) \\
&- C_{12}\left((m_1 - m_3)^2\left({m_1}^2 - 2m_3m_1 - {m_2}^2 + {m_3}^2\right)\right) \\
&- C_{22}\left(m_1(m_1 - m_3)\left({m_1}^2 - 2m_3m_1 - {m_2}^2 + {m_3}^2\right)\right)\Bigg)
\end{aligned}
\tag{C.9}
$$

where the same assignments as in (C.2) are used for the masses of the particles. B_i, C_i and C_{ij} appearing in (C.9) are the scalar and tensor integrals defined in [67] with

$$
\begin{aligned}
B_i &= B_i\left(m_2^2, m_3^2, m_1^2\right) \\
C_i &= C_i\left(m_3^2, m_2^2, m_1^2, 0, m_3^2, m_1^2\right) \\
C_{ij} &= C_{ij}\left(m_3^2, m_2^2, m_1^2, 0, m_3^2, m_1^2\right)
\end{aligned}
$$

For the $\mathcal{O}\left(\alpha_s\right)$ correction to the the residual (C.5), we obtain the result

$$
\begin{aligned}
\Delta Z = -\frac{1}{3\pi} + \frac{2}{3\pi}\Bigg(&B_0\left(m^2, 0, m^2\right) + B_1\left(m^2, 0, m^2\right) - \\
&2m^2\frac{\partial}{\partial p^2}\left(B_0\left(p^2, 0, m^2\right) - B_1\left(p^2, 0, m^2\right)\right)\Big|_{p^2=m^2}\Bigg)
\end{aligned}
\tag{C.10}
$$

with the fermion mass m.

Both (C.9) and (C.10) contain a infrared divergence which originates from the vanishing gluon mass and which is understood to be regularized by a small gluon mass ω. The divergence in ω drops out once the contributions of gluon radiation are added, allowing for a finite limit $\omega \to 0$. By the virtue of gauge invariance, the dependence on the renormalization scale μ drops out of the NLO result (C.3), leaving the running of α_s as the only source of the scale uncertainty.

Real corrections

The remaining piece to calculate is the decay width of the heavy quark going into a quark, a heavy gauge boson and an on-shell gluon

$\Gamma_{\text{real}} \propto$ 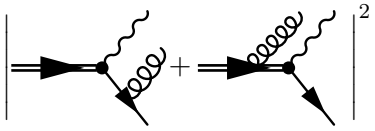

For the calculation, we choose a mass and momentum assignment analogous to (C.2)

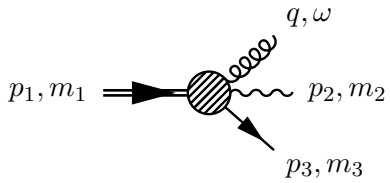

and label the phasespace integrals appearing in the calculation in accordance with [67] as

$$I^{j_1\ldots i_m}_{i_1\ldots i_n} = \frac{1}{\pi^2}\int \frac{d^3p_2}{2p_2^0}\frac{d^3p_3}{2p_3^0}\frac{d^3q}{2q^0}\delta\left(p_1+p_2+p_3-q\right)\frac{(\pm 2qp_{j_1})\ldots(\pm 2qp_{j_m})}{(\pm 2qp_{i_1})\ldots(\pm 2qp_{i_n})} \tag{C.11}$$

with the minus signs belonging to p_1 and the plus signs to $p_{2/3}$. Analytical expressions for the integrals (C.11) can be found in [67].

The calculation has been carried out with FORM [68] and we choose to decompose the results as

$$\Gamma_{\text{real}} = -\frac{\alpha_s}{3\pi^2 m_2^2 m_1}\left(g_V A_V + g_A A_A\right) \tag{C.12}$$

A_V is defined in terms of the integrals (C.11) as

$$\begin{aligned} A_V = {} & (m_3-m_1)^2 I + \\ & \left((m_3-m_1)^2 - m_2^2\right)\left((m_3+m_1)^2 + 2m_2^2\right)\times \\ & \left(I_1 + I_3 + m_1^2 I_{11} + \left(m_1^2 - m_2^2 + m_3^2\right) I_{13} + m_3^2 I_{33}\right) + \\ & \left(m_2^2 + \frac{1}{2}(m_3-m_1)^2\right)\left(I_3^1 + I_1^3\right) \end{aligned}$$

and A_A can be obtained from A_V by swapping the sign of m_1 (just in the polynomials, not in the integrals (C.11)).

Appendix D

Code

This chapter is intended to give an overview over some of the code written in the course of this thesis. However, it does not intended to cover the whole source which can be downloaded from

`http://theorie.physik.uni-wuerzburg.de/~cnspeckn/`

D.1 Coupling Library

The coupling library is split into four core modules and a number of support modules and programs. The core consists of:

- **module** `tdefs`: Global definitions.
- **module** `threeshl`: Actual implementation of the model; calculates masses, couplings and widths.
- **module** `nlowidth`: Contains the numerical code for the calculation of the $\mathcal{O}(\alpha_s)$ QCD corrections, c.f. app. C.2.
- **module** `tglue`: Definitions and functions for access from the O'Mega-generated amplitudes.

The support components are

- **module** `tscript`: Allows to access to masses, widths, couplings etc. by text identifiers like e.g. `lhcoupling(T b W)` for the left-handed $t'bW'$ coupling.
- **program** `spektrum`: Dumps spectrum and couplings for a specific point in parameter space (c.f. app. B).
- **program** `threeshleval`: Simple command-line tool which evaluates a quantity as specified by a `tscript` function.
- **program** `paraplot`: Generates a density plot of a `tscript` function over parameter space, taking a list of constraints into account.

- `scan`: Bash script for creating a "catalogue" of density plots.
- `plotter.pl`: Perl frontend to `threeshleval` for plotting quantities over $m_{W'}$ or M_{bulk}.
- `threeshl_mlink`: Mathematica wrapper around the libraries. Allows to access quantities via `tscript` functions.

In this section, some pieces of code will be presented to illustrate organization, implementation and usage of the package. The interested reader should consult the woven documentation generated from the noweb source which can be downloaded from the URL quoted at the beginning of this chapter which is more detailed and also gives the analytic formulae employed by the module.

Definitions: `module tdefs`

The module `tdefs` defines some basic constants

```
integer, parameter :: double=selected_real_kind &
  (precision(1.)+1, range(1.)+1)
integer, parameter :: slength = 256
real(kind=double), parameter :: &
  pi=3.1415926535897932385_double
```

`slength` defines a standard length for character variables, and the other two constants are self-explanatory. In addition, the module defines the `output_unit` and `error_onit` either via the `iso_fortran_env` (a FORTRAN 2003 feature) or as an ordinary constant in case this module is not supported by the compiler.

The actual calculations: `module threeshl`

The first duty of this module is to provide the necessary infrastructure to store the masses, widths, wavefunctions and couplings. To this end, each particle is assigned a number between 0 and 64 whose bits encode different quantum numbers

bits	meaning
0	0: Light state, 1: Heavy state
1	0: Fermion, 1: Boson
2	0: Lepton, 1: Quark (0: W, 1: Z)
3	0: Isospin $\frac{1}{2}$, 1: Isospin $-\frac{1}{2}$
4-5	Fermion generation

```
integer, parameter, public :: e_bcd=B'001000', nue_bcd=B'000000', &
  mu_bcd=B'011000', numu_bcd=B'010000', tau_bcd=B'101000', &
  nutau_bcd=B'100000', he_bcd=B'001001',hnue_bcd=B'000001', &
  hmu_bcd=B'011001', hnumu_bcd=B'010001', htau_bcd=B'101001', &
  hnutau_bcd=B'100001', u_bcd=B'000100', d_bcd=B'001100', &
```

```
  c_bcd=B'010100', s_bcd=B'011100', t_bcd=B'100100', &
  b_bcd=B'101100', hu_bcd=B'000101', hd_bcd=B'001101', &
  hc_bcd=B'010101', hs_bcd=B'011101', ht_bcd=B'100101', &
  hb_bcd=B'101101', w_bcd=B'010', hw_bcd=B'011', z_bcd=B'110', &
  hz_bcd=B'111', a_bcd=63
```

(although it doesn't fit into the quantum number scheme, the photon snaps nicely into its place). For the indexing of the coupling arrays, index ranges are defined which are nontrivial and disjunct in order to allow for better compile-time and run-time consistency checks

specifier	meaning
`l_chir, r_chir`	chirality
`l_mode, h_mode, lh_mode`	KK modes / mode combinations
`iso_up, iso_down`	isospin
`lat_0, lat_1, lat_2`	lattice sites
`gen_0, gen_1, gen_3`	fermion generations
`ftype_l, ftype_q`	lepton / quark
`ptype_b, ptype_f`	boson / fermion
`btype_w, btype_z, btype_a`	W / Z

```
integer, parameter, public :: l_chir=100, r_chir=101, &
  l_mode=110, h_mode=111, lh_mode=112, iso_up=120, &
  iso_down=121, lat_0=130, lat_1=131, lat_2=132, &
  gen_0=140, gen_1=141, gen_2=142, ftype_l=150, &
  ftype_q=151, ptype_b=160, ptype_f=161, btype_w=170, &
  btype_z=171, btype_a=172
```

The masses and widths of the particles are then stored in arrays indexed by the integer assigned to the particle

```
real(kind=double), public, target :: &
  mass_array(0:63)=0., width_array(0:63)=0.
```

while the couplings are stored in arrays which are indexed by the quantum numbers of the lines meeting at the vertex

```
real(kind=double), public, target :: &
  g_w_lep(l_mode:h_mode, l_mode:h_mode, gen_0:gen_2, &
    l_mode:h_mode, gen_0:gen_2, l_chir:r_chir)= 0., &
  g_w_quark(l_mode:h_mode, l_mode:h_mode, gen_0:gen_2, &
  l_mode:h_mode, gen_0:gen_2, l_chir:r_chir)= 0.
real(kind=double), public, target :: &
  g_z_lep(l_mode:h_mode, l_mode:lh_mode, gen_0:gen_2, &
    iso_up:iso_down, l_chir:r_chir)= 0.,&
  g_z_quark(l_mode:h_mode, l_mode:lh_mode, gen_0:gen_2, &
    iso_up:iso_down, l_chir:r_chir)= 0.
real(kind=double), public, target :: &
  g_wwz(l_mode:lh_mode, l_mode:h_mode)= 0.
```

```
real(kind=double), public, target :: &
  g_wwww(0:4)=(/(0.,i=1,5)/), &
  g_wwzz(l_mode:lh_mode, l_mode:lh_mode)= 0., &
  g_wwza(l_mode:lh_mode, l_mode:h_mode)= 0.
```

(the coupling between four $W^{(\prime)}$ is an exception and is enumerated by the number of W' at the vertex). All other couplings are fixed by electromagnetic or $\mathbf{SU}(3)_C$ gauge invariance. For convenience when calculating the couplings, the wavefunctions are organized in a similar way

```
real(kind=double) :: &
  wfunct_w(l_mode:h_mode, lat_0:lat_1)= 0., &
  wfunct_z(l_mode:h_mode, lat_0:lat_2)= 0.
real(kind=double) :: &
  wfunct_lep_l(l_mode:h_mode, gen_0:gen_2, &
    iso_up:iso_down, lat_0:lat_1)= 0.,&
  wfunct_lep_r(l_mode:h_mode, gen_0:gen_2, &
    iso_up:iso_down, lat_1:lat_2)= 0.,&
  wfunct_quark_l(l_mode:h_mode, gen_0:gen_2, &
    iso_up:iso_down, lat_0:lat_1)= 0.,&
  wfunct_quark_r(l_mode:h_mode, gen_0:gen_2, &
    iso_up:iso_down, lat_1:lat_2)= 0.
```

The parameters of the Three-Site Lagrangian are defined as

```
real(kind=double), target :: sigma_vev=0., g0=0., g1=0., &
  g2=0., x=0., lambda=0., t=0., eps_l, &
  eps_r(ftype_l:ftype_q, gen_0:gen_2, iso_up:iso_down)= 0., e
```

where t is redundant and defined for convenience only. `sigma_vev` must be divided by $\sqrt{2}$ to obtain the symmetry breaking scale v defined in chapter 3.3, and `lambda` has to be multiplied by 2 to obtain $\tilde{\lambda}$ (due to a difference in convention).

The Standard Model parameters are defined as variables which have to be set prior to calling the diagonalization routines

```
real(kind=double), public :: &
  me_pdg=0._double, mmu_pdg=0.106_double, mtau_pdg=1.78_double, &
  muq_pdg=0._double, mdq_pdg=0._double, mcq_pdg=1.25_double, &
  msq_pdg=0.95_double, mtq_pdg=174._double, mbq_pdg=4.2_double, &
  mw_pdg=80.403_double, mz_pdg=91.188_double, &
  e_pdg=0.313329_double, ww_pdg=2.048_double, &
  wz_pdg=2.443_double, wt_pdg=1.523_double
```

In addition, there is an error reporting system built into the module which traps invalid function calls or points in parameter space at which the analytic formulae contain complex roots. Each function pushes its name via a call to `estack_push` on a stack when it begins execution and removes it again via `estack_pop` at the end. A subprogram `panic` is called if an error occurs, which then prints an error message and the contents of the error stack to help localizing the origin of the failure. A version of the square root `msqrt` is provided which traps complex roots.

Apart from the Standard Model parameters and the mass / width arrays, most variables, subprograms and functions are declared as **private** and prefixed with `threeshl_` for export (the variables are exported by pointers).

Prior to using the library, the subprogram `init` must be called

```
subroutine init
# ifdef __NLOW__
  call nlow_init
# endif
  call set_names
  call init_pointers
end subroutine init
```

which initializes a couple of internal quantities (if the $\mathcal{O}(\alpha_s)$ corrections have been enabled at compile time, the corresponding library is also initialized). Afterwards, the Standard Model variables can be redefined if desired and the Model is then initialized by a call to

```
subroutine pdg_init_wgap_bmass (mhw, bmass, el)
real(kind=double), intent(in) :: mhw, bmass
real(kind=double), optional, intent(in) :: el
character(len=slength), parameter :: fname="pdb_init_wgap_bmass"
  call errstack_push(fname)
  if ((mhw < mw_pdg) .or. (bmass < 0.)) &
    call panic(err_invalid_parameters, 0)
  call gauge_cpl_from_sm_wgap(mw_pdg, mz_pdg, e_pdg, mhw)
  if (present (el)) then
    eps_l = el
  else
    eps_l = eps_l_of_x(x)
  end if
  lambda = bmass / sqrt(2._double) / sigma_vev
  call translate_fermion_masses( (/me_pdg, mmu_pdg, mtau_pdg/), &
    (/muq_pdg, mcq_pdg, mtq_pdg/), (/mdq_pdg, msq_pdg, mbq_pdg/))
  call diagonalize
  call errstack_pop
end subroutine pdg_init_wgap_bmass
```

The call to `gauge_cpl_from_sm_wgap` first calculates the gauge couplings from the W, W' and Z masses and the electromagnetic gauge coupling e. If ϵ_L is not given, ideal delocalization is assumed and ϵ_L is calculated from x. $\tilde{\lambda}$ is then set from M_{bulk} and `translate_fermion_masses` is called to calculate the ϵ_R from the SM fermion masses. Finally, `diagonalize` is called.

For more information on the guts of `diagonalize` refer to the woven source. In a nutshell, this subprogram performs the following steps

- Calculate the gauge boson wavefunctions and masses.
- Calculate the fermion wavefunctions and masses.
- Calculate the couplings.

In particular, the masses of the Standard Model particles are not taken from the input parameters, but are also calculated from the mass matrices in order to provide a simple consistency check.

An error during the calculation usually triggers the termination of the program. This behavior can be modified by setting the flag `threeshl_quit_on_panic` to `.false.`, in which case the library returns to the caller, printing an error message to STDOUT and setting the flag `threeshl_error`.

After the couplings have been calculated, the user can call the subprogram `calculate_widths` in order to calculate the widths and fill the width array (only the widths of the KK particles are calculated, the t, W and Z widths are taken from the Standard Model parameters, and the other Standard Model particles are set to zero width). If activated at compile time, the $\mathcal{O}(\alpha_s)$ corrections to the heavy quark widths can be included. This can be controlled via the global flag `threeshl_use_nlow` which is set to `.true.` per default. In the calculation, α_s is evaluated at the heavy quark mass.

It is also possible to initialize the model in the massless limit described in chapter 5.3. To this end, the subprogram `init_ward` must be called

```
subroutine init_ward (mx, ct, ph)
real(kind=double), intent(in) :: mx, ct, ph
integer :: gen, iso
character(len=slength), parameter :: fname = "init_ward"
  call errstack_push(fname)
  if ( (ct .le. -1._double) .or. &
       (ct .ge. 1._double) .or. (mx == 0.)) &
    call panic (err_invalid_parameters, 0)
  mass_array = 0.
  t = msqrt(1._double/ct**2 - 1._double)
  x = mx
  e = e_pdg
  g0 = e * msqrt( 1._double + x**2 + 1._double/t**2 )
  g1 = g0 / x
  g2 = g0 * t
  sigma_vev = 0.
  lambda = 0.
  eps_l = 0.
  eps_r = 0.
  wfunct_w(l_mode, :) = (/cos(ph), sin(ph)/)
  wfunct_w(h_mode, :) = (/-sin(ph), cos(ph)/)
  wfunct_z(l_mode, :) = (/-g2/2._double/g1 - g1/g2 , &
    g2/2._double/g0 - g0/2._double/g2 , g1/g0 + g0/2._double/g1 /)
  wfunct_z(l_mode, :) = wfunct_z(l_mode, :) / &
    msqrt(wfunct_z(l_mode, lat_0)**2 + &
      wfunct_z(l_mode, lat_1)**2 + &
      wfunct_z(l_mode, lat_2)**2)
  wfunct_z(h_mode, :) = &
    (/-g0/2._double, g1, -g2/2._double/) / &
    msqrt(g0**2/4._double + g1**2 + g2**2/4._double)
```

```
  do gen = gen_0, gen_2 ; do iso = iso_up, iso_down
    wfunct_lep_l(l_mode, gen, iso, :) = (/cos(ph), sin(ph)/)
    wfunct_lep_l(h_mode, gen, iso, :) = (/-sin(ph), cos(ph)/)
    wfunct_lep_r(l_mode, gen, iso, :) = (/sin(ph), cos(ph)/)
    wfunct_lep_r(h_mode, gen ,iso, :) = (/cos(ph), -sin(ph)/)
    wfunct_quark_l(l_mode, gen, iso, :) = (/cos(ph), sin(ph)/)
    wfunct_quark_l(h_mode, gen, iso, :) = (/-sin(ph), cos(ph)/)
    wfunct_quark_r(l_mode, gen, iso, :) = (/sin(ph), cos(ph)/)
    wfunct_quark_r(h_mode, gen ,iso, :) = (/cos(ph),-sin(ph)/)
  end do; end do
  call calculate_couplings
  call errstack_pop
end subroutine init_ward
```

This first sets all masses to zero and calculates the wavefunctions and parameters according to chapter 5.3. Then, the couplings are calculated via the overlap of the wavefunctions just like in the physical case.

After using the library, the function `finalize` should be called.

$\mathcal{O}(\alpha_s)$ corrections to the fermion widths: `module nlowidth`

The module `nlowidth` implements the numerical calculation of the analytical expressions given in app. C.2. As this might be useful in other contexts than the Three-Site Model, this module is kept separate from the noweb source of the rest of the package and doesn't contain any dependencies on the other packages. The analytical expressions are included from external files which have been autogenerated from Mathematica, and a FORTRAN 90 wrapper around the LoopTools library (which is FORTRAN 77 code) is supplied. As there is no woven documentation for this module, it is completely reprinted and documented here

```
module nlowidth
use ltglue
```

The LoopTools library outputs status and error messages to STDOUT. Unfortunately, there is no way to change this behavior which disturbs the operation of programs like `spektrum` or `threeshl`. To this end, the module calls `libc` functions to redirect these messages to STDERR (a trick shamelessly stolen from the Mathematica wrapper around LoopTools). This relies on FORTRAN 2003 features and can be deactivated at compile time via the preprocessor variable `__NO__SILENCER__`.

```
#ifndef __NO_SILENCER__
use, intrinsic :: iso_c_binding
use, intrinsic :: iso_fortran_env
#endif

implicit none
private
```

All **`public`** qualifiers are prefixed with `nlow_`, everything else is **`private`**.

```
public :: nlow_dz, nlow_nlo, nlow_rrad, nlow_lo, nlow_width, &
  nlow_wrel, nlow_init, nlow_finalize, nlow_alfas, nlow_alfas_mz, &
  nlow_mt, nlow_mb, nlow_mc, nlow_mz, nlow_b2mode, &
  nlow_b2mode_series, nlow_b2mode_full, nlow_b2mode_auto, &
  nlow_b2auto_thresh
```

The parameter β_2 used in [67] for the definition of the three-particle phasespace integrals turns out to be numerically unstable in the massless limit for the final state fermion. Therefore, the module can either use the full analytic expression for β_2 or an expansion in

$$\epsilon = \frac{m_0 m_2}{m_0^2 - m_1^2}$$

to order $\mathcal{O}\left(\epsilon^{19}\right)$ (using the naming conventions from app. C). This choice can be controlled via `nlow_b2mode` with the default setting `nlow_b2mode_auto` using the full expression for β_2 above `nlow_b2auto_thresh` and the expansion below it. The remaining public parameters which can be modified are the c, b, t and Z masses and the value of α_s at the Z pole which are required for the evolution of the coupling.

```
integer, parameter :: nlow_b2mode_series=0, nlow_b2mode_full=1, &
  nlow_b2mode_auto=2
integer, parameter :: double=selected_real_kind&
  (precision(1.) + 1, range(1.) + 1)
real(kind=double), parameter :: pi=3.1415926535897932385_double
real(kind=double) :: nlow_alfas_mz=0.1176_double, &
  nlow_mt=174._double, nlow_mb=4.2, nlow_mc=1.25, &
  nlow_mz=91.188_double, nlow_b2auto_thresh=0.1_double
integer :: stdout_copy, nlow_b2mode=nlow_b2mode_auto
```

The following functions are overloaded and can be called with or without m_2. If m_2 is committed, then the limit $m_2 \to 0$ is performed (see the actual implementation below for details); otherwise, the treatment of m_2 is determined from `nlow_b2mode`.

`nlow_rrad` calculates the $1 \to 3$ decay width an external gluon, `nlow_width` the full $\mathcal{O}(\alpha_s)$ width (including virtual + real corrections) and `nlow_wrel` returns the $\mathcal{O}(\alpha_s)$ width normalized to the leading order result.

```
interface nlow_rrad
  module procedure rrad_nobs
  module procedure rrad_bs
end interface nlow_rrad

interface nlow_width
  module procedure width_nobs
  module procedure width_bs
end interface nlow_width

interface nlow_wrel
  module procedure wrel_nobs
  module procedure wrel_bs
end interface nlow_wrel
```

This is the C interface necessary for redirecting the LoopTools output.

```
#ifndef __NO_SILENCER__
interface
  function dup (s) result (t) bind (c, name="dup")
    import :: c_int
    integer (kind=c_int), value :: s
    integer (kind=c_int) :: t
  end function dup

  function dup2 (s, t) result (r) bind (c, name="dup2")
    import :: c_int
    integer (kind=c_int), value :: s, t
    integer (kind=c_int) :: r
  end function dup2
end interface
#endif

contains
```

`redirect` and `end_redirect` are responsible for the actual redirection.

```
subroutine redirect
integer :: dummy
# ifndef __NO_SILENCER__
  flush (output_unit, iostat=dummy)
  flush (error_unit, iostat=dummy)
  dummy = dup2 (2, 1)
# endif
end subroutine redirect

subroutine end_redirect
integer :: dummy
# ifndef __NO_SILENCER__
  flush (output_unit, iostat=dummy)
  flush (error_unit, iostat=dummy)
  dummy = dup2 (stdout_copy, 1)
# endif
end subroutine end_redirect
```

The following two functions should be called before and after using the library.

```
subroutine nlow_init
# ifndef __NO_SILENCER__
  stdout_copy = dup (1)
# endif
  call redirect
  call ffini
  call end_redirect
end subroutine nlow_init

subroutine nlow_finalize
```

```
  call redirect
  call ffexi
  call end_redirect
end subroutine nlow_finalize
```

Calculates the normalization factor for $1 \to 2$. `mt`, `mb` and `mw` are m_0, m_2 and m_1 (adhering to the conventions of app. C).

```
function wdnorm (mt, mb, mw) result (res)
real(kind=double), intent(in) :: mt, mb, mw
real(kind=double) :: res
  call redirect
  if ((min (mt, mb, mw) < 0.) .or. (mt < mb + mw)) &
    print *, "WARNING: calculating broken width!"
  res = sqrt((mt**2 - (mb + mw)**2)*(mt**2 - (mb - mw)**2)) / &
    mt**3 / 32._double / pi
  call end_redirect
end function wdnorm
```

This function calculates the $\mathcal{O}(\alpha_s)$ contribution to the residual of the quark propagator (C.10). The actual code for ΔZ is included from `dz.inc`. `m` is the fermion mass, and `l` the infinitesimal gluon mass ω

```
function nlow_dz (m, l) result (res)
real(kind=double), intent(in) :: m, l
real(kind=double) :: res
complex(kind=double) :: dz
  call redirect
  call setlambda (l**2)
# include "dz.inc"
  if (aimag (dz) /= 0._double) print *, &
    "WARNING: dz not strictly real! ", aimag (dz)
  res = real (dz)
  call end_redirect
end function nlow_dz
```

Calculates the $\mathcal{O}(\alpha_s)$ 1PI correction to the $1 \to 2$ width. Again, the actual code is included from an extra file. `gv` and `ga` are the vector and axial couplings and `l` is the gluon mass ω.

```
function nlow_nlo (mt, mb, mw, gv, ga, l) result (res)
real(kind=double), intent(in) :: mt, mb, mw, gv, ga, l
real(kind=double) :: res
complex(kind=double) :: nlo
  call redirect
  call setlambda (l**2)
# include "nlo.inc"
  if (aimag (nlo) /= 0._double) print *, &
    "WARNING: nlo not strictly real! ", aimag (nlo)
  res = real (nlo) * wdnorm (mt, mb, mw)
  call end_redirect
end function nlow_nlo
```

The next two **private** functions are the $m_2 \neq 0$ resp. $m_2 = 0$ branches of the **public** `nlow_rrad` and calculate the $1 \to 3$ decay width for real gluon radiation.

In the first case, the code for the analytical expressions of the phasespace integrals (C.11) is taken from [67] and included from external files. Depending on `nlow_b2mode` and m_2, the series expansion of β_2 (see above) is used. The analytical expression for the $1 \to 3$ in terms of the phase space integrals is read in from `rrad.inc`.

In the second case, an infrared singularity arises in the limit $m_2 \to 0$ which cancels between virtual and real corrections. The function sets $m_2 = 10^{-50}\,\mathrm{GeV}$ in order to regularize this divergence and then evaluates a version of the $2 \to 3$ width where only the logarithms in m_2 are retained.

```
function rrad_nobs (mt, mb, mw, gv, ga, l) result (res)
real(kind=double), intent(in) :: mt, mb, mw, gv, ga, l
real(kind=double) :: res, ep
complex(kind=double) :: rrad, k, b0, b1, b2, int0, int101, int10, &
  int11, int200, int201, int211, int110, b2_series
  call redirect
# include "k.inc"
# include "b0.inc"
# include "b1.inc"
  ep = mb*mt/(mt**2 - mw**2)
  select case (nlow_b2mode)
    case (nlow_b2mode_full)
#     include "b2.inc"
    case (nlow_b2mode_series)
#     include "b2_series.inc"
      b2 = b2_series
    case (nlow_b2mode_auto)
      if (ep < nlow_b2auto_thresh) then
#       include "b2_series.inc"
        b2 = b2_series
      else
#       include "b2.inc"
      end if
    case default
      print *, "WARNING: invalid nlow_b2mode; using nlow_b2mode_full!"
#     include "b2.inc"
  end select
# include "int0.inc"
# include "int101.inc"
# include "int10.inc"
# include "int11.inc"
# include "int200.inc"
# include "int201.inc"
# include "int211.inc"
# include "int110.inc"
# include "rrad.inc"
  if (aimag (rrad) /= 0._double) print *, &
```

```
      "WARNING: rrad not strictly real! ", aimag(rrad)
   res = real (rrad)
   call end_redirect
end function rrad_nobs

function rrad_bs (mmt, mmw, gv, ga, l) result (res)
real(kind=double), intent(in) :: mmt, mmw, gv, ga, l
real(kind=double) :: res
complex(kind=double) :: rrad_bsoft, mb, mt, mw
   mt = mmt; mw = mmw
   mb = (1.E-50_double, 0._double)
   call redirect
#  include "rrad_bsoft.inc"
   if (aimag (rrad_bsoft) /= 0._double) print *, &
      "WARNING: rrad_bsoft not strictly real! ", aimag (rrad_bsoft)
   res = real (rrad_bsoft)
   call end_redirect
end function rrad_bs
```

`nlow_lo` calculates the leading order $1 \to 2$ width.

```
function nlow_lo (mt, mb, mw, gv, ga) result (res)
real(kind=double), intent(in) :: mt, mb, mw, gv, ga
real(kind=double) :: res, lo
#  include "lo.inc"
   res = lo * wdnorm (mt, mb, mw)
end function nlow_lo
```

The following two functions are drivers which assemble the NLO width from the leading order result plus the real and virtual corrections. In the $m_2 = 0$ case, m_2 is set to the infrared regulator $m_2 = 10^{-50}\,\mathrm{GeV}$ in order to regularize the divergence which cancels between virtual and real corrections. `alfas` is the value for α_s to be used for the calculation (see below for a function which evolves α_s to the desired scale).

```
function width_bs (mt, mw, gv, ga, alfas, l) result (res)
real(kind=double), intent(in) :: mt, mw, gv, ga, l, alfas
real(kind=double) :: res, low, mb
   mb = 1.E-50_double
   low = nlow_lo(mt, mb, mw, gv, ga)
   res = low + alfas * &
        ((nlow_dz (mt, l) + nlow_dz (mb, l)) * low + &
        nlow_nlo (mt, mb, mw, gv, ga, l) + &
        nlow_rrad (mt, mw, gv, ga, l))
end function width_bs

function width_nobs (mt, mb, mw, gv, ga, alfas, l) result (res)
real(kind=double), intent(in) :: mt, mb, mw, gv, ga, l, alfas
real(kind=double) :: res, low
   low = nlow_lo(mt, mb, mw, gv, ga)
   res = low + alfas * &
```

```
       ((nlow_dz (mt, l) + nlow_dz (mb, l)) * low + &
       nlow_nlo (mt, mb, mw, gv, ga, l) + &
       nlow_rrad (mt, mb, mw, gv, ga, l))
end function width_nobs
```

These two function return the NLO with normalized to the LO result.

```
function wrel_nobs (mt, mb, mw, gv, ga, alfas, l) &
  result (res)
real(kind=double), intent(in) :: mt, mb, mw, gv, ga, l, alfas
real(kind=double) :: res
  res = nlow_width (mt, mb, mw, gv, ga, alfas, l) &
    / nlow_lo (mt, mb, mw, gv, ga)
end function wrel_nobs

function wrel_bs (mt, mw, gv, ga, alfas, l) result (res)
real(kind=double), intent(in) :: mt, mw, gv, ga, l, alfas
real(kind=double) :: res
  res = nlow_width (mt, mw, gv, ga, alfas, l) &
    / nlow_lo (mt, 1.E-50_double, mw, gv, ga)
end function wrel_bs
```

`nlow_alfas` evolves α_s to a given scale. The mass thresholds and the value α_s at the Z pole are global parameters which can be adjusted (see above).

```
function nlow_alfas (l) result (res)
real(kind=double), intent(in) :: l
real(kind=double) :: res, a
  call redirect
  a = nlow_alfas_mz
  if (l < 0) then
    print *, "WARNING: not evolving alfas to a negative scale!"
  elseif (l > nlow_mt) then
    a = evolve (nlow_mt, nlow_mz, a, 5)
    a = evolve (l, nlow_mt, a, 6)
  elseif (l > nlow_mb) then
    a = evolve (l, nlow_mz, a, 5)
  elseif ( l > nlow_mc) then
    a = evolve (nlow_mb, nlow_mz, a ,5)
    a = evolve (l, nlow_mb, a, 4)
  else
    a = evolve (nlow_mb, nlow_mz, a, 5)
    a = evolve (nlow_mc, nlow_mb, a, 4)
    a = evolve (l, nlow_mc, a, 3)
  end if
  res = a
  call end_redirect

contains

function evolve (l1, l0, a0, n) result (res1)
```

```
real(kind=double), intent(in) :: l1, l0, a0
integer, intent(in) :: n
real(kind=double) :: res1
  res1 = 1._double / &
    ( (11._double - 2._double*real(n, kind=double)/3._double) &
    / 2._double / pi * log (l1 / l0) + 1._double / a0)
end function evolve
end function nlow_alfas

end module nlowidth
```

Interfacing O'Mega: `module tglue`

The `tglue` module provides the interface to the matrix element code generated by O'Mega. This is necessary for several reasons:

- Several couplings to the photon and to the gluons are not defined in `threeshl` but are required for the matrix element code to function.
- The couplings between three gauge bosons must be defined with an additional factor i for usage in O'Mega.
- The $W^{(\prime)}ff$ type couplings calculated in `threeshl` are taken w.r.t. to the $W^{(\prime)}_{1/2}$ states and need to be divided by an additional factor of $\sqrt{2}$ in order to obtain the couplings to the $W^{\pm(\prime)}$.
- The couplings between gauge bosons and fermions are decomposed w.r.t. to the left- and right-handed projectors, while the O'Mega implementation uses VA-type couplings.

To this end, additional couplings are defined in this module

```
complex(kind=double), public :: &
  g_a_lep, g_a_quark (iso_up:iso_down), g_aaww, &
  ig_aww, ig_wwz (l_mode:lh_mode, l_mode:h_mode)
complex(kind=double), public :: &
  g_w_lep_va (1:2, l_mode:h_mode, l_mode:h_mode, &
    gen_0:gen_2, l_mode:h_mode, gen_0:gen_2), &
  g_w_quark_va (1:2, l_mode:h_mode, l_mode:h_mode, &
    gen_0:gen_2, l_mode:h_mode, gen_0:gen_2), &
  g_z_lep_va (1:2, l_mode:h_mode, l_mode:lh_mode, &
    gen_0:gen_2, iso_up:iso_down), &
  g_z_quark_va (1:2, l_mode:h_mode, l_mode:lh_mode, &
    gen_0:gen_2, iso_up:iso_down)
real(kind=double), public :: g_s=1.218_double
complex(kind=double), public :: ig_s_norm, g_s_norm, g_s_norm2
```

In order to initialize these couplings, the functions `tglue_init` (and `tglue_init_ward` for the massless limit) are provided which boast the same

interfaces as `threeshl_pdg_init_wgap_bmass` and `threeshl_ward` (see above). The `tglue` initialization automatically initializes the `threeshl` module (and the `tscript` module, see below). Similarly, a `tglue_finalize` is provided which calls all other initialization routines.

An example of how to use `tscript`: `program threeshleval`

Instead of discussing the `tscript` module in detail, the source `treeshleval` is reprinted, a small program which takes $m_{W'}$ M_{bulk} and optionally ϵ_L (for nonideal delocalization) as well as a tscript function definition as command line arguments and returns the evaluated function.

```
program threeshleval
use threeshl
use tdefs
use tscript
use tglue
implicit none
real(kind=double) :: mhw=-1., mbulk=-1., eps_l
real(kind=double), pointer :: value
logical :: el_present = .false.
character(len=slength) :: fun
```

The `tscript` module defines the `tscript_tokenize_object` data type which is initialized by a call to `tscript_create_tobject` with the character string which is to be interpreted as a function definition.

```
type(tscript_tokenize_object) :: tobject
```

First, the program checks if it has been correctly called. If this is not the case, it prints the syntax and quits (see below). Otherwise, the variables are set from the command line arguments.

```
if (.not. ((iargc () >= 3) .and. (iargc () <= 5))) call print_usage
call getarg (1, fun); mhw = str_to_double (fun)
call getarg (2, fun); mbulk = str_to_double (fun)
call getarg (3, fun)
if (iargc() == 4) then
  if (trim (fun) == "no_nlow") then
    threeshl_use_nlow = .false.
  else
    eps_l = str_to_double (fun)
    el_present = .true.
  end if
  call getarg (4, fun)
end if
if (iargc () == 5) then
  eps_l = str_to_double (fun)
  call getarg (4, fun)
  if (trim (fun) == "no_nlow") then
```

```
    threeshl_use_nlow = .false.
  else
    call print_usage
  end if
  call getarg (5, fun)
end if
```

In order to parse the function string, a `tscript_tokenize_object` must be created. This is then decoded by a call to `tscript_decode_fspec` in order to obtain a pointer to the corresponding quantity. If an error occurred during the parsing, the syntax is printed (can be switched off via the flag `tscript_show_syntax`) and the program is terminated if `threesh_quit_on_panic` is set.

```
tobject = tscript_create_tobject(fun)
value => tscript_decode_fspec(tobject)
```

The model is initialized by a call to `tglue_init` and the function value is printed to STDOUT. After calling `tglue_finalize`, the program quits.

```
if (el_present) then
  call tglue_init (mhw, mbulk, el=eps_l)
else
  call tglue_init (mhw, mbulk)
end if
print '(F25.15)', value
call tglue_finalize

contains
```

This subprogram prints the syntax and then in turn calls `tscript_print_syntax` which shows the `tscript` syntax and quits if `threeshl_quit_on_panic` is set.

```
subroutine print_usage
  print *, "usage: threeshleval mhw mbulk [eps_l] [no_nlow] function"
  print *
  print *, "mhw and mbulk are the mass of the heavy W and the bulk mass;"
  print *, "if eps_l is not present, it is determined via ideal"
  print *, "delocalization. As for the function specifier:"
  print *
  call tscript_print_syntax
end subroutine print_usage
```

This tries to interpret a character string as a floating point number.

```
function str_to_double (str) result(res)
character(len=slength), intent(in) :: str
real(kind=double) :: res
integer :: errstat
  read (unit=str, fmt='(F50.50)', iostat=errstat), res
  if (errstat .ne. 0) call print_usage
end function str_to_double

end program threeshleval
```

D.2 O'Mega Module

In this section, only a part of the O'Caml source of the model module is presented. The reader interested in studying the full code is referred to the commented ocaml-web source.

Options

In order to allow for an easy setup of the various options discussed 5.3, the O'Mega module is implemented as a functor which maps two option modules to the final model module. The signatures of these modules are

```
module type Threeshl_options =
  sig
    val include_ckm : bool
    val include_hf : bool
    val diet : bool
  end

type qcd_implementation = Disabled | Colflow

module type Threeshl_colopt =
  sig
    val o : qcd_implementation
  end
```

The meaning of the different options is:

- *include_ckm*: Include flavor violating couplings.
- *include_hf*: Include the heavy fermions.
- *diet*: Setting this to *true* discards all couplings between the W' and the leptons or the first two quark generations (only implemented in the case of *include_ckm=false*).
- *Theeshl_colopt.o*: Method for the treatment of color. Setting this to *Colflow* includes the gluons and the QCD couplings with the sign conventions choosen correctly for the colorizer module to work, *Disabled* excludes the gluons.

The functor is then defined as

```
module Threeshl' (Module_options : Threeshl_options)
  (Module_colopt : Threeshl_colopt) =
```

Other options that the user might want to control can be set via command line options when the binary is invoked

```
let default_width = ref Timelike
let all_feynman = ref false
```

```
let options = Options.create [
  "constant_width", Arg.Unit (fun _ → default_width := Constant),
    "use constant width (also in t-channel)";
  "custom_width", Arg.String (fun x → default_width := Custom x),
    "use custom width";
  "cancel_widths", Arg.Unit (fun _ → default_width := Vanishing),
    "use vanishing width";
  "all_feynman", Arg.Unit (fun _ → all_feynman := true),
    "assign feynman gauge propagators to all gauge bosons\n"
    ^ "\t(for checking the ward identities);"
    ^ "use only if you *really* know\n"
    ^ "\twhat you are doing"]
```

Flavors

The first duty of the module is the definition of a type *flavor* which enumerates the different particles. This is done by first defining quantum numbers that encode KK mode, generation, "charge" (differentiates between particles / antiparticles and is also defined for neutrinos) and isospin and then defining *flavor* through suitable constructors.

```
type kkmode = Light | Heavy
type generation = Gen0 | Gen1 | Gen2
type csign = Pos | Neg
type isospin = Iso_up | Iso_down

type fermion =
  | Lepton of (kkmode × csign × generation × isospin)
  | Quark of (kkmode × csign × generation × isospin)

type boson =
  | W of (kkmode × csign)
  | Z of kkmode
  | A
  | G

type flavor = Fermion of fermion | Boson of boson
```

Two functions *revmap* and *revmap2* are defined which apply a list of functions to a value or resp. each element of a list of values and return the result as a flat list.

```
let revmap funs v = List.map (fun x → x v) funs
let revmap2 funs vals = ThoList.flatmap (revmap funs) vals
```

Together with a couple of functions that map to the constructors

```
let lepton kk cs gen iso = Lepton (kk, cs, gen, iso)
let quark kk cs gen iso = Quark (kk, cs, gen, iso)
let w kk cs = W (kk, cs)
let z kk = Z kk
let flavor_of_f x = Fermion x
let flavor_of_b x = Boson x
```

and several functions which loop a list of functions over the quantum numbers

```
let loop_kk flist = revmap2 flist [Light; Heavy]
let loop_cs flist = revmap2 flist [Pos; Neg]
let loop_gen flist = revmap2 flist [Gen0; Gen1; Gen2]
let loop_iso flist = revmap2 flist [Iso_up; Iso_down]
let cloop_kk flist = match Module_options.include_hf with
  | true → loop_kk flist
  | false → revmap flist Light
```

these two functions allow for the easy creation of a list of all particles which is required by O'Mega

```
let all_leptons = loop_iso (loop_gen (loop_cs (cloop_kk [lepton] )))
let all_quarks = loop_iso( loop_gen (loop_cs (cloop_kk [quark] )))
let all_bosons = (loop_cs (loop_kk [w] )) @ [Z Light; Z Heavy] @ [A] @
  (match Module_colopt.o with Colflow → [G] | _ → [])

let flavors () = (List.map flavor_of_f (all_leptons @ all_quarks)) @
  (List.map flavor_of_b all_bosons)
```

(using *clopp_kk* instead of *loop_kk* automatically implements the option *include_hf* for the exclusion of the heavy fermions).

Helpers

Apart the enumeration of the particles, the module is required to provide some query functions which O'Mega can use in order to obtain information on the properties of the particles. The enumeration of the particles by quantum number allows to do this in a rather convenient way as demonstrated by the examples of $\mathbf{SU}(3)_C$ and Lorentz representation.

```
let color =
let quarkrep = function
  | (_, Pos, _, _) → Color.SUN 3
  | (_, Neg, _, _) → Color.SUN (-3)
in function
  | Fermion (Quark x) → quarkrep x
  | Boson G → Color.AdjSUN 3
  | _ → Color.Singlet
```

```
let lorentz =
let spinor = function
  | (_, Pos, _, _) → Spinor
  | (_, Neg, _, _) → ConjSpinor
in function
  | Fermion (Lepton x) | Fermion (Quark x) → spinor x
  | Boson (W _) | Boson (Z _) → Massive_Vector
  | Boson A → Vector
  | Boson G → Vector
```

Another type of helper which is very important for the interaction with WHIZARD is the function *pdg* which returns the PDG code assigned to a particle.

```
let int_of_csign = function Pos → 1 | Neg → -1
let int_of_gen = function Gen0 → 1 | Gen1 → 2 | Gen2 → 3

let pdg =
let iso_delta = function Iso_down → 0 | Iso_up → 1
in let gen_delta = function Gen0 → 0 | Gen1 → 2 | Gen2 → 4
in let kk_delta = function Light → 0 | Heavy → 9900
in function
  | Fermion ( Lepton (kk, cs, gen, iso)) →
    (int_of_csign cs) × (11 + (gen_delta gen) + (iso_delta iso) + (kk_delta kk))
  | Fermion ( Quark (kk, cs, gen, iso)) →
    (int_of_csign cs) × (1 + (gen_delta gen) + (iso_delta iso) + (kk_delta kk))
  | Boson (W (kk, cs)) → (int_of_csign cs) × (24 + (kk_delta kk))
  | Boson (Z kk) → 23 + (kk_delta kk)
  | Boson A → 22
  | Boson G → 21
```

This function is designed such that it adheres to the Monte Carlo numbering scheme for the Standard Model particles and assigns the PDG code of their partner prefixed with 99 to their KK partners, e.g. $11/-11$ to the e^-/e^+ and $9911/-9911$ to the $e^{-\prime}/e^{+\prime}$.

Although not included in the interface, a very important function is the translation of a flavor into the constant identifying it in the FORTRAN module (see app. D.1).

```
let bcdi_of_flavor =
let prefix = function
  | Fermion (Lepton (Heavy, _, _, _)) | Fermion (Quark (Heavy, _, _, _))
  | Boson (W (Heavy, _)) | Boson (Z Heavy) → "h"
  | _ → ""
in let rump = function
  | Fermion (Lepton spec) → (match spec with
    | (_, _, Gen0, Iso_up) → "nue"
```

```
    | (_, _, Gen0, Iso_down) → "e"
    | (_, _, Gen1, Iso_up) → "numu"
    | (_, _, Gen1, Iso_down) → "mu"
    | (_, _, Gen2, Iso_up) → "nutau"
    | (_, _, Gen2, Iso_down) → "tau")
  | Fermion (Quark spec) → (match spec with
    | (_, _, Gen0, Iso_up) → "u"
    | (_, _, Gen0, Iso_down) → "d"
    | (_, _, Gen1, Iso_up) → "c"
    | (_, _, Gen1, Iso_down) → "s"
    | (_, _, Gen2, Iso_up) → "t"
    | (_, _, Gen2, Iso_down) → "b")
  | Boson (W _) → "w" | Boson (Z _) → "z"
  | Boson A → invalid_arg "Csmodels1.bcd_of_flavor: no bcd for photon!"
  | Boson G → invalid_arg "Csmodels1.bcd_of_flavor: no bcd for gluon!"
in function x → (prefix x) ^ (rump x) ^ "_bcd"
```

Other functions which are required by O'Mega for example to translate particle flavors in character strings suitable for the backend or to communicate with the user on the command line are constructed in a likewise fashion.

Couplings and vertices

In order to be able to represent the coupling constants as closely to the conventions of the FORTRAN module as possible, another type referring to the combination of KK modes at a vertex rather than the individual modes is defined.

```
type kk2 = Light2 | Heavy2 | Light_Heavy
let loop_kk2 flist = revmap2 flist [Light2; Heavy2; Light_Heavy]
let cloop_kk2 flist = match Module_options.include_hf with
  | true → loop_kk2 flist
  | false → revmap flist Light2
```

The coupling constants are then defined to mimic their FORTRAN counterparts as closely as possible.

```
type constant =
  | G_a_lep | G_a_quark of isospin
  | G_aww | G_aaww
  | G_w_lep of (kkmode × kkmode × generation × kkmode × generation)
  | G_w_quark of (kkmode × kkmode × generation × kkmode × generation)
  | G_z_lep of (kkmode × kk2 × generation × isospin)
  | G_z_quark of (kkmode × kk2 × generation × isospin)
  | G_wwz of (kk2 × kkmode)
  | G_wwzz of (kk2 × kk2)
  | G_wwza of (kk2 × kkmode)
```

```
  | G_wwww of int
  | G_s
  | IG_s
  | G_s2
```

Using the *loop_xx* function allows for a compact definition of the vertex lists, e.g. for the γff and Zff type vertices

```
let vertices_all =
let vgen kk gen =
  ((Fermion (Lepton (kk, Neg, gen, Iso_down)), Boson A, Fermion (Lepton (kk, Pos, gen,
    Iso_down))), FBF(1, Psibar, V, Psi), G_a_lep)
in loop_gen (cloop_kk [vgen])

let vertices_aqq =
let vgen kk gen iso =
  ((Fermion (Quark (kk, Neg, gen, iso)), Boson A, Fermion (Quark (kk, Pos, gen,
    iso))), FBF(1, Psibar, V, Psi), G_a_quark iso)
in loop_iso (loop_gen (cloop_kk [vgen]))

let vertices_zll =
let vgen kkz kk_f kk_fbar gen iso =
  ((Fermion (Lepton (kk_fbar, Neg, gen, iso)), Boson (Z kkz),
    Fermion (Lepton (kk_f, Pos, gen, iso))),
    FBF (1, Psibar, VA2, Psi),
    G_z_lep (kkz, get_kk2 (kk_f, kk_fbar), gen, iso))
in loop_iso (loop_gen (cloop_kk (cloop_kk (loop_kk [vgen] ))))

let vertices_zqq =
let vgen kkz kk_f kk_fbar gen iso =
  ((Fermion (Quark (kk_fbar, Neg, gen, iso)), Boson (Z kkz),
    Fermion (Quark (kk_f, Pos, gen, iso))),
    FBF (1, Psibar, VA2, Psi),
    G_z_quark (kkz, get_kk2 (kk_f, kk_fbar), gen, iso))
in loop_iso (loop_gen (cloop_kk (cloop_kk (loop_kk [vgen] ))))
```

The Wff vertex lists are defined in different versions in order to implement the different options , e.g. for Wqq type vertices

```
let vertices_wqq_no_ckm =
let vgen kkw kk_f kk_fbar iso_f gen =
  ((Fermion (Quark (kk_fbar, Neg, gen, conj_iso iso_f)),
    Boson (W (kkw, (match iso_f with Iso_up → Neg | _ → Pos))),
    Fermion (Quark (kk_f, Pos, gen, iso_f))),
    FBF (1, Psibar, VA2, Psi),
    G_w_quark (kkw, (match iso_f with Iso_up → kk_f | _ → kk_fbar), gen,
      (match iso_f with Iso_up → kk_fbar | _ → kk_f), gen) )
in loop_gen (loop_iso (cloop_kk (cloop_kk (loop_kk [vgen] ))))
```

```
let vertices_wqq_no_ckm_diet =
let filter = function
  | ((Fermion (Quark (Light, _, gen, _)), Boson (W (Heavy, _)),
      Fermion (Quark (Light, _, _, _))), _, _) →
        (match gen with Gen2 → true | _ → false)
  | _ → true
in List.filter filter vertices_wqq_no_ckm
```

```
let vertices_wqq =
let vgen kkw kk_f gen_f kk_fbar gen_fbar iso_f =
  ((Fermion (Quark (kk_fbar, Neg, gen_fbar, conj_iso iso_f)),
      Boson (W (kkw, (match iso_f with Iso_up → Neg | _ → Pos))),
      Fermion (Quark (kk_f, Pos, gen_f, iso_f))),
      FBF (1, Psibar, VA2, Psi),
      G_w_quark (match iso_f with
        | Iso_up → (kkw, kk_f, gen_f, kk_fbar, gen_fbar)
        | Iso_down → (kkw, kk_fbar, gen_fbar, kk_f, gen_f)))
in loop_iso (loop_gen (cloop_kk (loop_gen (cloop_kk (loop_kk [vgen] )))))
```

The actual vertex list passed to O'Mega is then assembled according to the selected options.

```
let vertices () = (vertices_all @ vertices_aqq @
  (match Module_options.diet with
    | false → vertices_wll
    | true → vertices_wll_diet) @
  (match (Module_options.include_ckm, Module_options.diet) with
    | (true, false) → vertices_wqq
    | (false, false) → vertices_wqq_no_ckm
    | (false, true) → vertices_wqq_no_ckm_diet
    | (true, true) → raise (Failure
      ("Modules4.Threeshl.vertices: CKM matrix together with"^
        " option diet is not implemented yet!"))) @
  vertices_zll @ vertices_zqq @ vertices_aww @ vertices_zww @
  (match Module_colopt.o with
    | Colflow → vertices_gqq @ vertices_ggg
    | _ → []),
  vertices_aaww @ vertices_wwzz @ vertices_wwza @ vertices_wwww @
  (match Module_colopt.o with
    | Colflow → vertices_gggg
    | _ → [])
  , [])
```

D.3 WHIZARD Quirks

In WHIZARD, models are described by a model file and a piece of FORTRAN glue. The model file defines free and derived parameters, the particles and a vertex list. The FORTRAN glue is called prior to the evaluation of the first matrix element and has to take care of setting up and providing all parameters and couplings that are required by the matrix element generation code to function. In principle, writing the model file is a straightforward task, and the FORTRAN glue would be the perfect place to perform the `tglue` initialization. However, in the case of the Three-Site Model, implementing the masses of the particles in this fashion turns out to be a problem.

In the particle definition, WHIZARD requires the mass to be either zero or a free / derived parameter. In the Three-Site Model however, the masses are complicated functions which are calculated by the `threeshl` module and stored in the `mass_array` array. It is possible to assign the members of this array to derived parameters like

```
derived mhz          mass_array(hz_bcd)
```

However, the members of this array get only initialized upon calling the `tglue` initialization which, if this would be called from the FORTRAN glue, would be only after the derived parameters have been evaluated. This way, the correct masses would not propagate into the phasespace code which therefore would fail.

The only way to get around this without modifying WHIZARD would be to define the masses as free parameters and calculate them with an external program which writes out a WHIZARD input file. However, this would be rather cumbersome and error-prone. Therefore, the version of WHIZARD which contains the Three-Site Model has been modified to generate code which calls `tglue_init` before the derived parameters are calculated. The amplitude is modified not to use the usual FORTRAN glue (which is unnecessary for the Three-Site Model and therefore omitted) but instead use `threeshl` and `tglue`.

Other minor changes include the build system which is modified to properly use the external library and an external O'Mega tree (WHIZARD includes its own version of O'Mega). However, these are minor issues which could be avoided, while the problem discussed in the last paragraph can only be solved cleanly by a change to the WHIZARD infrastructure.

As a result of these issues, the Three-Site Model is currently not included in the official distribution of the 1.9x branch of WHIZARD but only available in a modified WHIZARD package which can be downloaded from the URL quoted at the beginning of this chapter. The upcoming WHIZARD 2.0, however, will remove these limitations and will contain the implementation as part of the official distribution.

Bibliography

[1] S. Weinberg. A Model of Leptons. *Phys. Rev. Lett.*, 19:1264–1266, 1967.

[2] S. L. Glashow, J. Iliopoulos, and L. Maiani. Weak Interactions with Lepton-Hadron Symmetry. *Phys. Rev.*, D2:1285–1292, 1970.

[3] M. Kobayashi and T. Maskawa. CP Violation in the Renormalizable Theory of Weak Interaction. *Prog. Theor. Phys.*, 49:652–657, 1973.

[4] R. S. Chivukula et al. A three site higgsless model. *Phys. Rev.*, D74:075011, 2006, hep-ph/0607124.

[5] M. E. Peskin. *An Introduction to Quantum Field Theory (Frontiers in Physics S.)*. HarperCollins Publishers, 1995.

[6] C. Itzykson and J.-B. Zuber. *Quantum Field Theory*. Dover Publications, 2006.

[7] S. Weinberg. *The Quantum Theorie of f Fields, Vol 1: Foundations*. Cambridge University Press, 1995.

[8] S. Weinberg. *The Quantum Theory of Fields, Vol.2: Modern Applications*. Cambridge University Press, 1995.

[9] A. Manohar and H. Georgi. Chiral Quarks and the Nonrelativistic Quark Model. *Nucl. Phys.*, B234:189, 1984.

[10] M. Jacob and G. C. Wick. On the general theory of collisions for particles with spin. *Ann. Phys.*, 7:404–428, 1959.

[11] C. Qigg. *Gauge Theories of the Strong, Weak and Electromagnetic Interactions*. The Benjamin/Cummings Publishing Company, 1983.

[12] T. Ohl. Electroweak gauge bosons at future electron positron colliders. 1999, hep-ph/9911437.

[13] C. Amsler et al. Review of particle physics. *Phys. Lett.*, B667:1, 2008.

[14] J. Goldstone. Field Theories with Superconductor Solutions. *Nuovo Cim.*, 19:154–164, 1961.

[15] B. W. Lee, C. Quigg, and H. B. Thacker. Weak Interactions at Very High-Energies: The Role of the Higgs Boson Mass. *Phys. Rev.*, D16:1519, 1977.

[16] S. R. Coleman, J. Wess, and B. Zumino. Structure of phenomenological lagrangians. 1. *Phys. Rev.*, 177:2239–2247, 1969.

[17] G. 't Hooft and M. J. G. Veltman. Regularization and Renormalization of Gauge Fields. *Nucl. Phys.*, B44:189–213, 1972.

[18] J. Alcaraz et al. Precision Electroweak Measurements and Constraints on the Standard Model. 2007, 0712.0929.

[19] M. E. Peskin and T. Takeuchi. Estimation of oblique electroweak corrections. *Phys. Rev.*, D46:381–409, 1992.

[20] M. E. Peskin and T. Takeuchi. A New constraint on a strongly interacting Higgs sector. *Phys. Rev. Lett.*, 65:964–967, 1990.

[21] G. Altarelli and R. Barbieri. Vacuum polarization effects of new physics on electroweak processes. *Phys. Lett.*, B253:161–167, 1991.

[22] G. Altarelli, R. Barbieri, and S. Jadach. Toward a model independent analysis of electroweak data. *Nucl. Phys.*, B369:3–32, 1992.

[23] C. Csaki, C. Grojean, H. Murayama, L. Pilo, and J. Terning. Gauge theories on an interval: Unitarity without a Higgs. *Phys. Rev.*, D69:055006, 2004, hep-ph/0305237.

[24] L. Randall and R. Sundrum. A large mass hierarchy from a small extra dimension. *Phys. Rev. Lett.*, 83:3370–3373, 1999, hep-ph/9905221.

[25] A. Hebecker and J. March-Russell. The structure of GUT breaking by orbifolding. *Nucl. Phys.*, B625:128–150, 2002, hep-ph/0107039.

[26] A. Muck, A. Pilaftsis, and R. Ruckl. Minimal Higher-Dimensional Extensions of the Standard Model and Electroweak Observables. *Phys. Rev.*, D65:085037, 2002, hep-ph/0110391.

[27] R. Sundrum. To the fifth dimension and back. (TASI 2004). 2005, hep-th/0508134.

[28] M. Göckeler and T. Schücker. *Differential geometry, gauge theories , and gravity*. Cambridge University Press, 1987.

[29] H.-C. Cheng, C. T. Hill, S. Pokorski, and J. Wang. The standard model in the latticized bulk. *Phys. Rev.*, D64:065007, 2001, hep-th/0104179.

[30] N. Arkani-Hamed, A. G. Cohen, and H. Georgi. (De)constructing dimensions. *Phys. Rev. Lett.*, 86:4757–4761, 2001, hep-th/0104005.

[31] C. T. Hill and A. K. Leibovich. Deconstructing 5-D QED. *Phys. Rev.*, D66:016006, 2002, hep-ph/0205057.

[32] H. Georgi. A TOOL KIT FOR BUILDERS OF COMPOSITE MODELS. *Nucl. Phys.*, B266:274, 1986.

[33] R. Casalbuoni, S. De Curtis, D. Dominici, and R. Gatto. Effective Weak Interaction Theory with Possible New Vector Resonance from a Strong Higgs Sector. *Phys. Lett.*, B155:95, 1985.

[34] H.-J. He et al. LHC Signatures of New Gauge Bosons in Minimal Higgsless Model. *Phys. Rev.*, D78:031701, 2008, 0708.2588.

[35] T. Abe, S. Matsuzaki, and M. Tanabashi. Does the three site Higgsless model survive the electroweak precision tests at loop? *Phys. Rev.*, D78:055020, 2008, 0807.2298.

[36] R. Barbieri, A. Pomarol, R. Rattazzi, and A. Strumia. Electroweak symmetry breaking after LEP-1 and LEP-2. *Nucl. Phys.*, B703:127–146, 2004, hep-ph/0405040.

[37] R. S. Chivukula, E. H. Simmons, H.-J. He, M. Kurachi, and M. Tanabashi. Universal non-oblique corrections in Higgsless models and beyond. *Phys. Lett.*, B603:210–218, 2004, hep-ph/0408262.

[38] R. S. Chivukula, E. H. Simmons, H.-J. He, M. Kurachi, and M. Tanabashi. Ideal fermion delocalization in Higgsless models. *Phys. Rev.*, D72:015008, 2005, hep-ph/0504114.

[39] S. Matsuzaki, R. S. Chivukula, E. H. Simmons, and M. Tanabashi. One-Loop Corrections to the S and T Parameters in a Three Site Higgsless Model. *Phys. Rev.*, D75:073002, 2007, hep-ph/0607191.

[40] R. S. Chivukula, E. H. Simmons, S. Matsuzaki, and M. Tanabashi. The three site model at one-loop. *Phys. Rev.*, D75:075012, 2007, hep-ph/0702218.

[41] K. Hagiwara, R. D. Peccei, D. Zeppenfeld, and K. Hikasa. Probing the Weak Boson Sector in e+ e- → W+ W-. *Nucl. Phys.*, B282:253, 1987.

[42] The LEP Collarborations ALPEH, DELPHI, L3, OPAL and the LEP TGC Working Group. A Combination of Results on Charged Triple Gauge Boson Couplings Measured by the LEP experiments. *LEPEWWG/TC/2005-01*, 2005.

[43] H. Georgi. On-shell effective field theory. *Nucl. Phys.*, B361:339–350, 1991.

[44] N. D. Christensen and C. Duhr. FeynRules - Feynman rules made easy. *Comput. Phys. Commun.*, 180:1614–1641, 2009, 0806.4194.

[45] J. C. Collins and D. E. Soper. The Theorems of Perturbative QCD. *Ann. Rev. Nucl. Part. Sci.*, 37:383–409, 1987.

[46] W. Kilian, T. Ohl, and J. Reuter. WHIZARD: Simulating Multi-Particle Processes at LHC and ILC. 2007, 0708.4233.

[47] A. Pukhov. CalcHEP 3.2: MSSM, structure functions, event generation, batchs, and generation of matrix elements for other packages. 2004, hep-ph/0412191.

[48] M. Moretti, T. Ohl, and J. Reuter. O'Mega: An optimizing matrix element generator. 2001, hep-ph/0102195.

[49] T. Ohl. Vegas revisited: Adaptive monte carlo integration beyond factorization. *Comput. Phys. Commun.*, 120:13–19, 1999, hep-ph/9806432.

[50] G. P. Lepage. A new algorithm for adaptive multidimensional integration. *J. Comput. Phys.*, 27:192, 1978.

[51] T. Stelzer and W. F. Long. Automatic generation of tree level helicity amplitudes. *Comput. Phys. Commun.*, 81:357–371, 1994, hep-ph/9401258.

[52] H. Plothow-Besch. PDFLIB: A Library of all available parton density functions of the nucleon, the pion and the photon and the corresponding alpha-s calculations. *Comput. Phys. Commun.*, 75:396–416, 1993.

[53] M. R. Whalley, D. Bourilkov, and R. C. Group. The Les Houches Accord PDFs (LHAPDF) and Lhaglue. 2005, hep-ph/0508110.

[54] T. Sjostrand, S. Mrenna, and P. Skands. PYTHIA 6.4 Physics and Manual. *JHEP*, 05:026, 2006, hep-ph/0603175.

[55] F. Maltoni, K. Paul, T. Stelzer, and S. Willenbrock. Color-flow decomposition of QCD amplitudes. *Phys. Rev.*, D67:014026, 2003, hep-ph/0209271.

[56] T. Hahn and M. Perez-Victoria. Automatized one-loop calculations in four and D dimensions. *Comput. Phys. Commun.*, 118:153–165, 1999, hep-ph/9807565.

[57] T. Hahn. Generating Feynman diagrams and amplitudes with FeynArts 3. *Comput. Phys. Commun.*, 140:418–431, 2001, hep-ph/0012260.

[58] T. Gleisberg et al. Event generation with SHERPA 1.1. *JHEP*, 02:007, 2009, 0811.4622.

[59] J. R. Ellis, M. K. Gaillard, and D. V. Nanopoulos. A Phenomenological Profile of the Higgs Boson. *Nucl. Phys.*, B106:292, 1976.

[60] J. Bagger et al. CERN LHC analysis of the strongly interacting W W system: Gold plated modes. *Phys. Rev.*, D52:3878–3889, 1995, hep-ph/9504426.

[61] J. Pumplin et al. New generation of parton distributions with uncertainties from global QCD analysis. *JHEP*, 07:012, 2002, hep-ph/0201195.

[62] T. Ohl and C. Speckner. Production of Almost Fermiophobic Gauge Bosons in the Minimal Higgsless Model at the LHC. *Phys. Rev.*, D78:095008, 2008, 0809.0023.

[63] F. Bach. Phenomenonology of the Three Site Higgsless Model at the ATLAS detector of the LHC, Master's Thesis, 2009.

[64] F. Mandl and G. Shaw. *Quantum Field Theory*. John Wiley and Sons Ltd, 1993.

[65] J.-a. Liu and Y.-P. Yao. One loop radiative corrections to a heavy top decay in the standard model. *Int. J. Mod. Phys.*, A6:4925–4948, 1991.

[66] T. Hahn. New features in FormCalc 4. *Nucl. Phys. Proc. Suppl.*, 135:333–337, 2004, hep-ph/0406288.

[67] A. Denner. Techniques for calculation of electroweak radiative corrections at the one loop level and results for W physics at LEP-200. *Fortschr. Phys.*, 41:307–420, 1993, 0709.1075.

[68] J. A. M. Vermaseren. New features of form. 2000, math-ph/0010025.

Danksagung

Wohl keine Doktorarbeit dieser Welt entsteht ohne die Unterstützung des Autors durch seine Mitmenschen. Daher sind an dieser Stelle (ohne besondere Reihenfolge oder Anspruch auf Vollständigkeit) diejenigen Menschen aufgeführt, ohne deren Unterstützung die vorliegende Arbeit in dieser Form nicht möglich gewesen wäre.

- Meine Familie, die mich mein gesamtes Studium hindurch in jeder Hinsicht unterstützt hat und ohne deren Rückhalt diese Doktorarbeit niemals entstanden wäre.
- Meine Frau Barbara, deren Geduld durch die Physik manchmal schwer strapaziert wird und die dennoch immer zu mir und meiner Arbeit stand und steht.
- Prof. Dr. Thorsten Ohl, der diese Arbeit geduldig betreut und mir in zahllosen Diskussionen immer wieder zu neuen Erkenntnissen verholfen hat.
- Prof. Dr. Rückl, der mir die Durchführung dieser Arbeit an seinem Lehrstuhl ermöglicht hat.
- Prof. Dr. Hans Fraas, der in seinen Vorlesungen mein Interesse an der Theoretischen Physik geweckt hat.
- Dem Graduiertenkolleg GRK4711 (wenn auch keine Person im eigentlich Sinne), welches durch ein Stipendium diese Arbeit wesentlich unterstützt und mir zudem einen fünfwöchigen Aufenthalt an der MSU ermöglicht hat.
- Meinen Mitkollegiaten für eine angenehme und anregende Arbeitsatmosphäre, in der ich auch das eine oder andere gelernt habe, was nichts mit Teilchenphysik zu tun hat.
- Brigitte Wehner, die in allen formalen Angelegenheiten immer hilfreich zur Seite stand, und ohne die ich sicherlich die Erstattung von so mancher Dienstreise verbummelt hätte.
- Meinen Freunden, Kollegen und Bürogenossen Lisa Edelhäuser, Alexander Knochel und Thomas Schutzmeier für viele Diskussionen über Physik und noch mehr völlig unphysikalischen Spaß.

- Fabian Bach für viele erhellende Diskussionen über meine Arbeit.
- Lisa für das Korrekturlesen.
- Elizabeth Simmons und Sekhar Chivukula, die meinen sechswöchigen Aufenthalt an der Michigan State University ermöglicht und durch Ihre Gastfreundlichkeit angenehm gemacht haben.
- Neil Christensen für die angenehme und fruchtbare Zusammenarbeit an dem FeynRules-WHIZARD-Interface sowie für den ausführlichen Vergleich der verschiedenen Implementationen des Modells.
- Alle meine Freunde, die ich hier zwar leider nicht aufzählen kann, aber ohne deren Unterstützung vieles schwerer und manches unmöglich wäre.
- Zahllose Open-Source-Entwickler, ohne deren unermüdlichen und leider viel zu selten honorierten Einsatz kaum eines der Programme existieren würde, welche die Umsetzung dieser Arbeit erst möglich gemacht haben.

Lebenslauf

Persönliche Daten

Name	Christian Sepp Wolfgang Speckner
Geburtsdatum	19.08.1980
Geburtsort	Würzburg
Familienstand	verheiratet (04.04.2009), keine Kinder
Nationalität	Deutsch

Ausbildung

1986 – 1990	Grundschule Mistelbach
1990 – 1999	Graf-Münster-Gymnasium Bayreuth
Frühjahr 1999	Abitur
Wintersemester 2000 – Wintersemester 2003	Studium Mathematik und Physik für das Lehramt an Gymnasien, Universität Würzburg
Sommer 2003	Staatl. Zwischenprüfung für das Lehramt an Gymnasien
Wintersemester 2003 – Wintersemester 2006	Studium Diplomphysik, Universität Würzburg
Januar 2007	Verleihung des Titels „Diplom-Physiker (Univ.)“
Januar 2007	Beginn der Promotion an der Universität Würzburg
Januar 2007	Aufnahme als Stipendiat in das DFG-Graduiertenkolleg GRK4711 „Theoretische Teilchenphysik und Astrophysik“ in Würzburg

Versicherung an Eides Statt

Ich versichere hiermit an Eides statt, daß ich diese Dissertation eigenständig, selbständig und insb. ohne Hife eines kommerziellen Promotionsberaters angefertigt habe und keine anderen als die angegebenen Quellen und Hilfsmittel benutzt habe.

Würzburg, den _____

(Christian Speckner)

Erklärung

Ich erkläre hiermit, daß die vorliegende Dissertation weder in gleicher noch anderer Form bereits in einem anderen Prüfungsfach vorgelegen hat.

Würzburg, den _____

(Christian Speckner)